Transcription factor movement and tissue patterning in Arabidopsis root meristem

Mobiele transcriptiefactoren en weefsel patronenpatroonvorming van weefsels in het Arabidopsis wortelmeristeem

(with a summary in English)

Proefschrift

ter verkrijging van de graad van doctor aan de Universiteit Utrecht op gezag van de rector magnificus, prof.dr. G.J. van der Zwaan, ingevolge het besluit van het college voor promoties in het openbaar te verdedigen op maandag 28 september 2015 des middags te 12.45 uur

door

Yuchen Long

geboren op 28 april 1987

te Beijing, China

Promoter: Prof. dr. B.J.GW. Scheres

Copromoter: Dr. I. Blilou

This thesis was accomplished with financial support by an NWO VIDI grant to to Dr. I. Blilou, and an ERC Advanced Grant SysArc and an NWO Spinoza Grant to Prof. dr. B.J.GW. Scheres.

Table of contents

Chapter 1
The logic of communication: roles for mobile transcription factors in plants.

Yuchen Long*, Ben Scheres, Ikram Blilou[#]

Plant Developmental Biology, Plant Sciences, Wageningen University and Research Centre, Droevendaalsesteeg 1, Wageningen, 6708PB, The Netherlands.

*Current address: Laboratoire de Reproduction et Développement des Plantes, INRA, CNRS, ENS, UCB Lyon 1, 46 Allée d'Italie, 69364 Lyon Cedex 07, France.

[#] To whom correspondience should be addressed. E-mail: ikram.blilou@wur.nl

ABSTRACT

Mobile transcription factors play many roles in plant development. Here, we compare the use of mobile transcription factors as signals with some canonical signal transduction processes in prokaryotes and eukaryotes. After an initial survey, we focus on the SHORT-ROOT pathway in Arabidopsis roots to show that, despite the simplicity of the concept of mobile transcription factor signaling, many lines of evidence reveal a surprising complexity in control mechanisms linked to this process. We argue that these controls bestow precision, robustness and versatility on mobile transcription factor signaling.

INTRODUCTION

Development of multicellular organisms relies on coordination and cooperation of individual cells. These cells communicate via precise intercellular signals to coordinate proliferation, differentiation, and programmed cell death during tissue formation. The emergence of multicellular organisms is thought to rely on the evolution of mandatory cooperation amongst single cells (Bonner, 1998). However, intercellular signaling predates multicellularity, as cell-cell communication-based cooperativeness is also used

by unicellular organisms to maximize collective fitness (Xavier, 2011). In this review, specific examples of intercellular signaling pathways in different organisms will be detailed to illustrate the logic of intercellular communication during development. We begin with examples of pathways regulating biofilm and fruiting-body formation in prokaryotes, the EGFR-Ras-Raf-MEK-ERK pathway and JAK/STAT pathway regulating stem cell and embryonic development in animals, and then turn to plants to describe the SHR-SCR pathway which is key to regulating stem cell activities and radial patterning in the root.

Intercellular signaling in prokaryotes

Many unicellular prokaryote and eukaryote species are known to collaboratively form multicellular structures, thus effectively behaving transiently as multicellular organisms. Biofilm, for example, is a surface-adhering aggregation of individual species or mixed unicellular communities held together by an extracellular matrix composed of various biomolecules (Hall-Stoodley et al., 2004). Within the biofilm, these communities can develop distinct multicellular structures with physiological functions absent in free-living bacteria populations (Lawrence et al., 1991). Successful biofilm development involves collective interpretation of environmental and intercellular signals (Davies et al., 1998; Petrova and Sauer, 2009; Irie et al., 2012). This process includes various stages of adhesion, production of extracellular matrix, maturation and dispersion which are regulated by intercellular signals (Jimenez et al., 2012); Figure 1a). For example, the polysaccharide Psl is secreted by the pathogen *Pseudomonas aeruginosa* both as building block of the extracellular matrix and as an intercellular signal molecule to stimulate further production of Psl and other matrix polysaccharides, forming a positive feedback loop which fortifies local biofilm development (Irie et al., 2012).

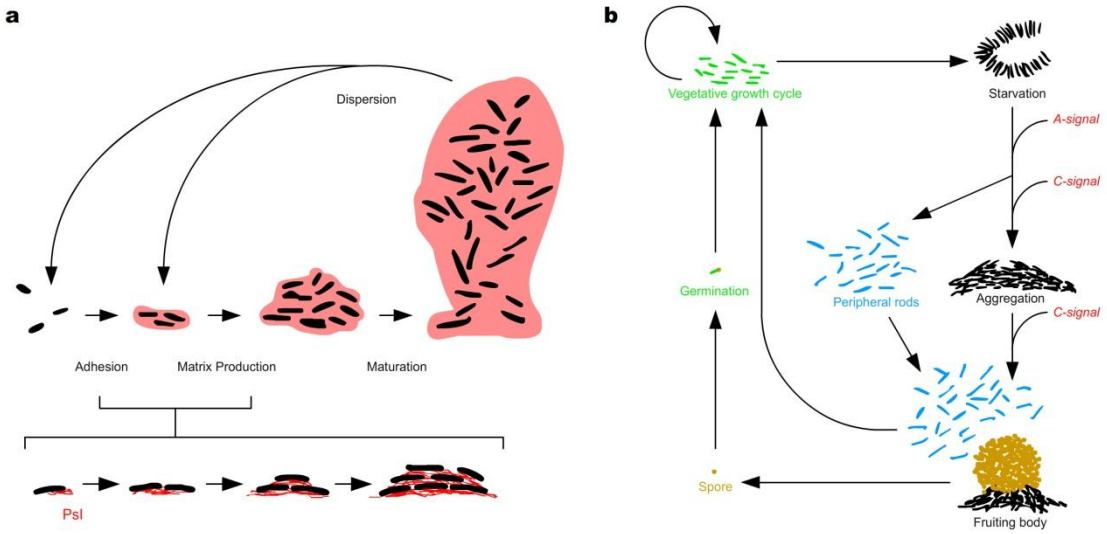

Figure 1. Life cycle of *Pseudomonas aeruginosa* and *Myxococcus xanthus*.

(a) *P. aeruginosa* biofilm formation includes various stages of adhesion, production of extracellular matrix, maturation and dispersion. During this process, secretion of Psl fortifies biofilm formation. (b) Fruiting-body formation of *M. xanthus* is triggered by starvation, upon which vegetative cells undergo different developmental processes guided by intercellular signals. The formed spore germinates under optimal conditions and initiates the vegetative growth cycle again.

Fruiting-body development of *Myxococcus xanthus*, a soil-borne predatory bacterium, also relies on intercellular signaling (Zusman et al., 2007); Figure 1). Exposed to stresses such as starvation, individuals of a *M. xanthus* biofilm can aggregate and develop fruiting-bodies, with 10%-20% of these cells differentiating into stress-resistant spores, another 10% differentiating into so-called peripheral rods, and the rest undergoing cell death (O'Connor and Zusman, 1991). Since around 10^5 of bacteria cells are needed for each fruiting-body, sensing the population size is crucial for successful body formation. To do this, *M. xanthus* employs a quorum-sensing signal (A-signal) to evaluate the population size, and triggers the first stage of aggregation. Later on, a cell-cell contact-based morphogenetic signal (C-signal) helps to pattern cell movement and shape the fruiting-body (Kaiser, 2004); Figure 1b). Although proposed to act independently (Konovalova et al., 2012), the fact that A-signaling and C-signaling require shared components suggests plausible interactions and convergence between these two pathways during fruiting-body formation.

Precise perception and regulation of intercellular signals are crucial for fruiting-body formation: mutants with decreased A-signaling require 10 to 20-fold higher cell density to trigger robust aggregation (Kuspa et al., 1992), while disruption in the negative feedback between a growth-promoting signal and C-signaling can lead to growth arrest and differentiation even in presence of excessive nutrients (Crawford and Shimkets, 2000). The example of *M. xanthus* development reveals a relatively simple module of self-amplification and regulatory feedbacks connected to intercellular signaling, which is sufficient for producing multicellular aggregates with different “cell types”.

Basic logics of intercellular signaling

To generate a multicellular organism, intercellular signaling must be tightly controlled during development. This holds true not only during the signaling events which specify cell type diversity and shape tissues and organs of higher organisms, but also during the formation of prokaryotic communities as described in the previous section. What are the most important requirements for appropriate intercellular signaling? Observations in many developmental processes highlight three important properties to be regulated during intercellular signaling: precision, robustness and versatility (Freeman, 2000).

Simply put, the property of “precision” describes the ability to deliver the right signals to the right place at the right time, “robustness” reflects maintenance of the correct signal output despite fluctuations, and “versatility” portrays the capacity to respond differently to the same signal under different circumstances (Freeman, 2000). Through decades of research, it is generally agreed that all three properties are controlled by signaling feedbacks during development (Freeman, 2000). Feedback describes mutual regulation of factors, and can produce different behaviors depending on the initial state or concentration of each factor. Simple feedback systems involving two components which can either activate or repress, and can be classified as one of three types: 1) mutual activation; each factor activates the other, 2) mutual inhibition; each factor inhibits the other, and 3) activation-inhibition; one factor activates and is inhibited by the other (Figure

2). The different topologies of these three feedback loops can generate distinct system outcomes.

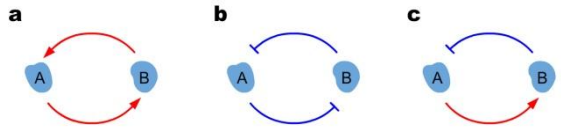

Figure 2. Two-component feedback loops between biomolecules.

(a) A and B mutually activate each other. (b) A and B mutually repress each other. (c) A activates B, while B represses A, forming a negative feedback loop.

In mutual activation, induction of one factor A can leads to the activation of the other factor B, which in turn activates even more A and results in high levels of both A and B (Figure 2a). This self-amplifying effect of positive feedback is seen in many signaling events, such as Psl fortification during *P. aeruginosa* biofilm development as previously mentioned, or in the case of vernalization in the model plant Arabidopsis, where the plant-homeodomain–polycomb repressive complex 2 (PHD–PRC2) initiates the trimethylation on Lysine 27 of Histone H3 (H3K27me3), which recruits more PHD–PRC2 complexes to spread the methylation mark to neighboring nucleosomes across the target *FLOWERING LOCUS C* (*FLC*) locus and therefore promote flowering transition after prolonged cold (Angel et al., 2011).

In mutual inhibition, an initial bias between two factors can be fortified and "locked in". For example, slightly more A than B can lead to the further repression of B, which in turn releases the repression on A. Such enhanced bias will result in the dominance of A in the system, or *vice versa* (Figure 2b). This kind of feedback can be found between *M. xanthus* growth and C-signaling during fruiting-body formation as previously mentioned, or during the development of Arabidopsis leaf pavement cells, where RHO-RELATED PROTEIN FROM PLANTS 2 (ROP2) and ROP6 indirectly inhibit each other's localization to the cell membrane, resulting in patches of ROP2 or ROP6-dominant domains on the cell periphery, and ultimately leading to the formation of lobes and indentations of the jigsaw-shaped pavement cells (Xu et al., 2010; Abley et al., 2013).

In activation-inhibition feedback loops, induction of the activating factor A can lead to higher level of the repressive factor B, which will immediately inhibit A and rebalance the

system (Figure 2c). Depending on the parameters of this feedback, either a robust homeostasis can be obtained, or the system can immediately shut down after an activation pulse. Notable example of this type of feedback can be found, among many other developmental processes, in the Arabidopsis shoot apical meristem, where the stem cell regulator WUSCHEL (WUS) promotes stem cell proliferation and activates CLAVATA3 (CLV3), a peptide signal which represses WUS and keeps the size of the stem cell pool in check (Reviewed by (Bäurle and Laux, 2005).

The beauty of feedback loops lies in their self-organization ability. When different feedback loops with varying parameters integrate, as during developmental signaling, self-organization may give rise to dynamic regulatory networks exhibiting different behaviors such as bistability (Cruz-Ramírez et al., 2012), periodicity (Moreno-Risueno et al., 2010; Traas and Vernoux, 2010), or spatiotemporal patterning (Abley et al., 2013; Mähönen et al., 2014). Thus, understanding feedback mechanisms is an essential step in describing intercellular signaling pathways.

Paradigms of intercellular signaling feedbacks in animals

Feedbacks in the EGFR-Ras-Raf MEK-ERK pathway

The EGFR-Ras-Raf-MEK-ERK pathway is a notable example of a classical intercellular signaling pathway in animals (Figure 3a). This pathway is involved in numerous processes such as growth, proliferation, differentiation, apoptosis and stem cell regulation (Aouadi et al., 2006; Oeztuerk-Winder and Ventura, 2012), and its deregulation can lead to tumorigenesis (Roberts and Der, 2007). Typically, signaling commences when the ligand, epidermal growth factor (EGF), binds to its receptor (EGFR), a tyrosine receptor kinase (Herbst, 2004). Upon self-phosphorylation, EGFR recruits a protein complex of growth factor receptor-bound protein 2 (Grb2) and son of sevenless (SOS) to swap the bound GDP on the membrane-associated Ras small guanosine triphosphatases (GTPase) with GTP, thus activating it (Margolis and Skolnik, 1994). Ras-GTP then activates the

serine/threonine-protein kinase Raf (MAPKKK), which will lead to the consecutive phosphorylation events of mitogen-activated protein kinase kinase (MAPKK / MEK) and extracellular-signal-regulated kinase (ERK / MAPK) (Johnson and Lapadat, 2002). This so-called mitogen-activated protein kinase (MAPK) cascade can trigger several target transcription factors to initiate immediate early gene (IEG) responses (O'Donnell et al., 2012). Amongst the IEG products are MAPK phosphatases (MKP) which dephosphorylate ERK and generate negative feedback in the pathway (Owens and Keyse, 2007). ERK, on the other hand, stimulates the activity of upstream regulator Raf and creates a positive feedback loop (Shin et al., 2009); Figure 3a). Scaffold proteins, regulators of the spatiotemporal specificity of MAPK cascade by compartmentalization, are also involved in the feedbacks of the signal transduction (Morrison and Davis, 2003; Dhanasekaran et al., 2007). Taken together, these highly entangled feedbacks enable a multitude of biological responses such as ultrasensitivity (Huang and Ferrell, 1996), oscillation (Kholodenko, 2000) and bistability (Markevich et al., 2004), turning the EGFR-Ras-Raf-MEK-ERK pathway into a highly dynamic signaling circuit.

Simplification of signal transduction

Other intercellular communication mechanisms in animals involve more direct signaling; nuclear receptors, for example, are transcription factors that upon ligand binding can directly regulate target expression (Tata, 2002). Numerous surface-perceived intercellular signals and their membrane receptors can also enter the target cell via endocytosis, and eventually translocate to the nuclei regulate target genes by directly binding to target transcription factors or coregulators (Planque, 2006). Such short signal transduction routes plausibly imply moderate simplification of regulations or feedbacks, but allow more immediate links between signal perception and target transcription factors. To compensate the reduced auto-regulation, extra feedback steps might be required for these simplified pathways.

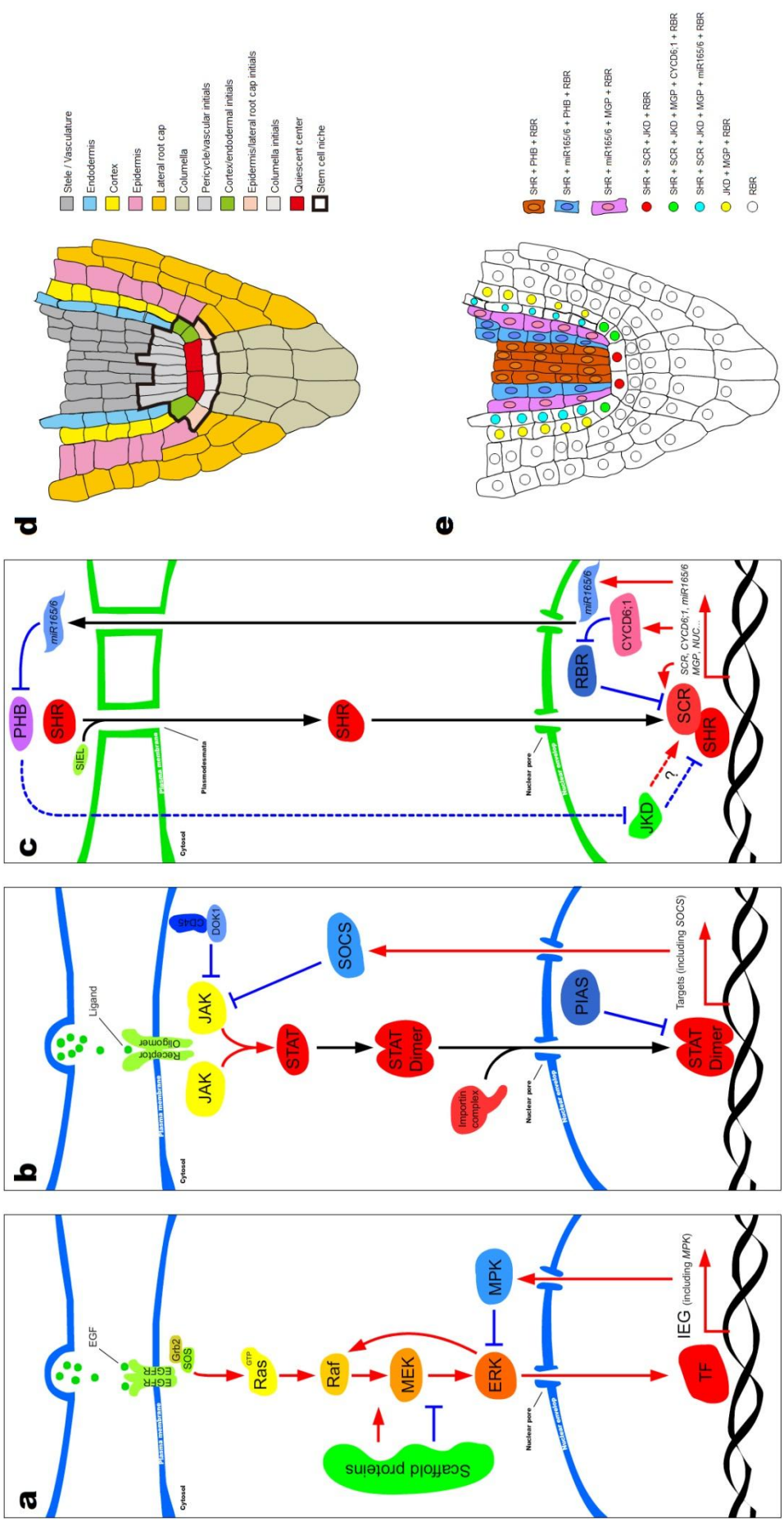
a
EGF
EGFR
Grb2
SOS
Ras
GTP
Raf
MEK
ERK
MPK
Scaffold proteins
Cytosol
Nuclear pore
IEG (including MPK)
TF
b
Ligand
Receptor Oligomer
JAK
JAK
STAT
STAT Dimer
CD45
DOK1
SOCS
PIAS
importin complex
Targets (including SOCS)
c
miR165/6
PHB
SHR
SIEL
Plasmodesmata
JKD
RBR
CYCD6;1
SCR
SHR
SCR, CYCD6;1, miR165/6 MGP, NUC...
d
Stele / Vasculature
Endodermis
Cortex
Epidermis
Lateral root cap
Columella
Pericycle/vascular initials
Cortex/endodermal initials
Epidermis/lateral root cap initials
Columella initials
Quiescent center
Stem cell niche
e
SHR + PHB + RBR
SHR + miR165/6 + PHB + RBR
SHR + miR165/6 + MGP + RBR
SHR + SCR + JKD + RBR
SHR + SCR + JKD + MGP + CYCD6;1 + RBR
SHR + SCR + JKD + MGP + miR165/6 + RBR
JKD + MGP + RBR
RBR

Figure 3. Simplified overview of three developmental signaling pathways.

(a) The EGFR-Ras-Raf-MEK-ERK pathway. (b) The JAK/STAT pathway. (c) The SHR-SCR pathway. (d) Illustration of the root meristem of *Arabidopsis thaliana*, where different cell types are marked by different colors. The bold line encircles the stem cell niche. (e) Expression patterns of the SHR-SCR circuit factors in the root meristem. EGF, epidermal growth factor; EGFR, epidermal growth factor receptor; Grb2, growth factor receptor-bound protein 2; SOS, son of sevenless; MEK, mitogen/extracellular signal-regulated kinase; ERK, extracellular-signal-regulated kinase; TF, transcription factor; IEG, immediate early gene; MPK, MAPK phosphatases; JAK, receptor-associated Janus kinases; STAT, signal transducer and activator of transcription; PIAS, nuclear protein inhibitor of activated STAT; SOCS, suppressor of cytokine signaling; DOK1, downstream of kinase 1; SHR, SHORT-ROOT; SIEL, SHORT-ROOT INTERACTING EMBRYONIC LETHAL; SCR, SCARECROW; JKD, JACKDAW; CYCD6;1, CYCLIND6;1; RBR, RETINOBLASTOMA-RELATED; MGP, MAGPIE; NUC, NUTCRACKER; miR165/6, miRNA165/6; PHB, PHABULOSA.

Feedbacks in the JAK/STAT signaling pathway

Another signal transduction system, the JAK/STAT pathway, can also provide quick access for intercellular signals to target regulation (Figure 3b). STAT stands for signal transducer and activator of transcription, and is known to regulate embryogenesis, stem cell regulation and regeneration in animals (Luo and Dearolf, 2001; Jiang et al., 2009). The JAK/STAT pathway can be activated by intercellular mediators such as cytokines (2000). As secreted polypeptides, cytokines can mediate specific cell-cell communication critical for the development and regulation of a range of cell types, particularly those of the immune and hematopoietic systems (Liongue et al., 2012).

The backbone of the JAK/STAT pathway is simple: it starts with dimerization or oligomerization of specific receptors upon binding to their ligands, leading to phosphorylation events at the receptor complex catalyzed by the receptor-associated Janus kinases (JAKs) (Figure 3b). Tyrosine phosphorylation of the receptor tails provides docking sites for inactive STATs in the cytoplasm, allowing STAT tyrosine phosphorylation by active JAKs. Phosphorylated STATs immediately homo- or heterodimerize with each other, translocate from cytoplasm into the nucleus, bind target DNA sequences and activate downstream target genes (Levy and Darnell, 2002); Figure 3b).

The signal transduction through the JAK/STAT pathway can be negatively regulated by other factors such as nuclear protein inhibitor of activated STAT (PIAS) and phosphatases such as suppressor of cytokine signaling (SOCS) and CD45 (Greenhalgh and Hilton, 2001); Figure 3b): PIAS is suggested to bind active STAT dimers not only to inhibit their transcriptional activity, but also to prevent them from DNA binding. Additionally, PIAS can mediate STAT sumoylation and attenuate JAK/STAT pathway sensitivity (Rogers et al., 2003; Begitt et al., 2011). SOCS proteins are directly induced by the STATs, and they create negative feedback on the JAK/STAT pathway by dephosphorylating JAKs or cytokine receptors, and can mediate signaling crosstalk and specificity (Murray, 2007). CD45 is a membrane bound phosphatase that negatively regulates JAK/STAT pathway by JAK dephosphorylation and recruitment of the inhibitory molecule downstream of kinase 1 (DOK1) (Irie-Sasaki et al., 2001; Wu et al., 2009).

Another important feature of the classical model for STAT-mediated signal transduction is the nucleocytoplasmic trafficking of STAT proteins, where STAT activation is coupled with nuclear import, and inactivation with nuclear export as reviewed by (Reich and Liu, 2006). Recent data has revealed that STAT proteins can exert functions beyond their role as transcription factors, and their subcellular localization can be highly dynamic in line with their specific functions (Yang et al., 2005; Ng et al., 2006; Lin et al., 2011; Hu et al., 2013; Macias et al., 2014), bringing another level of complexity to STAT signaling regulation.

The signal transduction process is simplified in the classic JAK/STAT pathway thanks to the dual nature of STAT, a transcription factor and signal transducer at the same time. This simplification, however, does not delimit regulation and feedback mechanisms within the pathway. One then may ask: can a functionally regulated intercellular signaling pathway be simplified further? Can one molecule integrate the roles of not only transcription factor and signal transducer, but also the intercellular signal itself? The answer is yes, as numerous mobile transcription factors are found to relay intercellular signaling events in plants.

Mobile transcription factors as intercellular signals during plant development

While plants make use of signal peptides, hormones and microRNAs as intercellular signaling intermediaries commonly employed in animals, they harbor in addition an arsenal of mobile transcription factors to deliver intercellular signals (Han et al., 2014). As plant cells are encaged in rigid cell walls, the mobility of these transcription factors is facilitated by the presence of plasmodesmata, membrane-bound intercellular channels that link almost all plant cells into one symplastic entity, permitting selective passage of macromolecules (Lucas and Lee, 2004).

The homeodomain protein KNOTTED1 (KN1) from *Zea mays* was the first described mobile transcription factor (Hake and Freeling, 1986; Lucas et al., 1995). Since then, the list of mobile transcription factors, or non-cell-autonomous transcription factors (NCATFs), has been growing constantly. Examples of such proteins with regulatory roles in plant development include LEAFY (LFY), regulator of flower development (Sessions et al., 2000), SHORT-ROOT (SHR), a GRAS-domain transcription factor regulating stem cell activity and radial patterning of the Arabidopsis root (Nakajima et al., 2001), CARPRICE (CPC) and TRANSPARENT TESTA GLABROUS1 (TTG1), mobile regulators of epidermis patterning (Kurata et al., 2005), FLOWERING LOCUS T (FT), long-distance signal inducing floral transition (Corbesier et al., 2007); TARGET OF MONOPTEROS 7 (TMO7), a basic helix-loop-helix (bHLH) transcription factor required for embryonic root initiation (Schlereth et al., 2010), WUSCHEL (WUS), a homeodomain transcription factor maintaining stem cell homeostasis in the shoot apical meristem (Yadav et al., 2011), PLETHORA 2 (PLT2), an AP2 domain transcription factor driving auxin-dependent root zonation (Mähönen et al., 2014), and many more (reviewed by (Han et al., 2014). A genome-wide screen in Arabidopsis revealed that many uncharacterized putative transcription factors are also capable of trafficking between cells with diverse movement patterns, and several observations have led to the hypothesis that plant transcription factors were all ancestrally mobile, while cell-autonomy was gained during evolution (Wu et al., 2003; Lucas et al., 2009; Rim et al., 2011).

Modes of NCATF movement can differ from protein to protein. LFY, for example, is smaller than the size exclusion limit of plasmodesmata in the Arabidopsis shoot apical meristem, and has been shown to diffuse between plant cells in a similar manner as free green fluorescent protein (GFP) (Wu et al., 2003). Domain deletions of LFY did not eliminate its movement capacity, indicating that no specific domain targets LFY movement (Wu et al., 2003). On the contrary, SHR movement is restricted to one cell layer in the Arabidopsis root, with multiple protein domains required for its mobility, suggesting tight regulation of movement at the protein level (Nakajima et al., 2001; Gallagher et al., 2004; Gallagher and Benfey, 2009). Indeed, many NCATFs exhibit highly controlled movement patterns which are tightly linked to their activities. To date, SHR remains the most intensively studied NCATF showing precise intercellular movement, and regulation of SHR movement and action range is crucial for proper root development in Arabidopsis. Therefore we focus on this example from here on.

SHR action range controls ground tissue development in Arabidopsis roots

The root of the model organism *Arabidopsis thaliana* has a simple yet well-defined structure, where concentric single-cell tissue layers of epidermis, cortex and endodermis encircle the central stele containing the vasculature, while columella and lateral root cap enclose the meristem at the root tip (Dolan et al., 1993); Figure 3d). All of these tissues are generated by four sets of stem cells residing in the root meristem. These stem cells surround the so-called quiescent center (QC) consisting of four mitotically less-active cells, and together they form the stem cell niche.

The cortex and endodermis layers make up the so-called “ground tissue”. Correct separation of the ground tissue relies on specific asymmetric cell divisions, or formative divisions (Scheres and Benfey, 1999), of the cortex/endodermal initial (CEI) stem cells. First, the CEI undergoes an anticlinal division, creating one daughter cell adjacent to the QC and maintaining CEI identity. The other cortex/endodermal initial daughter (CEID) which is displaced from the QC shifts its division plane by 90°, dividing periclinally and

giving rise to one cortex and one endodermis cell (van den Berg et al., 1995). Later during development, an additional cortex layer named middle cortex can be generated from endodermal lineage, residing between the original cortex and the recently divided endodermis (Baum et al., 2002).

Two transcription factors, SHR and SCARECROW (SCR), are required for the proper development of the ground tissue. Despite sharing similar phenotypes of reduced root length and loss of a ground tissue layer, a primary difference between *shr* and *scr* mutants is that endodermal cell fate is totally lost in the single ground tissue layer in *shr* but is retained in *scr* (Benfey et al., 1993; Scheres et al., 1995; Di Laurenzio et al., 1996; Helariutta et al., 2000). This difference uncouples SCR-dependent asymmetric cell division and SHR-dependent cell fate specification. However, subsequent loss- and gain-of-function analyses demonstrated that *SHR* can enhance *SCR* expression in the Arabidopsis root (Helariutta et al., 2000). Thus, SCR and SHR together control root radial patterning, where *SHR* relies on downstream *SCR* activation to initiate asymmetric cell division in the CEI, while other *SHR* targets are required to specify endodermal cell fate (Helariutta et al., 2000; Nakajima et al., 2001; Sena et al., 2004). Interestingly, *SHR* transcript was detected exclusively in the stele but not in the adjacent cell layer of QC, CEI and endodermis where *SCR* is being regulated (Helariutta et al., 2000). The difference in the *SHR* expression domain and domain of action as well as *SHR* local effect led to the postulation that SHR regulates a non-cell-autonomous signal carrying short-ranged positional information from the stele into the neighboring cells (Helariutta et al., 2000).

In 2001, Nakajima and colleagues demonstrated that SHR protein moves from the stele, its domain of transcription, into the outer adjacent cell layer of QC, CEI and endodermis. This observation suggested that the intercellular signal relayed during *SHR*-mediated signaling is actually SHR itself. The protein also shows distinct subcellular localization in different tissues: SHR resides both in the nuclei and cytoplasm in the stele cells, while in the “U-shaped domain” of the adjacent cell layer comprising QC, CEI and endodermis, SHR is exclusively detected in the nuclei (Nakajima et al., 2001).

SHR and *SCR* encode plant-specific putative transcription factors belonging to the GRAS protein family, which is named after three initially identified family members *GIBBERELLIN-ACID INSENSITIVE* (*GAI*), *REPRESSOR OF ga1-3* (*RGA*) and *SCR* itself (Pysh et al., 1999; Helariutta et al., 2000). Interestingly, GRAS proteins are reported to share similar domain organization with STATs and have been proposed to represent the STAT family in plants (Richards et al., 2000), although recent evidence to the contrary shows that this idea requires further investigation (Gallagher et al., 2004; Engstrom, 2011; Zhang et al., 2012).

In addition to controlling asymmetric cell divisions in CEI and formation of endodermis, SHR is also required for QC fate specification and maintenance in a SCR-dependent manner (Nakajima et al., 2001; Sabatini et al., 2003). Additionally, stele development also relies on SHR signaling. First described by Levesque et al (2006), an altered tissue pattern inside the stele occurs in *shr* mutant roots. Later on, it was demonstrated that the aspect of phloem development relies on SHR in the stele, while correct xylem patterning requires SHR's non-cell-autonomous action through a bidirectional signaling pathway: SHR moves out of the stele, and together with SCR induces the synthesis of microRNA165/6 in the endodermis. These microRNAs then move back into the stele and repress their target mRNA of a class III homeodomain leucine zipper (HD-ZIP III) transcription factor *PHABULOSA* (*PHB*) in a dose-dependent manner, thus patterning proper xylem layout inside the stele (Carlsbecker et al., 2010). *PHB* level also feeds back to ground tissue patterning, as a dominant *phb* allele insensitive to microRNA-mediated suppression resulted in ectopic periclinal division in the cortex in association with enhanced SHR outward movement (Miyashima et al., 2011). The ground tissue phenotype of dominant *phb* is suggested to be achieved by ectopic *PHB*-triggered repression of a SHR movement regulator *JACKDAW* (*JKD*, detailed in the following sections). In the wild-type situation, *PHB*-mediated repression of JKD is in turn repressed by sufficient SHR downstream signaling. To sum up, this chain of signaling events composes a self-regulating circuit that affects cell specification patterns in multiple tissues,

therefore allowing consistent exchange of spatial information across a robust stele / ground tissue boundary.

Regulation of SHR movement and action range has been intensively studied (summarized in Figure 3c and 3e). However, more questions remained to be answered about mechanisms that control the SHR signaling network. In the following sections, some major questions and findings pertinent to this network are described.

Regulation of SHORT-ROOT movement and action range

The cell fate determinant SHR relays positional information through stringent regulation of both its movement and perception. Whole-plant overexpression of *SHR* induces supernumerary periclinal divisions and over-proliferation of tissues bearing endodermal features (Helariutta et al., 2000), while ectopic *SHR* in QC and epidermal/lateral root cap initials also induces extra formative cell divisions locally (Nakajima et al., 2001; Sena et al., 2004). This indicates that a broad range of cells are competent to respond to SHR signal in the Arabidopsis root.

Several regulatory mechanisms have been proposed to explain the precise restriction of SHR protein movement: 1) SHR mobility might be facilitated by factors in the stele or across the stele / “U-shaped domain” boundary but absent in other cells; 2) SHR spreading might be restricted by other factors in the “U-shaped domain” or over the endodermis / cortex boundary but not in the stele; and 3) detectable SHR outside the “U-shaped domain” might be depleted through rapid SHR turnover mediated by protein degradation or backward flux. Evidence supporting each of these hypotheses has been reported (Welch et al., 2007; Koizumi et al., 2011; Cruz-Ramírez et al., 2012; Wu et al., 2014), and it is therefore likely that SHR movement regulation involves a combination of all of these proposed mechanisms.

Evidence for facilitated SHR movement

SHR has long been proposed to move through plasmodesmata (Nakajima et al., 2001), yet no direct evidence was available until 2011, when Vatén and colleagues demonstrated that plasmodesmata closure mediated by local callose deposition hampers SHR mobility out of the stele (Vatén et al., 2011). It is tempting to propose that more stringent symplastic permeability is established across the endodermis / cortex boundary to restrict further SHR spread. However, no general symplastic discontinuity was found between these two tissue layers (Sena et al., 2004), indicating that either SHR-specific selections are established across different tissue boundaries, or there are cell-autonomous factors actively facilitating SHR movement through plasmodesmata. The latter proposition is supported by the discovery of SHORT-ROOT INTERACTING EMBRYONIC LETHAL (SIEL), an endosome-associated SHR interactor which is suggested to promote SHR stele exit (Koizumi et al., 2011). *SIEL* expression is high in the stele and endodermis, and is activated by SHR and SCR, suggesting that SHR might promote its own movement in the stele, but not in the endodermis (Koizumi et al., 2011). The role of endodermal SHR-SIEL association remains to be evaluated. Interaction of SHR with SIEL was proposed to take place at the endosomes where other movement facilitators might aid SHR to traffick between cells (Wu and Gallagher, 2014). In addition, sufficient SHR mobility and correct SIEL subcellular localization were found to be dependent on intact microtubules (Wu and Gallagher, 2013). Taken together, these findings indicate that SHR intercellular movement is an active process which involves plasmodesmata apertures, endosomes and the microtubule cytoskeleton.

Evidence for SHR movement restriction

In wild-type root vasculature, SHR protein displays a nucleocytoplasmic dual subcellular localization; while in the “U-shaped domain” where it is immobile, SHR is restricted to cell nuclei (Nakajima et al., 2001). The correlation of SHR immobility and enhanced nuclear localization can also be found in the phloem companion cells as well as when SHR is expressed ectopically in the epidermis (Sena et al., 2004). These observations led to the

hypothesis that SHR movement is blocked by physical nuclear retention. Indeed, SHR tethered with an extra NLS exhibits predominantly nuclear localization in the stele and fails to move into the “U-shaped domain”, suggesting the necessity of cytoplasmic availability for its intercellular movement (Gallagher et al., 2004). Within the “U-shaped domain” where SHR is both immobile and highly enriched in the nucleus, SCR is also expressed and nuclear-localized in QC, CEI and endodermis (Di Laurenzio et al., 1996; Gallagher et al., 2004; Heidstra et al., 2004). This specific expression pattern and subcellular localization has raised the speculation that SCR might be involved in SHR nuclear retention, SHR movement restriction, or both. In *scr* mutants, SHR exhibits a nucleocytoplasmic dual localization in the mutant ground tissue layer (Nakajima et al., 2001) or in the epidermis when ectopically expressed (Sena et al., 2004), consistent with ground tissue expressed-SCR being necessary for SHR nuclear retention. Along the occasional periclinal ground tissue divisions in *scr*, SHR is detected in both the inner and outer cells, indicating that SCR indeed restricts SHR movement or turnover in the endodermis (Heidstra et al., 2004). Additionally, incomplete reduction of *SCR* level by an RNA interference approach (*SCRi*) can result in extended outward SHR movement and triggers extra periclinal divisions in the root ground tissue (Cui et al., 2007). On the other hand, misexpression of *SCR* in the stele can induce SHR nuclear localization and restrict its outward movement (Koizumi et al., 2012a), possibly through physical binding (Cui et al., 2007; Welch et al., 2007). These results indicate that SCR plays a prominent role in regulating SHR subcellular localization and intercellular movement. However in *scr* loss-of-function mutants, SHR produced in the stele or ectopically in the epidermis can only move one cell layer away from its transcriptional domain (Nakajima et al., 2001; Sena et al., 2004), to the same extent as in wild-type (Nakajima et al., 2001).

Recent work has shown that SHR orthologs from *Brachypodium distachyon* and *Oryza sativa* can move from the stele into the ground tissue when ectopically tested in Arabidopsis roots (Wu et al., 2014). Despite their strong interaction with AtSCR, their movement was not limited to a single layer of ground tissue, indicating that additional factors are required to restrict intercellular movement of SHR orthologs within Arabidopsis

roots. Another factor which regulates SHR mobility was named JACKDAW (JKD; (Welch et al., 2007) after the intelligent bird species known to “bypass the regulations of a scarecrow”. The *JKD* expression domain covers the QC, CEI, endodermis and cortex, overlapping with the “U-shaped domain”. In *jkd* mutants, SHR spreads one extra cell layer further into the cortex and initiates an extra round of periclinal cell division, creating three ground tissue layers. This extra division is asymmetric, generating a new endodermis between the preexisting endodermis and recently divided cortex. The original endodermis, on the other hand, is subsequently reprogrammed to pericycle identity, a cell type of the stele (Welch et al., 2007). The ectopic division can be rescued by introducing JKD back into the “U-shaped domain”, revealing its cell-autonomous effect in restricting SHR movement (Hassan et al., 2010). JKD belongs to a plant-specific C2H2 zinc finger protein family defined by the conserved INDETERMINATE DOMAIN (IDD) (Colasanti et al., 1998; Kozaki et al., 2004; Welch et al., 2007). Its homolog MAGPIE (MGP), a direct SHR and SCR target (Levesque et al., 2006; Cui et al., 2007), seems to counter JKD effects, where sufficient reduction of *MGP* activity in the *jkd* mutant background delimits the extra periclinal division in the cortex (Welch et al., 2007). The potential action of MGP on SHR movement regulation remains to be analyzed.

Evidence for SHR turnover

SHR turnover also plays a role in defining SHR range. After the periclinal asymmetric cell division in the ground tissue, SHR protein is equally distributed into the two daughter cells of endodermis and cortex (Nakajima et al., 2001). Residual SHR in the cortical cell is subsequently lost, suggesting that there is a rapid SHR turnover (Nakajima et al., 2001). Recently it was confirmed that SHR is subjected to protein degradation in a cell cycle-dependent manner (Cruz-Ramírez et al., 2012). Unwinding the responsible protein degradation pathway will provide more insights into the relevance of the SHR degradation for its actions.

A circuit regulating CEI formative division

SHR is capable of triggering formative divisions in a broad range of tissues, and its expression together with SCR is abundant in the whole “U-shaped domain” of QC, CEI and endodermis. However in wild-type plants, SHR-SCR–driven divisions only occur in a very small fraction of this “domain”, namely at the CEI position. To explain this discrepancy, experimental studies were combined with mathematical modeling, resulting in a circuit model which recreates the scenario that SHR-SCR activity on asymmetric cell division is spatially restricted only to the stem cell niche (Cruz-Ramírez et al., 2012). A bistable “flip-flop" circuit forms the core of this model. This circuit can integrate spatiotemporal cues using a nested positive feedback loop consisting of SHR, SCR, CYCLIND6;1 (CYCD6;1) and RETINOBLASTOMA-RELATED (RBR) proteins. RBR physically binds to SCR and forms a SHR-SCR-RBR ternary protein complex, rendering the bound SHR-SCR complex inactive. In the model, free SHR-SCR complex activates its downstream target *CYCD6;1* to disrupt SCR-RBR interaction via RBR phosphorylation, mediated by the CYCD6;1-CYCLIN DEPENDENT KINASE B1 (CDKB1) complex, thus activating the SHR-SCR complex (Figure 3c). *CYCD6;1* expression is enhanced by high auxin concentration, a condition encountered in the stem cell niche, thereby “flipping” the circuit into SHR-SCR activation status in the CEI. To ensure that the formative division occurs only once, SHR, SCR and RBR proteins are subjected to degradation during mitosis, resetting the circuit to “flop” status in the resulted endodermal cell where unphosphorylated RBR can maintain repression over newly formed SHR-SCR complex. In this circuit, spatial distribution of CEI formative division is defined by the radial axis of SHR movement range and the longitudinal axis of auxin concentration gradient, while position-based bistability is secured by degradation-mediated circuit reset after each cell cycle in the CEI lineage (Cruz-Ramírez et al., 2012).

The circuit needs refinement

The aforementioned circuit portrays a robust CEI cell fate specification process, however it does not explain why SHR-SCR-–dependent formative division does not frequently occur in the QC cells, where the circuit encounters maximal auxin concentrations (Cruz-Ramírez et al., 2012). Despite the lower frequency relative to CEI, the QC also performs asymmetric cell divisions, creating a shootward QC cell and a rootward columella initial stem cell (Cruz-Ramírez et al., 2013). This process, comparable to that in CEI, is controlled by a similar genetic circuit, where RBR maintains QC quiescence by repressing SHR-SCR activity (Cruz-Ramírez et al., 2013). However, *CYCD6;1* was not detected in the QC prior to asymmetric division under any tested circumstances (Cruz-Ramírez et al., 2013), indicating that 1) there are QC-specific factors repressing *CYCD6;1* activation and 2) the QC-specific version of this circuit consists of components which functionally replace the CYCD6;1-CDKB1 complex. Similarly, another modified version of this circuit might be responsible for regulating the formation of middle cortex during later stage of root development; however the nature of this hypothetical regulatory mechanism remains to be elucidated.

The middle cortex is formed from an extra round of periclinal cell divisions in the endodermal layer outside the stem cell niche, and it is known to be regulated by SHR and SCR (Paquette and Benfey, 2005; Cui and Benfey, 2009). Additionally, other GRAS proteins such as GAI and RGA, together with three other RGA homologs collectively termed DELLA proteins (Pysh et al., 1999), and SCARECROW-LIKE3 (SCL3) regulate middle cortex formation via the integration of plant hormone gibberellin (GA) signaling homeostasis and SHR-SCR activity (Heo et al., 2011). Specifically, middle cortex formation is SHR-dependent, while *SCR* expression and GA stimulus were reported to delay middle cortex formation (Paquette and Benfey, 2005). Being a target of SHR, SCR, DELLA proteins and itself, SCL3 serves as a positive regulator of GA signaling and antagonizes the repressive effect of DELLA proteins, which are subjected to degradation upon GA signal perception (Heo et al., 2011; Zhang et al., 2011). The antagonistic regulation of GA response of SCL3 and DELLA is accomplished via protein-protein

interaction and binding competition to JKD, MGP and their homologs, which delivers these GRAS proteins to target promoters, including the *SCL3* promoter itself (Yoshida et al., 2014). In addition, GA-mediated middle cortex repression also relies on SHRUBBY (SHBY), a vacuolar sorting protein and a positive regulator of GA signaling identified from a SHR-interactor screen (Koizumi and Gallagher, 2013). The convergence of SHR and GA signaling pathways by SCL3 and SHBY serves as a good example of how formative divisions can be established in the ground tissue. However it does not provide mechanistic spatial coordination of such divisions to the positions of CEI or middle cortex initiation, where formative divisions naturally occur.

A new parameter to be considered

Another mechanism has been proposed to explain the regulation of formative divisions at both CEI and middle cortex initiation. In this mechanism, SHR is described as a morphogen, where lower levels of SHR induce formative divisions while high levels exhibit a repressive effect (Koizumi et al., 2012a). The primary evidence supporting this proposition comes from *SHR/shr* heterozygous plants, in which middle cortex formation occurs earlier than in wild-type (Koizumi et al., 2012a). In addition, in wild-type roots, SHR levels exhibit large variations along the endodermal cell file, where formative divisions occur in cells with reduced SHR abundance to generate middle cortex (Koizumi et al., 2012a). Subsequently, a high level of nuclear SHR was proposed to be reinforced by SCR, as reduction of *SCR* by *SCRi* results in reduced SHR concentration and ectopic formative divisions in the ground tissue (Koizumi et al., 2012b; Cui et al., 2007).

The proposed SHR level-dependent mechanism opens the door to new interpretations of the regulatory interactions in the SHR signaling network. However, it must be reconciled with earlier observations, where overexpression and overaccumulation of SHR also induced ectopic formative divisions in the root ground tissue (Helariutta et al., 2000; Nakajima et al., 2001; Sena et al., 2004). Additionally, reducing endodermal SHR levels fails to trigger formative divisions in the circuit model (Cruz-Ramírez et al., 2012). Further

analysis is required to clarify the exact mechanism. One possibility when considering the phenotype of *SCRi*, and the fact that *SCR* is a direct SHR target, is that it is not the absolute level of SHR protein, but rather the level ratios or stoichiometry between SHR, SCR and other effector proteins dictate the occurrence of formative divisions.

Other possible effectors

In addition to its role as SHR movement regulator, JKD can also be considered as a transcriptional co-regulator within the SHR-SCR feedback, as JKD is required for normal *SCR* expression (Welch et al., 2007; Ogasawara et al., 2011). In addition, JKD and its homolog MGP can physically bind to SHR, SCR and each other, implicating them as potential SHR-SCR complex components. It is known that JKD, MGP and other homologs can bind DELLA and SCL3 in a competitive manner to direct these GRAS proteins to target DNA sequences (Yoshida et al., 2014). It is therefore possible that JKD and its homologs can, in a similar manner, competitively shuttle SHR-SCR complexes to different downstream target loci. However the exact action of JKD and its homologs requires further examination in regards to the SHR signaling circuit, SHR-SCR complex activity and root development.

Unwinding SHR signaling circuit – future perspectives

The SHR signaling circuit represents a versatile element for patterning multiple tissues in the root, and is subjected to a façade of regulations and feedbacks. Nonetheless, the exact executions of these regulations remain to be unraveled. It is becoming evident that although intensive studies have revealed many components of this entangled network, the complete composition and spatiotemporal dynamics of the SHR-SCR circuit remain to be measured.

GENERAL CONCLUSION

From examples in unicellular and multicellular organisms, we observe that intercellular signaling systems efficiently integrate signals into logical data processing networks, allowing cells to adjust and adapt their behavior based on the status of their neighbors. The utilization of mobile transcription factors as signals in plants is no exception to this rule, however the simplicity of this signaling strategy is deceptive as detailed studies reveal many layers of control which impart precision, robustness and versatility to the signaling process.

Chapter 2

The zinc finger BIRD proteins jointly stabilize tissue boundaries by confining the cell fate regulator SHORT-ROOT and contributing to fate specification in Arabidopsis

Yuchen Long[1,2], Wouter Smet[1,2], Alfredo Cruz-Ramírez[2,+], Bas Castelijns[2], Wim de Jonge[2], Ari Pekka Mähönen[3], Benjamin P. Bouchet[4], Gabino Sanchez Perez[5], Anna Akhmanova[4], Ben Scheres[1,2], Ikram Blilou[1,2,*].

[1]Plant Developmental Biology, Plant Sciences, Wageningen University, Droevendaalsesteeg 1, Wageningen, 6708PB, The Netherlands.

[2]Molecular Genetics, Department Biology, Utrecht University, Padualaan 8, Utrecht, 3581CH, The Netherlands.

[3]Institute of Biotechnology & Department of Biosciences, University of Helsinki, Helsinki 00014, Finland.

[4]Cell Biology, Faculty of Science, Utrecht University, Padualaan 8, Utrecht, 3581CH, The Netherlands.

[5]Bio-informatics, Plant Sciences, Wageningen University, Droevendaalsesteeg 1, Wageningen, 6708PB, The Netherlands.

[+]Current Address: Laboratorio Nacional de Genómica para la Biodiversidad, CINVESTAV, 18 Irapuato, Irapuato, Mexico.

* Address correspondence to ikram.blilou@wur.nl

ABSTRACT

Plant cells cannot rearrange their positions; therefore, sharp tissue boundaries must be accurately programmed. Movement of the cell fate regulator SHORT-ROOT from the stele to the ground tissue has been associated with transferring positional information across tissue boundaries. The zinc finger BIRD protein JACKDAW has been shown to constrain SHORT-ROOT movement to a single layer and other BIRD family proteins were

postulated to counteract JACKDAW's role in restricting SHORT-ROOT action range. Here we report that regulation of SHORT-ROOT movement requires additional BIRD proteins whose action is critical for the establishment and maintenance of the boundary between stele and ground tissue. We show that BIRD proteins act in concert and not in opposition. The exploitation of asymmetric redundancies allows the separation of two BIRD functions: constraining SHORT-ROOT spread through nuclear retention and transcriptional regulation of key downstream SHORT-ROOT targets including *SCARECROW* and *CYCLIND6*. Our data indicate that BIRD proteins promote formative divisions and tissue specification in the *Arabidopsis thaliana* root meristem ground tissue by tethering and regulating transcriptional competence of SHORT-ROOT complexes. As a result, a tissue boundary is not ''locked in'' after initial patterning like in many animal systems, but possesses considerable developmental plasticity due to continuous reliance on mobile transcription factors.

Key words

BIRD proteins; asymmetric cell division; SCR, SHR; JKD; BIB; MGP; NUC; CYCD6; nuclear retention; protein movement; ground tissue.

INTRODUCTION

In multicellular organisms, a precise organization of different tissues and distinct cell types within tissues is critical for proper establishment and maintenance of a functional body. This structural organization relies on the formation of sharp borders between distinct cell populations, as cells with distinct functions must be kept physically separated. Such spatial patterning is achieved in part through intercellular signaling that induces specific tissues or cell types at boundary positions.

Plant cells are encased in rigid cell walls, which prevent their rearrangement during

pattern formation. Therefore, cells must coordinate growth and development by interpreting a multitude of signals from their neighbors. Intercellular signalling through mobile transcriptional regulators has been shown to be essential for plant growth and development (Lucas et al., 1995b; Nakajima et al., 2001b; Kim et al., 2003a; Kurata et al., 2005b; Gallagher and Benfey, 2009b). In the *Arabidopsis thaliana* root meristem, the cell fate determinant SHORT-ROOT (SHR) is produced in the stele and moves one cell layer outward to instruct ground tissue development (Nakajima et al., 2001; Helariutta et al., 2000; Sena et al., 2004; Gallagher et al., 2004; Gallagher and Benfey, 2009). After movement from the stele, SHR binds to its target SCR (SCARECROW) and promotes the asymmetric cell division (ACD) of the Cortex-Endodermis Initial/daughter (CEI/CEID) as a bipartite SCR-SHR complex to generate the ground tissue (GT) consisting of two layers: cortex and endodermis (Di Laurenzio et al., 1996; Helariutta et al., 2000; Cui et al., 2007). The spatiotemporal distribution of ACDs at the CEI/CEID is regulated by a bistable circuit integrating cues provided by the radial movement of SHR and longitudinal auxin distribution patterns (Cruz-Ramírez et al., 2012). The establishment of the auxin gradient along the longitudinal axis has been extensively studied (Grieneisen et al., 2007; Santuari et al., 2011; Band et al., 2014), and deciphering SHR movement mechanisms is of equal importance to understand tissue boundary formation.

Several molecular factors that contribute to the generation of the SHR protein distribution are emerging. The HEAT domain protein SHR INTERACTING EMBRYONIC LETHAL (SIEL) was suggested to facilitate SHR movement through an endosome- and microtubule-dependent process (Koizumi et al., 2011; Wu and Gallagher, 2013). In addition, callose accumulation at plasmodesmata, symplastic channels which allow passage of hormones, proteins and RNAs (Du et al., 2007; Schlereth et al., 2010; Matsuzaki et al., 2010), results in plasmodesmata closure and reduces SHR intercellular trafficking (Vatén et al., 2011). Furthermore, nuclear targeting of SHR by fusing a nuclear localization signal or by expressing SCR in the vasculature blocks SHR movement (Gallagher et al., 2004; Koizumi et al., 2012), suggesting that nuclear retention determines the range of SHR movement. Finally, JACKDAW (JKD) was identified as a

factor that constrains SHR movement to a single cell layer and regulates the action range of SHR and SCR, *while the JKD-homolog* MAGPIE (MGP) promotes SHR-dependent ACD (Welch et al., 2007). Both proteins bind to and are transcriptionally regulated by the SCR-SHR complex (Levesque et al., 2006; Cui et al., 2007, 2012) but the available data suggested that they had opposite roles in GT patterning (Welch et al., 2007).

Here we report that JKD and its close homolog BALDIBIS (BIB) constrain SHR movement through nuclear retention in Arabidopsis. We show that JKD and BIB activate SCR expression and that the SHR-SCR complex requires JKD and BIB in transcriptional assays. We also show that JKD and BIB restrict *CYCLIND6* (*CYCD6*) expression to the CEI/CEID. In addition, we demonstrate that two other homologs MGP and NUTCRACKER (NUC) are required for periclinal cell divisions generating the two GT layers and, together with SCR, are necessary for endodermal fate specification in conjunction with JKD and not in opposition. Our findings illustrate a dual function of these proteins in maintaining sharp tissue boundaries within the root meristem and highlight a mechanism that can provide a high degree of developmental plasticity in patterning.

RESULTS

BALDIBIS and JACKDAW act redundantly to restrict SHR movement and ACD in the ground tissue.

In *jkd* mutants, SHR moves outward one layer beyond the endodermis and induces one additional endodermal file originating from the cortex (Welch et al., 2007). This phenotype is subtle and suggests that other factors or pathways may act in parallel to restrict SHR movement. JKD is a member of a plant-specific INDETERMINATE DOMAIN (IDD) C2H2 zinc finger protein family (Colasanti et al., 1998; Kozaki et al., 2004; Welch et al., 2007); members of this family are referred to as BIRD proteins hereafter. BIRD proteins share high sequence similarity within Arabidopsis (Supplemental Data Set 1; see Supplemental Methods) and between species (Englbrecht et al., 2004; Colasanti et al., 2006a),

suggesting plausible functional redundancy. To identify potentially redundant partners of JKD, we first examined the expression patterns of its closest homologs BULBUL (BLB) and BALDIBIS (BIB) (Supplemental Figure 1A). Promoter and protein fusions indicated that BLB was not expressed in roots, whereas BIB expression was similar to that of JKD (Figure 1A-D), with high levels in the cortex, endodermis and quiescent center (QC). BIB could also be detected in vascular initials (Figure 1D). Therefore, we reasoned that BIB might act redundantly with JKD.

BIB knockouts were not available, so we generated RNAi (*bib-i*) and artificial miRNA constructs, specifically targeting *BIB* and not its close homologs (Supplemental Figure 1). Both methods resulted in similar phenotypes; so we focused our analysis on RNAi-based *bib-i* lines.

Whereas wild-type (WT) and *bib-i* mature embryos did not reveal abnormal divisions at the root pole, 80% of *jkd* embryos and 95% of *jkd bib-i* embryos displayed one additional layer resulting from ectopic divisions in the GT region (Figure 1E-H). Cortical cells divided more frequently in *jkd bib-i* compared to *jkd* (n=25, 47% and 22%, respectively, measured by counting the number of cells in the cortex showing ectopic divisions). After germination, roots of *bib-i* displayed aberrant divisions in the QC (Figure 1J) however its radial cellular organization was similar to WT with single layers of endodermis, cortex and epidermis encircling the vasculature (Figure 1I, J, M, N; Dolan et al., 1993). In *jkd* mutant roots, at least one extra GT cell file was evident (Figure 1K) with increased numbers of cells in the circumference within each layer (Figure 1O; Welch et al., 2007). More extensive divisions took place in *jkd bib-i*, resulting in roots with wider meristems (Figure 1L). Within these roots, additional layers were observed between the central stele and the epidermis (Figure 1P). Besides an increased number of cell layers, in *jkd bib-i* roots possessed an increased cell number per layer and lacked clear morphological tissue distinctions (Figure 1P; Table 1).

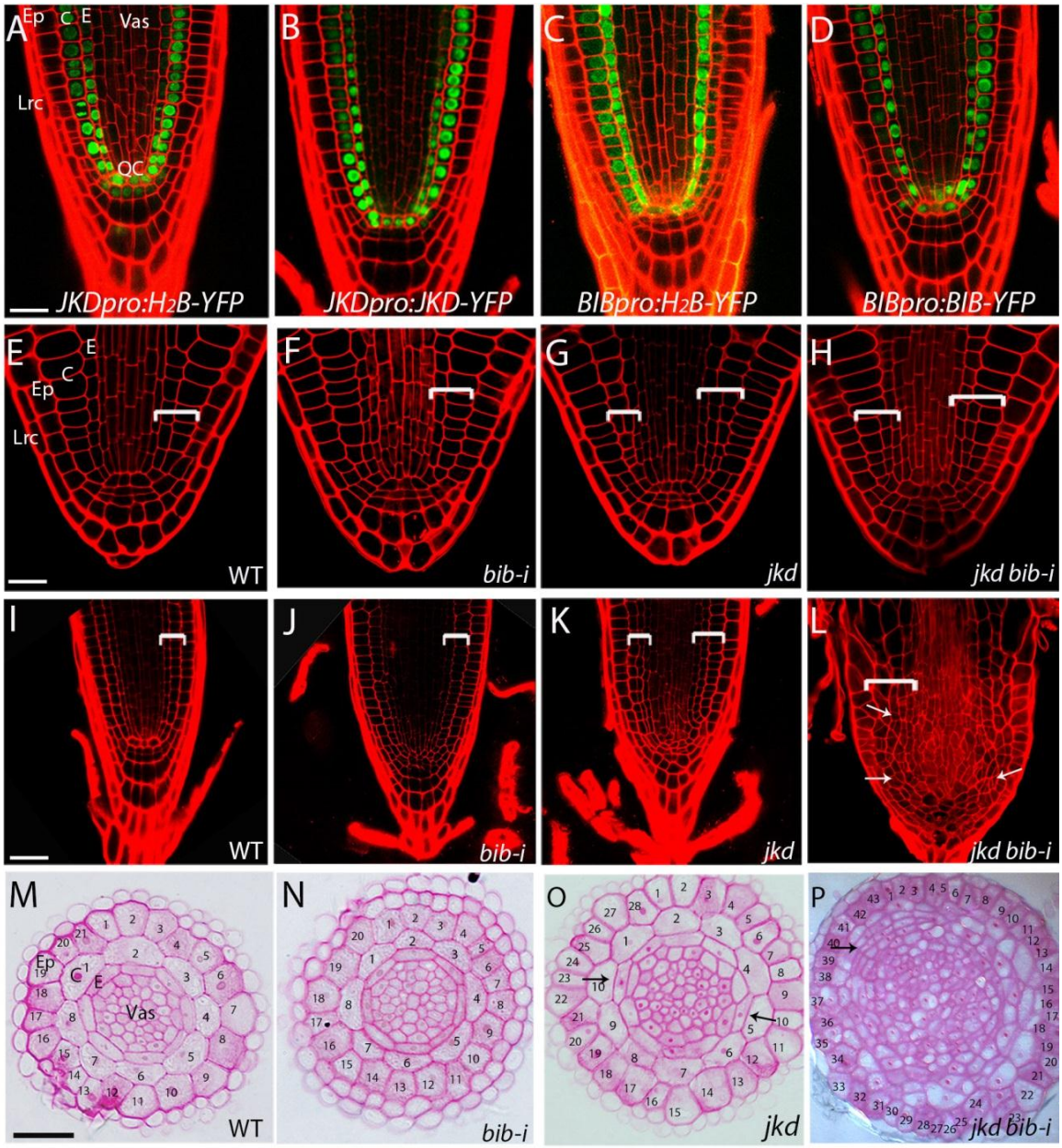

Figure 1. JKD and BIB act redundantly to restrict cell divisions in the ground tissue.

A-D Median longitudinal confocal sections of 4-day-old root expressing *JKDpro:H2B-YFP* (A), *JKDpro:JKD-YFP* (B), *BIBpro:H2B-YFP* (C) and *BIBpro:BIB-YFP* (D). Scale bar represents 20 µm. E-H Median longitudinal confocal sections of mature embryos of WT (E), *bib-i* (F), *jkd* (G) and *jkd bib-i* (H), brackets indicate GT. Scale bar represents 20 µm. I-L Median longitudinal confocal sections of 7-day-old roots of WT (I), *bib-i* (J), *jkd* (K) and *jkd bib-i* (L), brackets indicate GT; arrows point to examples of ectopic and disoriented divisions in *jkd bib-i.* Scale bar represents 50 µm. M-P Transverse sections of 5-day-old root meristem of WT (M), *bib-i* (N), *jkd* (O) and *jkd bib-i* (P). Note the increased cell number, disorganization of the circumferential pattern and the expansion of the vasculature in *jkd bib-i*. Arrows point to examples of ectopic divisions derived from the cortex. Scale bars represent 50 µm. Ep: Epidermis; C: Cortex; E: Endodermis; Vas: Vasculature; QC: Quiescent Center; Lrc: Lateral root cap.

Genotype		Epidermis	Cortex	Endodermis
Wild type	*n* = 13	22.9 ± 1.9	8 ± 0	8 ± 0
bib-i	*n* = 11	22.5 ± 1.2	8 ± 0	8 ± 0
jkd	*n* = 12	27.5 ± 1.6	9.2 ± 1.0	9.3 ± 1.1
		Layer 1	Layer 2	Layer 3
jkd bib-i	*n* = 12	40.0 ± 2.9	26.3 ± 1.8	21.3 ± 1.6

Table 1. Cell numbers at the circumference in root sections of WT, *jkd* and *jkd bib-i* homozygotes.

In *jkd bib-i*, cells were counted in the outermost layer at the corresponding position of the epidermis (Layer 1) and two layers inward (Layer 2 and 3). (n) represents the number of roots counted, numbers are average and SD.

The increased number of layers in *jkd bib-i* roots reminded us of reported effects of ectopic SHR expression which include extra layers displaying endodermal identity (Helariutta et al., 2000; Sena et al., 2004). Using the Casparian strip as a morphological marker for endodermal identity, we found that *jkd bib-i* roots possessed only one cell layer bearing endodermal features, located directly in contact with the epidermis, as recognized by emerging root hairs (Figure 2C, D). Occasionally Casparian strip features were present in the epidermis of the double mutant (Figure 2C). These data indicated that the extra divisions occurring in *jkd bib-i* did not produce supernumerary endodermal layers and thus was different from SHR overexpression phenotype.

We next monitored SCR expression in *jkd bib-i* using a *SCRpro:SCR-mRFP* protein fusion. In WT, SCR is strongly expressed in the QC and endodermis (Supplemental Figure 2A). In the *bib-i* mutant, SCR expression was similar to WT but weaker in the QC (Supplemental Figure 2B). In *jkd*, as previously reported, SCR could be detected in the endodermis and at most in one additional GT layer, and was absent from the QC (Supplemental Figure 2C; Welch et al., 2007). In *jkd bib-i* root meristems, also only a subset of layers expressed SCR. Shootwards in the meristem, strong SCR-mRFP localization was observed in two layers (Supplemental Figure 2D). However in the rootward meristematic region, where extensive divisions created additional layers, SCR expression decreased dramatically in its native stele-adjacent domain and was detected in cells located at, or internal to, the epidermal layer (Supplemental Figure 2D).

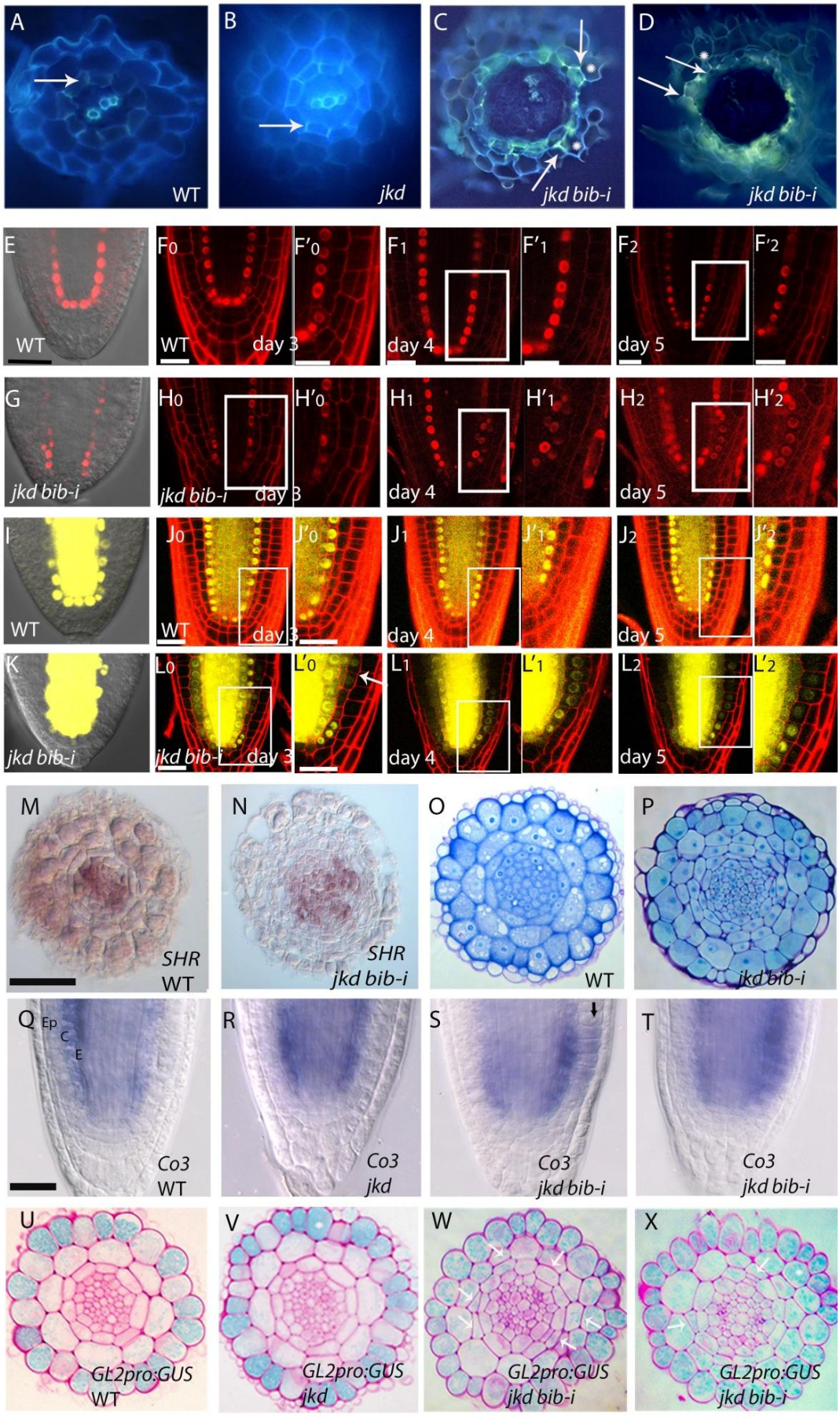
A
WT
B
jkd
C
jkd bib-i
D
jkd bib-i
E
WT
F0
WT
day 3
F'0
F1
day 4
F'1
F2
day 5
F'2
G
jkd bib-i
H0
jkd bib-i
day 3
H'0
H1
day 4
H'1
H2
day 5
H'2
I
WT
J0
WT
day 3
J'0
J1
day 4
J'1
J2
day 5
J'2
K
jkd bib-i
L0
jkd bib-i
day 3
L'0
L1
day 4
L'1
L2
day 5
L'2
M
SHR
WT
N
SHR
jkd bib-i
O
WT
P
jkd bib-i
Q
Ep
C
E
Co3
WT
R
Co3
jkd
S
Co3
jkd bib-i
T
Co3
jkd bib-i
U
GL2pro:GUS
WT
V
GL2pro:GUS
jkd
W
GL2pro:GUS
jkd bib-i
X
GL2pro:GUS
jkd bib-i

Figure 2. JKD and BIB determine tissue boundaries in the Arabidopsis root meristem.

A-D Free hand cross sections of 7-day-old roots stained with berberine hemisulfate and aniline blue, showing Casparian strips in WT (A), *jkd* (B) and *jkd bib-i* (C and D), arrows mark Casparian strips, asterisks mark epidermis bearing root hair (C and D). E-F'$_2$ *SCR:proSCR-mRFP* localization in WT embryo (E) and root at 3, 4 and 5 days after germination (F_0-F_2; F'$_0$, F'$_1$ and F'$_2$ are insets from F_0, F_1 and F_2). G-H'$_2$ *SCRpro:SCR-mRFP* localization in *jkd bib-i* embryo (G) and root at 3, 4 and 5 days after germination (H_0-H_2; H'$_0$, H'$_1$ and H'$_2$ are insets from H_0, H_1 and H_2). For both WT and *jkd bib-i* the same root was observed for three consecutive days. Scale bars are 20 µm. I-J'$_2$ *SHR:proSHR-YFP* localization in WT embryo (I) and root at 3, 4 and 5 days after germination (J_0-J_2; J'$_0$, J'$_1$ and J'$_2$ are insets from J_0, J_1 and J_2). K-L'$_2$ *SHR:proSHR-YFP* localization in *jkd bib-i* embryo (K) and root at 3, 4 and 5 days after germination (L_0-L_2; L'$_0$, L'$_1$ and L'$_2$ are insets from L_0, L_1 and L_2). For both WT and *jkd bib-i* the same root was observed for three consecutive days. Scale bars are 20 µm. M, N Expansion of the vascular tissue in *jkd bib-i*. *In situ* hybridization shows *SHR* mRNA localization in transverse sections of 5 days old root meristem in WT (M) and *jkd bib-i* (N), note the expanded *SHR* domain in *jkd bib-i* compared to WT. Scale bar represents 100 µm. Arrows point to residual lateral root cap. O, P Cross sections 5 days old roots stained with toluidine blue showing more cells in the vasculature in *jkd bib-i* (P) compared to WT (O). Scale bar represents 50 µm Q-T mRNA localization by whole mount *in situ* hybridization of cortex marker *Co3* in 3 days old seedlings in WT (Q), *jkd* (R), *jkd bib-i* (S, T). Arrow points to epidermal expansion of *Co3* expression. U-X Expression pattern of *GL2pro:GUS* in transverse root sections of 4-day-old WT (U), *jkd* (V) and *jkd bib-i* (W, X). Unstained cells develop hairs while blue stained cells remain hairless. Arrows point to ectopic divisions. Asterisk indicates cortical cell expressing *GL2* gene.

In *jkd bib-i,* only one layer occupying either the epidermal position or adjacent to it displayed endodermal features, while the inner layers did not. We monitored SCR expression dynamics in *jkd bib-i* to assess whether a shift in the SCR domain correlated with the occurrence of the divisions. In mature embryos of both WT and *jkd bib-i*, SCR expression was restricted to the stele-adjacent layer at the root pole although *jkd bib-i* roots occasionally revealed expression one layer further out (Figure 2E, G). In a time lapse experiment, SCR showed predominant expression in the endodermis in the WT roots from 3 to 5 days after germination (dag, Figure 2F_0-F'$_2$). Similarly, we observed strong SCR expression the endodermis in *jkd bib-i* roots and weak expression in the adjacent outer layer at 3 dag (Figure 2H_0, H'$_0$). However on day 4, the additional divisions became more apparent in *jkd bib-i* and are correlated with an increase of SCR levels in the new cells (Figure 2H_1, H'$_1$). On day 5, SCR levels were more elevated in the epidermal layer, while a decrease of expression was observed in the original SCR-expressing domain (Figure 2H_2, H'$_2$), consistent with SCR expression in 7-day-old

jkd bib-i roots (Supplemental Figure 2D). These data indicate that the SCR expression pattern observed in later stages in *jkd bib-i* roots results from cell fate respecifications, where outer cell layers acquire endodermal fate while inner layers gradually lose it, thereby maintaining a one-layered, outward shifting “endodermis”.

In *jkd* mutants, a low level of SHR moves one extra layer outward from the endodermis, correlated with ectopic divisions in the cortex (Supplemental Figure 2G; Welch et al., 2007). We investigated whether SHR movement was enhanced further in *jkd bib-i*. In *bib-i* single mutants, SHR localization did not differ from WT; the protein was nuclear and cytoplasmic in vascular tissue while it was retained in the nuclei in the endodermis (Supplemental Figure 2E, F). In *jkd bib-i*, however, SHR protein not only accumulated in the expanded inner vascular tissue where it retained its cytoplasmic and nuclear localization, but was also detected in all surrounding cell layers, including epidermis (Supplemental Figure 2G).

To assess whether the ectopic divisions occurring in *jkd bib-i* correlated with enhanced SHR mobility and reduction of nuclear localization, we monitored SHR dynamics in a time lapse experiment similar to the previous description for SCR. In *jkd bib-i* mature embryos, we did not observe SHR in the outer layers (Figure 2I, K). We then tracked SHR expression in the same root and found that WT root exhibited nuclear SHR localization in the endodermis from 3 to 5 dag (Figure 2J_0-J’$_2$). In *jkd bib-i* at 3 dag, nuclear and cytoplasmic SHR could be detected in cells located at the cortex position spanning the entire meristem (Figure 2L_0, L’$_0$); in the same lineage we also detected early divisions, with nuclear and cytoplasmic SHR in the vasculature-facing inner cells, while in the epidermis-facing outer cells SHR expression was predominantly nuclear (Figure 2L’$_0$, arrow). At 4 and 5 dag SHR could be detected in cells at the epidermal position and occasionally in lateral root cap cells (Figure 2L_1-L’$_2$).

These findings clearly show that in *jkd bib-i*, inefficient SHR nuclear retention promotes its spread outside its transcription domains. Consistent with this, we did not observe *SHR* mRNA in the outer layers (Figure 2M, N), confirming that this spreading of SHR protein

was a result of enhanced SHR mobility.

Previous data indicated that the extra cortical division in the *jkd* mutant leads to a fate shift of the original endodermis to pericycle, evidenced by this layer producing lateral roots (Welch et al., 2007). We thus questioned whether the over-proliferating inner cells in *jkd bib-i* resulted in an increase of the vasculature. Toluidine blue and basic fuchsin staining revealed that the central domain in *jkd bib-i* contained more vascular cell files (Figure 2P, Supplemental Figure 3) when compared to WT and *jkd* (Figure 1O, 2O, Supplemental Figure 3).

In mature embryos, additional divisions in *jkd* and *jkd bib-i* originated from the cortex, so we asked whether the newly formed layers in roots carried cortex identity. In WT, the *Co3* promoter is highly expressed in the cortex, weakly in the endodermis and excluded from the QC (ten Hove et al., 2010). Consistent with this reported promoter activity, *in situ* hybridization detected *Co3* transcripts in the cortex of WT (Figure 2Q, Supplemental Figure 4A). In *jkd*, expansion of *Co3* expression coincided with the additional ground tissue layer (Figure 2R, Supplemental Figure 4B). In *jkd bib-i*, *Co3* expression expanded radially and could also be detected in the epidermis already at early stages (Figure 2S, T) and in the QC at later stages when extensive division has taken place (Supplemental Figure 4C-D).

Subsequently, we assessed whether the epidermis layer was also affected by the extensive divisions. In Arabidopsis, the epidermal layer comprises two cell types: cells directly in contact with a single cortex cell (N position) will adopt a non-hair fate, while cells located at the cleft between two cortical cells (H position) will generate root hairs. We checked the expression of the epidermal expressed homeobox gene *GLABRA 2* (*GL2*), specifically marking non-hair cells (Lee and Schiefelbein, 1999), by monitoring its promoter activity fused to the GUS reporter (*GL2pro:GUS*). In WT, *GL2* was expressed in epidermal cells located at the N position (Lee and Schiefelbein, 1999; Figure 2U), whereas in *jkd* ectopic *GL2* expression could also be observed in cells located at the H position (Figure 2V) in agreement with a previous report that JKD affects epidermal fate

specification (Hassan et al., 2010). In *jkd bib-i, GL2* expression was observed in all epidermal cells, suggesting that BIB might also contribute to the JKD function in epidermal fate specification (Figure 2W). Interestingly, *GL2* expression also extended inwards to the sub-epidermal layer (Figure 2X).

Collectively, our data indicate that tissue boundaries between layers in *jkd bib-i* mutant roots are destabilized, creating reprogrammed fates that correlate with SHR outspread.

BIB and JKD cooperate with SCR to retain SHR in the nucleus.

We explored the molecular basis by which BIB and JKD could restrict SHR movement. JKD can directly interact with both SCR and SHR (Welch et al., 2007; Supplemental Figure 5). We assessed whether BIB, similar to JKD, could interact with both SCR and SHR in yeast two-hybrid and bimolecular fluorescence complementation (BiFC) assays and found this to be the case (Supplemental Figure 5). In addition, BIB could directly bind to JKD in BiFC assays (Supplemental Figure 5B). These data are in agreement with previously reported findings that BIRD proteins are capable of binding among themselves and with SCR and SHR (Welch et al., 2007; Supplemental Figure 5).

Based on the observed SHR spread in *jkd bib-i*, and the potential for the BIRD proteins to bind SHR and SCR, we reasoned that BIRD proteins may restrict SHR movement by a nuclear retention mechanism, where these nuclear proteins bind SHR and prevent its nuclear exit. In support of this idea we observed SHR-YFP in both the nuclei and cytoplasm in Arabidopsis protoplasts and *Nicotiana benthamiana* epidermal cells (Supplemental Figure 5B, Supplemental Figure 6A, A'), but in the presence of SCR, BIB or JKD, SHR localization became largely nuclear (Supplemental Figure 6B-E") indicating a role of BIRD proteins in SHR nuclear retention. In agreement, in BiFC assays of SHR with BIRD proteins and SCR, the reconstituted YFP fluorescence signal was predominantly nuclear, indicating that SCR-SHR or BIRD-SHR protein complexes were largely nuclear (Supplemental Figure 5B).

To validate the observed effects on SHR nuclear retention in plants, we misexpressed JKD, BIB and SCR using the promoter of the *WOODENLEG* (*WOLpro*) gene, which is normally expressed in the procambial region of the vascular tissue (Bonke et al., 2003a; Vatén et al., 2011b), where SHR is both nuclear and cytoplasmic (Figure 3A, A'). Expression of SCR in the vasculature directed nuclear SHR retention, consistent with a previous report (Koizumi et al., 2012; Figure 3B, B'). When BIB and JKD were ectopically expressed together or individually in the vasculature, they were also able to efficiently retain SHR in the nuclei (Figure 3C-E''' compare to A, A'). To quantify the effect of BIRD proteins in retaining nuclear SHR, we measured nuclear and cytoplasmic SHR-YFP fluorescence intensity in the vasculature with ectopic SCR or BIRD proteins expression, and found that in the roots, the presence of BIRD proteins enhanced SHR nuclear portion to similar levels as SCR (Supplemental Figure 6F).

As JKD is required to activate SCR expression (Ogasawara et al., 2011), we tested whether SHR nuclear localization mediated by JKD and BIB operated in part through induction of SCR. We first analyzed SCR expression in lines misexpressing JKD and BIB in the vascular domain, and found that SCR was ectopically induced in the vascular tissue (Figure 3F-I'). This was in line with promoter assays using a dual-luciferase system where both JKD and BIB were able to significantly induce *SCR* promoter activity in Arabidopsis protoplasts (Supplemental Figure 7). In contrast, SCR and SHR were not sufficient to activate the *SCR* promoter effectively (Supplemental Figure 7). Additionally, we misexpressed JKD and BIB in the vasculature of *scr* mutants and found that JKD and BIB were not sufficient to fully retain SHR in the nuclei in the absence of functional SCR (Figure 4). Quantifications of nuclear SHR in *scr* background confirmed that ectopic JKD and BIB on their own are able to promote SHR nuclear retention to a certain extent, and that their action is more efficient in presence of functional SCR (Supplemental Figure 6F).

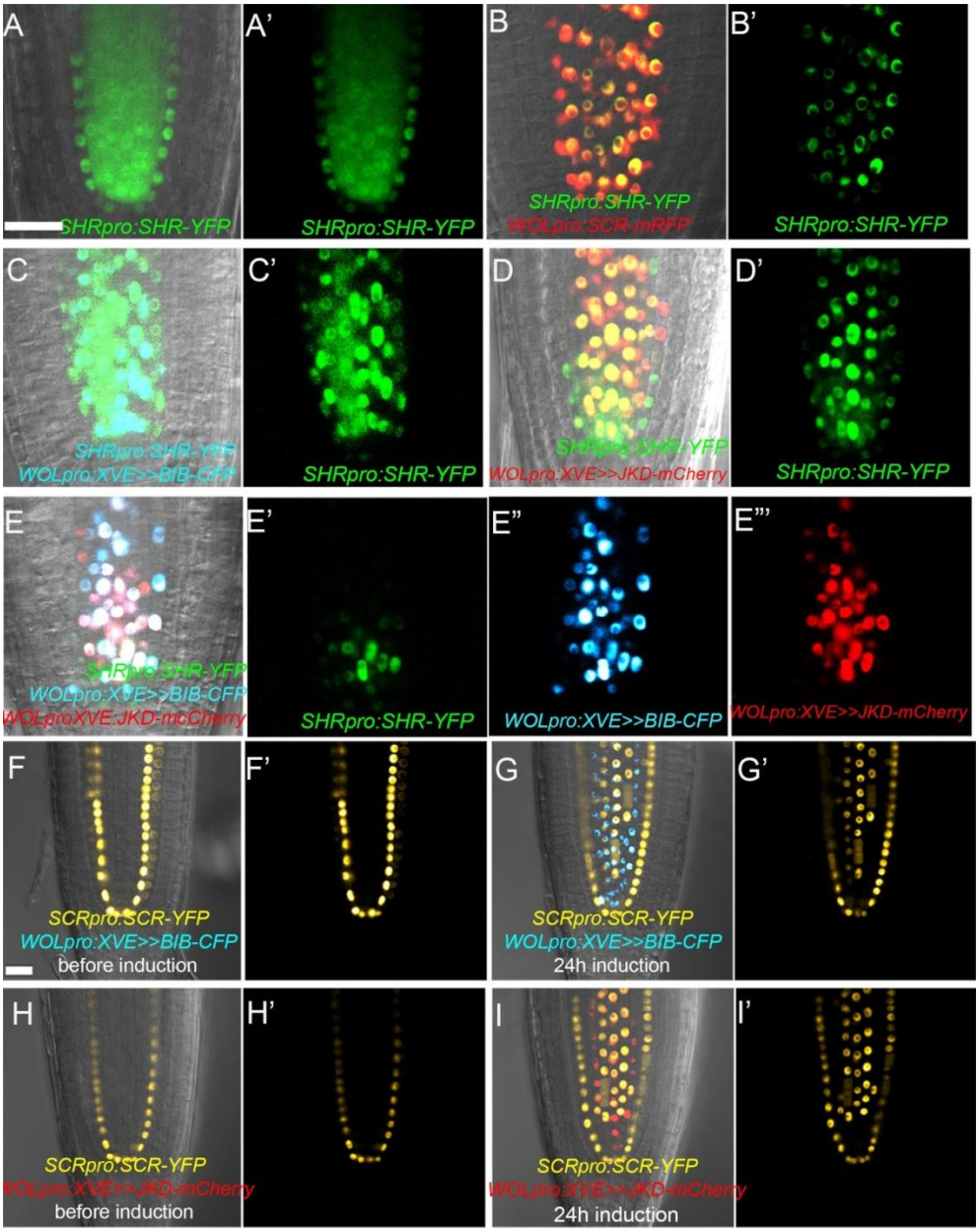

Figure 3. JKD, BIB and SCR promote SHR nuclear retention *in planta*.

A-E"' BIRD proteins and SCR are able to retain SHR in the nuclei when expressed in vasculature under *WOODENLEG* promoter (*WOLpro*). 3-day-old roots expressing *SHRpro:SHR-YFP* alone (A, A') or in combination with *WOLpro:SCR-mRFP* (B, B'), *WOLpro:XVE>>BIB-CFP* (C, C'), *WOLpro:XVE>>JKD-mCherry* (D, D'), and both *WOLpro:XVE>>JKD-mCherry* and *WOLpro:XVE>>BIB-CFP* (E-E"'). Scale bar represents 20 µm. F-I' Confocal images of 3-4-day-old roots containing *SCRpro:SCR-YFP* and *WOLpro:XVE>>BIB-CFP* or *WOLpro:XVE>>JKD-mCherry* before induction (F, F', H, H') and 24h after estradiol induction (G, G', I, I'). Note ectopic SCR expression in the vasculature. Scale bar represents 20 µm.

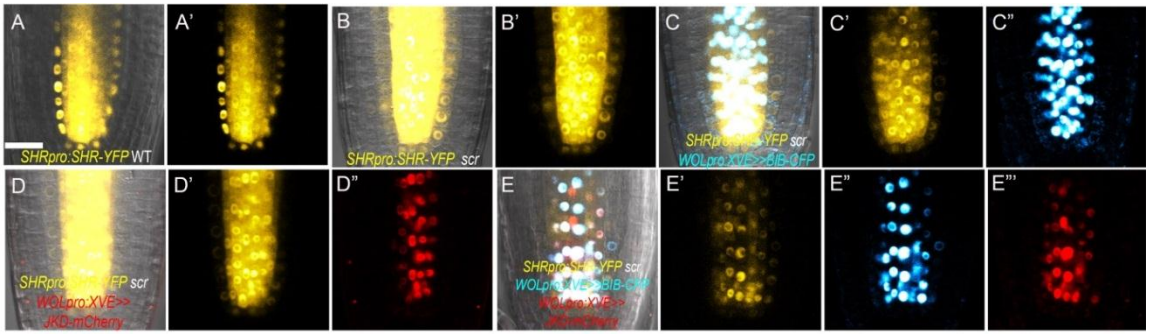

Figure 4. JKD and BIB require SCR to promote full SHR nuclear retention *in planta*.

A-A' Confocal images of roots expressing *SHRpro:SHR-YFP* in WT. B-E"' Confocal images of 3-day-old *scr-3* roots expressing *SHRpro: SHR-YFP* (B, B') and co-expressing *WOLpro:XVE>>-BIB-CFP* (C-C"); *WOLpro:XVE>>JKD-mCherry* (D-D") and both *WOLpro:XVE>>BIB-CFP* and*WOLpro:XVE>>JKD-mCherry* (E-E"'). Note that in vasculature JKD and BIB are not able to fully retain SHR to the nuclei in the absence of SCR. Scale bar represents 20 µm.

Besides being SHR targets, JKD and SCR also regulate each other's expression (this study; Welch et al., 2007). To reveal a direct nuclear retention effect of SCR and BIRD proteins on SHR without the background effects of endogenous proteins involved in the pathway, we used Hela cells as a heterologous system to prevent any plant-specific downstream regulation induced by SHR, SCR or the tested BIRD proteins. When SHR-YFP alone was expressed in this system, it localized to both nuclei and cytoplasm (Figure 5A-A", F) similar to its localization in the plant vasculature. When co-expressed with BIB and/or JKD, SHR-YFP nuclear localization was enhanced (Figure 5B-D", F), but not to the same level as in plants (Supplemental Figure 6F). Interestingly, when SCR was added, SHR-YFP localization became fully nuclear (Figure 5-E", F). We conclude that BIB, JKD and SCR all individually promote SHR nuclear targeting, with SCR showing the strongest effect.

Together, our data suggest that JKD and BIB restrict SHR movement through SHR nuclear retention mediated by formation of nuclear complexes. In addition, JKD and BIB can promote SHR nuclear retention through activating *SCR* transcription.

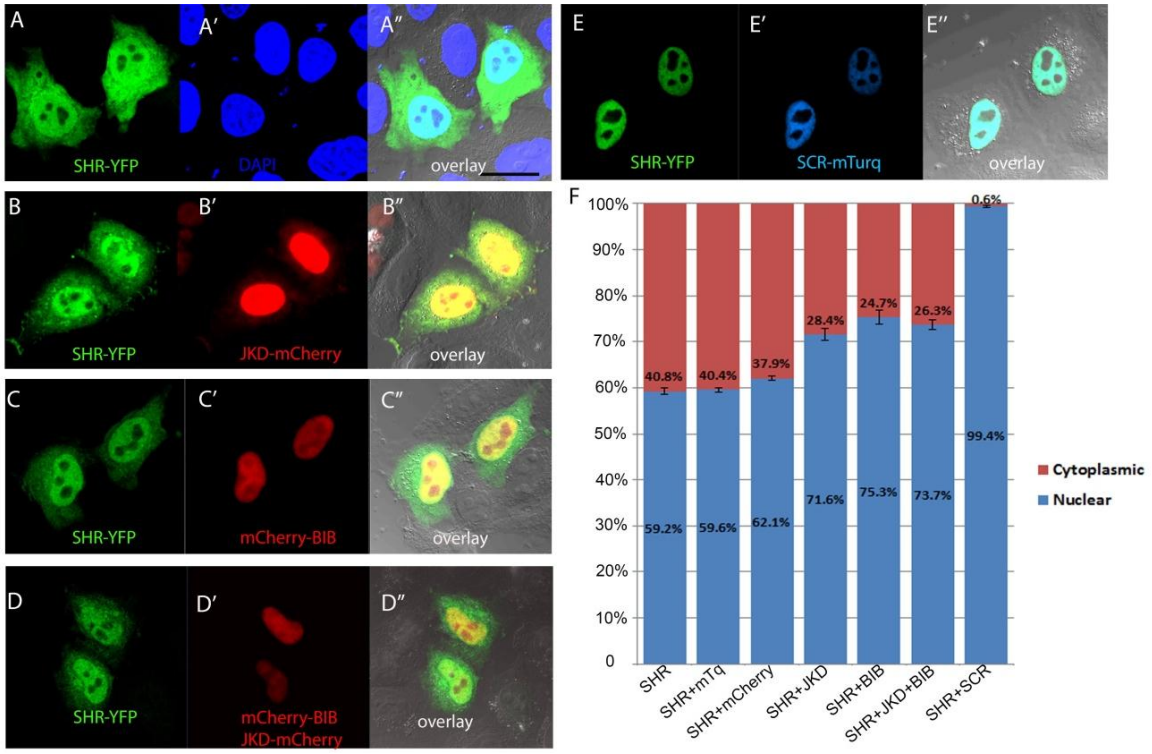

Figure 5. JKD, BIB and SCR promote SHR nuclear retention in Hela cells.

A-E" BIRD proteins and SCR are able to retain SHR in the nuclei of Hela cells. After transfection, cells were stained with DAPI for nuclear visualization and protein colocalization. Images showing cells transfected with SHR-YFP only (A-A"), in combination with JKD-mCherry (B-B"), mCherry-BIB (C-C"), JKDm-Cherry + mCherry-BIB (D-D") and SCR-mTurquoise (SCR-mTurq) (E-E"). Scale bar represents 20 µm. F Level of SHR nuclear retention in presence of BIRD proteins and SCR is indicated in percentages. Free mTurquoise (mTq) and mCherry were used as controls. Error bars represent standard error of mean, n>15.

MGP and NUC promote formative divisions and endodermal cell fate in the ground tissue.

MGP and *NUC* were previously described as direct SCR and SHR transcriptional targets (Levesque et al., 2006; Cui et al., 2007). Both proteins are expressed in the cortex, endodermis, and a subset of the vasculature, and are predominantly excluded from the QC (Figure 6A, B). Since the additional GT divisions in *jkd* mutants were suppressed in *jkd mgp-i* (Welch et al., 2007), we wondered whether this suppression was enhanced in *jkd mgp-i nuc-i.* To assess NUC function in the root meristem, we generated RNAi to specifically reduce *NUC* levels (*nuc-i*, Supplemental Figure 1). We did not observe significant differences in meristem size in roots of double *mgp-i nuc-i* RNAi lines and triple

jkd mgp-i nuc-i when compared to WT (Supplemental Figure 8A). Interestingly, *jkd mgp-i nuc-i* triple mutant roots contained patches of undivided GT, indicating that cortex and endodermis layers were not fully separated (Figure 6F, J). These cells maintained endodermal characteristics as revealed by the presence of Casparian strips (Figure 6N). This phenotype is reminiscent of *scr* mutants where an undivided layer maintains endodermal and cortical fate (Figure 6G, K, O; Di Laurenzio et al., 1996; Heidstra et al., 2004).

In contrast, the undivided GT layer in *shr* mutants lacks endodermal characteristics (Helariutta et al., 2000). To assess whether endodermal fate specification relies on the SHR targets MGP, NUC, SCR and JKD, we generated a quadruple mutant line *jkd mgp-i nuc-i scr*. Similar to *shr*, these plants displayed shorter root meristems and no Casparian strip (Supplemental Figure 8A; Figure 6H, L, P), suggesting a loss of endodermis. We then checked whether the remaining GT layer still retained cortex characteristics by *in situ* hybridization using the cortex specific gene *Co3* (ten Hove et al., 2010) and revealed that the mutant GT layer of *jkd mgp-i nuc-i scr* still expressed a cortex marker (Supplemental Figure 8B, C), suggesting that SHR specification of endodermis requires these four targets.

Given the dual function of BIRD genes as transcriptional activators and SHR movement regulators, the lack of endodermal specification could be a result of SHR-targets removal or inefficient SHR movement. To test these hypotheses, we monitored SHR protein in *jkd mgp-i nuc-i scr* mutant (Figure 6Q-T), and found that SHR movement was not hindered but rather enhanced, reaching the epidermis (Figure 6T). This effect was similar to that observed in *jkd bib-i*. Interestingly, *jkd bib-i* failed to induce divisions when combined with *scr* or *shr* mutants (Figure 7A-D), indicating that ectopic divisions in *jkd bib-i* depend on SCR and SHR activity. To test whether such dependency requires MGP and NUC, we generated *jkd bib-i mgp-i nuc-i*. The quadruple mutant failed to generate supernumerary layers, and patches of undivided cells were observed in the GT (Figure 7E, F).

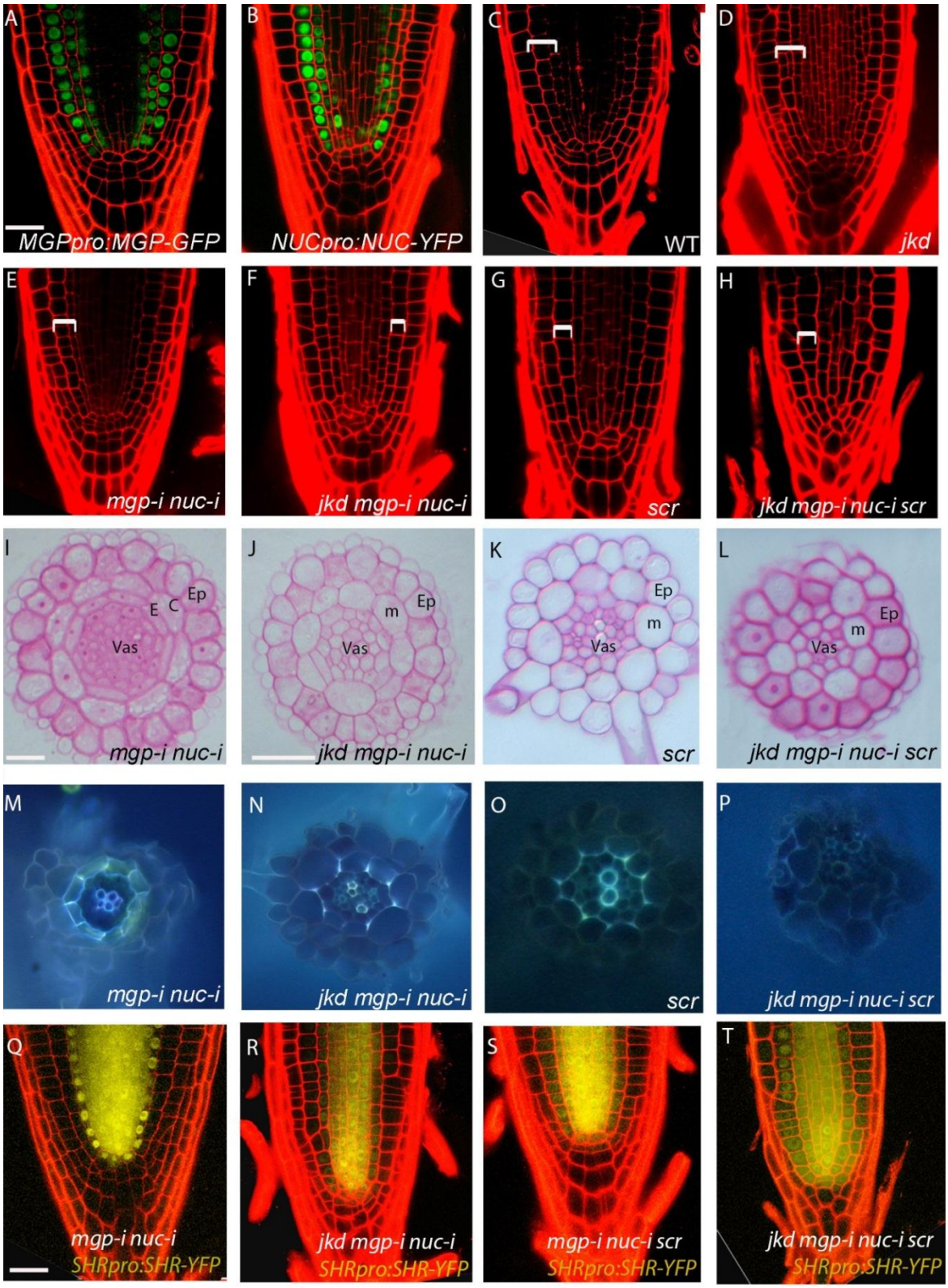
A
MGPpro:MGP-GFP
B
NUCpro:NUC-YFP
C
WT
D
jkd
E
mgp-i nuc-i
F
jkd mgp-i nuc-i
G
scr
H
jkd mgp-i nuc-i scr
I
Ep
E
C
Vas
mgp-i nuc-i
J
m
Ep
Vas
jkd mgp-i nuc-i
K
Ep
m
Vas
scr
L
Ep
m
Vas
jkd mgp-i nuc-i scr
M
mgp-i nuc-i
N
jkd mgp-i nuc-i
O
scr
P
jkd mgp-i nuc-i scr
Q
mgp-i nuc-i
SHRpro:SHR-YFP
R
jkd mgp-i nuc-i
SHRpro:SHR-YFP
S
mgp-i nuc-i scr
SHRpro:SHR-YFP
T
jkd mgp-i nuc-i scr
SHRpro:SHR-YFP

Figure 6. MGP, NUC and JKD cooperate with SCR to specify endodermal fate.

A-B Median longitudinal confocal images of 4-day-old roots expressing *MGPpro:MGP-GFP* (A) and *NUCpro:NUC-YFP* (B) showing expression in cortex, endodermis and pericycle. C-H Median longitudinal confocal sections of 4-day-old roots, where *mgp-i nuc-i* (E) exhibiting normal GT similar to WT (C), *jkd* roots showing divisions in the cortex layer (D), while *jkd mgp-i nuc-i*; *scr* and *jkd mgp-i nuc-i scr* displaying one monolayer of ground tissue (F-H). Brackets indicate GT. Scale bar represents 20 µm. I-L Transverse sections of 4-day-old roots showing WT ground tissue layers in *mgp-i nuc-i* (I) and a reduction of ground tissue layers in *jkd mgp-i nuc-i* (J) and *jkd mgp-i nuc-i scr* (L) similar to *scr* (K). Scale bar represents 50 µm. Ep: Epidermis; C: Cortex; E: Endodermis; Vas: Vasculature; m: mutant GT layer. M-P Free hands sections of 4-day-old roots stained with berberine hemisulfate and aniline blue to visualize Casparian strips in *mgp-i nuc-i* (M), *jkd mgp-i nuc-i* (N), *scr* (O), *jkd mgp-i nuc-i scr* (P). Note absence of Casparian strips in *jkd mgp-i nuc-i scr*. Q-T Confocal images of 4-day-old roots expressing *SHRpro:SHR-YFP* in *mgp-i nuc-i* (Q), *jkd mgp-i nuc-i* (R), *mgp-i nuc-i scr* (S) and *jkd mgp-i nuc-i scr* (T). Note SHR spreads to epidermis in *jkd mgp-i nuc-i scr*. Scale bar represents 20 µm.

Taken together, our data suggest that BIRD proteins are collectively required for formative divisions in the GT. Endodermal fate is generated by combined transcriptional activity of SHR targets in the GT, and these transcriptional regulations can be uncoupled from the regulation of SHR movement in *jkd bib-i* background.

JKD and BIB confine *CYCD6* expression to CEI/CEID.

It has been shown that the SCR-SHR protein complex activates *CYCD6* transcription and that ectopic *CYCD6* expression is sufficient to induce formative divisions in the GT (Sozzani et al., 2010a; Cruz-Ramírez et al., 2012b). We thus asked whether divisions in *jkd* and *jkd bib-i* were associated with ectopic *CYCD6* expression.

In WT roots, *CYCD6* expression is predominantly constrained to the CEI/CEID (Figure 7H; Sozzani et al., 2010). In both *jkd* and *jkd bib-i* roots, *CYCD6* expression expanded along the cortex and endodermis and occasionally could be found in the vasculature, correlating with the occurrence of extra divisions (Figure 7I-K).

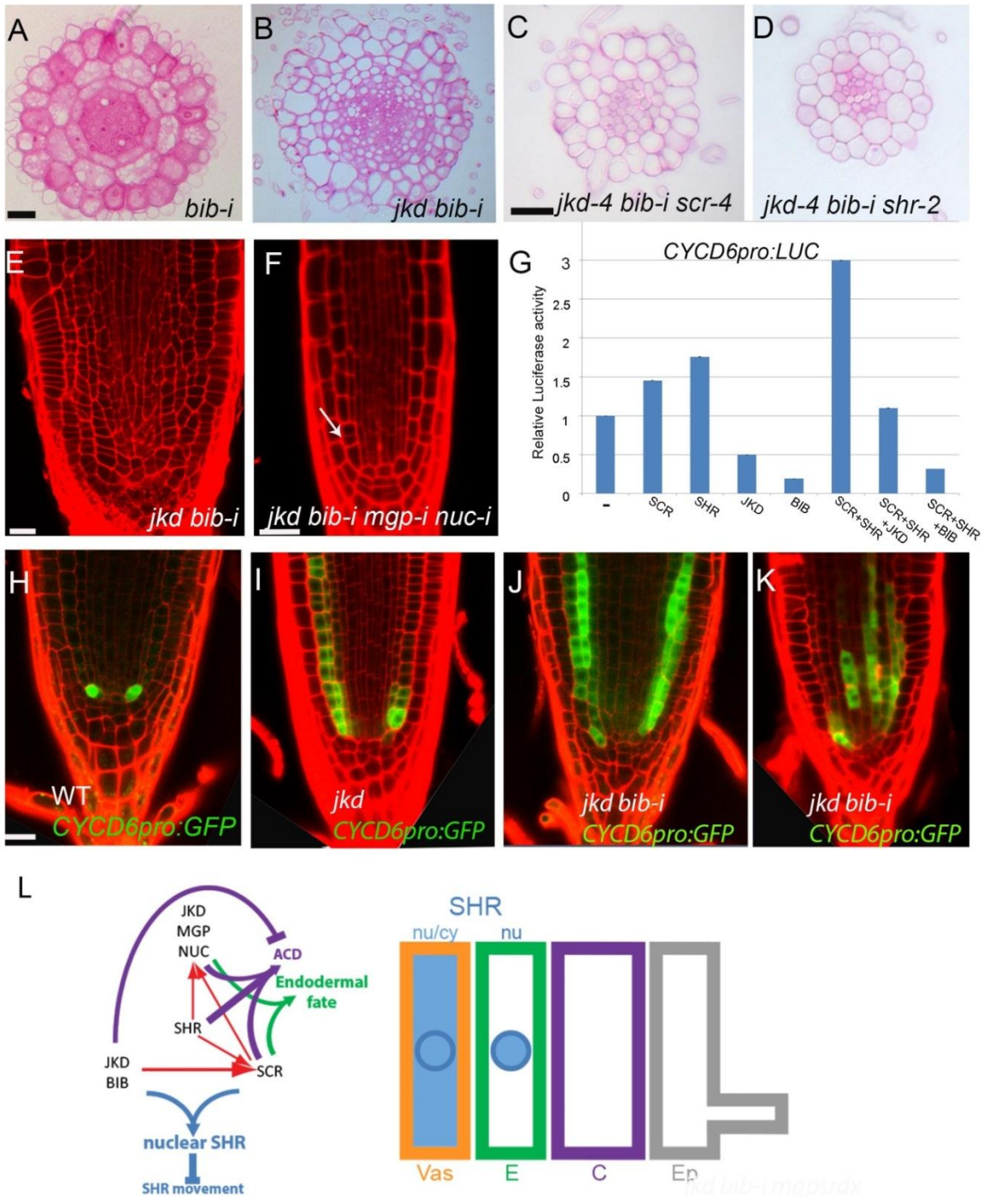

Figure 7. BIRD proteins regulate formative divisions through modulation of transcription.

A-D Root transverse sections of 4-day-old roots showing normal ground tissue layers in *bib-i* (A), multiple layers in *jkd bib-i* (B) and reduction of layers in both *jkd bib-i scr* (C) *and jkd bib-i shr* (D). Scale bars are 20 µm. E-F Confocal images of roots showing reduction of ground tissue divisions in *jkd bib-i mgp-i nuc-i* (F) compared to *jkd bib-i* (E), arrow points to GT separation. Scale bars represent 20 µm. G BIB and JKD reduce *CYCD6* promoter activity, as measured by Dual Luciferase assay using protoplasts transiently co-transformed with firefly luciferase under *CYCD6* promoter (*CYCD6pro*) and effectors plasmids carrying SCR, SHR, BIB or JKD driven by CaMV 35S promoter. Values represent average of

(Figure 7 continues) three replicates. The error bars represent SD. Each experiment was repeated at least three times with three technical replicates. H-K Confocal images *CYCD6pro:GFP* expression in 5-day-old roots of WT (H), *jkd* (I) and *jkd bib-i* (J and K). Induced expression of *CYCD6pro:GFP* correlates with ectopic divisions in *jkd* and *jkd bib-i*. Scale bar represents 20 µm. L. Model illustrating BIRD action on SHR movement range and root radial pattern specification. In WT, JKD, BIB and SCR promote SHR nuclear retention (thick blue arrow) and restrict SHR movement (thick inhibition sign) in part through *SCR* activation (red arrow), which in turn together with SHR promotes *JKD*, *NUC* and *MGP* expression. All together they contribute to asymmetric cell division (thick purple arrow) and endodermal fate specification (thick green arrow). JKD and BIB restrict ACD and promote normal boundary specification leading to one layer from each tissue.

To assess whether JKD and BIB can repress *CYCD6* transcription, we tested the effect of JKD and BIB on the *CYCD6* promoter in a transient protoplast dual-luciferase system. The SCR-SHR protein complex was able to activate the *CYCD6* promoter in this assay. However, JKD and BIB countered SCR-SHR action: addition of JKD to SCR-SHR reduced *CYCD6* promoter activity back to basal levels, while BIB was able to repress it beyond basal levels (Figure 7G). Taken together, the genetic and molecular data suggest that JKD and BIB constrain *CYCD6* expression to CEI/CEID by repressing its transcription in GT cells, showing an extra layer of regulation in a highly robust process.

DISCUSSION

Our work highlights the dual functions of BIRD proteins in setting up and maintaining boundaries between tissues in the root meristem, by being critical regulators of SHR movement, formative divisions and endodermal fate specification. To achieve their function, BIRD proteins integrate two processes, nuclear retention and transcriptional regulation, as means to promote correct patterning. Our data suggest a mechanism by which the range of SHR action is restricted to one cell layer by a combined activity of BIRD proteins and SCR. We also pinpoint SHR targets required for endodermal fate specification. In addition we show that BIRD proteins are required for *CYCD6* restriction to the CEI/CEID. Furthermore, our transcription assays indicate that SCR and SHR are not sufficient to activate key downstream target genes such as *SCR* but require tethering by BIRD proteins, which have been demonstrated to bind DNA (Kozaki et al., 2004).

Consistent with this notion, we also show that BIRD proteins on their own have the potential to act both as activators and repressors depending on the target promoters (Figure 7L, Supplemental Figure 9).

We present strong evidence that regulation of SHR movement mediated by BIRD proteins is important for setting up tissue boundaries, as the *jkd bib-i* mutant displays multiple cell layers in which such boundaries are no longer stable but shift (Supplemental Figure 9). A one-cell boundary shift was already observed in *jkd* mutants (Welch et al., 2007), but our current data highlight extreme boundary instability and underscore the potential of root cell files to continuously assess positional information and redirect cell fates. The boundary destabilization phenotype does not resemble the effect caused by ectopically expressing SHR under the *SCR* promoter, where all the multiple cell files exhibited endodermal fate. One major difference between the two phenotypes is that the first is a direct consequence of an enhanced SHR motility and spontaneous cell fate re-specification while the latter is a direct consequence of an hyperactive positive feedback loop of SHR on the *SCR* promoter (Nakajima et al., 2001; Sena et al., 2004).

Our present study shows that BIRD proteins employ nuclear retention as a mechanism to regulate SHR movement. As JKD and BIB form nuclear complexes with both SCR and SHR, it is plausible that BIRD proteins and SCR cooperate in the endodermis to prevent movement of SHR beyond one cell layer, in agreement with previously described data on the role of SCR (Gallagher et al., 2004; Cui et al., 2007; Koizumi et al., 2012).

In a heterologous system, JKD and BIB promoted SHR nuclear retention independently from SCR. However, in plants this activity also involves SCR. Since both JKD and BIB were able to enhance *SCR* promoter activity in a protoplast system and induce SCR protein expression in the vasculature when expressed under the *WOL* promoter, it is likely that the *in vivo* role of the BIRD proteins in constraining SHR activity requires both nuclear retention and transcriptional activation of *SCR* (Supplemental Figure 9) to reinforce SCR action in this process. Finally, we show that SHR targets (*SCR* and *BIRD* genes studied here) cooperate to regulate GT divisions and endodermal fate specification. Reduction of

MGP and NUC activities in *jkd* background not only suppressed the extra GT divisions in *jkd* but also prevented periclinal divisions generating the two GT layers, indicating that BIRD proteins act similarly to SCR in promoting periclinal divisions in the GT. The resulting GT monolayer, however, retained endodermal fate, which is only removed when *scr* is additionally mutated even in the presence of SHR. These data show that BIRD proteins and SCR are essential SHR targets for endodermal fate. Interestingly, in *jkd mgp-i nuc-i scr*, SHR spreads to the epidermis and is both cytoplasmic and nuclear in all cells. Therefore, nuclear retention capacity is bestowed on SHR by a combination of BIRD proteins and SCR.

ACDs in the GT were shown to rely on a bistable circuit involving SCR-SHR interaction with RETINOBLASTOMA-RELATED (RBR) protein, which is in turn regulated by CYCD6 (Cruz-Ramírez et al., 2012). Expression of *CYCD6*, a direct SCR-SHR target, is usually constrained to the CEI/CEID (Sozzani et al., 2010a; Cruz-Ramírez et al., 2012b). In both *jkd* and *jkd bib-i*, *CYCD6* expression expanded and correlated with ectopic divisions. This indicates that BIRD proteins can act not only as transcriptional activators, as shown by their action on *SCR* expression, but also as repressors. Alternatively, BIRD proteins might either activate a repressor to compete with the activation by SHR and SCR or bind to SCR-SHR complex to prevent it from activating *CYCD6*. Our data indicate that BIRD proteins can differentially regulate target genes. A recent study supports dual roles of BIRD proteins in differential transcriptional regulation of gibberellin-mediated downstream gene expression (Yoshida et al., 2014). A next step is to determine possible binding of BIRD proteins to these promoters, dissect which motifs in the sequences specify these activities, and test their relevance for GT patterning. Another question arising from our results is how BIRD proteins specifically restrict *CYCD6* expression to the CEI/CEID, as BIRD expression domains are not excluded from the CEI/CEID. Taking into account that some BIRD proteins are part of the SCR-SHR complex and are also transcriptionally regulated by RBR (Wildwater et al., 2005a; Cruz-Ramírez et al., 2012b), further research is needed to address how BIRD proteins are involved in the regulation of the bistable circuit described by Cruz-Ramírez et al. (2012). As BIRD proteins can interact with both

SCR and SHR and among each other, it will be interesting to map these interactions at cellular resolution to correlate the occurrence of specific complexes with cell type-specific activities.

Finally, our study indicates that SHR protein activity is regulated by dynamic interactions with BIRD proteins and SCR for the correct establishment of tissue boundaries. The continuous activity of this system may illustrate a major difference between plants and many animals. We show that, in plants, tissue boundaries can undergo major rearrangements under certain circumstances, indicating that plants maintain plasticity at adult stages whereas in many animal systems boundaries are locked after an initial patterning and cell movement phase.

METHODS

Plant growth and transformation

Growth conditions of *Arabidopsis thaliana* plants were described in Sabatini et al. (1999). Mutants and transgenic lines used in this study are as follows: *jkd-4* (Col-0) *and mgp-i* as described in Welch et al. (2007); *scr-3* as described in Fukaki et al. (1996); *scr-4* (WS) as in Fukaki et al. (1998); *shr-2* as in Nakajima et al. (2001).

For *bib-i* lines, an RNAi clone was obtained from pAGRIKOLA (www.agrikola.org) and transformed into Col-0. For *nuc-i* lines, a 300 bp fragment of *NUC* coding sequence was amplified and sub-cloned into pDONR221 in a gateway reaction. The resulting entry clone was then recombined into a pHellsgate vector. Plants were transformed by floral dip as described in Clough and Bent (1998) and primary transformants were selected on Basta for *bib-i* and Kanamycin for *nuc-i.* For every transgenic construct at least 20 transformants were analyzed and 10 lines were selected to check RNA levels. Lines with more than 50% reduced transcripts were chosen for phenotypic analysis and follow up experiments.

Double *jkd bib-i* was generated by crossing *bib-i* lines into *jkd-4* followed by genotyping for *jkd-4* as described in Welch et al., 2007. Information on the genotyping protocol for *bib-i* can be found in www.agrikola.org. *mgp-i nuc-i and jkd mgp-i nuc-i* were generated by transforming the pHellsgate vector containing the *NUC* RNAi construct into either *mgp-i* or *jkd mgp-i. jkd bib-i scr, jkd bib-i shr, jkd bib-i mgp-i nuc-i and jkd mgp-i nuc-i scr* were generated by crossing. Homozygous lines were selected by genotyping.

Constructs for cells and plant transformation

For mammalian constructs, *JKD*, *BIB*, *SCR* and *SHR* CDS were amplified using primers described in Supplemental Table 1 and subcloned by ligation into mammalian vector containing *mTurquoise*, *SYFP2* or *mCherry* under the constitutive CMV (cytomegalovirus) promoter (Kremers et al., 2006a; Goedhart et al., 2010a, 2007a). The resulting clones are listed in Supplemental Table 2. For constructs tested as effectors after protoplast transformation, CDS of *SCFP3A*, *SYFP2*, *mCherry*, and *mRFP* were recombined in a multiple gateway reaction using the CAMV *35S* promoter combined with *SCR*, *SHR*, *BIB* or *JKD* (Supplemental Table 3). Information on primers and transgenic constructs can be found in Supplemental Table 4 and 5. Clones were generated using the multigateway system (Invitrogen) and introduced to plants by floral dip (Clough and Bent, 1998).

RT-qPCR Analysis

Total RNA was extracted from 4-day-old roots (Spectrum™ Plant Total RNA Kit | Sigma-Aldrich). DNase treatment, cDNA synthesis were performed according to manufactured description (Fermentas). RT-qPCR was performed using SYBR Green Mastermix (Applied Biosystems, Warrington, UK). Results were normalized against *ACTIN* expression. qPCR primers are described in Supplemental Table 4.

Each experiment was repeated for three biological replicates.

Transient transfection assays

Hela cell culture and transfection were as described in Jiang et al. (2014), constructs were transfected using FuGENE 6 (Promega). Cells were fixed with formaldehyde and mounted in VectaShield mounting media with DAPI.

Four-week-old *Nicotiana benthamiana* plants were used for infiltration by agrobacterium containing different constructs as described in Liu et al. (2010). The infiltrated region of the leaf was then mounted in water and checked for expression.

Promoter Luciferase activity in protoplast

CYCD6 and *SCR* promoters were amplified using primers described in Supplemental Table 4, cloned into pDONR221 and transferred to pUGW35 (Nakagawa et al., 2007) containing a minimal 35S promoter and the Firefly Luciferase (LUC) reporter.

Protoplasts were prepared from Arabidopsis mesophyll cells as described in Yoo et al. (2007). A suspension of protoplasts (100µl, approximately 10^5 protoplasts per ml) was co-transfected with 5 µg of *CYCD6pro:LUC* or *SCRpro:LUC* and the effector plasmids (See Supplemental Table 3). 1µg of *35Spro:Renilla-LUC* was used as internal control for transfection efficiency. Protoplasts were incubated overnight. Cells were checked for the expression of the effectors by confocal laser microscopy prior to measurement. Luciferase activities were measured using the Dual-Luciferase Reporter assay system in a Glomax 96 microplate luminometer (Promega). LUC activity was normalized using Renilla luciferase and the relative ratio was determined by comparing this to the obtained with the promoter activity without effectors.

Time lapse analysis

SCRpro:SCR-mRFP and *SHRpro:SHR-YFP* roots were initially visualized 3 days after germination and followed daily up to 5 days after germination.

Fluorescence Microscopy

All confocal images were done using Zeiss LSM 710 confocal laser scanning microscope (Carl Zeiss GmbH) with a C-Apochromat 40x/1.20 W Korr water-immersion objective. Cyan fluorescence was detected at 465 – 500 nm with 458 nm excitation and 458/514 beam splitter; yellow detected at 520 – 560 nm with 514 nm excitation and 458/514 beam splitter; and red detected at 600 – 660 nm with 543 nm excitation and 488/543/633 beam splitterwas used. Images were processed using Zeiss ZEN software and Adobe Photoshop CS6.

For mature embryo, seeds were incubated overnight in water before dissection and staining with Periodic acid/ Schiff as described in Truernit et al. (2008). Samples were mounted in Hoyer solution and analyzed.

For roots, samples were mounted in 10µM Propidium iodide. Casparian strip staining was performed in hand sectioned roots as described in Scheres et al. (1995). Images were acquired using an Olympus Fluorescence microscope. Fuchsin staining was done as described in Mähönen et al., (2000).

For Hela cells, images were acquired as described above. For nuclear-cytoplasmic ratio quantification, 3 regions-of-interests (ROI) in the nucleus excluding nucleoli and 3 ROI in the cytoplasm of each cell were measured with background subtraction using ImageJ with Multi Measure plugin (http://www.optinav.com/Multi-Measure.htm).

Light microscopy

Roots sections were performed as described in Scheres et al. (1995). Sections were then stained either with Rutenium red or toluidine blue and photographed using Normaski microscope (Axio Imager; Carl Zeiss).

Histochemical staining of plant material containing the *GL2pro*:*GUS* reporter gene was performed as described in Hassan et al., 2010. For *in situ* hybridization in sections using *SHR* probe; sectioning, preparation of probes were done as described in Mahonen et al. (2000). For cortex-specific expression, whole mount *in situ* hybridizations were performed as described in Hejátko et al., (2006). Primers used to generate cortex probe are described in Supplemental Table 4.

Yeast 2-Hybrid assay

Yeast two-hybrid (Y2H) interactions were analysed using the ProQuest Two-Hybrid System (Invitrogen Life Technologies). The coding sequences (CDS) of *BIB* and *NUC* were amplified using Phusion High-Fidelity DNA Polymerase (Thermo Scientific) and Gateway compatible primers (See Supplemental Table 4). PCR products were cloned into pDONR221 with a Gateway BP II kit (Invitrogen) and sequences were verified. The resulting clones were used in a Gateway (Invitrogen) LR reactions, in combination with the destination yeast expression vectors pDEST22 (Gal4 AD) and pDEST32 (Gal4 BD), and were then checked by restriction analysis and sequencing. A non-autoactivating form of SHR was generated by eliminating acidic amino acids 58-64 as described in Koizumi et al. (2011). The resulting protein was fused to pDEST32 BD vector. Constructs for *JKD, MGP, SCR and SHR* CDS were described in Welch et al. (2007). *SCR* and *SHR* were used as bait and interactions were selected using drop out medium supplemented by 5mM 3-Amino-1,2,4-triazole (3AT) as described in Welch et al. (2007).

Bimolecular fluorescence complementation assay

For BiFC analysis, we subcloned *BIB* and *NUC* CDS in vectors pARC233, pARC234 by single Gateway LR reactions to generate N-terminal fusions to the two YFP fragments as described in Welch et al. (2007). *JKD, MGP*, *SCR* and *SHR* CDS were described in Welch et al. (2007). *Arabidopsis thaliana* Col-0 mesophyll protoplasts were transfected according to Yoo et al. (2007). YFP fluorescence was visualized using a Zeiss LSM 710 confocal laser scanning microscope and images were processed with the confocal microscope Zeiss ZEN software and Adobe Photoshop CS6. Results from at least three independent experiments and more than 20 protoplast cells were visualized.

Image processing

Images were processed using Adobe Photoshop CS6 as follows. Figure 1: Images were rotated to vertical position and background filled with black bucket paint in I and J. Contrast was adjusted in I and L to enhance red color. Color balance tool was used to equalize background in M-P. Figure 2G images were rotated to vertical position and the generated empty space was filled in with bucket paint tool. Figure 6: levels were enhanced in T.

Figure 7: Images were rotated to vertical position and background filled with black bucket paint in I and K.

Contrast was enhanced in Supplemental Figure 5 and Brightness in Figure 2 J_0-J'_2 to improve the quality of the signal in each panel.

SUPPLEMENTARY DATA

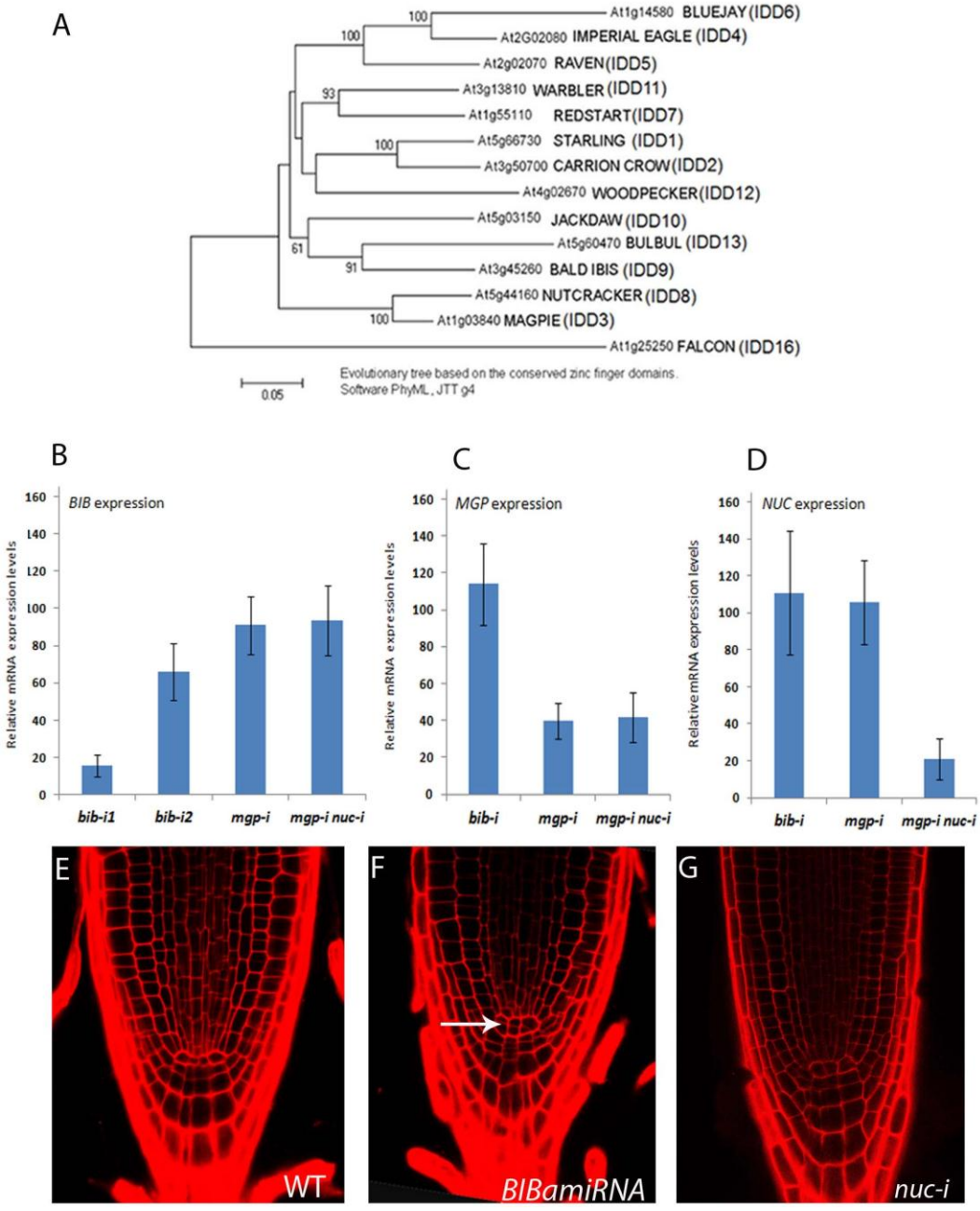

Supplemental Figure 1. Transcript levels in *BIRD* RNAi lines relative to that in WT determined by RT-qPCR.

A Phylogenetic tree of *Arabidopsis thaliana* BIRD proteins (also known as IDD proteins) based on their conserved zinc finger domains. B-D Transcripts levels of *BIB* (B), *MGP* (C) and *NUC* (D). For *BIB*, RNA levels were determined in two independent *BIB* RNAi lines (*bib-i1* and *bib-i2*), *mgp-i* and *mgp-i nuc-i. MGP* and *NUC* expression levels were also determined in *bib-i*, *mgp-i* and *mgp-i nuc-i*. Relative mRNA levels were determined by quantitative real time PCR represented as percentages. Numbers on y-axes are in percentage, error bars represent standard deviations. E-G Median longitudinal confocal sections of 7 days old roots of WT (D), *BIBamiRNA* (E) and *nuc-i* (G). Arrow indicates abnormal divisions occurring in the QC.

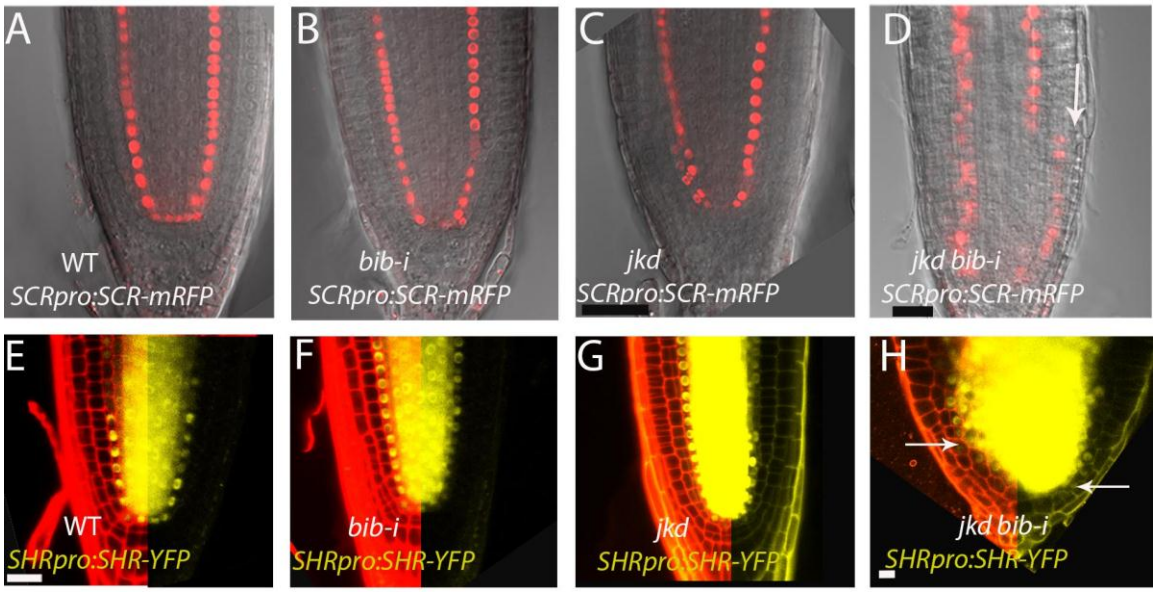

Supplemental Figure 2. Outward shift of SCR expression domain *in jkd bib-i* correlates with SHR spread.

A-D Confocal images showing 7 days old roots expressing *SCRpro:SCR-mRFP* in WT (A), *bib-i* (B), *jkd* (C) and *jkd bib-i* (D), arrow points to expression of SCR-mRFP in the epidermis in *jkd bib-i* (D). Scale bars represent 20 µm. E-H Confocal images of 7 days old roots expressing *SHRpro:SHR-YFP* of WT (E), *bib-i* (F), *jkd* (G) and *jkd bib-i* (H). Scale bars are 20 µm.

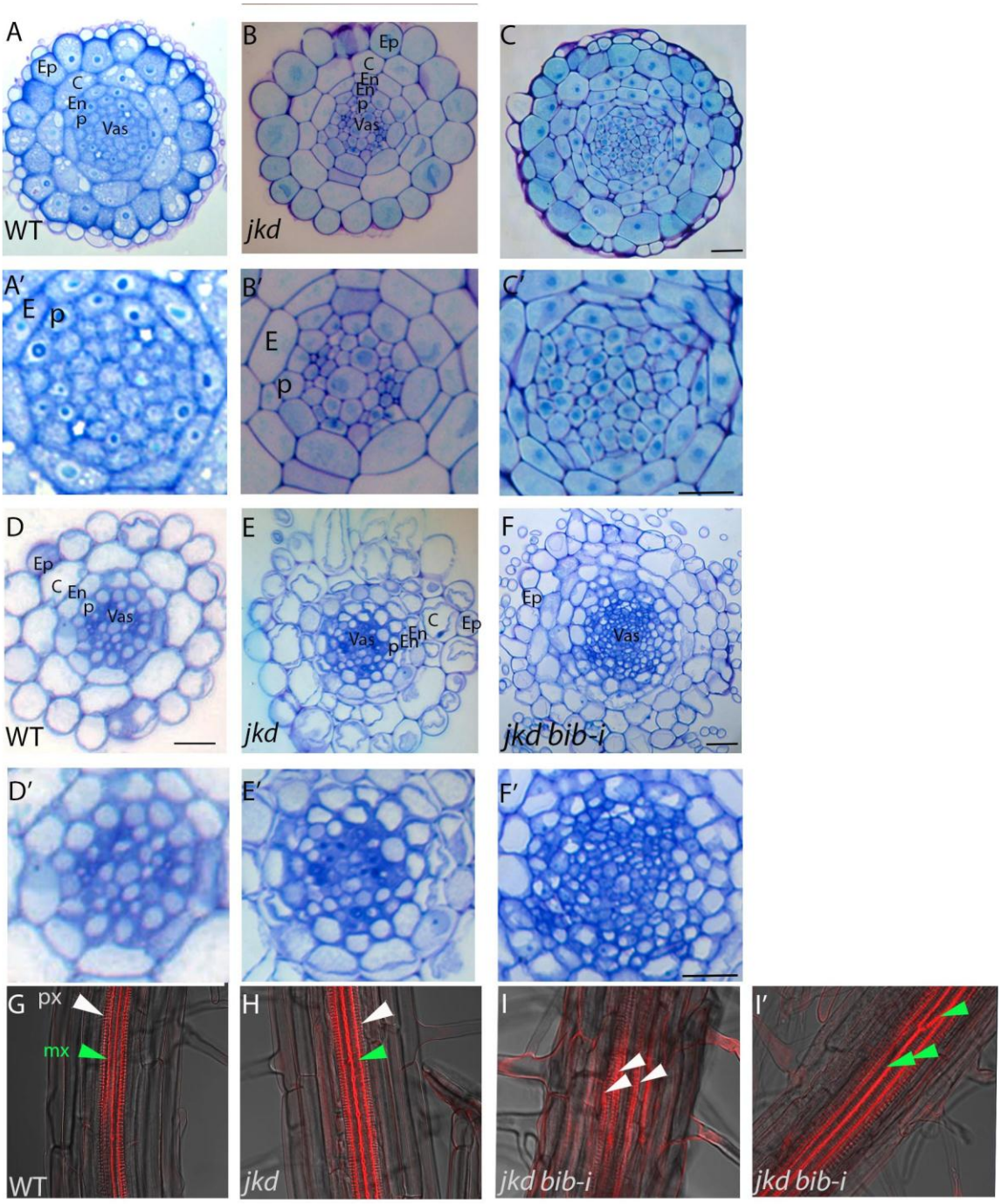

Supplemental Figure 3. Increased cell number of vasculature in *jkd bib-i.*

A-F' Toluidine blue images of stained cross sections taken from different zones of 5 days old roots of WT (A, A'; D, D''), *jkd* (B, B'; E, E'), *jkd bib-i* (C, C'; F, F'). A-C: Sections are from the meristematic region. D-F: Sections are at the differentiation zone. A', B', C', D', E' and F' are enlarged images from A, B, C, D, E and F. Note the increase in cell number of the vascular bundle in F and F''. A and C are the same images of roots sections in Figure 2 O and P. Ep: epidermis, C: cortex, En: endodermis; Vas: vasculature, P: pericycle.

G-I' Confocal images of fuchsin-stained xylem in roots of WT (G), *jkd* (H) and *jkd bib-i* (I, I'). Note increased number of protoxylem (px, white arrowheads in I) and metaxylem (mx, green arrowheads in I').

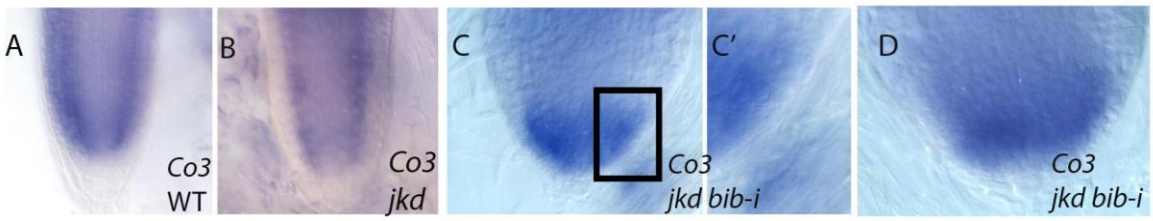

Supplemental Figure 4. JKD and BIB constrain cortex marker to one single layer.

A-D Whole mount *in situ* hybridization using a cortex specific gene *Co3* in 7 days old roots of WT (A), *jkd* (B), *jkd bib-i* (C-D). Note expansion of cortex marker inwards and outwards the radial axis *in jkd bib-i*.

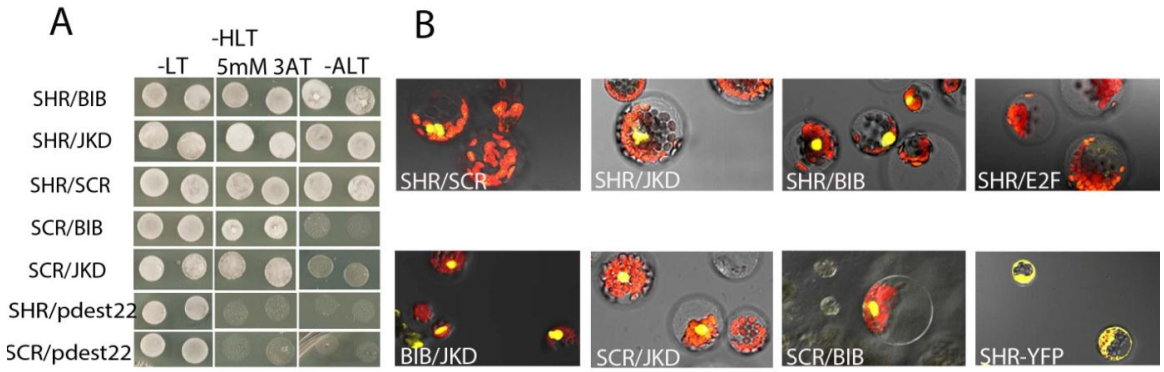

Supplemental Figure 5. BIB and JKD proteins interact with SCR, SHR and among themselves.

Supplemental Figure 5. BIB and JKD proteins interact with SCR, SHR and among themselves.

A Yeast two-hybrid assay determining interactions by growth rates on selective medium His-Leu-Trp- (-HLT) supplemented with 5mM of 3-Amino-1,2,4-triazole (3-AT) and Ala- Leu-Trp- (-ALT). BIRD proteins were used as prey while SCR and a non-autoactivating form of SHR were used as bait. The SCR and SHR pair was used as a positive control while SCR/pdest22 and SHR/pdest22 pairs were used as negative controls. B Bimolecular fluorescence complementation assay in protoplasts reveals that BIRD proteins interact with SCR, SHR and themselves. The SHR/SCR pair was used as a positive control, SHR/E2F pair was used as a negative control. Note that SHR-SYFP showing nuclear and cytoplasmic localization.

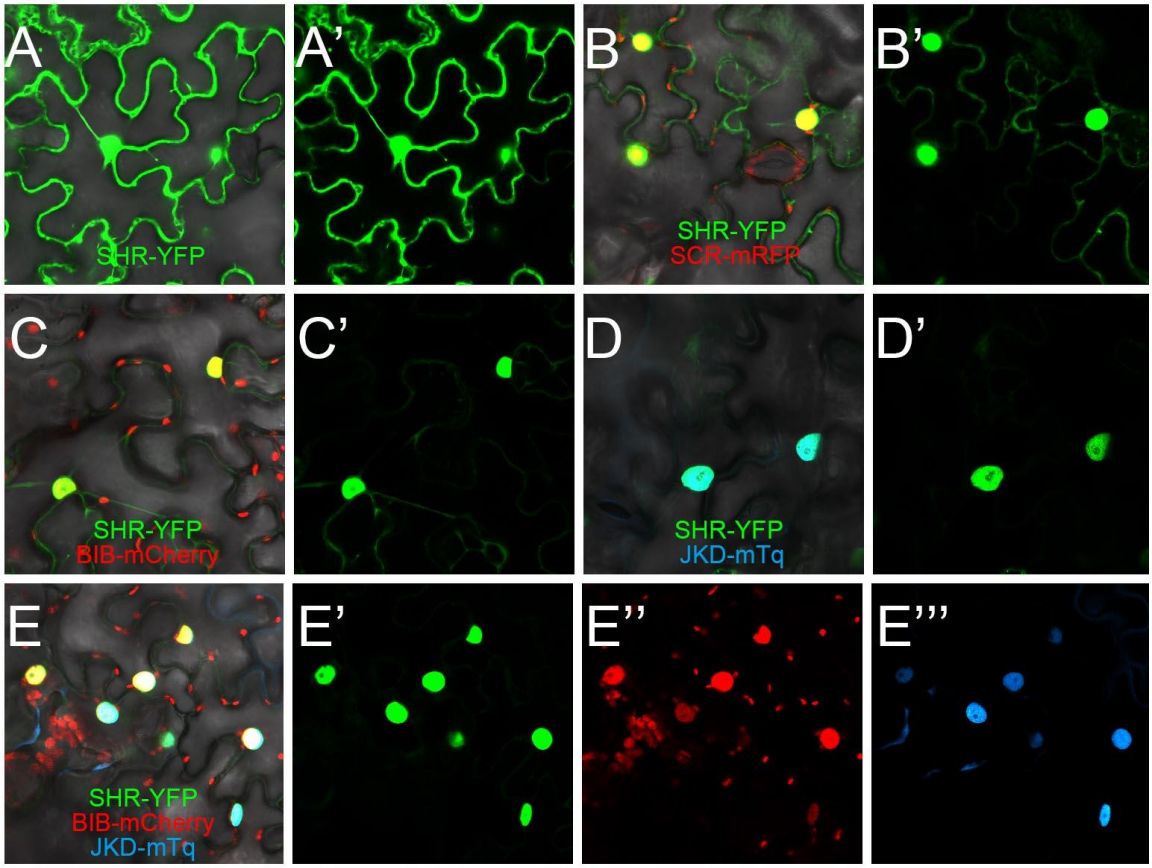

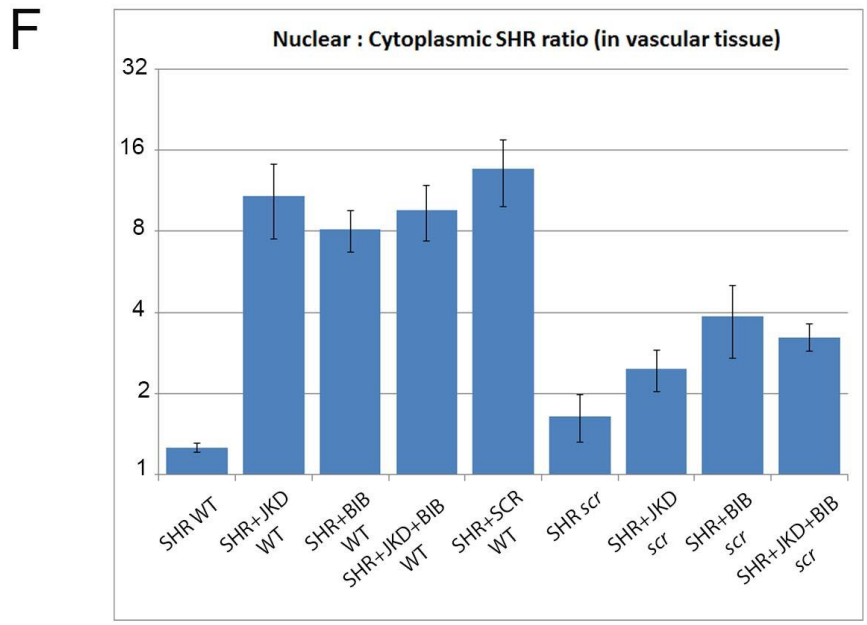

Supplemental Figure 6. BIRD proteins contribute to SHR nuclear retention together with SCR.

A-E'" Transient expression assays in *Nicotiana bentamiana* leaf epidermal cell of SHR-YFP (A, A'), SHR-YFP in presence of SCR-mRFP (B,B'), BIB-mcherry (C,C'); JKD-mTq (D,D') and BIB-mcherry + JKD-mTq (E, E"'). F Quantification of nuclear and cytoplasmic fluorescence signal ratio in plant expressing BIRDs and SCR in vascular tissue in presence and absence of *SCR*.

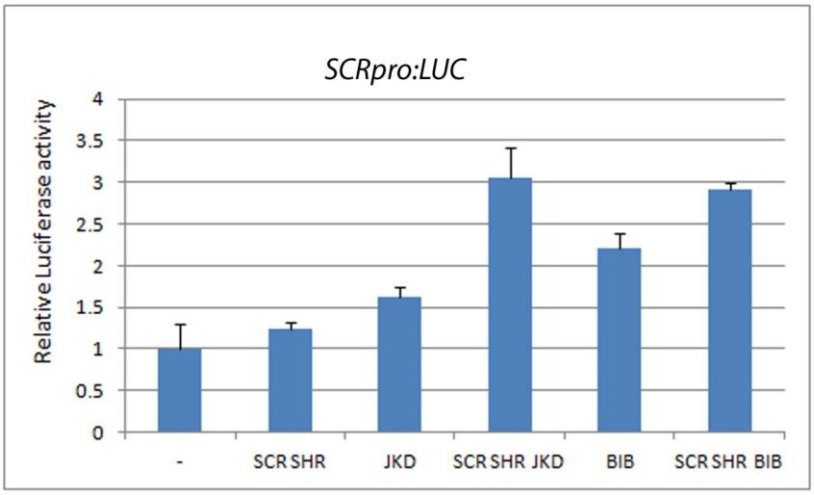

Supplemental Figure 7. JKD and BIB activate *SCR* expression more efficiently than SCR-SHR complex.

Promoter activity measured by Dual Luciferase assay using protoplasts transiently co-transformed with firefly luciferase under *SCR* promoter and effectors plasmids carrying SCR, SHR, BIB or JKD driven by CaMV 35S promoter. BIB and JKD induce *SCR* promoter activity independently from SCR-SHR complex.

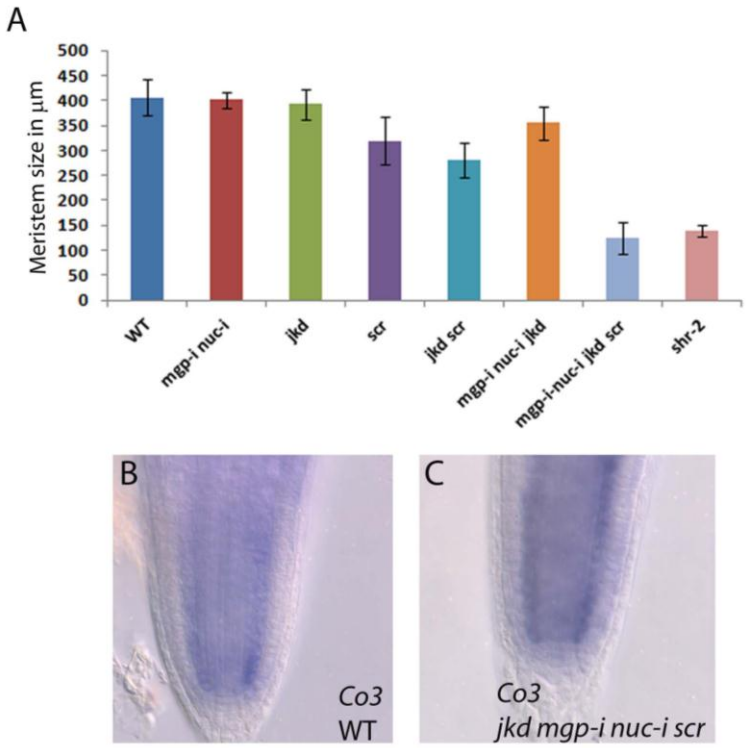

Supplemental Figure 8. *JKD, MGP, NUC* and *SCR* genes control root meristem size but do not influence cortex cell fate.

A *jkd mgp-i nuc-i scr* roots display a reduction of meristem size similar to the one observed in *shr*. Y-axis represents the meristem size in µm. Error bars represent standard deviations. For each line the meristems of at least 20 plants were measured. B, C Whole mount *in situ* hybridization using a cortex-specific gene *Co3* in 3 days old roots of WT (B) and *jkd mgp-i nuc-i scr* (C).

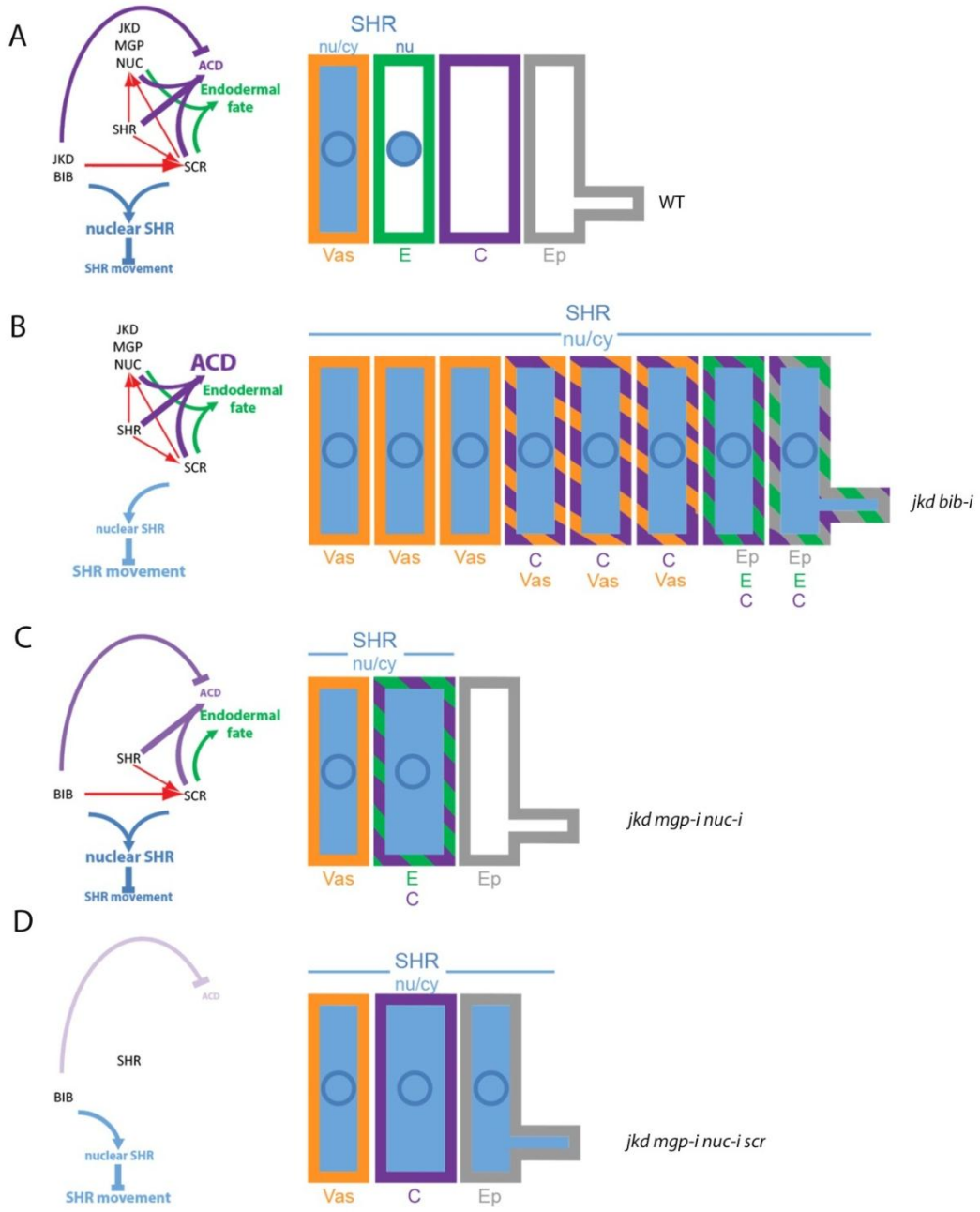

Supplemental Figure 9. Model illustrating BIRD action on SHR movement range and root radial pattern specification.

A In WT, JKD, BIB and SCR promote SHR nuclear retention (thick blue arrow) and restrict SHR movement (thick inhibition sign) in part through *SCR* activation (red arrow) which in turn together with SHR promotes *JKD*, *NUC* and *MGP* expression. All together they contribute to asymmetric cell division (thick purple arrow) and endodermal fate specification (thick green arrow). JKD and BIB restrict ACD and promote normal boundaries specification leading to one layer from each tissue. B In *jkd bib-i,* SHR spread is accompanied by excessive divisions leading to loss of tissue boundaries. C In *jkd mgp-i nuc-i,* ACD in ground tissue is restricted but endodemal fate is still maintained. D In *jkd mgp-i nuc-i scr,* excessive SHR movement is not sufficient to trigger ACD and endodemal fate requires activity of the four proteins.

Supplemental Tables

Primers	Forward	Reverse
EcoRI-SHR-BamHI	CCGGAATTCATGGATACTCTCTTTAGAC	CGCGGATCCGCCGTTGGCCGCCACGC
KpnI-SCR-AgeI	CGGAATTCATGGATACTCTCTTTAGAC	CGCGGATCCGCCGTTGGCCGCCACGC
AfeI-JKD-AgeI	GCTAGCGCTATGCAGATGATTCCAGG	GCGACCGGTATACCCAATGGAGCAAACC
mCherry-BIB	GGAATTCCATGATGATGCCAGATGATC	GACGTCGACTTACTGGTTCATGTCGGCGG

Supplemental Table 1: primers used to generate Constructs for transformation in Hela cells

Constructs	Reference
SHR-YFP	This study
JKD-mCherry	This Study
mCherry-BIB	This Study
SCR-mTurquoise	This Study

Supplemental Table 2: Constructs used for Hela cells transformation

Construct	Vector	Reference
SHR-YFP	pB7m34GW	This Study
JKD-mCherry	pH7m34GW	This Study
SCR-mRFP	pH7m34GW	This Study
BIB-CFP	pH7m34GW	This Study
CYCD6pro:LUC	pUWG35	This Study
SCRpro:LUC	pUWG35	This Study

Supplemental Table 3: Effectors and promoter constructs used for Luciferase activity in protoplast

Primer name	Forward	Reverse
qPCR MGP	CGCTCTCTTTATGGTCGGGAGG	CGGAAAGAGAAGTTGCCCCGTTAGCG
qPCR NUC	CAACCATTTGTACCACAACCGC	GGGGCAGAGAGAGTAGTGGTAGTGG
qPCR BIB	CAAGCTCAAGCAATAGCAAGAC	GTGGAGGCCGGAGGAGACGAGTCTGG
qPCR ACTIN	GGCGAAGATGTGGCAGAGCA	ACGAGGATTCGGTGCAGGACCT
SCRpro	CCGATTGAGAGGAGAGGATTGACCGG	AGATTGCATGGTTATAAATAAGGT
CYCD6pro	CTCTGCAAGTGCAGAAACAAAGTACATTTTAG	TGGTGTTAGAAGATGAAGAAGAAG
Attsites pDNR221	GGGGACAAGTTTGTACAAAAAAGCAGGCTG	GGGGACCACTTTGTACAAGAAAGCTGGGTT
SHRpro 2.5KB	TTTCGAGAAATTACATAAGAAACTGAATT	TAAATCTTAGATATTGTGGGTCTTAC
NUCpro 2,6kb	CTCTCTTTATTAGTTTAGGAAG	GAGAGAGAGAGAGAGAGAAGGAGAC
BIBpro	ATTSITES-GAGTCTCTTTGACAACAGACA	ATT-SITESTCCCACAAGACTTATAGAGAAGTAAG

	TCTGGA	CAC
att sites pGMETeasy1R4	GGGGACAACTTTGTATAGAAAAGTTGCG	GGGGACTGCTTTTTTGTACAAACTTGC
NUC cds	ATGACAAGTGAAGTTCTTCAAACAATCTC AAGTGG	AATCCATCCATTGATAGACGATGGATGGCAC
BIB cds	ATGATGATGCCAGATGATCATCA	CTGGTTCATGTCGGCGGTTGGTGTGCCG
Co3 probe	CACTGTCTGGCCTGGGATC	TCGCAATGCTAGTTGGGTC

Supplemental Table 4: Primers sequences used in this study

Lines	Plant vector	Plant Resistance	Reference
SCRpro:SCR-YFP	pB7m34GW	ppt	Cruz Ramirez et al., 2012
SHRpro:SHR-vYFP	pGreenII0029	ppt	This study
JKDpro:JKD-YFP	pB7m34GW	ppt	This study
JKDpro:HIS2B-YFP	pGreenII0025	norf	This study
BIBpro:BIB-YFP	pB7m34GW	ppt	This study
BIBpro:HIS2B-YFP	pGreenII0025	norf	This study
NUCpro:NUC-YFP	pB7m34GW	ppt	This study
MGPpro:MGP-GFP	pGreenII0029	ppt	Cruz ramirez et al., 2012
SCRpro:SCR-mRFP	pH7m34GW	hyg	This study
WOLpro:SCR-mRFP	pH7m34GW	hyg	This study
WOLpro:XVE>>JKD-mcherry	pH7m34GW	hyg	This study
WOLpro:XVE>>BIB-CFP	pH7m34GW	hyg	This study
CYCD6pro:GFP	pKGWFS7-Dx	ppt	Sozzani et al., 2010
bib-i	pAGRIKOLA	ppt	This study
mgp-i	pGreenII0025	MTX	Welch et al., 2007
nuc-i	pHellsgate	Kan	This study

Supplemental Table 5: Transgenic lines used in this study

Supplemental methods

Phylogenetic analysis

The 13 protein sequences from the Arabidopsis members of the Zinc finger protein family A1a and one member of A1b (At1g25250), described in Englbrecht et al., 2004, were aligned using Muscle (Edgar et al., 2004) and careful manual adjustment of the alignment to remove unambiguously positions was done using Bioedit (Hall et al., 1999). Based on the final multiple sequence alignment containing 233 sites, a phylogenetic tree was constructed using maximum likelihood in PhyML (Guidon et al., 2003) using as model for amino acids substitution JTT with a discrete gamma distribution (4 categories). Statistical support to assess the significance of phylogenetic grouping was evaluated using 100 bootstrap replicates. The final unrooted tree was generated using MEGA Tree Explorer (Tamura et al., 2011).

Supplementary References

Englbrecht CC, Schoof H, Böhm S. Conservation, diversification and expansion of C2H2 zinc finger proteins in the Arabidopsis thaliana genome. BMC Genomics. 2004; 5(1):39

Edgar RC: MUSCLE: a multiple sequence alignment method with reduced time and space complexity. BMC Bioinformatics, 2004; 5:113.

Supplemental Data. Long et al. Plant Cell (2015) 10.1105/tpc.114.132407

Hall TA: BioEdit: a user-friendly biological sequence alignment editor and analysis program for Windows 95/98/NT. Nucleic Acids Symposium Series, 1999; 41:95-98

Guindon S, Gascuel O: A simple, fast, and accurate algorithm to estimate large phylogenies by maximum likelihood. Syst Biol 2003; 52(5):696-704.

Tamura K, Peterson D, Peterson N, Stecher G, Nei M, and Kumar S. MEGA5: Molecular Evolutionary Genetics Analysis using Maximum Likelihood, Evolutionary Distance, and Maximum Parsimony Methods. Molecular Biology and Evolution. 2011; 28: 2731-2739.

Chapter 3

Optimizing FRET-FLIM as a tool to detect nuclear protein interactions at cellular resolution in living Arabidopsis roots

Yuchen Long[1,2], Yvonne Stahl[3], Stefanie Weidtkamp-Peters[4], Wouter Smet[1,2], Yujuan Du[1,2], Alfredo Cruz-Ramírez[2,*], Benjamin Bouchet[5], Kai Jiang[5], Anna Akhmanova[5],Theodorus W.J. Gadella, Jr[6], Joachim Goedhart[6], Rüdiger Simon[3], Ben Scheres[1,2], and Ikram Blilou[1,2]

[1]Plant Developmental Biology, Plant Sciences, Wageningen University, Droevendaalsesteeg 1, Wageningen, 6708PB, The Netherlands

[2]Molecular Genetics, Department Biology, Padualaan 8, Utrecht, 3581CH, The Netherlands

[3]CEPLAS (Cluster of Excellence on Plant Sciences), and Institute of Developmental Genetics, Heinrich Heine University, Universitätsstraße 1, Düsseldorf, 40225, Germany

[4]Center for Advanced Imaging, Institute of Developmental Genetics, Heinrich Heine University, Universitätsstraße 1, Düsseldorf, 40225, Germany

[5]Cell Biology, Department Biology, Utrecht University, Padualaan 8, Utrecht, 3581CH, The Netherlands

[6]Swammerdam Institute for Life Sciences, Section of Molecular Cytology, van Leeuwenhoek Centre for Advanced Microscopy, University of Amsterdam, Science Park 904, Amsterdam, 1098 XH, The Netherlands

*Current Address; Laboratorio Nacional de Genómica para la Biodiversidad, CINVESTAV, Irapuato, Guanajuato, Mexico

ABSTRACT

Protein complex formation has been extensively studied in various biological systems. However, detection of protein interactions at cellular resolution in intact multicellular

organisms is difficult to achieve. Here we describe an optimization protocol for Förster resonance energy transfer (FRET) measured by fluorescence lifetime imaging microscopy (FLIM) to detect protein-protein interactions in living Arabidopsis roots. Using optimized tagged versions of the stem cell regulators SHORT-ROOT (SHR) and SCARECROW (SCR), we detect their complexes *in vivo*, with interaction peaks only in a subset of cells within broader domains where both proteins co-localize. We show that FRET-FLIM technology is a versatile tool to visualize protein binding with robust accuracy noninvasively using endogenous promoters and at cellular resolution in different developmental contexts. We also demonstrate that this approach provides new information on the spatial specificity of nuclear protein complexes. To our knowledge, this is the first report successfully showing spatiotemporal interaction of nuclear proteins in living multicellular organisms using FRET-FLIM. Additionally, our optimized *in vivo* FRET-FLIM procedure is applicable to any biological system.

Key words

Protein complex, protein-protein interaction, fluorophores, FRET-FLIM, SHORT-ROOT, SCARECROW

INTRODUCTION

In living organisms, many cellular functions are executed by protein complexes. In recent years, the concept of “protein-protein interaction networks” has emerged: rather than working as monomeric entities, most cellular proteins are viewed as dynamically engaging in protein binding events. To understand the dynamic nature of protein complexes, it is crucial to correlate the *in vivo* spatiotemporal bindings between key proteins and their impacts on different biological processes. This holds true especially in a multicellular context, where heterogeneity of protein complexes between cell populations can lead to different processes in distinct cells within an intact organism.

Protein interactions are frequently studied with biochemical methods. These methods can be challenging, especially for protein complexes of low abundance. Improvements of protein purification procedures and the increased sensitivity of mass spectrometers have dramatically enhanced protein complex detectability (Bensimon et al., 2012; Pardo and Choudhary, 2012; Young et al., 2012). In addition, automated methods have been developed to isolate specific cell populations, further allowing high throughput proteome-wide analysis of protein complexes in selected cellular environments (Bridgeman et al., 2010; Petricka et al., 2012). Despite these technical advances, biochemical methods remain demanding when dealing with dynamic interactions in transient protein complexes.

Alternatively, fluorescence-based microscopic techniques have been developed to study protein-protein interactions. Bimolecular fluorescence complementation (BiFC) is commonly employed to visualize protein interaction in living cells, where two non-fluorescent fragments of a fluorescent protein can form a bimolecular fluorescent complex upon interaction (Hu et al., 2002). Successful BiFC applications in intact living organisms have been reported (Gohl et al., 2010; Hudry et al., 2011; Smaczniak et al., 2012; Zhang et al., 2004). However, the irreversible formation of bimolecular complexes limits its use to follow dynamic protein interactions (Kodama and Hu, 2012). Conversely, other strategies such as employing Förster resonance energy transfer (FRET) can provide a means to visualize and quantify dynamic protein complexes in living cells, with the immediate spatial information conserved as a microscopic lifetime image. FRET describes the phenomenon of energy transfer from an excited donor fluorophore to a non-excited acceptor fluorophore in its direct vicinity through dipole-dipole coupling (Förster, 1948) (Figure 1a). Since FRET only occurs when the two fluorophores are within a short radius (on the scale of several nanometers), direct protein-protein interaction can be detected by tagging candidate proteins with appropriate fluorophores, such as different green fluorescent protein (GFP) variants (Kremers and Goedhart, 2009). Upon interaction, FRET will lead to a decreased donor emission, relative to that measured in a non-FRET situation, and an elevated acceptor emission (Clegg, 2009). These changes in emission

intensities can be used to reflect the level of protein interaction by directly monitoring donor-acceptor emission ratio change or measuring donor emission recovery after acceptor photobleaching (Adjobo-Hermans et al., 2011; Gu et al., 2004). However, these emission level-based techniques are highly dependent on the concentrations and good signal-to-noise ratios of both donor and acceptor, complicating the analysis with lowly expressed proteins at endogenous levels.

FRET can also be quantified by measuring the fluorescence lifetime decrease of the donor molecules by fluorescence lifetime imaging microscopy (FLIM) (Gadella Jr. et al., 1993). Since FLIM measures a kinetic parameter namely the fluorescence lifetime of the donor, the analysis is less sensitive to intensities. Moreover, only the donor fluorescence signal needs to be acquired for FRET-FLIM measurement, making it less demanding with respect to acceptor fluorescence. Applications of FRET-FLIM are mostly applied to analyze protein-protein interaction in living cells or as means to analyze biosensors (Bücherl et al., 2013; Crosby et al., 2011; Hamers et al., 2014; Kardash et al., 2011; Stahl et al., 2013; Tonaco et al., 2006). FRET-FLIM can be especially useful to detect the interaction between lowly expressed proteins, as accurate measurement is less dependent on emission intensity. Therefore, dynamic protein complex association at cellular resolution can be detected noninvasively using a microscopy-based approach. With these technical advantages, one would be able to follow such interactions in living multicellular organisms and determine their specificity in different cell types and developmental contexts.

Here, we used *Arabidopsis thaliana* as a model organism to establish FRET-FLIM in living tissues. The Arabidopsis root is ideal for live imaging with confocal microscopy due to its transparency and its simple and organized structure. In order to set up *in planta* FRET-FLIM in the Arabidopsis roots, we exploited the intensively-studied interaction between the two GRAS domain transcription factors SHORT-ROOT (SHR) and SCARECROW (SCR). SHR and SCR control the radial pattern of the Arabidopsis root through generating formative cell divisions in the stem cell called the cortex-endodermis initial (CEI) (Helariutta et al., 2000a; Di Laurenzio et al., 1996a). SHR protein is

synthesized in the vasculature and moves outward into the surrounding cell layer consisting quiescent center (QC), CEI and endodermis cells (Nakajima et al., 2001a) (Supplementary Fig. 1). SHR physically interacts with SCR, and this interaction has been shown to regulate downstream target expression and SHR movement itself (Cruz-Ramírez et al., 2012a; Cui et al., 2007a; Long et al., 2015a). However, it is hitherto unknown whether this interaction is spatially homogenous within the cell layer that contains both proteins. Here, we optimize the FRET-FLIM approach and visualize the SHR-SCR complex in living Arabidopsis plants at cellular resolution. We show that in the root meristem, SHR–SCR interaction is stronger in the CEI than in the QC and endodermis. We expanded our analysis to Arabidopsis embryos and lateral root primordia (LRP), showing that *in vivo* FRET-FLIM can be applied in different developmental contexts. Our work demonstrates that nuclear protein interactions can be visualized in a living intact organism and provides evidence that the SHR-SCR interaction is not homogenous throughout their domain of co-localization. Our optimization procedure to detect *in vivo* protein-protein interaction can be applied to any protein pair in any biological system.

RESULTS

Experimental design for *in vivo* FRET-FLIM optimization

The FRET-FLIM technology allows visualization and quantification of protein-protein interactions in living cells. However, many considerations have to be taken into account when using these techniques. Here we addressed and optimized important conditions as prerequisites for measurable FRET to occur in the Arabidopsis. These include 1) position of fluorescent tags, 2) system-specific fluorophores, and 3) *in vivo* fusion protein functionality.

Our optimization procedure featured an *ex vivo*-to-*in vivo* pipeline, where we first employed the transient Arabidopsis protoplast expression system as a convenient tool to

test a large number of FRET-FLIM pair combinations for condition 1 and 2, before evaluating condition 3 in Arabidopsis roots. For rapid data acquisition, we exploited widefield frequency-domain FLIM (Verveer and Hanley, 2009) measurements for protoplast samples with high transgene expression levels. *In planta* lifetime measurements were conducted with time-correlated single photon counting (TCSPC)-based time-domain FLIM (Gerritsen et al., 2009) to maximize photon usage with confocal imaging of lowly-expressed proteins at endogenous levels.

We chose SHR and SCR as the interacting protein pair to optimize FRET-FLIM, because their mutual binding has been reported using different approaches (Cui et al., 2007a; Cruz-Ramírez et al., 2012a; Long et al., 2015a; Welch et al., 2007a).

Position of fluorescent tags

A short distance between the donor and the acceptor requires proper tag positioning on fusion proteins to achieve measureable FRET at sufficient level (Figure 1b). We first optimized the tagging position to detect FRET-FLIM between SHR and SCR with a cyan-emitting mTurquoise (mTq) (Goedhart et al., 2010b) as donor and a yellow-emitting SYFP2 (Kremers et al., 2006b) as acceptor in Arabidopsis protoplasts.

Since there are no available crystallographical data or predicted protein structures of SHR or SCR to guide the choice of tagging positions, we opted to fuse mTq and SYFP2 to both the amino- and carboxyl-termini of the SHR and SCR proteins. We constructed *SCR:mTq*, *mTq:SCR*, *SHR:SYFP2* and *SYFP2:SHR* under the constitutive promoter of Cauliflower Mosaic Virus 35S RNA (*35S*) by the Gateway cloning system, and introduced them into Arabidopsis protoplasts as pairs (example in Figure 1c). As a negative control, we co-transfected *SYFP2:SHR* with a nuclear-localizing mTq variant (*NLS-mTq*), while for positive control we constructed a nuclear-localizing fusion between SYFP2 and mTq (*NLS-SYFP2:mTq*), where continuous FRET occurs due to the fluorophores' close vicinity. Upon paired co-transfection, we analyzed FRET between each SHR-SCR combination by

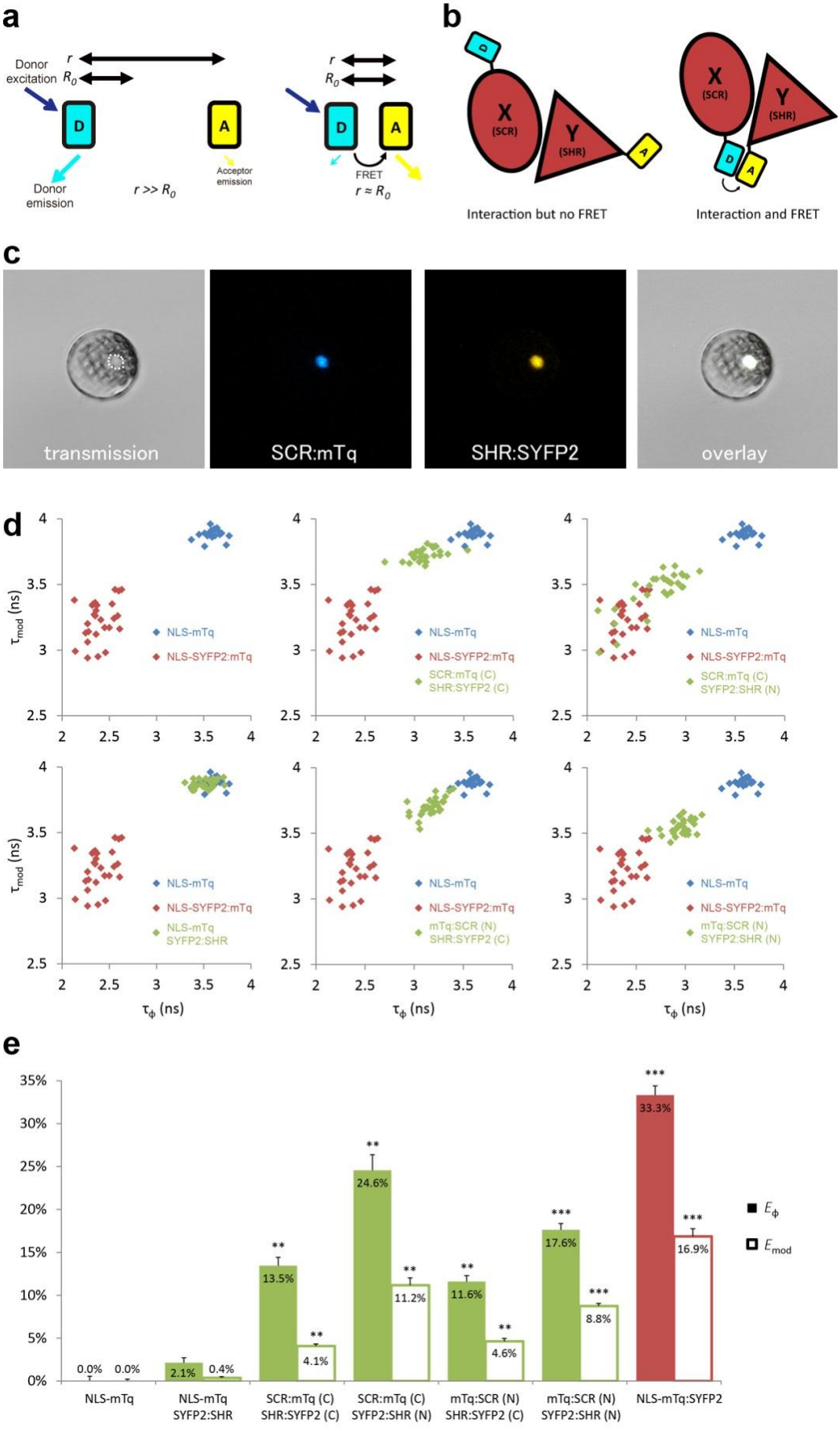
a
Donor excitation
r
R0
D
A
Donor emission
r >> R0
Acceptor emission
FRET
r ≈ R0
b
X (SCR)
Y (SHR)
Interaction but no FRET
Interaction and FRET
c
transmission
SCR:mTq
SHR:SYFP2
overlay
d
τmod (ns)
τϕ (ns)
NLS-mTq
NLS-SYFP2:mTq
SCR:mTq (C) SHR:SYFP2 (C)
SCR:mTq (C) SYFP2:SHR (N)
NLS-mTq SYFP2:SHR
mTq:SCR (N) SHR:SYFP2 (C)
mTq:SCR (N) SYFP2:SHR (N)
e
0.0%
0.0%
2.1%
0.4%
13.5%
4.1%
24.6%
11.2%
11.6%
4.6%
17.6%
8.8%
33.3%
16.9%
Eϕ
Emod
NLS-mTq
NLS-mTq SYFP2:SHR
SCR:mTq (C) SHR:SYFP2 (C)
SCR:mTq (C) SYFP2:SHR (N)
mTq:SCR (N) SHR:SYFP2 (C)
mTq:SCR (N) SYFP2:SHR (N)
NLS-mTq:SYFP2

Figure 1: Optimization of tagging orientation for FRET-FLIM detection.

(a) Illustration of FRET principle. D, donor fluorophore; A, acceptor fluorophore; *r*, distance between D and A; R_0, Förster radius for D and A. (b) Illustration emphasizing the necessity to optimize tagging orientation for FRET. X and Y, two proteins of interest. Limited to no FRET might be observed when fluorophores are located at the distant ends of X and Y, yielding false negative result. (c) Arabidopsis mesophyll protoplast co-expressing SCR:mTq and SHR:SYFP2. Dotted line circles the nucleus. (d) Scatterplots showing distribution of phase lifetime τ_φ against modulation lifetime τ_{mod} from protoplast measurements. Each FRET pair was plotted against the same positive and donor-only samples. n > 10 for each sample. (e) Bar chart showing FRET efficiency *E* derived from τ_φ and τ_{mod} in (d), error bars represent standard errors within one set of experiment. * represent *p*-values, **, $10^{-20} < p < 10^{-2}$; ***, $p < 10^{-20}$, *p*-values calculated by Student's t-test compared to the donor-only samples.

frequency-domain FLIM measurements. Frequency domain FLIM measurements yield a fluorescence lifetime based on the phase-shifted (τ_φ) and demodulated (τ_m) fluorescence emission relative to the modulated excitation source (Verveer and Hanley, 2009). From these lifetimes and the lifetime of the donor-only sample the average FRET efficiency was calculated, yielding E_φ and E_{mod}. As shown in Figure 1d and 1e, different combinations of tagging orientations gave varying levels of FRET, reflected by different shifts of lifetimes in the scatterplots and the unequal FRET efficiencies in the bar chart. The SCR:mTq SYFP2:SHR combination scored the highest FRET efficiency of E_φ = 24.6% ± 1.8% and E_{mod} = 11.2% ± 0.9% (Figure 1d and 1e). These results suggest that the carboxyl-terminus of SCR and the amino-terminus of SHR are in close proximity. Up to 33.3% FRET efficiency was measured in the positive control NLS-SYFP2::mTq (Figure 1e), comparable to the previous description (Goedhart et al., 2010b). The NLS-mTq SYFP2:SHR negative control gave near-ground level FRET (Figure 1e), indicating that FRET between each SHR-SCR combination reflects specific binding. To achieve the highest sensitivity, we selected carboxyl-terminal-tagged SCR and amino-terminal-tagged SHR for further optimizations and analyses.

System-specific fluorophores

Often, fluorescent proteins show variable performance in altered pH, temperature or other conditions introduced by different biological systems. To identify the optimal fluorophores

suitable for FRET-FLIM measurement in Arabidopsis, we compared the performances of several fluorescent proteins in protoplasts and roots.

First, we evaluated whether cyan fluorescent protein (CFP) variants SCFP3A and mTq, in the context of our FRET pair combination SCR and SHR, could be used in a common cyan-yellow FRET-FLIM setup in plant cells (Hamers et al., 2014; Kremers et al., 2006b). As shown in Figure 2a, SCR:mTq yielded a higher FRET efficiency than SCR:SCFP3A in combination with SYFP2:SHR in protoplasts, most likely due to mTq's higher quantum yield. However, SCR:SCFP3A SYFP2:SHR measurements were more precise, indicated by the smaller standard errors (Figure 2a) and decreased spread in scatterplots (Supplementary Fig. 2a). The reduced precision of mTq-SYFP2 measurements might reflect suboptimal mTq performance in plant nuclei (see Discussion).

We next tested the performance of SCFP3A, mTq and SYFP2 in Arabidopsis roots. Since SHR and SCR co-localize in QC, CEI and endodermis, it is essential to detect them in these cells to assess where they potentially interact. Under endogenous promoters, both cyan-variant-tagged *SCR* and *SHR* transgenic lines displayed low fluorescence: signal of *pSCR::SCR:SCFP3A*, *pSCR::SCR:mTq* and *pSHR::SHR:SCFP3A* could be detected in the endodermis with low signal-to-noise ratios (SNR); while endodermal signal of *pSHR::SHR:mTq* was indistinguishable from background signal (Figure 2b).

Since FRET-FLIM is more dependent on donor fluorescence, the poor detection of these two cyan variants made them unsuitable as donor tags. On the contrary, *pSCR::SCR:SYFP2* and *pSHR::SYFP2:SHR* yielded readily detectable emissions supported by higher SNR (Figure 2b). To this end, we favored SYFP2 as donor tag and proceeded to optimize a yellow-red FRET-FLIM setup.

We have previously shown that red fluorescent proteins are efficient FRET acceptors in combination with SYFP2 with Förster radii > 5.6 nm (Goedhart et al., 2007b). Three red-emitting variants, mStrawberry, mCherry and mRFP, were tested for their performance as mentioned above. In protoplasts, SHR and SCR tagged with all three red variants and SYFP2 gave comparable FRET efficiency, with SYFP2-mStrawberry pair

slightly lower (Figure 2a, Supplementary Fig. 2b). When expressed in roots, *pSCR::SCR:mRFP* exhibited higher detectability than *pSCR::SCR:mStrawberry* and *pSCR::SCR:mCherry*. Therefore, we selected SYFP2:SHR and SCR:mRFP for *in vivo* FRET-FLIM studies.

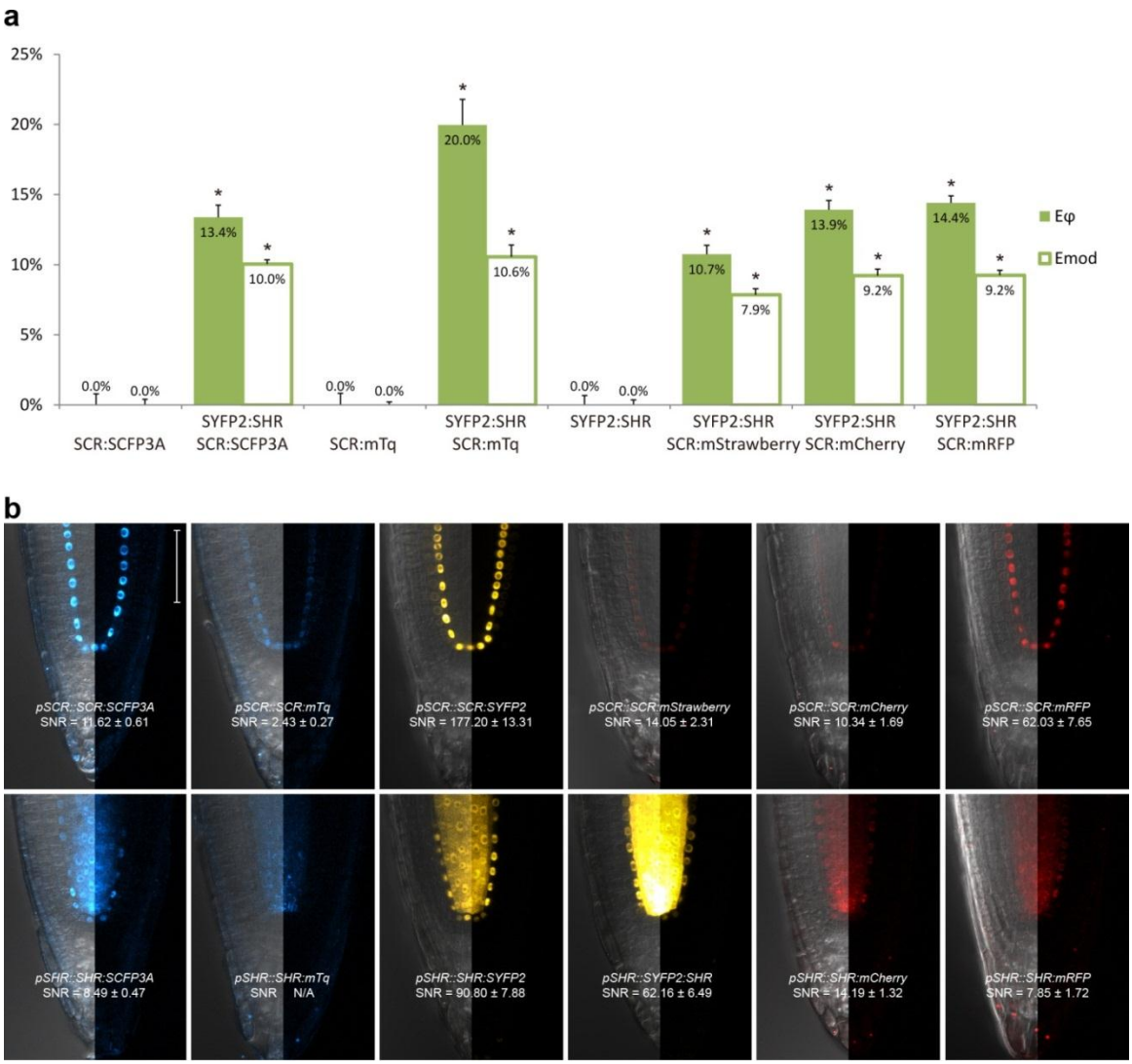

Figure 2: Selection of an appropriate fluorescent protein pair for FRET-FLIM analysis.

(a) Bar chart of FRET efficiency E_{φ} and E_{mod} between SCR and SHR tagged with different fluorescent proteins, with error bars of standard error of mean, n > 10 for each sample. *, $p < 10^{-2}$, *p*-values calculated by Student's t-test compared to the donor-only samples. (b) Confocal images of roots expressing SCR and SHR tagged with different fluorescent proteins, with signal-to-noise ratio (SNR) calculated from endodermal nuclear fluorescence signal. Scale bar, 50 µm. For every image, the left half displays the overlay image and the right half fluorescence channel from the same root.

In vivo fusion protein functionality

Fusion protein engineering has a potential pitfall: the resulted fusions might lose biological function due to undesired conformational changes introduced by tagging. Measurements carried out with such nonfunctional fusions might not accurately reflect their endogenous behaviors. Therefore it is crucial to evaluate the functionality of fusion proteins before FRET-FLIM measurements.

Despite its high detectability in the endodermis, we noticed that only 11% of the roots harboring *pSHR::SYFP2:SHR* showed clearly visible signal in the stem cell niche (Figure 3b), while such signal was readily visible in 80% of roots harboring the carboxyl-terminal-tagged *pSHR::SHR:SYFP2* (Figure 3a). This indicated that SYFP2:SHR might not move sufficiently between certain cells. As previously shown, SHR movement from the vasculature is essential for root growth regulation, and altering its mobility can cause abnormal CEI division and disrupted root architecture (Cui et al., 2007a; Koizumi et al., 2012b; Long et al., 2015a; Vatén et al., 2011a). Additionally, SHR and SCR co-localize in the endodermis and stem cell niche, it is thus essential to have sufficient SHR movement into the stem cell niche to measure SHR-SCR interaction. Since amino-terminal tagging on SHR was not reported to disrupt SHR movement (Heidstra et al., 2004a), we reasoned that the Gateway linker between SYFP2 and SHR might cause an undesired conformational change to the fusion, and attempted to restore SYFP2:SHR mobility by linker alteration. Using site-directed mutagenesis, we generated *pSHR::SYFP2-SHRΔ1a* by removing 5 amino acids from the linker, shortening it from 5'-DPAFLYKVA-3' to 5'-DKVA-3'. As shown in Figure 3c, up to 71% of the roots harboring *pSHR::SYFP2-SHRΔ1a* showed significant improvement of SHR fusion signal in the stem cell niche. The linker alteration of SYFP2-SHRΔ1a did not change the FRET efficiency between SHR and SCR in protoplasts (Supplementary Fig. 3a and 3b). This enabled us to measure FRET-FLIM between SHR and SCR in their endogenous conditions.

Our optimization procedure revealed that the combination of analysis in protoplasts (*ex vivo*) and intact plants (*in vivo*) is essential for the selection of the appropriate donor-acceptor pairs, and fortifies the notion that such systematic procedure should be utilized for any biological context prior to *in vivo* FRET-FLIM measurements

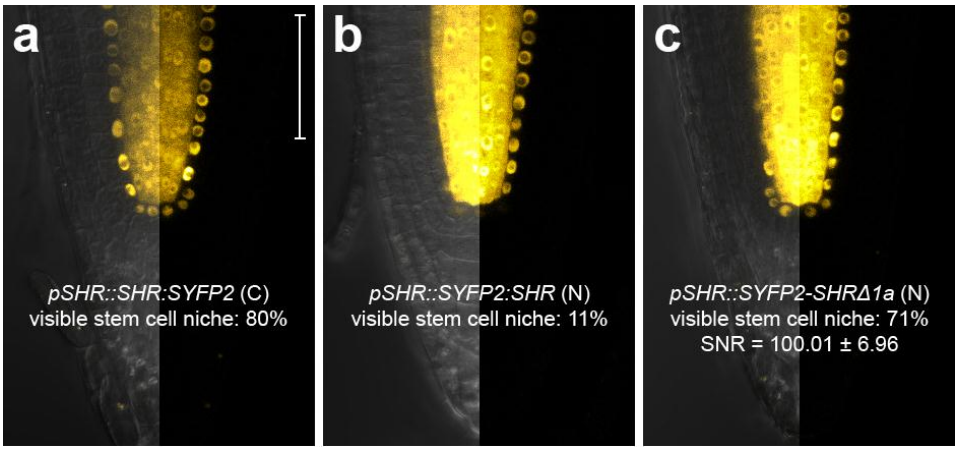

Figure 3: Improvement of SHR fusion protein mobility.

Confocal images of roots expressing SHR fusion proteins differentially tagged with SYFP2, with signal-to-noise ratio (SNR) calculated from endodermal nuclear fluorescence signal. (a) *pSHR::SHR:SYFP2*, (b) *pSHR::SYFP2:SHR*, (c) *pSHR::SYFP2-SHRΔ1a*, n > 10 for each sample. Scale bar, 50 µm. For every image, the left half displays the overlay image and the right half fluorescence channel from the same root.

Measuring FRET-FLIM in Arabidopsis roots

After optimization, we measured the fluorescence lifetime of SYFP2-SHRΔ1a in living Arabidopsis seedlings containing both *pSHR::SYFP2-SHRΔ1a* and *pSCR::SCR:mRFP* transgenes (Figure 4a). The measurements utilized a single-pixel fluorescence lifetime analysis pipeline (see Methods) to yield confocal fluorescence lifetime heatmaps as shown in Figure 4b. Long lifetime regions were pseudo-colored as red pixels, while lower lifetime pixels were characterized by a “blue-shift”. When only SYFP2-SHRΔ1a was expressed in the Arabidopsis roots, fluorescence lifetime was generally high in the root, indicated by the homogenous reddish pseudo-color (Figure 4b). Upon *pSCR::SCR:mRFP* co-expression, SYFP2-SHRΔ1a fluorescence lifetime was observed to decrease where it co-localized with SCR:mRFP, indicated by the enhanced bluish tint in the QC, CEI and endodermal nuclei on the heatmap (Figure 4b). This result confirms that SHR and SCR interact in the QC, CEI and endodermis in Arabidopsis roots (Cruz-Ramírez et al., 2012a; Long et al., 2015a).

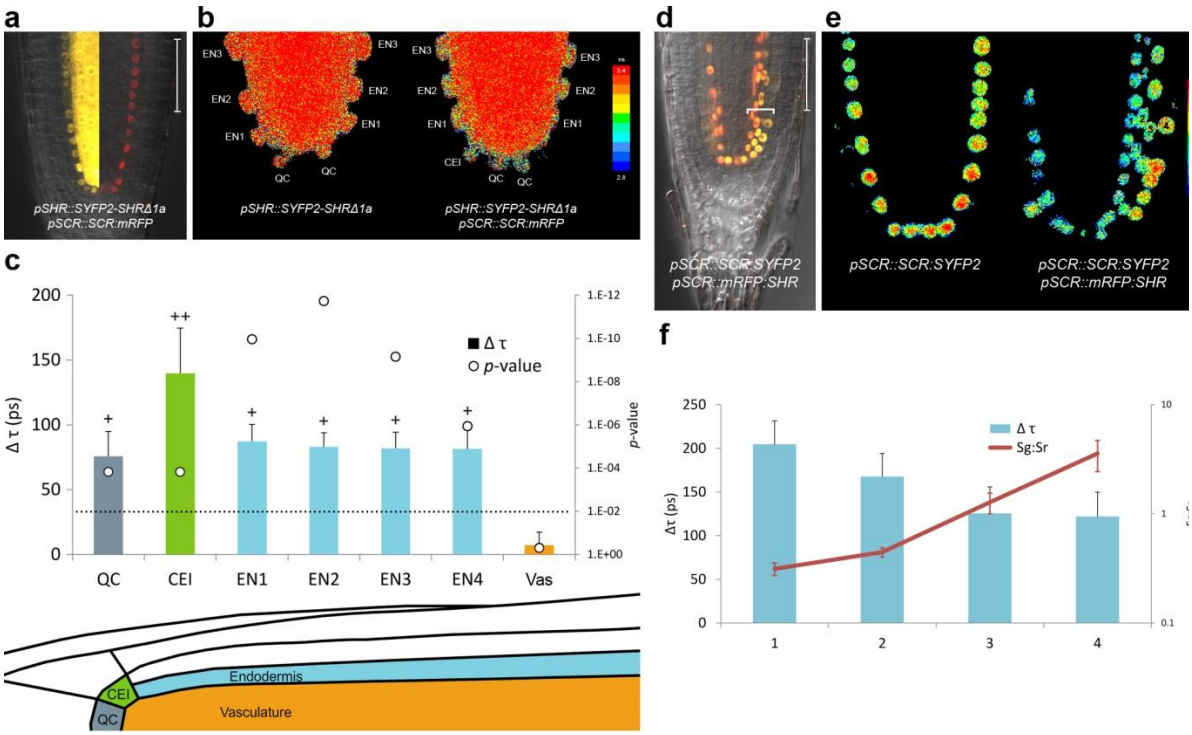

Figure 4: FRET-FLIM between SHR and SCR in Arabidopsis roots.

(a) Arabidopsis root co-expressing *pSHR::SYFP2-SHRΔ1a* and *pSCR::SCR:mRFP*. Scale bar, 50 µm. Yellow fluorescence channel (left) and red fluorescence channel (right) were overlaid with transmission image from the same root. (b) Heatmaps of fluorescence lifetime in donor-only and sample root. Note the lifetime decrease indicated by the "blue-shift". (c) Quantification of lifetime change ($\Delta\tau$) in single cells. Column color matches with tissue type indicated in the schematic root section below the chart. Circles indicate *p*-value calculated by Student's t-test of sample lifetimes comparing to donor-only lifetimes at each cell position, with the dotted line marking the 0.01 significant value. + indicates that FRET at the cell position is significantly different to that in vasculature ($p < 10^{-2}$). ++ indicates FRET at CEI position is significantly different to QC and endodermis ($p < 10^{-2}$). Donor roots n = 86, FRET sample roots n = 109. EN 1-4, first 4 endodermal cells starting from CEI. Vas, vasculature. (d) Root expressing *pSCR::SCR:SYFP2* and *pSCR::mRFP:SHR*, showing SHR fused with fluorophore on amino-terminal with Gateway linker retains its ability to induce ectopic formative division (marked by bracket) when expressed in *SCR* domain. Scale bar, 50 µm. (e) Heatmaps of fluorescence lifetime in donor-only and sample root. (f) Quantifications of lifetime change ($\Delta\tau$) of SCR:SYFP2 and yellow-to-red fluorescence ratio (Sy:Sr) of cells numbered in (e). Donor roots n = 17, FRET sample roots n = 16.

We quantified the FRET level between SHR and SCR fusions in different cells. As shown in Figure 4c, FRET between SYFP2-SHRΔ1a and SCR:mRFP was detected in the QC, the CEI and endodermis cell 1 (rootward) to 4 (shootwad). Furthermore, SHR and SCR fusions displayed a significantly higher FRET level in the CEI than in the QC or endodermis (Figure 4c), suggesting a possible biological significance for higher SHR-SCR complex levels in the CEI where formative cell divisions take place. The same

interaction profile reappeared in different measurements with comparable results at most cell positions (p > 0.01, Supplementary Fig. 4). In the vasculature, where only SYFP2-SHRΔ1a was present, FRET remained at basal levels (Figure 4c). This further confirmed that the FRET detected in QC, CEI and endodermis accurately reflects SHR-SCR interactions.

We also tested SHR-SCR interaction in *pSCR::SCR:SYFP2 pSCR::mRFP:SHR* roots, where ectopic SHR drove extensive formative cell divisions in a SCR-dependent manner (Nakajima et al., 2001a) (Figure 4d). As shown in Figure 4e and 4f, we found that FRET levels between SCR:SYFP2 and mRFP:SHR were higher in the inner ectopic cell layers (position 1 and 2 in Figure 4e) compared to the outer cell layers (position 3 and 4 in Figure 4e). Such observation indicates that SHR-SCR complex level is enriched in the ectopically dividing inner cells. Alternatively, this could also be a consequence of reduced expression level of *pSCR::mRFP:SHR* in the outmost layer (Figure 4f), resulting in varied donor-to-acceptor ratio in different cell files and thus altering the FRET outcome. Nevertheless, this result confirmed that high FRET between SHR and SCR correlates with CEI-like formative divisions in Arabidopsis roots.

FRET-FLIM in different developmental contexts

After establishing FRET-FLIM measurements between SYFP2-SHRΔ1a and SCR:mRFP in the Arabidopsis root meristem, we extended the application of this technique in Arabidopsis embryos and lateral root primordia (LRP).

In heart stage embryos, SHR and SCR expression domains at the root pole are similar to those in the postembryonic roots (Figure 5a). Similar to the root meristem, we found that SYFP2-SHRΔ1a exhibited strong FRET with SCR:mRFP in QC, CEI and endodermis of late heart- / early torpedo-stage embryos (Figure 5b and 5c). Interestingly, FRET between SYFP2-SHRΔ1a and SCR:mRFP in the embryo was enhanced in QC and endodermis 1, to similar levels occurring in the CEI (Figure 5c). This observation might reflect enhanced

SHR-SCR interaction in these embryonic cells. Alternatively, the contribution of high background signal (reduced SNR in Figure 5a) with generally shorter lifetimes in the embryos might have influenced FRET detections and resulted in a general lifetime reduction.

New root meristems are formed from differentiated root tissue in a process called lateral root formation. Lateral root initiation is marked by a series of cell divisions originating from the vasculature (Malamy and Benfey, 1997). Using FRET-FLIM, we studied the interaction between SHR and SCR during lateral root formation. As shown in Figure 5d, SHR and SCR only co-localized in a subset of cells in the developing stage III LRP: SCR:mRFP was detected in both of the two outer layers (OL1 and OL2), while SYFP2-SHRΔ1a resided in the OL2 nuclei and maintained nuclear-and-cytoplasmic localization in the inner layer (IL), similar to mature vasculature. Within OL2 where SYFP2-SHRΔ1a and SCR:mRFP co-localized, FRET was detected higher in the central cells (OL2-1, Figure 5e and 5f), reaching the levels observed in CEI of primary roots (Figure 4c). In contrast, OL2 cells displaced from LRP midline (OL2-2 and OL2-3, Figure 5f) exhibited similar FRET levels to those in the endodermis in the primary root (Figure 4c). No FRET was detected in the IL or vasculature due to the absence of detectable SCR:mRFP (Figure 5f).

After emergence, the lateral root morphology resembles the primary root, with similar cellular organization and expression patterns of *pSHR::SYFP2-SHRΔ1a* and *pSCR::SCR:mRFP* (Figure 5g). However, the FRET levels between SYFP2-SHRΔ1a and SCR:mRFP in emerged lateral roots were generally higher with no significant difference between QC, CEI and endodermis (Figure 5i).

Analyses between SYFP2-SHRΔ1a and SCR:mRFP in Arabidopsis embryos and LRP show that *in vivo* FRET-FLIM can be utilized to different developmental contexts. Additionally, FRET-FLIM between SYFP2-SHRΔ1a and SCR-mRFP could also be performed in heterologous systems such as HeLa cells (Supplementary Fig. 3c and 3d), promising the applicability of these techniques to other biological systems.

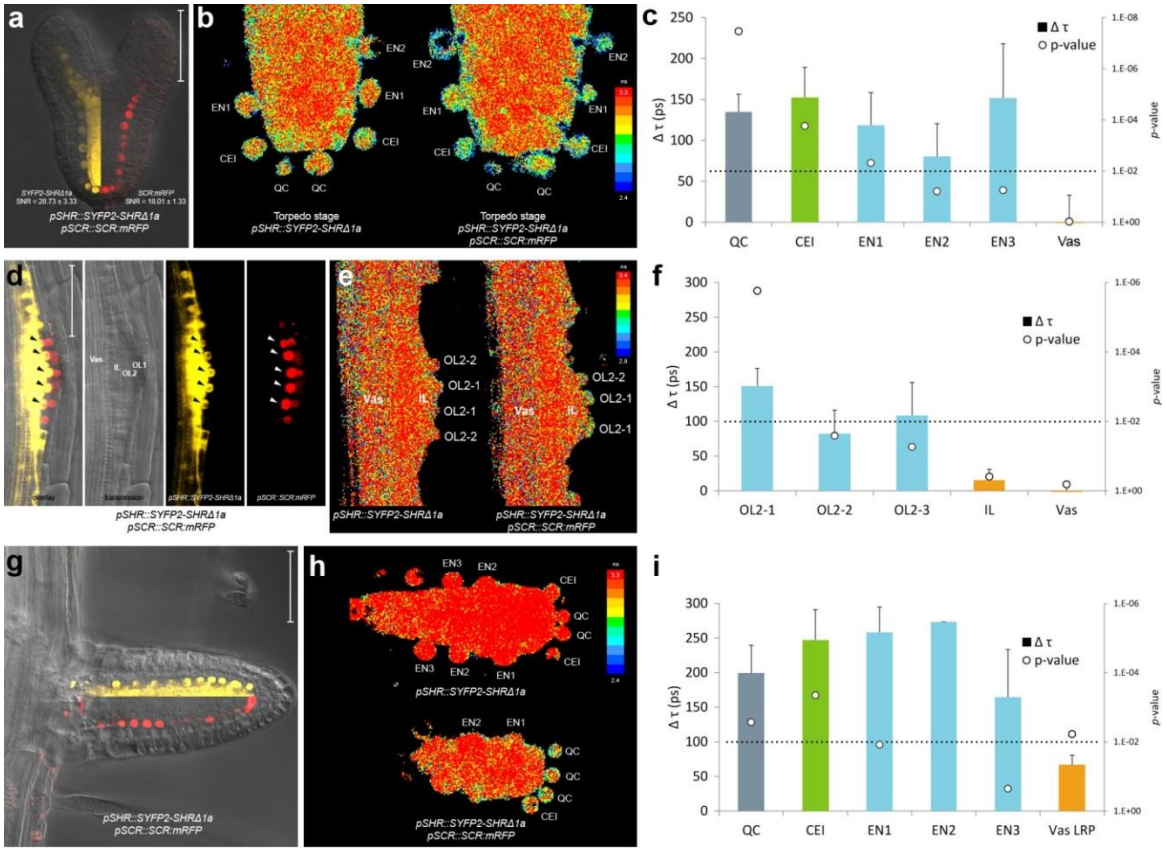

Figure 5: Spatiotemporal dynamics of SHR-SCR interaction.

(a) Early torpedo stage Arabidopsis embryo co-expressing *pSHR::SYFP2-SHRΔ1a* and *pSCR::SCR:mRFP*, with signal-to-noise ratio (SNR) calculated from endodermal nuclear fluorescence signal. Scale bar, 50 μm. Yellow fluorescence channel (left) and red fluorescence channel (right) were overlaid with transmission image from the same root. (b) Heatmaps of fluorescence lifetime in donor-only and sample embryo. (c) Quantification of lifetime change ($\Delta\tau$) in single cells. Column color matches with tissue type illustrated in Figure 4. Circles indicate *p*-value calculated by Student's t-test of sample lifetimes comparing to donor-only lifetimes at each cell position, with the dotted line marking the 0.01 significant value. Donor embryos n = 18, FRET sample embryos n = 34. (d) Arabidopsis stage III LRP co-expressing *pSHR::SYFP2-SHRΔ1a* and *pSCR::SCR:mRFP*. Scale bar, 50 μm. OL1 and OL2, outer layer 1 and 2; IL, inner layer; Vas, primary root vasculature. Arrowheads point to OL2 cells where SHR and SCR co-localize. (e) Fluorescence lifetime heatmaps of donor-only and sample LRP. OL2 cells were numbered with OL2-1 in the middle of the LRP and OL2-2 and -3 progressively further from LRP midline. (f) Quantification of FRET between SYFP2-SHRΔ1a and SCR:mRFP measured in (e). Donor LRP n = 13, FRET sample LRP n = 17. (g) Arabidopsis emerged lateral root co-expressing *pSHR::SYFP2-SHRΔ1a* and *pSCR::SCR:mRFP*. Scale bar, 50 μm. Yellow fluorescence channel (upper) and red fluorescence channel (lower) were overlaid with transmission image from the same root. (h) Fluorescence lifetime heatmaps of donor-only and sample emerged lateral root. (i) Quantification of FRET between SYFP2-SHRΔ1a and SCR:mRFP measured in (h). Donor lateral roots n = 11, FRET sample lateral roots n = 3. Vas LRP, vasculature of LRP.

DISCUSSION

In the present study, we optimized the FRET-FLIM technology to inspect nuclear protein interactions in living plants. We show that protein complex formation can be mapped to specific cells in different organs *in vivo*. This technique therefore overcomes current limitations to studying protein complex dynamics at cellular resolution.

We show that fluorophores exhibit different performances in plant cells when fused to two interacting transcription factors. For example, mTq is well recognized as a preferred CFP variant for use as a FRET donor (Goedhart et al., 2010b). In the Arabidopsis root, endodermal signal was low for SCR:mTq and undetectable for SHR:mTq (Figure 2b). Such low mTq detectability, however, was not reported when localized to cell membranes, cytoplasm or cytoskeleton in intact Arabidopsis plants (Peremyslov et al., 2012; Roppolo et al., 2011; Waadt et al., 2014). This is possibly due to high expression levels of these fusion proteins concentrated at different subcellular domains, or might suggest that mTq protein is sensitive to the plant nuclear microenvironment. The new cyan variant mTurquoise2, with improved folding properties, might be an alternative that remains to be tested in Arabidopsis (Goedhart et al., 2012). Nevertheless, our optimization procedure highlights the importance of selecting appropriate fluorophores for different cellular and subcellular conditions.

Optimizing FRET-FLIM in living Arabidopsis roots allowed visualization of spatiotemporal bindings between endogenous SHR and SCR during different developmental stages, which cannot be addressed by *in vivo* over-expressions or cell lines. We found that the FRET levels between SYFP2-SHRΔ1a and SCR:mRFP vary among different developmental contexts, and among different cell types within each developmental stage. The enhanced FRET-FLIM signals in specific cells could reflect a higher concentration of SHR-SCR heterodimers, but we cannot exclude that the FRET signal can be modified by the presence of other binding partners which may have an effect on the FRET levels through conformational effects. Such a scenario is plausible, as we have previously shown that SHR interacts with a variety of BIRD proteins which regulate SHR intercellular

mobility and transcriptional activity (Long et al., 2015a). Other protein such as RETINOBLASTOMA-RELATED (RBR) also physically associates with the SHR-SCR complex to repress ectopic formative divisions in the endodermis (Cruz-Ramírez et al., 2012a). The binding dynamics of these proteins to SHR-SCR complexes and each other have not yet been tested. To this end, extending our optimized FRET-FLIM technique for proteins interacting with SHR-SCR complex to create a protein interaction map at cellular resolution will be a big step towards understanding the cell-specific protein complex dynamics *in vivo* and their functions during Arabidopsis development.

The discovery of plausible SHR-SCR interaction heterogeneity highlights the spatiaotemporal sensitivity of *in vivo* FRET-FLIM. However, FRET requires the donor and acceptor being within the stringent Förster radius, making it especially sensitive to close-ranged protein associations but inefficient to detect interactions between far-end-tagged proteins due to functionality obligations or associations of proteins within big protein complexes that exceed Förster radii. Meanwhile, single molecule spectroscopy analyses such as fluorescence correlation spectroscopy (FCS)-based techniques, can detect protein-protein association without Förster radius requirement. Application of *in planta* FCS-related analyses between SHR and SCR is presented by Sozzani et al (2014, accompanied manuscript), where SHR-SCR interactions and their relative stoichiometry are documented in complementary fashions to our findings in the Arabidopsis root. Single molecule tracking of SHR-SCR complex, however, was proven impractical in the stem cell niche due to high background level, while *in vivo* FRET-FLIM succeeded in obtaining interaction information thanks to the stringently controlled fitting procedure. To sum up, one can obtain a broader spectrum of information regarding to protein-protein interaction when combining FRET-FLIM and FCS-based techniques *in vivo*.

Nevertheless, our heterologous analyses forecast future applications of *in vivo* FRET-FLIM in studying protein-protein interactions in other biological systems. Indeed, attempts of applying FRET-FLIM measurements in living animals or intact tumors to study interactions between exogenous proteins or monitor biosensors have been reported

(Kardash et al., 2011; Kelleher et al., 2009; Nobis et al., 2013; Venugopal et al., 2012), indicating the possibility of *in vivo* FRET-FLIM usage. Following our optimization procedure, endogenous protein interactions should be readily analyzable in living animals. In addition, one should take advantage of exploiting heterologous systems (HeLa cells for plants, protoplasts for animals, etc.) to study cellular processes without interferences from system-specific endogenous factors.

In conclusion, our optimization of FRET-FLIM allows detection of protein complexes in living tissue at cellular resolution. Our optimization procedure is, in principle, appropriate for any protein interaction pair. Low abundance of certain proteins and potential limitations in engineering effective fusions without disruption of protein function still remain major challenges for *in vivo* FRET-FLIM measurements. Technical advances will rely on continuous improvements of fluorescent tags and detection sensitivity. Combined with optimization and application of other microscopic techniques such as single-molecule FRET-FLIM or FCS-based techniques in living organisms, FRET-FLIM will allow us to precisely monitor the composition of multiprotein complexes and their dynamics *in vivo*.

METHODS

DNA constructs

Coding sequences (CDS) of *SCFP3A*, *mTurquoise*, *SYFP2*, *mCherry*, *mStrawberry* and *mRFP* (Goedhart et al., 2007b, 2010b; Kremers et al., 2006b) were subcloned into multiple Gateway cassettes with flanking *att*B sites. A general SV40 nuclear localizing signal (NLS) (Lassner et al., 1991) was attached to the N-terminal of *mTq* and *SYFP2* to generate *NLS-mTq* and *NLS-SYFP2*. For C-terminal tagging, fluorescent protein sequences were recombined into pGEMTeasyR2R3 vector by Gateway BP reaction; while pGEMTeasyR1R2-derived entry clones were generated for N-terminal tagging. *SHR* and *SCR* coding sequence in pDONR221-derived entry clones (Welch et al., 2007a) were

used for C-terminal tagging clones; while for N-terminal tagging *SHR* and *SCR* were subcloned into pGEMTeasyR2R3. For protoplast transfection, *35S* promoter-driven fusions of *SHR* and *SCR* with N- or C-terminal tagging were created in pB7m34GW or pH7m34GW binary vectors (Karimi et al., 2007) by multiple Gateway LR reactions (Invitrogen). Positive controls of *35S::NLS-SYFP2:mTq* and *35S::NLS-SYFP2:SCFP3A* were generated by combining previously described tags in entry clones. Root expression vectors of *SHR* and *SCR* were created similarly with endogenous *pSHR* and *pSCR* promoters (Long et al., 2015a). For better stem cell niche localization, *pSHR::SYFP2-SHRΔ1a* was generated by site-directed mutagenesis (QuikChange II, Aligent) from *pSHR::SYFP2:SHR* vector. For HeLa cell expression, SYFP-Δ1a-SHR was generated by subcloning *SHR* CDS with flanking restriction sites (5'-BsrGI-SHR-BamHI-3') into pSYFP2-C1 (Kremers et al., 2006b) followed by site-directed mutagenesis as described. SCR-mCherry was generated by subcloning *SCR* CDS with flanking restriction sites (5'-KpnI-SCR-AgeI-3') into pmTurquoise-N1 (Goedhart et al., 2010b), followed by swapping mTurquoise with mCherry (5'-AgeI-mCherry-NotI-3') (Goedhart et al., 2007b). Primers for cloning are listed in Supplementary Table 1.

Arabidopsis growth condition and transformation

Arabidopsis thaliana ecotype Columbia (Col-0) plants containing *SHR* and *SCR* transgenes were grown as previously described[43]. Stably transformed lines were generated by *Agrobacterium tumefaciens*-mediated transformation via floral dip method (Clough and Bent, 1998).

Protoplast preparation and transfection

A. thaliana Col-0 mesophyll protoplasts were prepared and transfected according to Yoo et al. (2007) with following adaptations: 4th and 5th leaves from young seedings were incised on the abaxial side and laid on the surface of enzyme solution for overnight

digestion. During transfection, 40% PEG-calcium transfection solution was used. 2×10^5 protoplast cells were used for each transfection. For donor saturation, donor and acceptor vectors were transfected in 1:2 ratio, with 10 µg DNA in total. After transfection, W5 solution was used instead of WI, and transfected protoplasts were cultivated overnight under constant light before observation.

A. thaliana Col-0 tissue culture protoplasts were prepared and transfected according to Axelos et al. (1992). 10 µg donor vector and 20 µg acceptor vector were transfected.

Transfection of heterologous systems

HeLa cell culture and transfection were as described in Jiang et al. (2014), constructs were transfected using FuGENE 6 protocol (Promega).

Fluorescence lifetime imaging microscopy in protoplasts

Living transfected protoplasts were collected in LabTek chambered coverglass (Nunc) for frequency-domain FLIM measurements. Samples with cyan fluorescent donors were acquired according to Goedhart et al. (2010) and samples with yellow fluorescent donor werer acquired according to Goedhart et al. (2007). Briefly, CFP-variants were excited with a 440 nm modulated diode laser (LDH-M-C-440; PicoQuant) at 75.1MHz, the light was reflected by a 455DCLP dichroic mirror and emission was passed through a D480/40 band-pass emission filter (Chroma Technology). SYFP2 fluorescence was excited with a 514 nm Argon laser (Melles-Griot) intensity-modulated at a frequency of 75.1 MHz and the light was reflected by a 525DCXR dichroic mirror and emission was passed through a HQ545/30 band-pass emission filter (Chroma Technology). Emission was detected using a radio frequency (RF)-modulated image intensifier (Lambert Instruments II18MD) coupled to a charge-coupled device (CCD) camera (Photometrics HQ) as detector. FLIM stacks of 18 phase images were acquired in permutated recording order with an exposure time of 50-1000 ms per image depending on sample brightness. The average

fluorescence lifetime of individual nuclei was quantified from which an average lifetime for the sample was determined. FRET efficiency was calculated as described in Goedhart et al. (2007). More than 10 cells were analyzed for each sample.

Confocal microscopy

Protoplasts and Arabidopsis roots were imaged with a LSM 710 laser-scanning confocal microscope (Carl Zeiss GmbH) with a C-Apochromat 40x/1.20 W Korr water-immersion objective. A 2 air unit (AU) pinhole was set for weak *SHR* expression. Cyan fluorescence was detected at 465 – 500 nm with 458 nm excitation and 458/514 beam splitter; yellow detected at 520 – 560 nm with 514 nm excitation and 458/514 beam splitter; and red detected at 600 – 660 nm with 543 nm excitation and 488/543/633 beam splitter, respectively. Images were taken with no offset, and signal-to-noise ratio (SNR) was calculated as follows:

$$\mathrm{SNR} = \frac{S}{N}$$

where *S* is the nuclear fluorescence signal from imaged root endodermis, and *N* auto-fluorescence signal in the adjacent non-fluorescent area in the root to emphasize the challenge of measurement in Arabidopsis root with high background signal. More than 10 roots were analyzed for each SNR calculation, except for *pSCR::SCR:mStrawberry* (n=8), *pSCR::SCR:mCherry* (n=7) and *pSHR::SHR:mRFP* (n=9).

Arabidopsis root meristems and LRP were mounted in water and embryos in 5% glucose prior to observation.

Fluorescence lifetime imaging microscopy in living Arabidopsis

Roots of 3 day-post-germination (dpg) and 6 dpg seedlings were mounted in water for measurements in primary roots and LRP, respectively. Late heart- / early torpedo-stage

embryos were mounted in 5% glucose for measurements. Fluorescence lifetime imaging microscopy was performed on a confocal laser scanning microscope (Zeiss LSM 780) additionally equipped with a single-photon counting device with picosecond time resolution (PicoQuant Hydra Harp 400). SYFP2 fluorescence was excited at 485 nm using a linearly polarized diode laser (LDH-D-C-485) operated at a repetition rate of 32 MHz. Excitation power was around 1 µW at objective (40x water immersion, Zeiss C-PlanApo, NA 1.2). The emitted light was collected in the same objective and separated into its perpendicular and parallel polarization (Thorlabs PBS 101, Thorlabs GmbH, Germany). Fluorescence was then detected by Tau-SPADs (PicoQuant) in a narrow range of SYFP2's emission spectrum (band-pass filter: HC535/30 AHF). Images were taken with 12.6 µs pixel time and a resolution of 0.1 µm/pixel for roots and embryos and 0.21 µm/pixel for LRP (Zoom 4 and 2, 256x256). A series of 60 frames were merged into one image and further analyzed (Widengren et al., 2006).

Single-Pixel Fluorescence lifetime analysis

The fluorescence lifetime of SYFP2 was determined and analyzed pixel-wise in merged images to increase photon numbers for analysis using the software tools "AnI-3SF" and "Margarita" developed in Prof. C.A.M Seidel group [Software Package for Multiparameter Fluorescence Spectroscopy, Full Correlation and Multiparameter Fluorescence Imaging (http://www.mpc.uni-duesseldorf.de/seidel)] for Multiparameter Fluorescence Image Spectroscopy (MFIS) (Kudryavtsev et al., 2007; Weidtkamp-Peters et al., 2009). In fluorescence lifetime measurements, high spatial resolution microscopy and low excitation power prevent photo bleaching; the number of photons per pixel is exceptionally low, ranging from 100 to 2000 photons per pixel. Therefore, a model to fit the data with a minimal number of parameters has to be applied in conjunction with a maximum likelihood estimator (MLE) (Eggeling et al., 2001; Schaffer et al., 1999; Sisamakis et al., 2010; Weidtkamp-Peters et al., 2009; Widengren et al., 2006). The decay of SYFP2 is approximated in the subsequent fluorescence lifetime analysis by an

(fluorescence-weighted) average lifetime, τ. We therefore used a monoexponential model function with two variables (fluorescence lifetime τ and scatter contribution γ); as described elsewhere (Stahl et al., 2013), fitted with MLE. The instrument response function was measured using the dye erythrosine, which exhibits a very short fluorescence lifetime, which is additionally quenched in an aqueous, saturated potassium iodide solution.

FRET-FLIM quantification in living Arabidopsis

Nuclear areas of no smaller than 25 pixels, based on the nuclei's appearances after the 100-photon-per-pixel background subtraction, were selected from independent cells. Cellular fluorescence lifetimes were computed by least-square fitting the Gaussian peaks of each cells' lifetime distributions. Fluorescence lifetimes at the same cell position were pooled from independent measurements without normalization, enabled by the robust FRET-FLIM acquisition between samples and between experiments. Reduction of fluorescence lifetime ($\Delta\tau$) between donor-only and FRET samples were calculated from the means of donor-only and FRET samples at each cell position, with inclusion of fractional standard errors. Significances, between donor-only and FRET samples at specific cell positions in the same or different experiments, were resolved by Student's t-test with critical value of $p < 0.01$.

SUPPLEMENTARY DATA

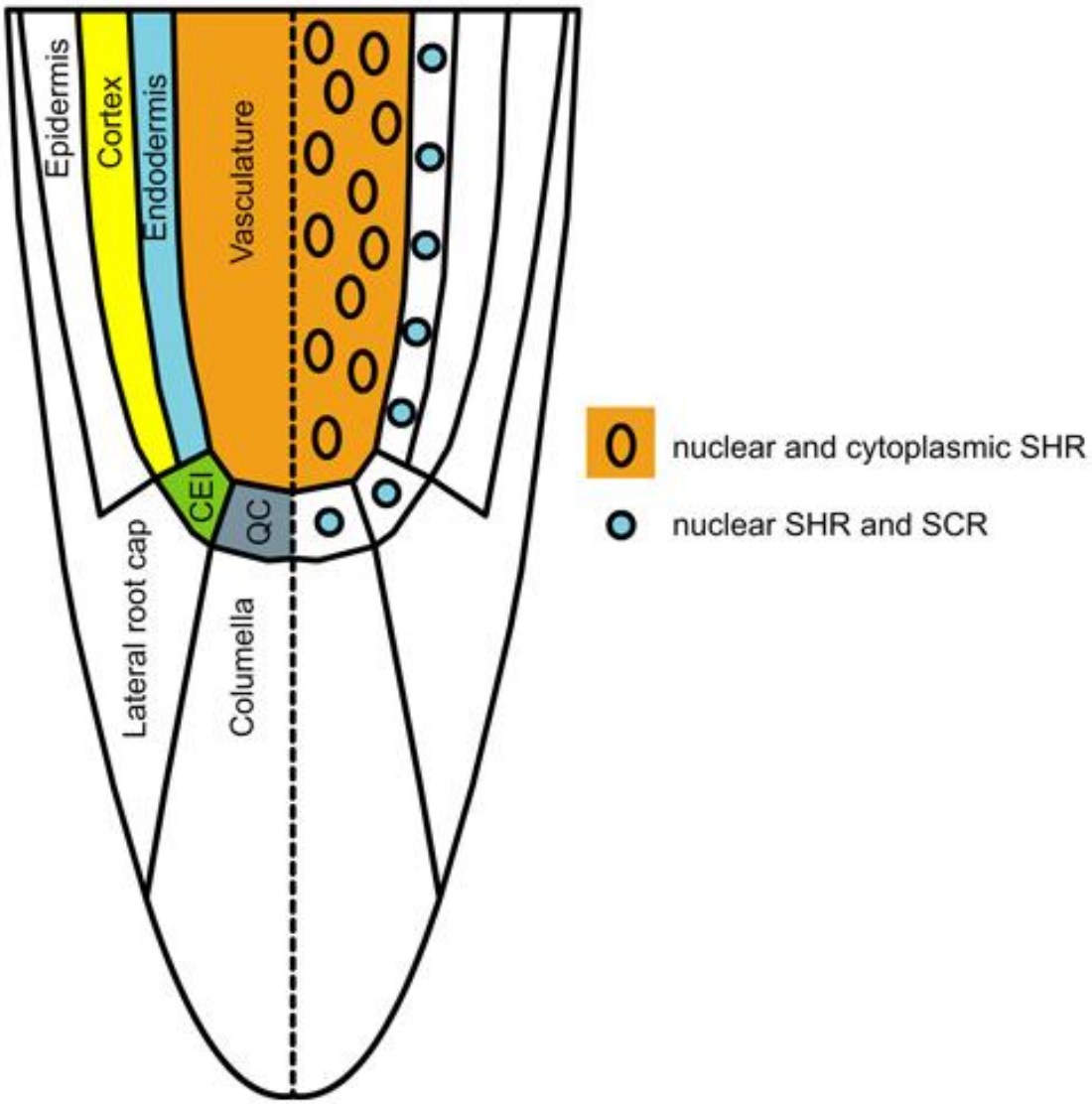

Supplementary Figure 1: Diagram of *Arabidopsis thaliana* root meristem.

Arabidopsis thaliana root meristem marked with different cell types. QC, quiescent center; CEI, cortex-endodermal initial. Right half panel summarizes SHR and SCR localization.

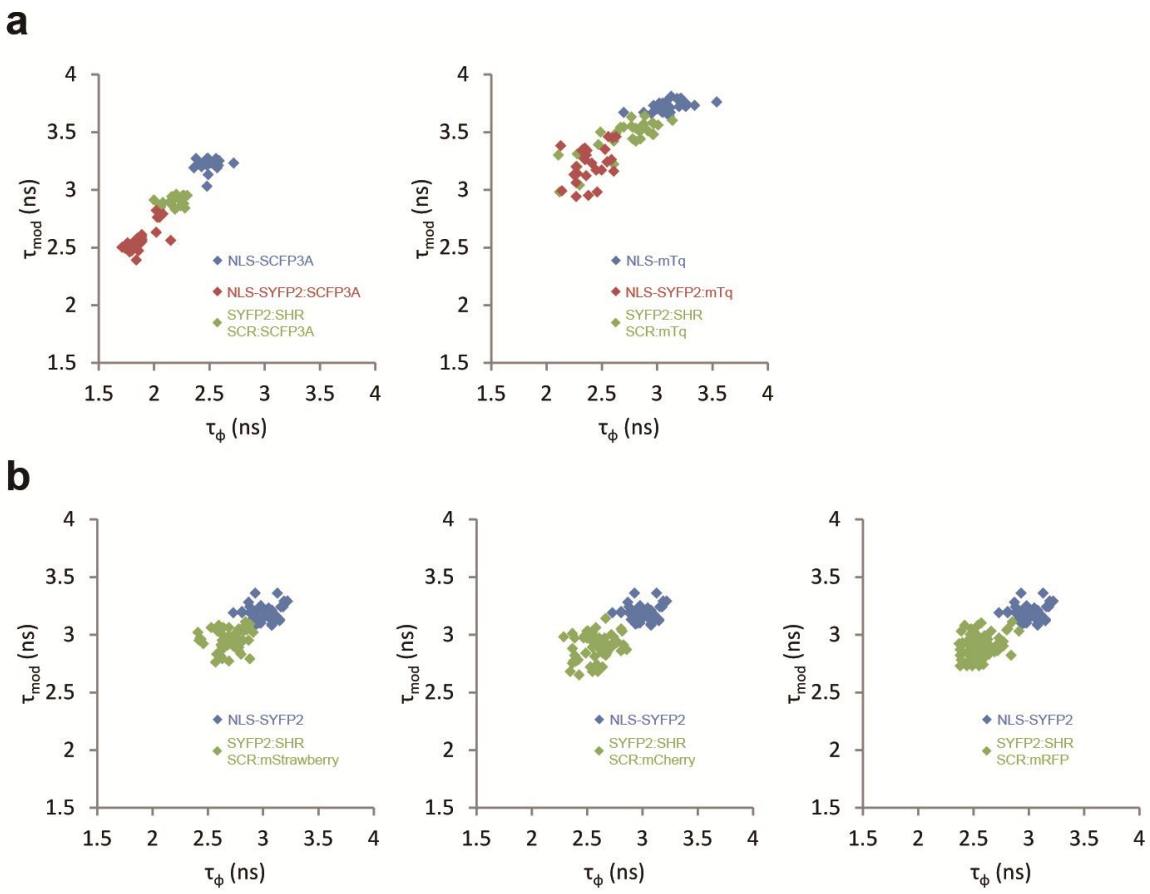

Supplementary Figure 2: Optimization of tags-of-choice for FRET-FLIM between SHR and SCR.

(a) Scatterplots showing distribution of phase lifetime τ_{φ} against modulation lifetime τ_{mod} from protoplast measurements between SYFP2:SHR and SCR:SCFP3A or SCR:mTq. (b) Scatterplots of fluorescence lifetime measurements between SYFP2:SHR and SCR:mStrawberry, SCR:mCherry or SCR:mRFP in protoplasts.

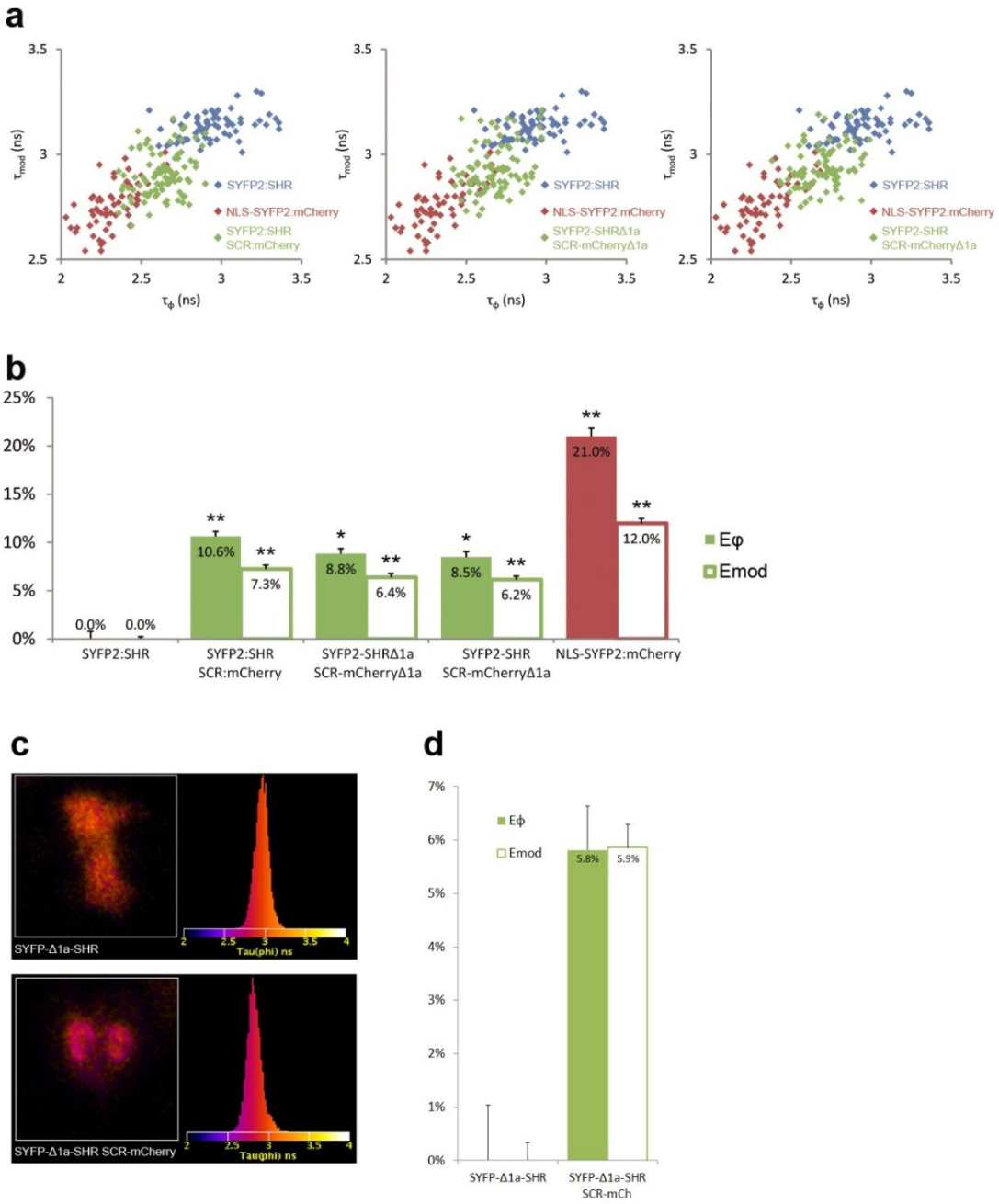

Supplementary Figure 3: Optimization of linker composition for FRET-FLIM between SHR and SCR.

(a) Scatterplot of fluorescence lifetime measurements between SHR and SCR with different linker composition in protoplasts. SYFP2-SHRSΔ1a has 5'-DKVA-3' linker, SCR-mCherryΔ1a has 5'-NKVA-3' linker, while SYFP2-SHR has no linker between SYFP2 and SHR. (b) Bar chart of FRET efficiency *E* derived from (a), with error bars of standard error of mean. *, $10^{-20} < p < 10^{-2}$; **, $p < 10^{-20}$. (c) Fluorescence ifetime heatmaps and histograms of SYFP-Δ1a-SHR in donor-only or FRET sample HeLa cells. (d) Bar chart showing FRET efficiency *E* derived from τ_{φ} and τ_{mod} in (c), error bars represent standard errors within one set of experiment, n > 10.

Supplementary Table 1. Primer list for cloning

SCFP3A/mTurquoise-R2R3 F	5'-GGGGACAGCTTTCTTGTACAAAGTGGCTATGGTGAGCAAGGGCGAGGAG-3'
SCFP3A/mTurquoise-R2R3 R	5'-GGGGACAACTTTGTATAATAAAGTTGCTTACTTGTACAGCTCGTCCATGC-3'
SCFP3A/mTurquoise-221 F	5'-GGGGACAAGTTTGTACAAAAAAGCAGGCTTCATGGTGAGCAAGGGCGAGGAG-3'
SCFP3A/mTurquoise-221 R	5'-GGGGACCACTTTGTACAAGAAAGCTGGGTCCTTGTACAGCTCGTCCATGC-3'
SYFP2-R2R3 F	5'-GGGGACAGCTTTCTTGTACAAAGTGGCTATGGTGAGCAAG-3'
SYFP2-R2R3 R	5'-GGGGACAACTTTGTATAATAAAGTTGCTCACTTGTACAGC-3'
SYFP2-221 F	5'-GGGGACAAGTTTGTACAAAAAAGCAGGCTTCATGGTGAGC-3'
SYFP2-221 R	5'-GGGGACCACTTTGTACAAGAAAGCTGGGTCTCACTTGTACAGC-3'
mCherry/mStrawberry-R2R3 F	5'-GGGGACAGCTTTCTTGTACAAAGTGGCTATGGTGAGCAAGGGCGAGGAG-3'
mCherry/mStrawberry-R2R3 R	5'-GGGGACAACTTTGTATAATAAAGTTGCTTACTCACTTGTACAGCTCGTCCATGCC-3'
mCherry/mStrawberry-221 F	5'-GGGGACAAGTTTGTACAAAAAAGCAGGCTGTATGGTGAGCAAGGGCGAGGAG-3'
mCherry/mStrawberry-221 R	5'-GGGGACCACTTTGTACAAGAAAGCTGGGTTCTTGTACAGCTCGTCCATGCCG-3'
mRFP-R2R3 F	5'-GGGGACAGCTTTCTTGTACAAAGTGGCTATGGCCTCCTCCGAGGACGTCATC-3'
mRFP-R2R3 R	5'-GGGGACAACTTTGTATAATAAAGTTGCTCAGGCGCCGGTGGAGTGGCGGCCC-3'
mRFP-221 F	5'-GGGGACAAGTTTGTACAAAAAAGCAGGCTGTATGGCCTCCTCCGAGGACGTC-3'
mRFP-221 R	5'-GGGGACCACTTTGTACAAGAAAGCTGGGTTGGCGCCGGTGGAGTGGCGG-3'
NLS 5'-attachment F	5'-ATGCCAAAGAAGAAGAGAAAGGTCATGGTGAGCAAGGGCG-3'
NLS-221 F	5'-GGGGACAAGTTTGTACAAAAAAGCAGGCTTCATGCCAAAG-3'
SHR-R2R3 F	5'-GGGGACAGCTTTCTTGTACAAAGTGGCTATGGATACTCTCTTTAGACTAGTCAGTCTCC-3'
SHR-R2R3 R	5'-GGGGACAACTTTGTATAATAAAGTTGCTTACGTTGGCCGCCACGCACTAGCCCAAAC-3'
SCR-R2R3 F	5'-GGGGACAGCTTTCTTGTACAAAGTGGCTATGGCGGAATCCGGCGATTTCAACGGTGG-3'
SCR-R2R3 R	5'-GGGGACAACTTTGTATAATAAAGTTGCCTAAGAACGAGGCGTCCAAGCTGAAGC-3'
SYFP2-SHRΔ1a sense	5'-GACGAGCTGTACAAGGACAAAGTGGCTATGGATACT-3'
SYFP2-SHRΔ1a antisense	5'-AGTATCCATAGCCACTTTGTCCTTGTACAGCTCGTC-3'
SYFP2-SHR sense	5'-CATGGACGAGCTGTACAAGATGGATACTCTCTTTAGAC-3'

SYFP2-SHR antisense	5'-GTCTAAAGAGAGTATCCATCTTGTACAGCTCGTCCATG-3'
SCR-mCherryΔ1a sense	5'-GGACGCCTCGTTCTAACAAAGTGGCTATGGTGAG-3'
SCR-mCherryΔ1a antisense	5'-CTCACCATAGCCACTTTGTTAGAACGAGGCGTCC-3'
BsrGI-SHR-BamHI F	5'-TTGTGTACAAGATGGATACTCTCTTTAGACTAGTCAGTCTCC-3'
BsrGI-SHR-BamHI R	5'-GCGGATCCTTACGTTGGCCGCCACGCACTAGCCCAAACC-3'
KpnI-SCR-AgeI F	5'-CGGGGTACCATGGCGGAATCCGGCGATTTCAACGGTGGTC-3'
KpnI-SCR-AgeI R	5'-TTGACCGGTTTAGAACGAGGCGTCCAAGCTGAAGCAGTGAG-3'
AgeI-mCherry-NotI F	5'-GCTACCGGTCGCCACCATGGTGAGCAAGGG-3'
AgeI-mCherry-NotI R	5'-CCGCGGCCGCTTACTCGTCCATGCCGCCGG-3'

Chapter 4

Spatial segregation of transcription factor complexes correspond to different cell fates in Arabidopsis root

Yuchen Long[1,2], Yvonne Stahl[3], Stefanie Weidtkamp-Peters[4], Sara Díaz-Triviño[1,2], Wenkun Zhou[1], Joachim Goedhart[5], Theodorus W.J. Gadella, Jr[5], Rüdiger Simon[3], Ben Scheres[1,2], and Ikram Blilou[1,2]

[1]Plant Developmental Biology, Wageningen University and Research Centre, Droevendaalsesteeg 1, Wageningen, 6708PB, The Netherlands.

[2]Molecular Genetics, Department Biology, Padualaan 8, Utrecht, 3581CH, The Netherlands.

[3]CEPLAS (Cluster of Excellence on Plant Sciences), and Institute of Developmental Genetics, Heinrich Heine University, Universitätsstraße 1, Düsseldorf, 40225, Germany.

[4]Center for Advanced Imaging, Institute of Developmental Genetics, Heinrich Heine University, Universitätsstraße 1, Düsseldorf, 40225, Germany.

[5]Swammerdam Institute for Life Sciences, Section of Molecular Cytology, van Leeuwenhoek Centre for Advanced Microscopy, University of Amsterdam, Science Park 904, Amsterdam, 1098 XH, The Netherlands.

ABSTRACT

In the Arabidopsis root meristem, the transcription factor complex of SHORT-ROOT (SHR) and SCARECROW (SCR) regulates asymmetric cell division (ACD) in the cortex-endodermis initial (CEI), the stem cell playing a central role in defining root radial pattern. The spatial restriction of ACD to CEI requires the joined inhibitory inputs of RETINOBLASTOMA-RELATED (RBR) and the BIRD/INDETERMINATE DOMAIN proteins JACKDAW (JKD) and BALDBIBS (BIB) on the activity of SHR-SCR complex. These proteins and their tangled transcriptional regulations form a complex network with yet undefined molecular behavior to precisely activate or repress ACD in designated cells.

One plausible hypothesis is that SHR and SCR form cell-specific protein complexes with binding partners to differentially regulate target gene expression and thus ACD. However, visualization of transcription factor complexes in living roots at the cellular resolution, and correlating their distribution to cellular activities, have never been reported. Here we show that spatial partitioning of SHR and SCR complexes, mediated by BIRD and RBR proteins, is pivotal to maintain radial pattern in the root meristem. Using Förster resonance energy transfer measured by fluorescence lifetime microscopy (FRET-FLIM), we show that BIRD proteins form different cell type-specific complexes with SHR and SCR in living Arabidopsis roots. Additionally, elevated SHR-SCR interaction could be detected in mutants with increased ACD, in agreement with SHR-SCR function in promoting ACD. Binding assays indicate that JKD and SHR-SCR form a ternary complex, suggesting that the observed spatial interaction distribution in roots does not reflect exclusive heterodimers but rather dynamic conformational changes of the studied complexes. Taken together, our transcription factor complex distribution analysis shows that, in a complex regulatory network, spatial separation of protein complexes can modify network topology and regulate segregation of different cell fates in a multicellular organism.

Keywords

cell fate, asymmetric cell division, protein-protein interaction, transcription factor complex, FRET-FLIM, spatiotemporal network

INTRODUCTION

Precise cell fate determination is key to proper establishment of multicellular body plans. Cell fate determination relies on accurately patterned gene expressions, which are in turn regulated by designated transcription factors (TFs). These “master regulator” TFs often do not function alone, but are required in different TF complexes via protein-protein interactions (Lemon and Tjian, 2000; Spitz and Furlong, 2012). Within their expression

domains, different TF complexes and their dynamics can generate distinct transcriptional outcome, thereby differentially regulating downstream targets and specifying various developmental processes in space and time (Spitz and Furlong, 2012). For example, during the segmentations of several animal species, different Hox TF complexes are spatially segregated to generate the correct body plan (reviewed by Ladam and Sagerström, 2014). Though expressed in largely separate bodily compartments, it has been suggested that Hox TFs and their numerous interactors can form different complexes with distinct activities in many overlapping domains, highlighting the significance of TF complex assembly in transcriptional regulations.

As plant cells cannot migrate nor reorganize in intact tissues, precise cell fates are determined by accurately patterned TFs. In the root of the model plant *Arabidopsis thaliana*, two GRAS-domain TFs SHORT-ROOT (SHR) and SCARECROW (SCR) bind and maintain the stem cell niche and contribute to the radial patterning by promoting asymmetric cell divisions (ACD). One of the ACD at the position of the stem cell cortex/endodermis initial (CEI) separates the two ground tissue layers: cortex and endodermis (Scheres et al., 1995a; Di Laurenzio et al., 1996a; Helariutta et al., 2000a; Cui et al., 2007a; Welch et al., 2007a).

Being a mobile protein, SHR moves out of the vasculature, where it localizes to both nuclei and cytoplasm, and is halted in the adjacent cell layer of QC, CEI and endodermis by SCR and several BIRD/INDETERMINATE DOMAIN (IDD) protein family members by nuclear retention (Fig. 1; Nakajima et al., 2001; Cui et al., 2007; Welch et al., 2007; Koizumi et al., 2012; Long et al., 2015). Within this “U-shaped” single cell layer, SHR-SCR complex can be detected in all three cell types, with enrichment in the CEI (Chapter 3).

SHR and SCR form a regulatory network with RETINOBLASTOMA-RELATED (RBR) to confine SHR-SCR activity in the CEI and quiescent center (QC) position (Cruz-Ramírez et al., 2012a, 2013). RBR physically binds SHR-SCR complex to repress its action on ACD, while the plant hormone auxin enhances the expression of a SHR-SCR target *CYCLIN D 6;1* (*CYCD6;1*) to phosphorylate RBR in a CYCD6;1-CDKB1 complex and

release SHR-SCR to induce ACD (Cruz-Ramírez et al., 2012a). Spatial control on ACD position is achieved by convergence of the longitudinal auxin gradient and the radial SHR distribution, together with protein degradation-driven network reset (Cruz-Ramírez et al., 2012a). A similar network is also found regulating the less frequent QC division, however *CYCD6* expression might be repressed by an unidentified factor in the QC, where ACD regulation might involve a different cyclin-CDK complex (Cruz-Ramírez et al., 2013).

The regulation of SHR-SCR pathway activity also relies on several BIRD/IDD family C2H2 zinc finger proteins. To ensure proper ground tissue separation, the BIRD proteins JACKDAW (JKD), MAGPIE (MGP) and NUTCRACKER (NUC) are required together with SCR as key SHR downstream targets and coregulators to activate ACD and specify endodermal cell fate (Long et al., 2015a). However, to prevent extra ACD, JKD redundantly acts with BALDIBIS (BIB) to restrict SHR outspread together with SCR by SHR nuclear trapping and repress the ACD-associated *CYCD6;1* expression (Long et al., 2015a). These BIRD/IDD proteins are expressed in overlapping domains with SHR-SCR complex in the QC, CEI and endodermis, and different interaction assays indicate that they bind to SHR, SCR and each other (Fig. 1; Welch et al., 2007; Long et al., 2015). Consequently, we asked whether BIRD proteins form distinct TF complexes with SHR and SCR in different cell types. To determine protein-protein interactions in their relevant developmental context, we performed Förster resonance energy transfer measurement by fluorescence lifetime microscopy (FRET-FLIM) in living Arabidopsis roots. We show that BIRD proteins form different cell type-specific complexes with SHR and SCR in living Arabidopsis roots: JKD-SHR was predominant in the QC and CEI, and JKD-SCR interaction occurred in the endodermis. SHR-SCR interaction is found predominantly present in the stem cells in wild-type (WT) roots, and mutant roots with extra ACD harbor increased SHR-SCR interaction, in agreement with SHR-SCR function in promoting ACD. Co-immuoprecipitation (Co-IP) show that JKD and SCR-SHR form a ternary complex, while binding assays demonstrate that BIRD proteins and RBR have the potential to reduce SHR-SCR association possibly through protein interaction competitions.

Collectively, our study allows spatial correlation of complex compositions with ACD

regulations in the roots and demonstrates that that a multicellular organism can regulate various cell fates by exchanging partners and/or conformations of TF complexes.

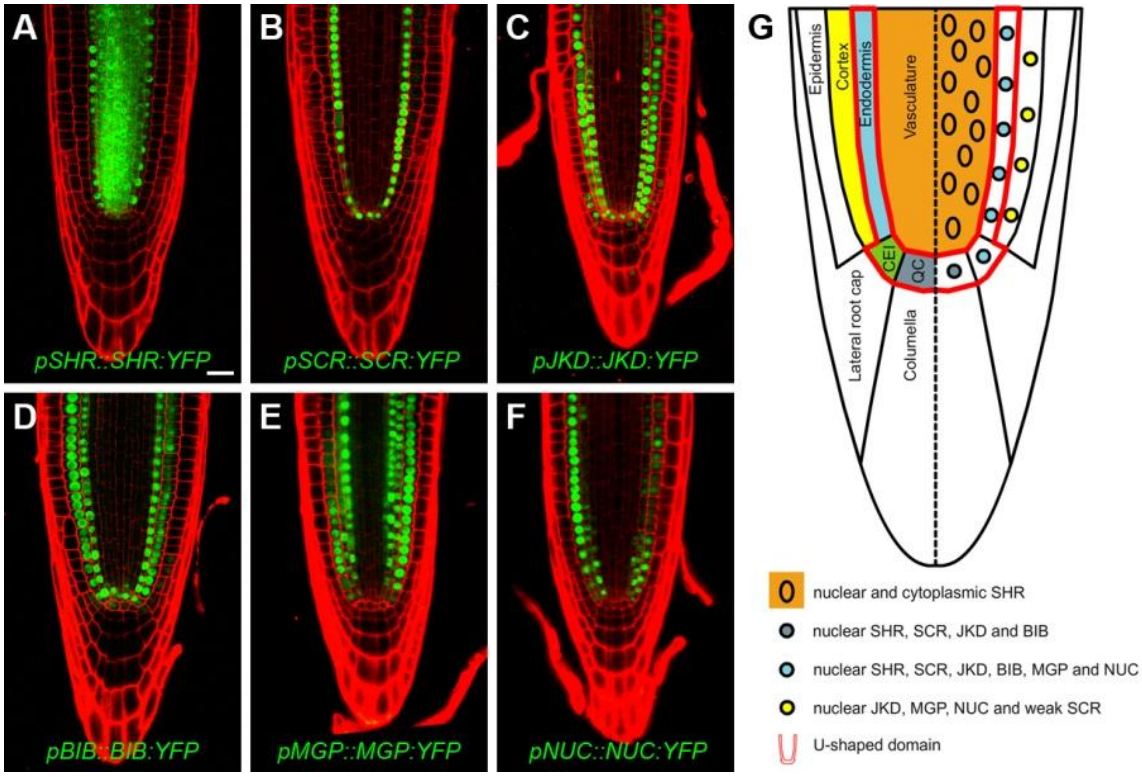

Fig. 1. Root expression patterns of SHR, SCR, JKD, BIB, MGP and NUC.

(**A-F**) Expression patterns of YFP fusions of SHR, SCR, JKD, BIB, MGP and NUC driven by their own endogenous promoters in the roots. Scale bar indicates 20μm. Images were rotated to vertical orientation, and the generated empty space were filled with black pixels to fill the panels. (**G**) Illustration of the Arabidopsis root meristem, with marked tissue types (left) and localization pattern of the six proteins (right). The "U-shaped domain" is encircled by bold red lines. QC, quiescent center; CEI, corte/endodermis initial.

RESULTS

JKD binds SHR and SCR in complementary patterns *in planta*

JKD localizes to the nuclei of QC, CEI, endodermis and cortex (Fig. 1; Welch et al., 2007; Long et al., 2015), overlapping the U-shaped domain where SHR-SCR complex was detected in the Arabidopsis roots (Chapter 3). JKD binds both SHR and SCR (Welch et al., 2007a; Long et al., 2015a), and regulates divisions along the radial root axis via SHR nuclear retention and differential regulation of two SHR-SCR targets, enhancing *SCR* while repressing *CYCD6;1* (Long et al., 2015a). As *SCR* and *CYCD6;1* are both

expressed within the U-shaped domain (Di Laurenzio et al., 1996a; Sozzani et al., 2010b), it is likely that JKD forms different protein complex configurations with SHR and SCR to regulate target expressions in cell type-specific manners. To test this, we measured interactions between JKD and SHR or SCR in their relevant spatial context of the root meristem by FRET-FLIM (Chapter 3) in living Arabidopsis roots.

First we established the JKD-SHR and JKD-SCR FRET pairs according to our optimization pipeline (described in Chapter 3) and found that, in Arabidopsis mesophyll protoplasts, both N- and C-terminal–tagged JKD showed high FRET efficiencies with C-terminal–tagged SHR and SCR (Fig. 2A, C). As C-terminal–tagged JKD rescued *jkd* phenotype (Hassan et al., 2010; Long et al., 2015a), we used this version for *in planta* FRET-FLIM analyses.

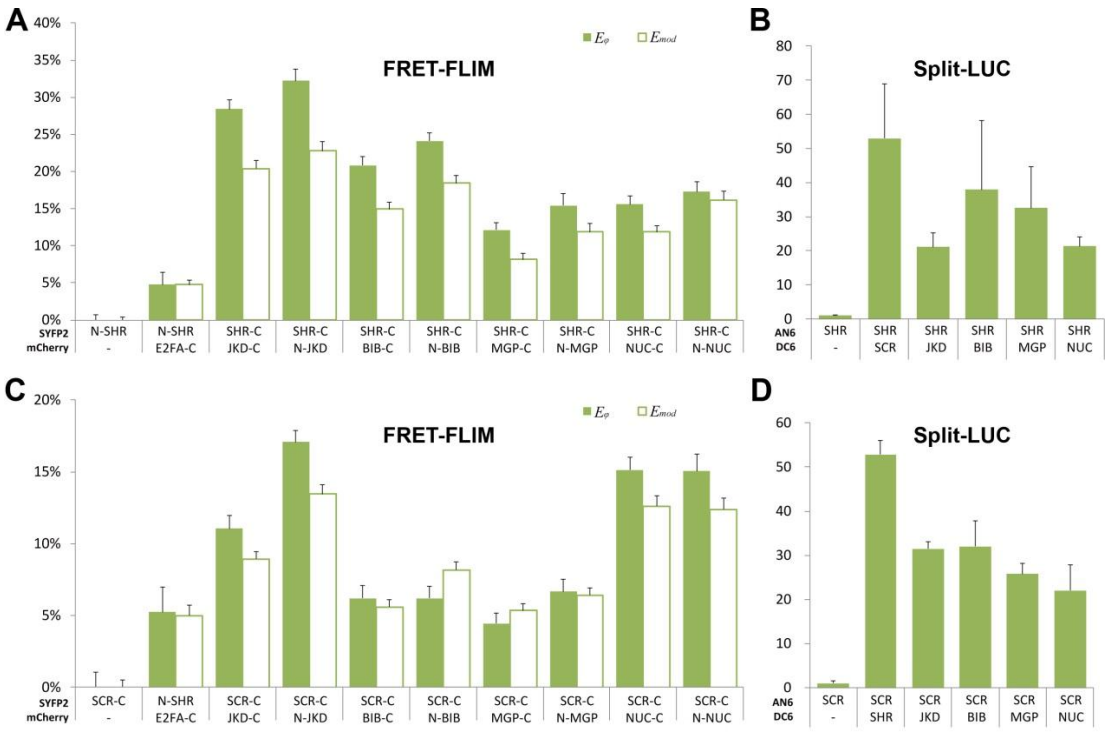

Fig. 2. FRET-FLIM optimization in Arabidopsis protoplasts.

(**A, C**) FRET quantification of phase efficiency (E_φ) and modulation efficiency (E_{mod}) between the studied BIRD/IDD proteins and SHR (**A**) or SCR (**C**). 60-120 protoplasts were measured for each sample. (**B, D**) Normalized quantification of the reconstituted luciferase activity of split-LUC assay determining binding between the studied BIRD proteins and SHR (**B**) or SCR (**D**). 3 biological replicas were performed. Error bars indicate standard errors.

Endogenous mRFP fusions of both *SHR* and *JKD* displayed suboptimal fluorescence level for FRET-FLIM (Chapter 3), which precluded using mRFP fusions for both proteins at endogenous levels. So we combined the bright *pSHR::SHR:Venus* (Chapter 3) with *JKD:mRFP* under the *SCR* promoter (*pSCR*) which is expressed higher in the JKD-SHR overlapping domain and rescued *jkd* phenotype (Fig. 3A; Hassan et al., 2010). We measured fluorescence lifetime of the YFP variant Venus in roots expressing *pSHR::SHR:Venus* and *pSCR::JKD:mRFP* and found that SHR:Venus lifetime significantly decreased in the QC and CEI nuclei in presence of JKD:mRFP, depicted by the blue-shift on the fluorescence lifetime heatmaps (Fig. 3B, C). This indicates that JKD and SHR interact in these cells.. In the endodermis where SHR and JKD also colocalize (Fig. 3A), such blue-shift was much less prominent (Fig. 3B, C), indicating reduced interaction. In the vasculature where JKD:mRFP is absent, SHR:Venus maintained its long lifetime (Fig. 3B, C), confirming the FRET-specific lifetime reduction in the QC and the CEI. Next, we quantified FRET cell-by-cell within the U-shaped domain and verified the distribution of FRET efficiency, with high peak in the QC, and medium in the CEI (Figure 3D).

Subsequently, we monitored YFP fluorescence lifetime in roots expressing *pJKD::JKD:SYFP2* and *pSCR::SCR:mRFP* (Fig. 3E), and found that JKD-SCR association displayed complementary pattern to JKD-SHR interaction, portrayed by lifetime reduction in the endodermal nuclei (Fig. 3F, G). In the cortex, no significant life time reduction of JKD:SYFP2 was detected, in agreement with the low abundance of cortical SCR:mRFP (Fig. 3F, G). Lifetime quantification confirms the FRET pattern (Fig. 3H), and suggests that JKD-SCR complex is enriched in the endodermis, moderately present in the CEI and excluded from the QC and cortex.

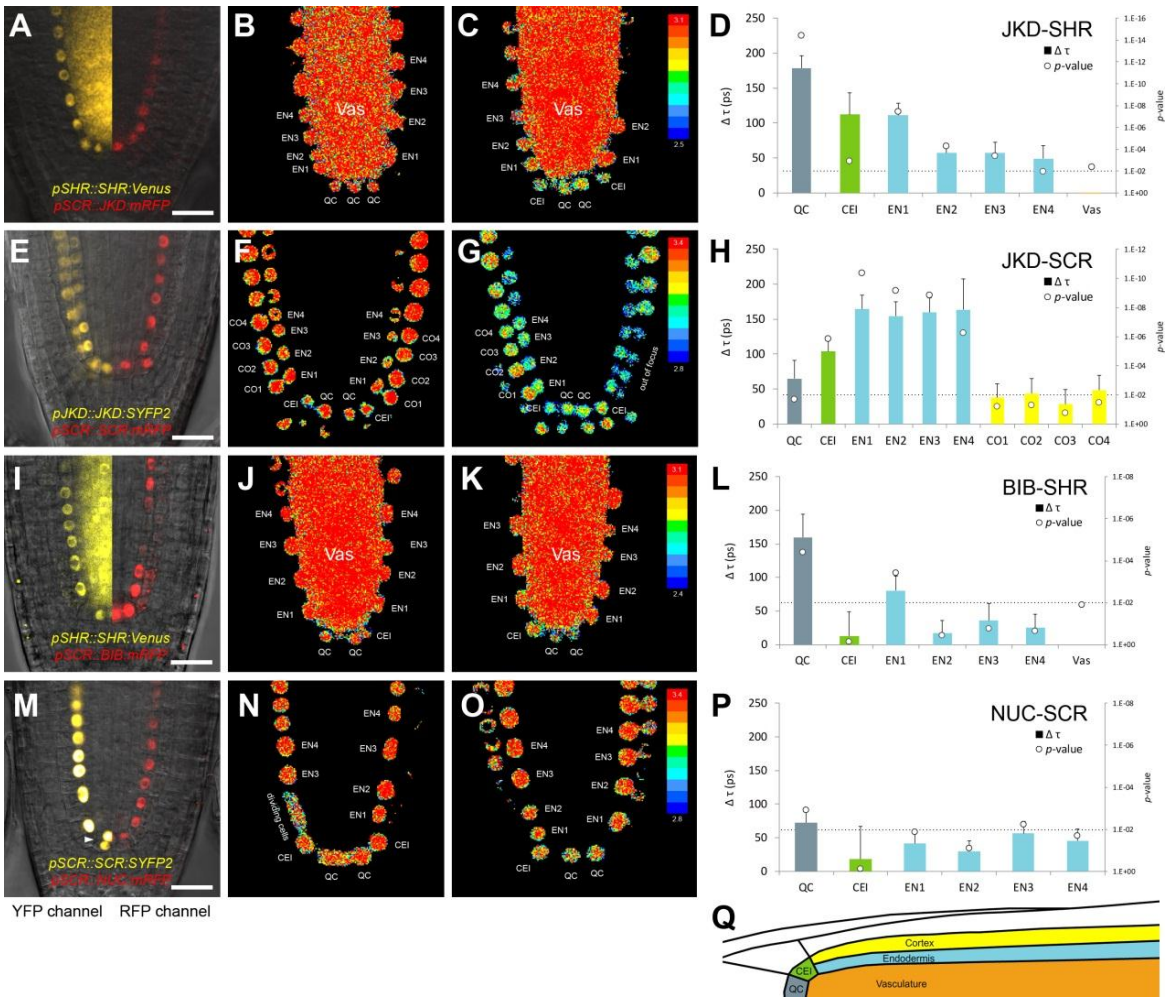

Fig. 3. FRET-FLIM of JKD-SHR, JKD-SCR, BIB-SHR and NUC-SCR in Arabidopsis roots.

FRET-FLIM measurements of *pSHR::SHR:Venus–pSCR::JKD:mRFP* (**A-D**, n=31 for SYFP2 donor-only samples and n=74 for FRET samples), *pJKD::JKD:SYFP2–pSCR::SCR:mRFP* (**E-H**, donor-only n=26, FRET sample n=68), *pSHR::SHR:Venus–pSCR::BIB:mRFP* (**I-L**, donor-only n=14, FRET sample n=25) and *pSCR::SCR:SYFP2–pSCR::NUC:mRFP* (**M-P**, donor-only n=8, FRET sample n=10) in WT Arabidopsis roots. (**A, E, I, M**) Root meristems with coexpression of each protein pair shown in YFP channel (left) and RFP channel (right). White arrowhead points to *pSCR::NUC:mRFP* induced QC division in (**M**). Scale bar indicates 20μm. (**B, F, J, N**) Fluorescence lifetime heatmaps of roots with donor (YFP fusion) expression only. (**C, G, K, O**) Fluorescence lifetime heatmaps of YFP fusions in roots with coexpression of each protein pair. (**D, H, L, P**) Bar chart represents cell-wise quantification of lifetime reduction of the YFP fusions in each protein pair, error bars indicate standard errors. Circles indicate *p*-value between donor-only and FRET sample measurements in each cell, dotted line marks the critical value of 0.01. Color of the columns in (**D, H, L, P**) indicates specific cell type, as illustrated in (**Q**). QC, quiescent center; CEI, cortex/endodermis initial; EN, endodermis; CO, cortex; Vas, vasculature.

BIB and NUC display distinct complex distributions compared to JKD

We have previously shown that at least three other BIRD proteins, BIB, MGP and NUC, interact with both SCR and SHR (Fig. 1; Welch et al., 2007; Long et al., 2015). Prior to

testing these interactions in living roots, we followed our FRET optimization pipeline (Chapter 3) in the Arabidopsis mesophyll protoplasts. Similar to JKD, both N- and C-terminal–tagged BIB, MGP and NUC were tested for binding to SHR and SCR (Fig. 2A, C). Prominent FRET was only measured from BIB-SHR and SCR-NUC combinations, while other BIB, NUC and MGP combinations with SHR or SCR yielded lower FRET efficiencies when compared to the negative control SHR-E2FA (Fig. 2A, C; Cruz-Ramírez et al., 2012), suggesting weak or no interactions. Other *in vivo* methods such as bimolecular fluorescence complementation (BiFC) and split Renilla luciferase (split-LUC) assays, however, confirmed that these BIRD proteins indeed interact with both SHR and SCR in protoplasts (Fig. 2B, D; Long et al., 2015). The observed differences between different assays indicate that the FRET levels might reflect the relative abundance of each heterodimer, or alternatively indicate that further optimization is required for protein pairs to achieve higher FRET efficiencies. In line of these limitations, we focused our further analysis on BIB-SHR and NUC-SCR protein pairs.

As endogenous *BIB* fusions displayed suboptimal fluorescence level for FLIM measurement we generated *pSCR::BIB:mRFP* to map FRET occurrence with *pSHR::SHR:Venus* in root nuclei (Fig. 3I). The lifetime heatmap indicates that BIB-SHR exhibited more FRET in the QC (Fig. 3J, K), similar to the JKD-SHR FRET pattern (Fig. 3B, C). Quantification confirmed the prominent BIB-SHR FRET in the QC but also revealed that, unlike JKD-SHR, FRET between BIB and SHR is not significant in the CEI or endodermis (Fig. 3L). This result implies that BIB-SHR complex is only abundant in the QC in the roots.

Thereafter, we checked FRET between NUC and SCR. NUC is expressed in the CEI, endodermis, cortex and pericycle of the root, and is largely excluded from the QC (Fig. 1; Long et al., 2015). However its endogenous level is low for sufficient FRET measurement, hence, we opted to enhance the NUC:mRFP level by expression under *pSCR* (Fig. 3M). Surprisingly, mild to no FRET were detected between NUC and SCR in the whole U-shaped domain of QC, CEI and endodermis (Fig. 3N, O). Interestingly, ectopic QC expression of *NUC* promoted QC divisions (Fig. 3M), consistent with its potential role in

inducing divisions, yet quantification indicates that ectopic QC NUC-SCR FRET is significant but barely detectable (Fig. 3P).

Enrichment of SHR-SCR complex correlates with CEI-like ACD

Previously we have shown that SHR-SCR complex is enriched in the CEI (Chapter 3). This enrichment correlates with the complex's function in inducing CEI divisions in WT and ectopic divisions in *pSCR::SHR:mRFP* expressing roots (Chapter 3), where endodermis repetitively divide in a CEI-like manner (Nakajima et al., 2001a). Extra SHR-SCR–dependent ACD are also found in roots with *JKD* knockdown (*jkd-i*) by RNA interference (RNAi) (Fig. 4B'; Welch et al., 2007). To examine if SHR-SCR binding is also associated with these extra ACDs in *jkd-i*, we thus measured florescence lifetime of SYFP2-SHR in the newly divided ground tissue cells with clear SHR nuclear localization, and found that FRET between SHR and SCR increased significantly in these cells comparing to WT endodermis (p<0.001), similar to the level in the WT CEI (p=0.55) (Fig. 4D). In *jkd-i* roots, *SCR* expression is abolished in the QC (Welch et al., 2007a), thus no FRET was measured (Fig. 4D; Fig. S1A-A'"; Welch et al., 2007). CEI is morphologically difficult to identify in *jkd-i*, so we did not quantify FRET at this position (Fig. 4D).

RBR knockdown by RNAi (*rbr-i*) induces ectopic cell divisions in both QC and ground tissue (Fig. 4C; Wildwater et al., 2005; Cruz-Ramírez et al., 2012, 2013). In addition, RBR binds to SCR and represses the SHR-SCR activity in inducing ACD (Cruz-Ramírez et al., 2012a). To assess the effect of reducing RBR level on SHR-SCR binding, we measured the FRET level in *rbr-i* lines. Similar to *jkd-i*, endodermal SHR-SCR FRET also exhibited a general increase in *rbr-i* roots (Fig. 4D). Additionally, we observed an enhanced SHR-SCR FRET level in the QC (Fig. 4D), where it correlates with the described phenotype of high QC division rate in *rbr-i* in a SHR-SCR–dependent manner (Wildwater et al., 2005b; Cruz-Ramírez et al., 2013).

Taken together, these results confirm that SCR-SHR complex is prominent in cells that

are in states of active ACD.

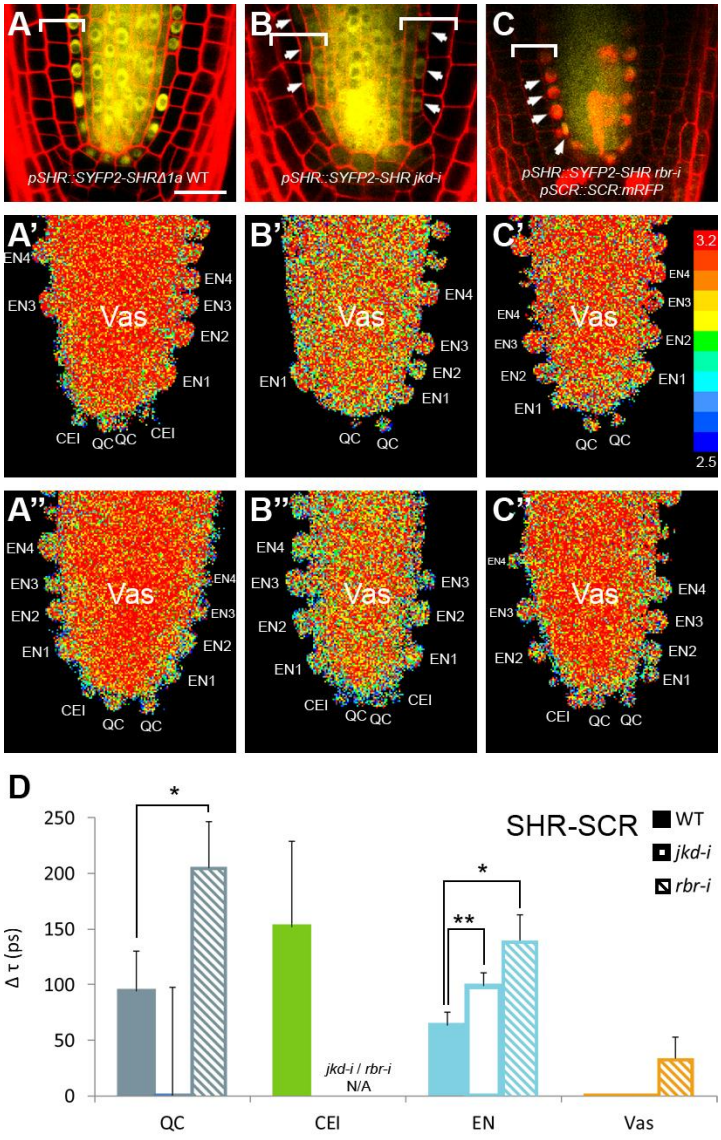

Fig. 4. FRET-FLIM measurements of SHR-SCR in mutant backgrounds.

(**A-C**) Root meristems of WT (donor-only n=25, FRET sample n=32), *jkd-i* (donor-only n=8, FRET sample n=5) and *rbr-i* (donor-only in WT n= 26, FRET sample n=4) lines. Brackets indicate ground tissue, note the extra divisions. White arrows point to examples of the measured nuclei. Red patches in *rbr-i* mark cell deaths specific to this background (**C**). Scale bar indicates 20μm. (**A'-C"**) Fluorescence lifetime heatmaps of roots expressing *pSHR::SYFP2-SHRΔ1a pSCR::SCR:mRFP* in WT (**A', A"**), *jkd-i* (**B', B"**) and *rbr-i* (**C',C"**). Upper penals are with *SYFP2-SHR* donor only (**B', C', D'**), and the lower panels are heatmaps with coexpression of both fusion constructs (**B", C", D"**). (**D**) Quantification of fluorescence lifetime reduction of SHR-SCR FRET pair in WT, *jkd-i* and *rbr-i*. For SHR-SCR in *jkd-i*, ground tissue cells with clear SHR nuclear localization and subjected to ACD were named "EN" (**C', C"**) and measured and plotted in the "EN" position on the bar chart to compare with SHR-SCR FRET in endodermis (**D**). QC, quiescent center; CEI, cortex/endodermis initial; EN, endodermis; Vas, vasculature; N/A, not available.

Strong JKD interaction to SHR and SCR requires the SHR-SCR complex

The increased SHR-SCR complex in the ground tissue of *jkd-i* and *rbr-i* indicates that JKD and RBR can repress SHR-SCR association. As RBR can bind SCR (Cruz-Ramírez et al., 2012a) while JKD binds both SHR and SCR (Welch et al., 2007a), we hypothesized that JKD and RBR might reduce SHR-SCR complex by protein binding competition. To test this without the interference of plant-specific transcriptional regulations, we performed split-LUC competition assays in the HeLa cells as a heterologous system. As shown in Figure 5A, SHR and SCR fused with each half of luciferase interacted readily in HeLa cells, showing more than 30-time increase of the reconstructed luciferase activity comparing to the ground level activity where only half of the luciferase is fused with SHR. Addition of JKD reduced SHR-SCR interaction by 66% (Fig. 5A), indicating that JKD indeed strongly interferes with SHR-SCR association. Expression of MGP, NUC and RBR also decreased SHR-SCR interaction, albeit to weaker extends by approximately one third (Fig. 5A). Addition of free mCherry or SYFP2 did not change SHR-SCR binding in HeLa cells (Fig. 5A), confirming the specificity of competitions. These results imply that JKD, MGP, NUC and RBR can reduce SHR-SCR association possibly through protein interaction competitions and independently from plant-specific downstream transcriptional regulations.

Our FRET-FLIM analysis *in planta* showed that JKD binds strongly to SHR or SCR in different cell types. To test if these binding specificities are also the result of protein interaction competitions, we performed binding competition assay also for JKD-SHR and JKD-SCR complexes in the HeLa system. Strikingly, JKD binding to SHR and SCR are much weaker than SHR-SCR interaction in HeLa cells, with approximately 1.5-time luciferase activity in both cases comparing to ground level (Fig. 5B, C). Interestingly, addition of SCR increased JKD-SHR interaction to roughly 3 times of ground level (Fig. 5B), while additional SHR boosted JKD-SCR association to 16 times compared to ground level (Fig. 5C). Addition of free mCherry or MGP could not alter JKD binding to SHR or SCR (Fig. 5B, C). These data indicate that instead of competition, JKD requires SHR to strongly bind SCR, and *vice versa*. Given the fact that JKD did not abolish SHR-SCR

interaction (Fig. 5A), it is likely that JKD binds strongly to the SHR-SCR complex, and suggest formation of a SHR-SCR-JKD ternary complex. Indeed, Co-IP from transfect tobacco leaves indicates that SHR, SCR and JKD can form ternary complex (Fig. 5D).

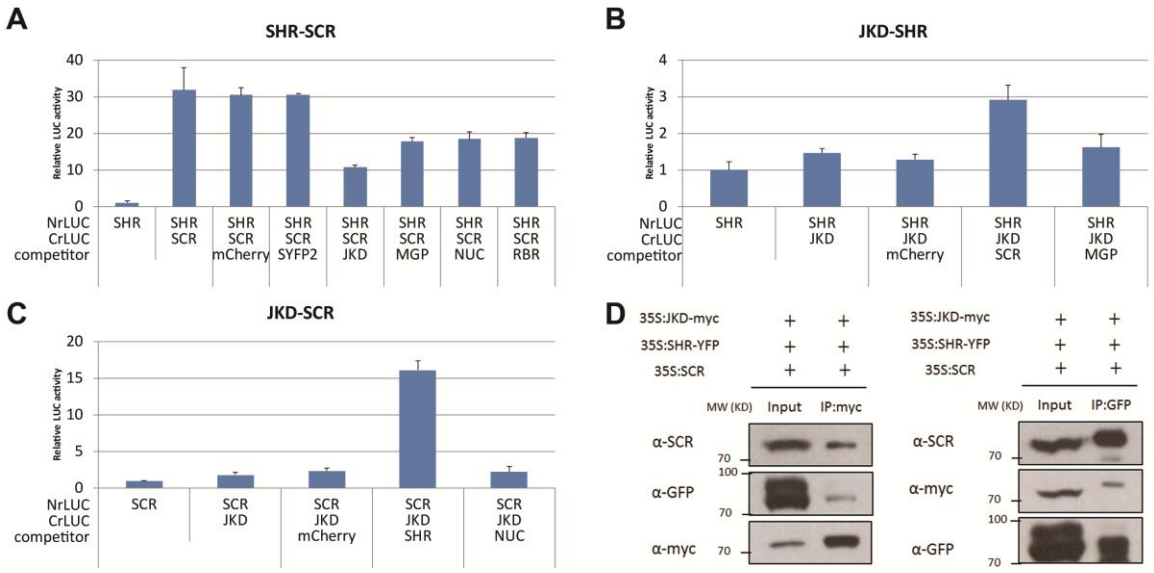

Fig. 5. SHR, SCR and JKD form ternary complex.

(**A-C**) Protein binding competition tested by split-LUC assay in HeLa cells. Error bars indicate standard deviations. (**D**) Co-immunoprecipitation of SHR, SCR and JKD from transfected tobacco leaves.

BIB-SHR and NUC-SCR complexes are also enhanced in *jkd* mutant

In WT roots, SCR and SHR predominantly bind to JKD or each other, meanwhile BIB-SHR complex formed in the QC and NUC-SCR complex was almost undetectable (Fig. 3). To test if JKD was interfering with BIB-SHR and NUC-SCR interactions, we measured FRET occurring in BIB-SHR and NUC-SCR pairs in the *jkd* mutant roots.

For FRET measurements, we used lines where BIB and NUC were expressed under *SCR* promoter. Expressing *pSCR::BIB:mRFP* in *jkd* roots rescued the ectopic division phenotype, consistent with the redundant role of BIB and JKD in restricting extra ACD (Fig. 6A). In these rescued roots, BIB-SHR showed similar FRET pattern to JKD-SHR in the WT, namely that BIB-SHR FRET was not only highly found in the QC, but also moderately in the CEI and endodermis (Fig. 6B comparing to Fig. 3D). Since *JKD* and *BIB* are partially redundant in regulating root patterning (Long et al., 2015a), it is likely that BIB and JKD can form similar complexes with SHR, but JKD is the preferred SHR partner to

regulate their common transcriptional targets.

Contrastingly, *pSCR::NUC:mRFP* did not rescue the ectopic ACD in *jkd* roots, even though sufficient fluorescent signal can be detected in the cortex and endodermis for both NUC:mRFP and SCR:SYFP2 (Fig. 6C). This is consistent with NUC playing different role in ground tissue regulation comparing to BIB (Long et al., 2015a). In addition, NUC-SCR exhibited detectable and statistically significant FRET efficiency in the endodermis and the QC (Fig. 6D). In the cortex, NUC and SCR also displayed similar FRET level to endodermis, while insufficient data points were acquired for CEI (Figure 5D). The increased NUC-SCR complex in the *jkd* roots suggests that JKD might prevent NUC-SCR interaction by forming JKD-SCR complexes, thereby limiting free SCR for NUC binding. Additionally, this also indicates that NUC-SCR complex is relevant for ACD regulation, a function attributed for *NUC* and *SCR* genetically (Long et al., 2015a).

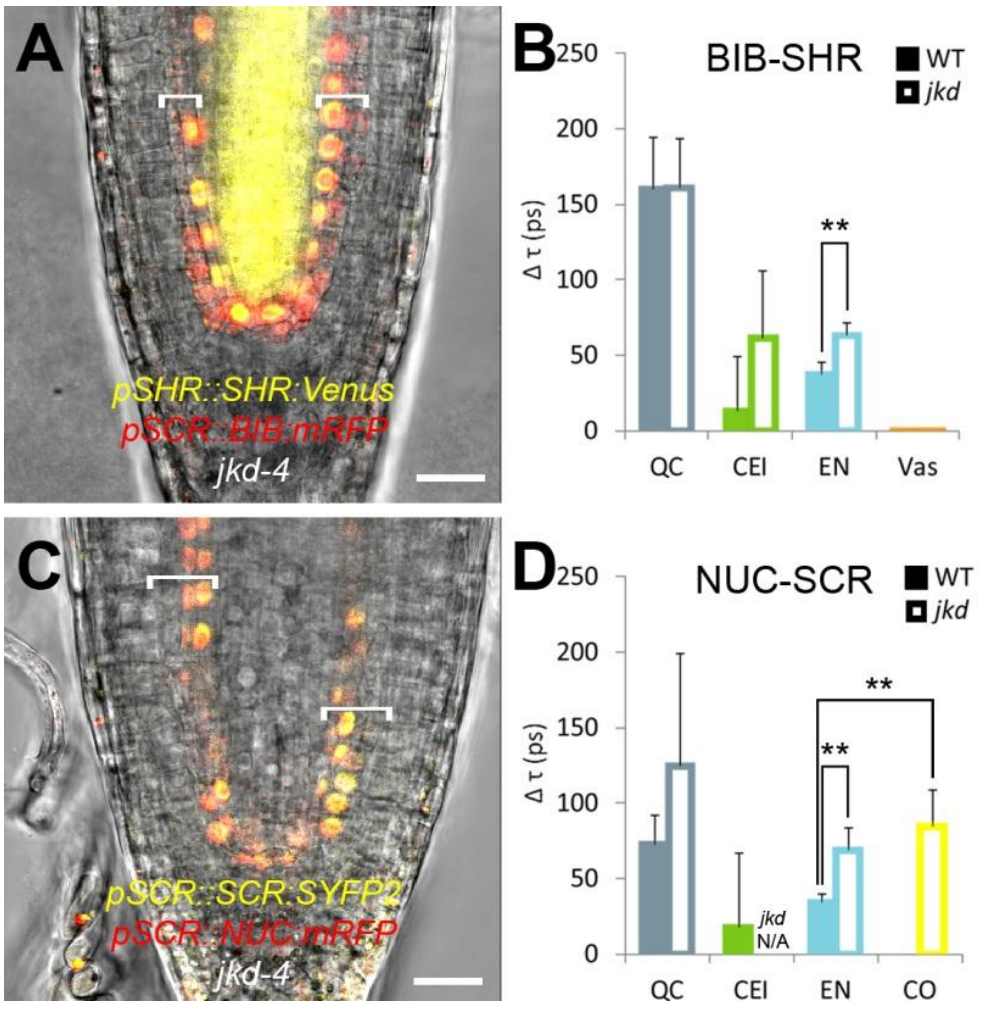

Fig. 6. FRET-FLIM measurements of BIB-SHR and NUC-SCR in *jkd* mutant.

(**A**) Coexpression of *pSHR::SHR:Venus* and *pSCR::BIB:mRFP* in *jkd* root. Brakets indicate ground tissue. Note the extra division phenotype of *jkd* is rescued in root expression *pSCR::BIB:mRFP*. Scale bars indicate 20μm. (**B**) Cell-wise quantification of fluorescence lifetime reduction of BIB-SHR FRET pair in WT and *jkd* (n=17). As *pSCR::BIB:mRFP* rescued the extra divisions in *jkd*, donor-only in WT was used (n=14). (**C**) Coexpression of *pSCR::SCR:SYFP2* and *pSCR::NUC:mRFP* in *jkd* root. Brakets indicate ground tissue. Scale bars indicate 20μm. (**D**) Cell-wise quantification of fluorescence lifetime reduction of NUC-SCR FRET pair in WT and *jkd* (donor-only n=4, FRET sample n=11). * indicates the *p*-value is smaller than the significance level 0.05, while ** indicates $p<0.01$ (**B, D**). Error bars indicate standard errors in (**B, D**). QC, quiescent center; CEI, cortex/endodermis initial; EN, endodermis; CO, cotex; N/A, not available.

DISCUSSION

In this report, we used FRET-FLIM measurements to identify the spatial distribution of several plant TF complexes consisting of SHR, SCR, JKD, BIB and NUC in the growing root tip of Arabidopsis plant. Combining our previous report on SHR-SCR complex distribution in the QC, CEI and endodermis (Chapter 3), we generated a protein "interaction map" in living roots (Fig. 7). The map highlights the different TF complex compositions in the three cell types of QC, CEI and endodermis: in the QC SHR mainly interacts with JKD and BIB with a moderate SCR interaction. The endodermis is predominated by JKD-SCR complex and also a moderate SHR-SCR level. In the CEI, however, the tested JKD homologs seem to bind less efficiently to SHR and/or SCR, while SHR-SCR complex level is specifically enriched (Fig. 7). The particular distribution pattern of these TF interactions indicates that, despite general coexpression in multiple tissues, certain TF complexes are only favored in one specific cell type. As FRET is sensitive to small distances between tested molecules (less than 10nm), proteins sitting on the far ends of a relatively big complex can exhibit low or no FRET. Thus, the tested proteins might form higher level complexes, and the detected FRET-FLIM data indicate different complex configurations. Our preliminary data indicate this is most likely the case, as Co-IP revealed a SHR-SCR-JKD ternary complex, while interaction studies in HeLa cells using split luciferase system showed that JKD-SCR and JKD-SHR complexes are enriched by adding either SHR or SCR, respectively. When SHR, SCR and JKD were coexpressed in HeLa cells, JKD-SCR is much more abundant than JKD-SHR, suggesting that the "JKD-SCR" variant of the ternary complex is the "default mode", as was also

found in the endodermis. These data also indicate that the spatial complex distribution observed with FRE-FLIM reflects the active complex and not specific heterodimers.

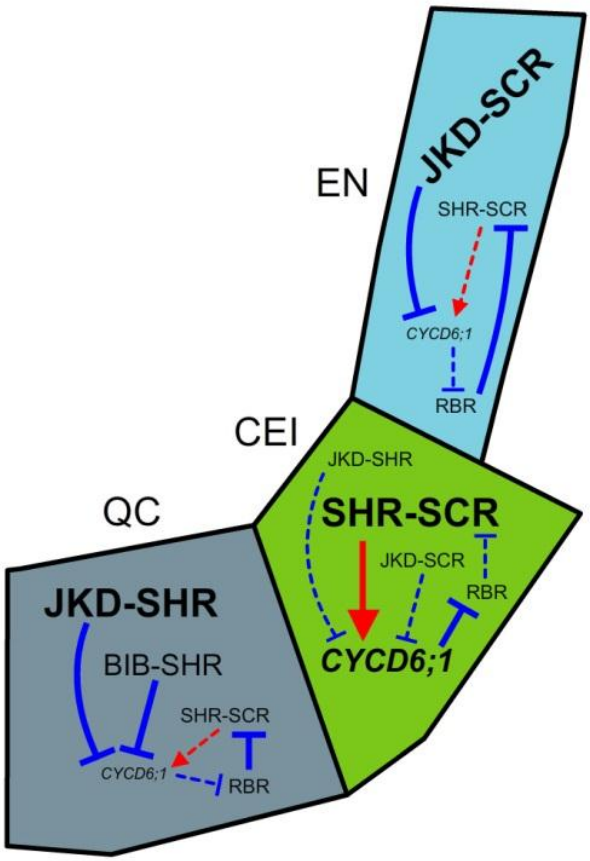

Fig. 7. Spatiotemporal network regulating ACD.

The spatial protein complex distribution and the cellular sub-networks in the QC, CEI and endodermis. Red arrows indicate activation, blue flat-end arrows indicate repression. Font size reflects the abundance of protein complex or *CYCD6;1* level. QC, quiescent center; CEI, cortex/endodermis initial; EN, endodermis.

In HeLa cells, JKD-SHR was also enhanced with additional SCR, albeit to lower extend, indicating that whenever there are abundant “JKD-SCR”, there should also be a certain amount of “JKD-SHR”. Upon JKD coexpression, SHR-SCR abundance decreased but was not depleted. Taken together with the presence of ternary complex, the default “high JKD-SCR, low JKD-SHR and low SHR-SCR” interaction profile in the endodermis indicates one specific higher order complex configuration, rather than of three different complexes. Other complex configurations found in QC and CEI indicate that there are uncharacterized interaction competitions or facilitations involved in establishing cell type-specific differences.

The cell type-specific complex configurations we identified spatially correlate with their potential biological functions during root development. For example, the CEI division and *CYCD6;1* expression are both SHR- and SCR-dependent (Sozzani et al., 2010b; Cruz-Ramírez et al., 2012a), and their occurrence in WT root is focused to the CEI position where SHR-SCR interaction within a complex is the highest (Chapter 3). While in the QC, JKD and BIB preferentially binds SHR either to prevent ACD through repressing specific QC cyclin, or alternatively JKD and BIB might change SCR-SHR conformation to activate target genes required for QC specification and maintenance such as *SCR* (Sabatini et al., 2003) and *WUSCHEL-RELATED HOMEOBOX 5* (*WOX5*; Sarkar et al., 2007). In the endodermis, JKD and BIB would bind SCR to repress unwanted divisions and *CYCD6;1* expression promoted by the SCR-SHR complex. This complex configuration is also likely to confer endodermal specification, and analyzing the complex's activity on key targets for this process is necessary to confirm the hypothesis.

We also demonstrated that JKD is a buffering molecule for the TF complex compositions, as when genetically removed the complex distribution largely changes in accordance to their functions. JKD-redundant BIB binds more SHR to prevent divisions, while SHR-SCR level inevitably increases along the extra cell divisions. Interestingly, the almost non-existing NUC-SCR interaction increased in the ectopically dividing cells in *jkd* background, indicating that JKD normally prevents NUC-SCR interaction. Additionally, NUC-SCR complex is associated with the extra divisions in *jkd* roots in both the QC and ground tissue, supporting their roles as positive regulators of cortex-endodermis separation (Long et al., 2015a). It is possible that NUC, similar to JKD and BIB, can also transcriptionally enhance *SCR* expression, resulting in the increased NUC-SCR abundance in the *jkd* cortex. NUC-SCR observed only in the absence of JKD, suggesting that JKD might prevent NUC from binding to SCR and activating divisions. Ectopic QC expression of *NUC* also induced ACD, and it is likely that *NUC* and thus NUC-SCR complex are largely kept away from QC in WT roots to prevent these undesired divisions. The absence of NUC-SCR complex in the CEI, however, seems to suggest that NUC might interact with other yet unidentified molecules to execute the CEI division, or its

close homolog MGP redundantly takes over its role in WT conditions. The possibilities remain to be tested. Nevertheless, these data indicate that there can be extensive cross-regulations between protein complexes and the expression of complex components, and suggest a very plausible auto-regulating system.

Previously it has been reported that a regulatory network consisting of SHR, SCR and RBR are responsible to restricting the CEI-like divisions to the stem cell niche, although it did not explain how such division is repressed in the QC (Cruz-Ramírez et al., 2012a). Our current report introduces other players to explain the distinct behaviors of QC and CEI; it is likely that RBR, another SCR interactor, is also involved in the establishment of distinct TF complexes in the root, as SHR-SCR complex is also elevated in the *rbr-i* background. Completing the "interaction map" with SHR/SCR binding to RBR, MGP and inter-BIRD interactions and identifying their actions on specific target gene expressions will be essential to fully understand the dynamics of the complex distribution conformation pattern and its role in cell specification and regulation of ACD. Resolving the molecular structure of the SCR-SHR-BIRD complexes will also be critical to determine their exact composition, binding conformation and binding sites. In addition, identifying how the complexes bind to DNA and dissecting the binding motifs will be the next steps toward understanding the mechanism of transcriptional regulation.

Taken together, we demonstrate that different TF complexes are associated with different states among neighboring cells in the Arabidopsis root. The next challenge will be to decipher different complexes' functions and the mechanism which generates this dynamic interaction pattern. For the former, transcriptional analysis will be necessary; while for the latter, protein competition assays will explain the formation and configuration of different complexes. Given both transcriptional dependencies and protein interactions, a combination of these mechanisms might be at the basis of the conformation switches that we report here.

MATERIAL AND METHODS

DNA constructs

JKD, *BIB*, *MGP* and *NUC* coding sequences (CDS) were cloned with primers listed in Supplementary Table 1 and subcloned into pGEMTeasyR2R3 for generating N-terminal fusions downstream of the cauliflower mosaic virus *35S* promoter and *mCherry* by MultiSite Gateway® cloning (Invitrogen). Other constructs for FRET-FLIM measurements are as described in Long et al. (2015) and Chapter 3. For split-LUC assay in protoplasts, entry clones containing CDS of *SHR*, *SCR*, *JKD*, *BIB*, *MGP* and *NUC* (Long et al., 2015a) were introduced to pDuEx-An6 and pDuEx-Dc6 by Gateway recombination (Fujikawa and Kato, 2007). For split-LUC assay in HeLa cells, vectors were generated from HeLa expression vectors described in Long et al. (2015) by substituting the fluorescence protein tag with N- or C-ternimal half of LUC (NrLUC or CrLUC). Primers used for subcloning NrLUC and CrLUC are listed in Supplementary table 1. NrLUC-SHR was created from SYFP2-SHR; SHR-NrLUC from SHR-SYFP2 with a linker of 2 times Gly-Gly-Gly-Gly-Ser in addition to the restriction site; SCR-CrLUC from SCR-mTurquoise and CrLUC-JKD from mCherry-JKD with same linkers for SHR-NrLUC.

Plant growth and transformation

Growth conditions of *Arabidopsis thaliana* are as described by Sabatini et al. (1999). Mutant and transgenic lines used are as follows: *jkd-4* and *jkd-i* (Welch et al., 2007a), *rbr-i* (Wildwater et al., 2005b). *In planta* FRET-FLIM constructs were introduced into wild-type *Arabidopsis thaliana* ecotype Colombia-0 (Col-0) by floral dipping (Clough and Bent, 1998). FRET-FLIM double construct lines in wild-type and mutant backgrounds were generated by crossing.

Transient split-LUC assay in protoplast and HeLa cells

A. thaliana Col-0 mesophyll protoplasts were prepared according to Long et al. (2015). Recombined pDuEx-An6 and pDuEx-Dc6 constructs of 2µg each were cotransfected with

1µg of the constitutive *pUBQ::Firefly-LUC* vector. Luciferase activities were measured by using the Dual-Luciferase® Reporter Assay System in a GloMax® 96 Microplate Luminometer (Promega). The obtained LUC levels were normalized using Firefly luciferase, and the relative ratio was determined by comparing this to the obtained with the single transfected pDuEx-An6 fusion samples as described in Cruz-Ramírez et al. (2012).

HeLa cells were transfected according to Long et al. (2015). Cells were transfected with 100ng NrLUC fusion, 100ng CrLUC fusion and 300ng competitor. Vectors used are as followed: NrLUC-SHR and SCR-CrLUC for SHR-SCR interaction; SHR-NrLUC and CrLUC-JKD for JKD-SHR interaction; SCR-NrLUC and CrLUC-JKD for JKD-SCR interaction. Free mCherry, free SYFP2, SHR-SYFP2, SCR-mCherry, JKD-SYFP2, MGP-mCherry, NUC-mCherry and RBR-SYFP2 were used as competitors. Luciferase activity was measured and calculated as described above.

Fluorescence lifetime measurements

FRET-FLIM measurements and analysis in mesophyll protoplasts and Arabidopsis roots are as described in Chapter 3. Frequency-domain FRET-FLIM was performed for protoplast measurements, while time-domain FRET-FLIM for roots. For protoplast measurements, 60-120 cells were measured for each sample. Root measurements are as followed: JKD-SHR, *pSHR::SHR:Venus* in WT (n=31) and coexpression of *pSHR::SHR:Venus* and *pSCR::JKD:mRFP* in WT (n=74). JKD-SCR, *pJKD::JKD:SYFP2* in WT (n=26) and coexpression of *pJKD::JKD:SYFP2* and *pSCR::SCR:mRFP* in WT (n=68). BIB-SHR, *pSHR::SHR:Venus* in WT (n=14) and coexpression of *pSHR::SHR:Venus* and *pSCR::BIB:mRFP* in WT (n=25). NUC-SCR, *pSCR::SCR:SYFP2* in WT (n=8) and coexpression of *pSCR::SCR:SYFP2* and *pSCR::NUC:mRFP* in WT (n=10). SHR-SCR, *pSHR::SYFP2-SHRΔ1a* in WT (n=25) and coexpression of *pSHR::SYFP2-SHRΔ1a* and *pSCR::SCR:mRFP* in WT (n=32). SHR-SCR in *jkd-i*, *pSHR::SYFP2-SHRΔ1a* in *jkd-i* (n=8) and coexpression of *pSHR::SYFP2-SHRΔ1a* and

pSCR::SCR:mRFP in *jkd-i* (n=5). SHR-SCR *rbr-i*, *pSHR::SYFP2-SHRΔ1a* in WT (n=26) and coexpression of *pSHR::SYFP2-SHRΔ1a* and *pSCR::SCR:mRFP* in *rbr-i* (n=4). BIB-SHR in *jkd*, *pSHR::SHR:Venus* in WT (n=14, as SHR showed different distribution in *jkd* comparing to roots rescued with *pSCR::BIB:mRFP*, so WT was selected for FRET control) and coexpression of *pSHR::SHR:Venus* and *pSCR::BIB:mRFP* in *jkd* (n=17). NUC-SCR in *jkd*, *pSCR::SCR:SYFP2* in *jkd* (n=4) and coexpression of *pSCR::SCR:SYFP2* and *pSCR::NUC:mRFP* in *jkd* (n=11).

Co-immunoprecipitation and immunoblot assays

The Co-immunoprecipitation (Co-IP) experiments were performed according to published procedure Liu et al. (2010). Briefly, Agrobacterium with binary vectors containing CDS of SCR, SHR:GFP and JKD:myc were infiltrated into *N. benthamiana* leaves. The infiltrated leaf tissues were harvested, grounded in liquid nitrogen and resuspended in native extraction buffer [50mM TRIS-MES pH 8.0, 0.5M sucrose, 1mM $MgCl_2$, 10 mM EDTA, 5mM Dithiothreitol, protease inhibitor cocktail CompleteMini tablets (Roche)] on ice. Total extract was centrifuged at 16000g at 4°C for 15 minutes and protein complexes were captured using the uMACS GFP beads (Miltenyi Biotec) and c-myc beads (Santa Cruz).

For immunoblot analysis, proteins were separated by SDS-PAGE in a 10% acrylamide gel and electroblotted. Bands were detected with the Amersham ECL western blotting detection reagents (Amersham). Antibodies used in these experiments were as follows: anti-Myc antibody (sc-40, Santa Cruz), anti-GFP antibody (Roche), anti-SCR antibody (Santa Cruz), donkey anti-goat HRP-conjugated antibody, and goat anti-mouse HRP-conjugated antibody.

Confocal microscopy and image processing

Confocal microscopy was performed using a Zeiss LSM710 confocal as described in Long et al. (2015), or a Leica SP8 confocal with the same spectrum settings. Contrast of

confocal images was enhanced for fluorescence visualization, and roots were rotated to have vertical orientation. Resulted empty space was filled with black pixels to have rectangular panels (Fig. 1A-F).

SUPPLEMENTARY DATA

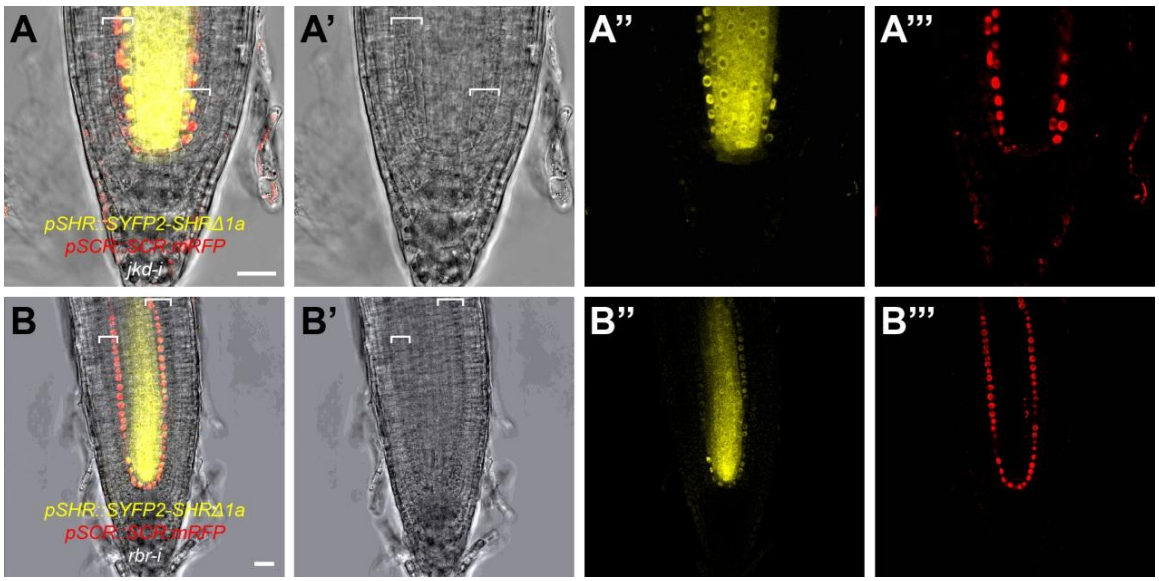

Fig. S1. Root meristems coexpressing SHR-SCR in mutant backgrounds

Coexpression of *pSHR::SYFP2-SHRΔ1a* and *pSCR::SCR:mRFP* in *jkd-i* (**A-A'''**) and *rbr-i* root (**B-B'''**). Brackets indicate the ground tissue. Note the extra division phenotype of *jkd* is rescued in root expression *pSCR::BIB:mRFP* (C-C'''). Scale bars indicate 20μm.

Primer name	**Sequence (5'-3')**
JKD-R2R3 F	GGGGACAGCTTTCTTGTACAAAGTGGCTATGCAGATGATTCCAGGAGATCC
JKD-R2R3 R	GGGGACAACTTTGTATAATAAAGTTGCTCATCAACCCAATGGAGCAAACC
BIB-R2R3 F	GGGGACAGCTTTCTTGTACAAAGTGGCTATGATGATGCCAGATGATCATC
BIB-R2R3 R	GGGGACAACTTTGTATAATAAAGTTGCTTACTGGTTCATGTCGGCGGTTGG
MGP-R2R3 F	GGGGACAGCTTTCTTGTACAAAGTGGCTATGACAACTGAAGATCAGAC
MGP-R2R3 R	GGGGACAACTTTGTATAATAAAGTTGCTCAAATCCATCCATTGATAGAGGAAGAATGG
NUC-R2R3 F	GGGGACAGCTTTCTTGTACAAAGTGGCTATGACAAGTGAAGTTCTTCAAACAATC
NUC-R2R3 R	GGGGACAACTTTGTATAATAAAGTTGCTCAAATCCATCCATTGATAGACGATGG

	ATGG
SHR-NrLUC BamHI F	CGGGATCCCGGCGGCGGCGGCAGCGGCGGCGGCGGCAGCATGGCTTCCAAGGTGTACG
SHR-NrLUC NotI R	TTTTCCTTTTGCGGCCGCTCAGCCACCCTTAACGAGAGG
NrLUC-SHR AfeI F	GCTAGCGCTCATGGCTTCCAAGGTGTACG
NrLUC-SHR BsrGI R	TTGTGTACAGTGTACAGGCCACCCTTAACGAGAGG
SCR-CrLUC AgeI F	TTGACCGGTGGGCGGCGGCGGCAGCGGCGGCGGCGGCAGCATGAAGCCCGACGTCGTCC
SCR-CrLUC NotI R	TTTTCCTTTTGCGGCCGCTCACTGCTCGTTCTTCAGCACG
CrLUC-JKD AfeI F	GCTAGCGCTCATGAAGCCCGACGTCGTCC
CrLUC-JKD EcoRI R	GGAATTCCCGCCGCCGCTGCCGCCGCCGCCCTGCTCGTTCTTCAGCACG

Supplementary Table 1. Primers used in this study.

Chapter 5

Site-directed mutagenesis in JACKDAW reveals a potential mechanism of target regulation by subnuclear compartmentalization

Yuchen Long[1,2], Wim de Jonge[2], Wouter Smet[1,2], Wenkun Zhou[1], Joachim Goedhart[3], Theodorus W.J. Gadella, Jr[3], Ben Scheres[1,2], Ikram Blilou[1,2]

[1]Plant Developmental Biology, Plant Sciences, Wageningen University, Droevendaalsesteeg 1, Wageningen, 6708PB, The Netherlands.

[2]Molecular Genetics, Department Biology, Padualaan 8, Utrecht, 3581CH, The Netherlands.

[3]Swammerdam Institute for Life Sciences, Section of Molecular Cytology, van Leeuwenhoek Centre for Advanced Microscopy, University of Amsterdam, Science Park 904, Amsterdam, 1098 XH, The Netherlands.

ABSTRACT

In Arabidopsis root, the zinc finger protein JACKDAW binds the mobile transcription factor SHORT-ROOT to restrict its intercellular movement and attenuates its transcriptional regulatory activity. In an attempt to assess how JACKDAW could physically achieve these functions, we modeled and analyzed JKD protein structure and created multiple mutants by site-directed mutagenesis. Detailed analysis of JACKDAW expression indicates that it has a punctuated subnuclear localization, and can superpose this localization on SHORT-ROOT. In addition, our site-directed mutagenesis approach revealed two JACKDAW mutants in its zinc finger domains that are still interacting with SHR, but show opposite effects on SHORT-ROOT nuclear localization and target regulation. The first mutant could transfer SHORT-ROOT into subnuclear bodies and repress the expression of two SHORT-ROOT targets, *SCARECROW* and *CYCLIN D 6;1*, resulting in delayed ground tissue separation. The second mutant abolished the punctuated nuclear localization of SHORT-ROOT, failed to restrict SHORT-ROOT movement and could not

rescue the extra ground tissue divisions in *jackdaw* mutant. Taken together, we provide evidence for a role of JACKDAW subnuclear compartmentalization in regulating target gene expressions.

INTRODUCTION

Plants form cellular patterns via strictly controlled cell divisions. In the root of *Arabidopsis thaliana*, the ground tissue (GT) encompasses two cell types, the outer cortex and the inner endodermis, which separate the epidermis from the central vasculature (Figure S1; Dolan et al., 1993). Cortex and endodermis originate from asymmetric cell divisions (ACDs) of one stem cell population, the cortex/endodermis initials (CEI), and precise GT pattern formation relies on a regulatory network involving transcriptional regulators such as SHORT-ROOT (SHR), SCARECROW (SCR), RETINOBLASTOMA-RELATED (RBR) and the BIRD proteins (Di Laurenzio et al., 1996a; Helariutta et al., 2000a; Cruz-Ramírez et al., 2012a; Long et al., 2015a). Subset of these proteins can form various protein complexes in different cell types, suggesting that they might differentially regulate the expressions of their downstream targets to trigger different cell behaviors (Long et al., 2015; Chapter 3; Chapter 4). For example, SHR-SCR complex is particularly enriched in the CEI or ectopically dividing GT cells in mutants with extra ACD, where they are required for the ACD and activation of the CEI-enriched expression of *CYCLIN D 6;1* (*CYCD6;1*) (Chapter 3; Chapter 4).

The BIRD protein JACKDAW (JKD) binds differentially to SHR and SCR: it interacts predominantly with SHR in the quiescent center (QC) and preferentially to SCR over SHR in the endodermis (Chapter 4). In CEI, JKD binds moderately to both SHR and SCR (Chapter 4). Together with JKD's effect on *SCR* activation and *CYCD6;1* repression (Long et al., 2015a), this suggests that JKD displays different spatial complex configurations that correlates with different target gene expression to promote specific cell fates. To gain insights on how JKD exerts its function in SHR movement restriction, it is important to identify motifs required for interaction with SHR and its nuclear retention, as well as

regulating JKD-mediated target transcription.

JKD belongs to the BIRD/INDERTERMINATE DOMAIN (IDD) protein family characterized by the conserved ID domain (Colasanti et al., 2006b; Welch et al., 2007a; Long et al., 2015a). The ID domain, consisting of ~170 amino acids (a.a.), starts with a putative nuclear localizing signal (NLS) and contains four C2H2 type, or so-called "classical", zinc finger motifs (Figure 1a; Kozaki et al., 2004; Colasanti et al., 2006). C2H2 type zinc finger motifs harbor two conserved cysteine and two histidine residues to bind a zinc ion and fold into a ββα structure containing an N-terminal β-hairpin and a C-terminal α-helix (Klug and Schwabe, 1995). C2H2 zinc finger motifs and their C2HC variants are known to bind DNA, RNA and proteins (Klug, 1999; Brown, 2005; Hall, 2005; Brayer and Segal, 2008). For instance, the maize IDD protein INDETERMINATE1 (ID1) uses its zinc fingers to bind a specific DNA sequence (Kozaki et al., 2004a), while JKD and it homolog MAGPIE (MGP) can bind SHR and SCR proteins through their N-terminal portions which harbor the zinc finger domains (Welch et al., 2007a). Additionally, JKD and its homologs can also bind the promoters of *SCR* (*pSCR*), *MGP* (*pMGP*) and *SCARECROW-LIKE3* (*pSCL3*) by their N-terminal regions which contain the zinc finger domains (Ogasawara et al., 2011a; Yoshida et al., 2014a). Thus it is possible that JKD mediate protein-protein and protein-DNA interactions with its zinc finger domains.

Despite the potential role of the zinc finger domains in mediating JKD-SHR complex formation and its transcriptional activity, little is known about the specific motifs and a.a. residues required for this interaction and/or transcriptional regulations. In an attempt to identify such motifs, we performed a mutant screen in JKD's ID domain, and isolated two mutants (we named JKD^{H133D} and JKD^{sub30}) with different effect on nuclear localization and ability to regulate divisions in the GT. Our first mutant (JKD^{H133D}) with alteration in a semi-conserved motif in the second zinc finger of JKD translocated itself to specific subnuclear regions seemingly away from DNA, and repressed ACD in the GT in *jkd* background, resulting into patches of undivided GT. The other mutant (JKD^{sub30}), with disturbed fourth zinc finger, failed to retain SHR into nuclei, restrict its movement or rescue *jkd* root phenotype while enhancing the expression of *SCR* and *CYCD6;1*. These

findings show that the second and fourth zinc fingers of JKD have different regulatory functions. Additionally, we show that mutation in the second zinc finger also triggers subnuclear relocation of the JKD homologs MAGPIE (MGP) and NUTCRACKER (NUC) but not BALDIBIS (BIB). Taken together, we show that JKD employs different protein domains to partition interactors into nuclear subdomains and to adjust target expression.

RESULTS

JACKDAW protein structure analysis and prediction

To decipher the structural base for JKD's binding capacity to its interactors, such as SHR, we first attempted to resolve its 3D structure *in silico*. Since no crystal structure is available for JKD, we opted to predict JKD structure using the homology modeling module of the YASARA software package (Krieger et al., 2009).

As shown in Figure 1b, homology modeling was able to recreate the four C2H2 zinc finger motifs, in agreement with previous predictions (Colasanti et al., 2006b), wrapping around the major groove of a superficial double-helix DNA fragment. The rest of the protein, however, showed poorly resolved structure: the N-terminal portion upstream the zinc fingers was predicted largely unstructured, while the C-terminal half exhibited several helices without clear ternary structures (Figure 1b). Lacking an overall predicted structure suggests that JKD might not share homology with any structurally-resolved proteins outside the zinc finger domains.

Interestingly, besides the four zinc ions in the four zinc fingers, the homology model also predicted binding capacity for two extra zinc molecules: one lying in the N-terminal strand bound by two histidines H20 and H24 (Figure 1d), the other situating between an antiparallel 2-stranded β-sheet and an α-helix in the C-terminal half (Figure 1e), similar to the structure of a C2H2 zinc finger. However the β-strands and α-helix are not consecutive, but are dispersed among the 314-316, 397-399 and 469-480 a.a positions (Figure 1a, e). Thus, the C-terminus of JKD might fold into a novel type of zinc finger.

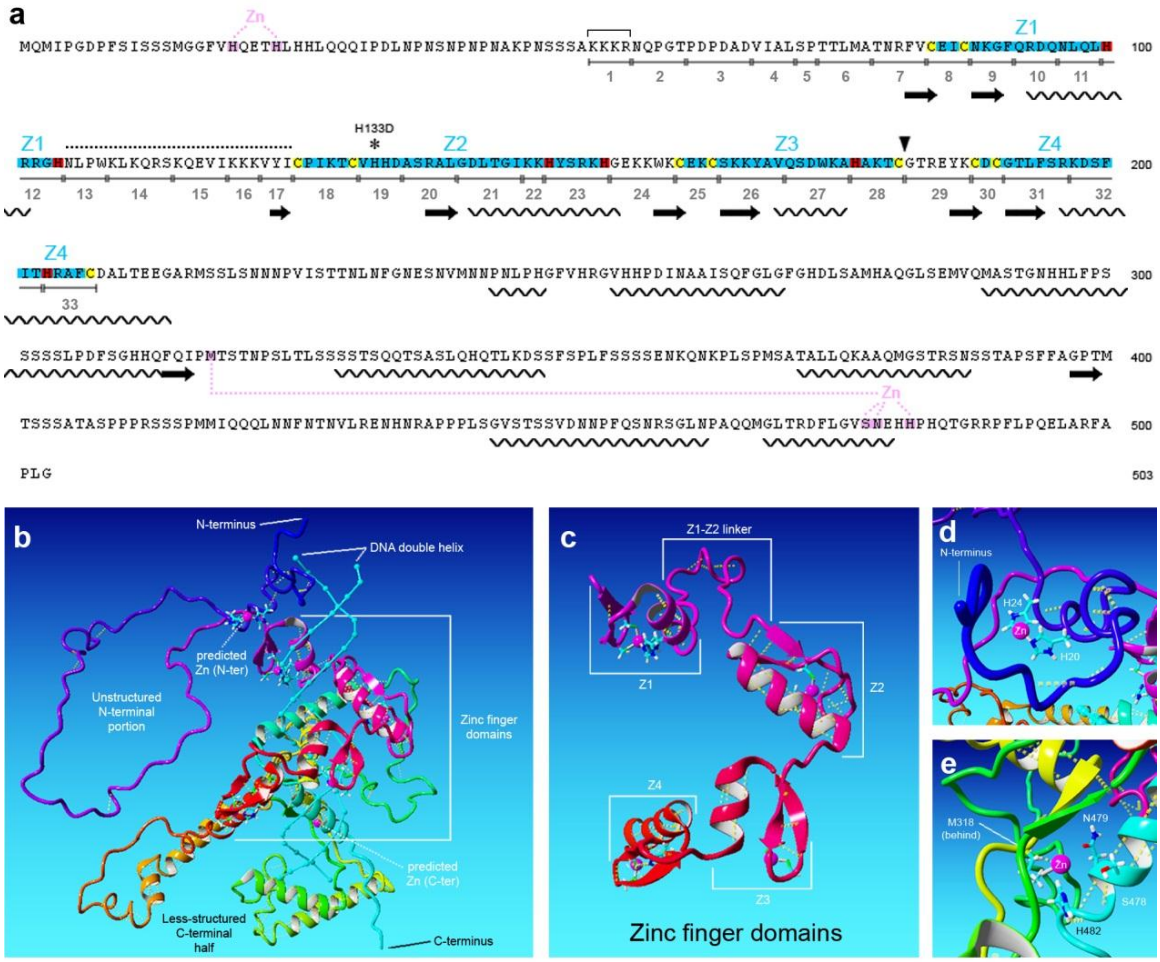
a
Zn
Z1
MQMIPGDPFSISSSMGGFVHQETHLHHLQQQIPDLNPNSNPNPNAKPNSSSAKKKRNQPGTPDPDADVIALSPTTLMATNRFVCEICNKGFQRDQNLQLH
100
Z1
H133D
Z2
Z3
Z4
RRGHNLPWKLKQRSKQEVIKKKVYICPIKTCVHHDASRALGDLTGIKKHYSRKHGEKKWKCEKCSKKYAVQSDWKAHAKTCGTREYKCDCGTLFSRKDSF
200
Z4
ITHRAFCDALTEEGARMSSLSNNNPVISTTNLNFGNESNVMNNPNLPHGFVHRGVHHPDINAAISQFGLGFGHDLSAMHAQGLSEMVQMASTGNHHLFPS
300
33
SSSSLPDFSGHHQFQIPMTSTNPSLTLSSSSTSQQTSASLQHQTLKDSSFSPLFSSSSENKQNKPLSPMSATALLQKAAQMGSTRSNSSTAPSFFAGPTM
400
Zn
TSSSATASPPPRSSSPMMIQQQLNNFNTNVLRENHNRAPPPLSGVSTSSVDNNPFQSNRSGLNPAQQMGLTRDFLGVSNEHHPHQTGRRPFLPQELARFA
500
PLG
503
b
N-terminus
DNA double helix
predicted Zn (N-ter)
Unstructured N-terminal portion
Zinc finger domains
predicted Zn (C-ter)
Less-structured C-terminal half
C-terminus
c
Z1-Z2 linker
Z1
Z2
Z4
Z3
Zinc finger domains
d
N-terminus
H24
Zn
H20
e
M318 (behind)
N479
Zn
S478
H482
f
JKD
N
Z1
Z2
Z3
Z4
C
Predictors
DisEMBL-465
DisEMBL-HL
ESpritz-DisProt
ESpritz-NMR
ESpritz-XRay
IUPred-long
IUPred-short
JRONN
VSL2b
58.65 %
32.01 %
32.80 %
01.39 %
68.39 %
58.85 %
67.40 %
55.07 %
66.20 %
76.74 %
Predicted Structure
Predicted Disorder
Disorder Deposition
P-FIT
VSL2B
VL3
VLXT
Residue Index
g
Z1
Z2
Z3
Z4
JKD CEICNKGFQRDQNLQLHRRGHNLPWKLKQRSKQEVIKKKVYICPIKTCVHHDASRALGDLTGIKKHYSRKHGEKKWKCEKCSKKYAVQSDWKAHAKTCGTREYKCDCGTLFSRKDSFITHRAFC 207
BIB CEVCNKGFKRDQNLQLHRRGHNLPWKLKQRTNKEQVKKKVYICPEKTCVHHDPARALGDLTGIKKHFSRKHGEKKWKCDKCSKKYAVMSDWKAHSKICGTKEYRCDCGTLFSRKDSFITHRAFC 193
MGP CEICGKGFQRDQNLQLHRRGHNLPWKLKQRTSKE-VRKRVYVCPEKSCVHHHPTRALGDLTGIKKHFCRKHGEKKWKCEKCAKRYAVQSDWKAHSKTCGTREYRCDCGTIFSRRDSFITHRAFC 194
NUC CEVCGKGFQRDQNLQLHRRGHNLPWKLKQRTSKE-VRKRVYVCPEKTCVHHHSSRALGDLTGIKKHFCRKHGEKKWTCEKCAKRYAVQSDWKAHSKTCGTREYRCDCGTIFSRRDSFITHRAFC 191

Figure 1. Amino acid sequence and homology model of JKD.

(**a**) Amino acid sequence of JKD, where predicted α-helix (zig-zag line) and β-strand (bold arrow) marked below the sequence. The predicted nuclear localizing signal (NLS) marks the start of ID domain (bracket). The four zinc fingers (Z1-Z4) are highlighted as blue, with their zinc-binding cysteine and histidine residues highlighted as yellow and red. The Z1-Z2 linker is marked with dotted lines. Possible extra zinc binding residues are selected based on side chain properties and facing, and are lighlighted as pink. Extra predicted zinc ions are also marked in pink. Asterisk marks the histidine residue substituted in JKD^{H133D}. Black arrow head marks the of N- and C-terminal JKD truncations site in Welch et al. (2007). (**b-d**) 3D ribbon model of the predicted JKD structure showing the whole protein and a superposed DNA fragment (**b**), the isolated zinc finger domains (**c**) and the predicted extra zinc ions in the N-terminal (**d**) and C-terminal (**e**). Predicted and possible zinc binding residues with side chains are depicted as stick model. Predicted hydrogen bonds are shown as yellow dotted lines, zinc ion as magenta balls. (**f**) Intrinsic disorder analysis of JKD protein. Corresponding position of zinc finger domains are marked by dotted lines. Middle panel shows the intrinsic disorder prediction by multiple tools on MobiDB website. Lower panel shows the intrinsic disorder prediction on Disprot website, the Y axis indicating level of predicted disorder disposition, with 0 indicating structural feature while 1 indicating disorder. (**g**) Alignment of the zinc finger domains of JKD, BIB, MGP and NUC. Red highlights small plus hydrophobic residues (AVFPMILW), blue acidic (DE), magenta basic (RK) and green other residues (STYHCNGQ). Asterisk (*) marks fully conserved residues, while codon (:) and dot (.) mark residues with strongly or weakly similar properties.

The lack of overall predicted structure also suggests that JKD may contain intrinsically disordered protein (IDP) domains. IDPs lack stable structures due to their a.a. sequence characteristics, and are known to carry out many biological functions, such as mediating protein-protein, protein-nucleotide interactions and regulating cellular signaling (Oldfield and Dunker, 2014; Wright and Dyson, 2015). Agreeing with the homology model, a collection of IDP predictions on the MobiDB database website indicate that the regions outside the zinc finger domains of JKD are indeed likely disordered (Figure 1f; Potenza et al., 2014; http://mobidb.bio.unipd.it/entries/Q700D2). An independent prediction with four prediction tools (P-FIT, VSL2B, VL3 and VLXT) also yielded similar results that JKD contains large IDP regions outside the zinc finger domains (Figure 1f; Obradovic et al., 2003, 2005; Xue et al., 2010; http://www.disprot.org/metapredictor.php).

JKD structural modeling indicates presence of four well-structured N-terminal C2H2 zinc fingers, one potentially novel C-terminal zinc finger, and large disordered regions.

Sequence analysis of the zinc finger domains of BIRD proteins

Binding between JKD and SHR requires the N-terminal half of the JKD protein, where the zinc fingers are located (Welch et al., 2007a). As the N-terminal portion upstream of the zinc fingers was predicted unstructured, we focused on the conserved zinc finger domains for further analysis.

JKD, as other IDD proteins, harbors 4 zinc fingers, Z1, Z2, Z3 and Z4 (Colasanti et al., 2006b). Z1 and Z2 are C2H2 zinc fingers, and are separated by a 21 amino acid (a.a.) spacer (Figure 1a, dotted line), while Z3 and Z4 are C2HC variants. Z2, Z3 and Z4 are spaced by linkers of 6 a.a. length, effectively forming a triple finger cluster (Figure 1a; Iuchi, 2001). The linker distribution suggests that Z2-Z4 might function together, while Z1 is spatially separated and might function differently. Alternatively, the long Z1-Z2 linker might loop and bring Z1 closer to the Z2-Z4 cluster (Figure 1c).

The zinc finger domains of the BIRD proteins are highly conserved (Welch et al., 2007a), with BIB, MGP and NUC sharing similar zinc finger arrangements as JKD, and most residues share conserved properties (Figure 1g). Several less conserved residues actually share similar structural properties (i.e. several a.a. with different properties are interchangeable for specific secondary structures such as α-helix, β-strand or turn), while one charged island strikes out immediately downstream of the zinc-binding cysteines of Z2, where JKD and BIB have a histidine-histidine-aspartate stretch (HHD, positive-positive-negative at near-physiological condition), while MGP and NUC have an all positive tri-histidine stretch (HHH) instead (Figure 1g, bracket). This stretch sits in the turn of the β-sheet, seems exposed to the outside of the protein, and might have specific function between the two conserved sub-clades of BIRD proteins.

The structural-sequence analysis of BIRD zinc finger domains reveals that they are highly conserved with only subtle differences, and the functional specificities of BIRD may either lie within these different residues or in the other parts of the protein.

Identification of SHR-binding motifs in the ID domain of JKD

To identify motifs in JKD potentially required for SHR interaction and nuclear retention, we created several JKD mutant variants by site-directed mutagenesis in the ID domain (Figure 1a) and tested for their binding capacity to SHR in the yeast two-hybrid (Y2H) system.

To cover the whole ID domain, 33 domains of 2 to 6 a.a. length were selected and numbered as 1 to 33, respectively (Figure 1a). Using deletions ($^{\Delta}$) or Alanine-substitutions (^{sub}), we found that yeast colonies with combinations of SHR and JKD mutants of domain 16, 18, 19, 25, 30 and 33 exhibited reduced growth to different levels (Table 1), indicating that these motifs might be required for JKD-SHR binding.

Among the domains which altered JKD-SHR binding in the Y2H system, domain 16 represents a newly identified tri-lysine (KKK) putative NLS located in the Z1-Z2 spacer; domain 18 covers the two zinc-binding cysteine residues of Z2; domain 19 consists of a valine (V) and the HHD stretch mentioned above; domain 25 contains the two zinc-binding cysteine residues of Z3; while domain 30 and 33 cover all four zinc-chelating residues in Z4, respectively. The Y2H analysis suggested that the Z1-Z2 linker and the Z2-Z3-Z4 triple-finger cluster of JKD contribute to SHR binding, while Z1 seems less likely to be involved in JKD-SHR interaction.

Substitutions of domain 19 and 25 resulted in much reduced interaction to SHR, while substitutions of domain 30 and 32 seemingly abolished SHR interaction. Primarily, we chose two representative mutations and focused on domain 19 and 30to further quantify the Y2H interaction between SHR and two of the JKD mutants: JKD^{sub19} with all-alanine substitutions (VHHD to AAAA), and JKD^{sub30} with alanine substitutions at the two zinc-chelating cysteine residues (CDC to ADA) to break Z4. Using *lacZ* as reporter gene, we found that JKD^{sub19} effectively halved the binding to SHR, while JKD^{sub30} abolished interaction to SHR *in vitro*, confirming the effect of these motifs in the Y2H selection system (Figure 2b). The effect of mutations in domain 25 and 32 are currently under analysis.

Deletions	Autoactivation	SHR Y2H	Substitutions	Autoactivation	SHR Y2H
WT	30	++	WT	30	++
Δ1	50+	++			
Δ2	20	++			
Δ3	10	++			
Δ4	10	++			
Δ5	10	++			
Δ7	35	++			
Δ8	35	++			
Δ9	20	++			
Δ10	20	++			
Δ12	20	++	Sub12 AAAAA	30	++
			Sub12 ARRGA	5	++
Δ13	35	++			
Δ14	50+	++			
Δ16	20	+/-	Sub16 AAA	N/A	++
Δ18	30	++	Sub18 AAAAAA	20	+
			Sub18 APIKTA	20	+
Δ19	30	++	Sub19 AAAA	5	+/-
Δ23	20	++	Sub23 AYSRKA	10	++
Δ24	10	++			
Δ25	10	+	Sub25 AAAA	10	+/-
Δ26	10	++	Sub26 AAAAAA	5	++
			Sub28 AAKTA	10	++
			Sub30 ADA	5	-
			Sub33 ARAFA	5	-
			Sub33 ARAFC	5	-

Table 1. Yeast 2-hybrid analysis between SHR and JKD mutants.

Substituted amino acids are underlined. Autoactivation is tested on –HT dropout medium with 3-AT supplement (mM). Alanine-substituted amino acids are underlined. Colony growth indicates interaction level, and is marked as: ++, strong growth; +, positive growth; +/-, scarce growth; -, no growth.

In vivo JKD-SHR interaction is enhanced by mutations in domain 19 or 30

To assess whether the mutations in JKD domain 19 and 30 affect SHR binding in plant cells, we performed split Renilla luciferase (SplitLUC) assay and Förster resonance energy transfer (FRET) assay to measure interactions between SHR and JKD^{sub19}, JKD^{sub30} and a point mutation at a.a. position 133 in JKD, substituting the first histidine residue of domain 19 into aspartic acid (JKD^{H133D}, VHHD to VDHD). Surprisingly, both assays in plant cells indicate that JKD-SHR interaction is not reduced by mutations in

these motifs, as suggested by Y2H assay, but rather enhanced (Figure 2e, f).

The *in vitro* and *in vivo* analyses suggested opposite conclusions for the interaction between SHR and JKD^{H133D} or JKD^{sub30}. However, because JKD and SCR have known transcriptional effects (readout of Y2H, Figure 2a), we surmised that the Y2H interactions were influenced by this characteristic. Therefore, we relied on the *in vivo* assays and concluded that JKD^{H133D} and SHR most likely exhibit strong interaction in plant cells (for details, see Discussion).

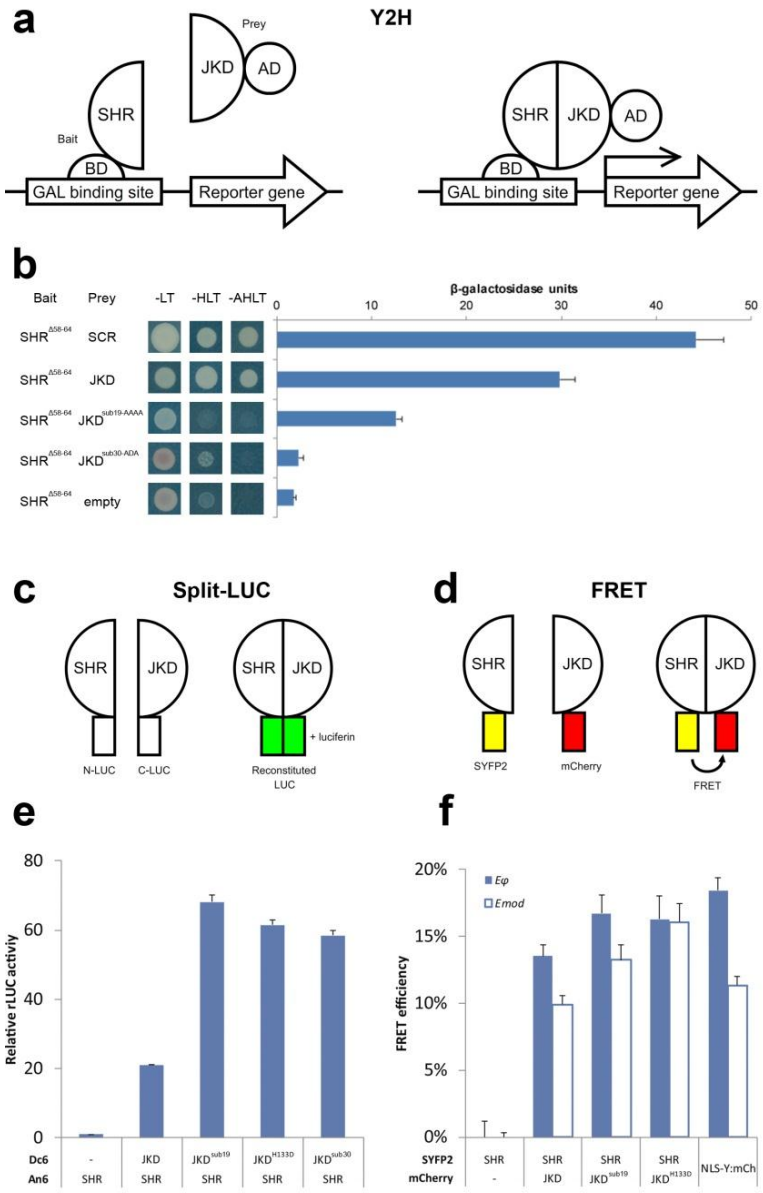

Figure 2. Interaction analysis of JKD zinc finger mutants.

(**a**) Principle of Y2H, where SHR is fused to the binding domain (BD) or GAL4 as bait and JKD with activation domain (AD) as prey. Upon interaction, AD drives report gene expression. (**b**) SHR and JKD interactions indicated by yeast colony growth on dropout medium and β-galactosidase reporter activity measured by CPRG assay. A non-aoutoactivating variant of SHR ($SHR^{\Delta 58\text{-}64}$) was used as bait, SHR-SCR pair was used as positive control, and SHR with an empty pDest22 vector was used as negative control. (**c**) Principle of split-LUC, where SHR and JKD are fused with the N- and C-terminal halves of Renilla luciferase. Upon interaction, the reconstituted luciferase generates light with the substrate luciferin. (**d**) Principle of FRET, where SHR and JKD are fused with SYFP2 or mCherry. Upon interaction, FRET occurs between the fluorophores, resulting into fluorescence lifetime reduction of SYFP2. (**e**) Split-LUC assay of SHR and JKD mutants. Note that all three mutants showed higher interaction than wild-type JKD to SHR. (f) FRET-FLIM analysis of SHR and JKD mutant interaction. The phase FRET efficiency (E_{φ}) and the modulation FRET efficiency (E_{mod}) both indicate that the tested JKD mutants showed increased interaction to SHR than wild-type JKD. Error bars indicate standard errors.

Mutations in different JKD motifs altered JKD nuclear localization

While expressed in the protoplasts for FRET-FLIM analysis, we noticed that JKD^{H133D} exhibited specific subnuclear localization (Figure 3). To assess this in detail, we monitored the localization of JKD:mRFP, JKD^{H133D}:mRFP and JKD^{sub30}:mRFP driven by the constitutive cauliflower mosaic virus *35S* promoter in protoplasts. Interestingly, JKD:mRFP exhibited a rather punctuated nuclear localization (Figure 3a, a') which was not previously observed in roots under endogenous promoter. JKD^{H133D}:mRFP is predominantly concentrated in certain subnuclear compartments (Figure 3b, b'), while JKD^{sub30}:mRFP displayed a more homogenous localization in the nucleoplasm comparing to JKD:mRFP (Figure 3c, c'). These data indicate that JKD^{H133D} and JKD^{sub30} exerted opposite effects on JKD subnuclear localization, with JKD^{H133D} enhancing its punctured localization while JKD^{sub30} diminishing it.

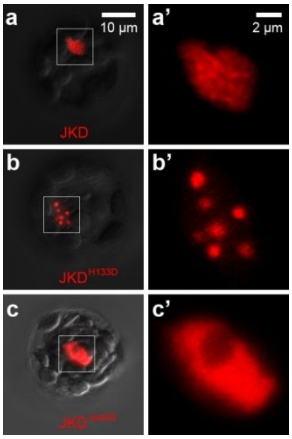

Figure 3. Subnuclear localization of JKD, JKD^{H133D} and JKD^{sub30}.

Subnuclear localization of mRFP fusions of wild-type JKD (**a, a'**), JKD^{H133D} (**b, b'**) and JKD^{sub30} (**c, c'**) in Arabidopsis mesophyll protoplasts. Right panels are zoom-in RFP channel images from the squares in the left panels.

JKD^{H133D} acts as a subnuclear localizer

JKD is known to promote SHR nuclear retention (Figure 4b-b"; Long et al., 2015). The fact that JKD^{H133D} is enriched in subnuclear bodies while maintaining interaction with SHR suggests that JKD^{H133D} may also shuttle SHR to the subnuclear compartments. To test this, we first coexpressed JKD^{H133D}:mRFP and SHR:YFP in Arabidopsis mesophyll protoplasts and observed their localization. When expressed alone, SHR exhibited a nucleocytoplasmic dual localization similar to that in the root vasculature (Figure 4a-a''). Addition of JKD restricted SHR signal to the protoplast nuclei, and superimposed a punctuated localization to SHR (Figure 4b-b''). Meanwhile, coexpressing JKD^{H133D} largely enriched SHR signal into the JKD^{H133D} subnuclear bodies (Figure 4c-c''). JKD^{H133D} and SHR nuclear-body enrichments were also observed in Arabidopsis roots (Figure 5). These results confirm that JKD^{H133D} can translocate SHR into certain subnuclear domains. On the contrary, JKD^{sub30} did not induce nuclear retention of SHR:YFP, nor did it trigger punctured SHR subnuclear localization as JKD did, resulting into a nucleocytoplasmic SHR dual localization similar to SHR alone (Figure 4d-d'').

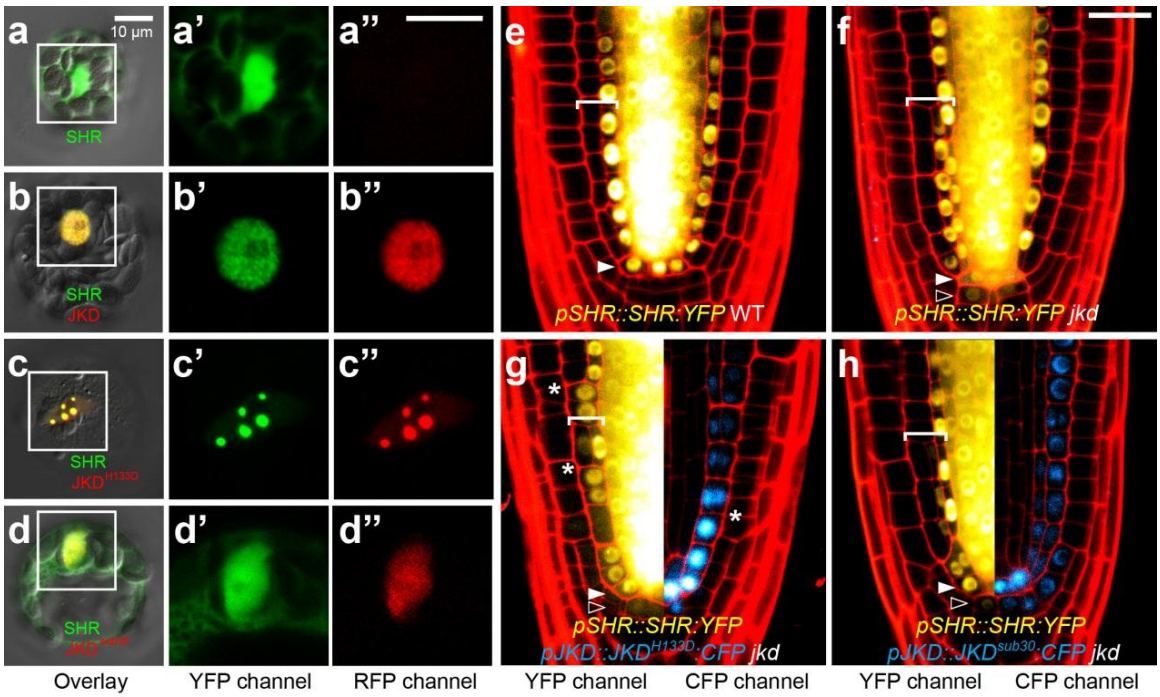

Figure 4. JKD, JKD^{H133D} and JKD^{sub30} have different effect on SHR localization and root radial patterning.

(**a-d"**) SHR:YFP expressed alone (**a-a"**) and coexpressed with JKD:mRFP (**b-b"**), JKD^{H133D}:mRFP (**c-c"**) and JKD^{sub30}:mRFP (**d-d"**). Panels of separate YFP and RFP channels are also zoomed in from the square in the left panels. Scale bar indicates 10µm. (**e-h**) SHR:YFP distribution in wild-type (**e**), *jkd* (**f**) and *jkd* roots expressing *pJKD::JKD^{H133D}:CFP* (**g**) and *pJKD::JKD^{sub30}:CFP* in *jkd* (**h**) roots. Brackets mark ground tissue, white arrowheads point to SHR localizatin at QC position, empty arrowheads to SHR at columella initial position, asterisks mark patchy ground tissue separation in *JKD^{H133D} jkd* root. Scale bar indicates 20µm.

As JKD binds SCR and other BIRD proteins involved in GT patterning (Welch et al., 2007a; Long et al., 2015a), we next assessed whether JKD^{H133D} mutation sequesters these proteins to subnuclear bodies in protoplasts. As shown in Supplementary Figure 2, we found that JKD-interactors also showed enrichment in the JKD^{H133D}-bodies. Specifically, MGP, NUC and wild-type JKD were predominantly translocated to JKD^{H133D}-containing bodies (Supplementary Figure 2b-d"). SCR and BIB showed partial enrichment in JKD^{H133D}-bodies (Supplementary Figure 2e-f"). JKD^{H133D} did not alter the homogenous nuclear localization of free mRFP (Supplementary Figure 2a-a"), confirming the specific confining effect of JKD^{H133D} to its interactors. Compartmentalization of these proteins might be achieved by direct binding to JKD^{H133D}, or alternatively by associating to other JKD^{H133D}-binding proteins, such as SHR.

JKD^{H133D} and JKD^{sub30} mutations exert different effects on root radial pattern

The altered subcellular localizations of SHR suggest that mutations in JKD^{H133D} and JKD^{sub30} might modify its function in controlling SHR intercellular movement, target gene expression and thus GT patterning. Therefore, we monitored the effect of *pJKD::JKD^{sub30}:CFP* and *pJKD::JKD^{H133D}:CFP* in *jkd* mutants by testing complementation. Roots of *jkd* are characterized by one extra GT layer, a result of ectopic cortical ACD triggered by insufficient endodermal SHR nuclear retention and enhanced SHR outspread (Figure 4f; Welch et al., 2007). Additionally, SHR also moves one layer further from QC into the position of the columella initial, and has a nucleocytoplasmic dual localization in both cells (Figure 4f). As SHR is not retained in protoplast nuclei by

JKD^{sub30}, we predicted that JKD^{sub30} could not rescue the *jkd* phenotype. Indeed, *pJKD::JKD^{sub30}:CFP* failed to rescue the extended SHR:YFP movement nor the extra ACD in the *jkd* mutants (Figure 4h).

Intriguingly, JKD^{H133D} not only abolished the ectopic ACD in *jkd* roots, but also caused incomplete GT separation with patches of undivided cells (Figure 4g). Interestingly, SHR:YFP exhibited nucleocytoplasmic dual localization in the positions of QC, columella initials and unseparated GT cells (Figure 4g), with its nuclear portion showing enrichment in the JKD^{H133D}-triggered subnuclear bodies (Figure 5).

These data confirm that JKD^{H133D} and JKD^{sub30} have different effects on root radial pattern, and suggest that Z2 and Z4 play different regulatory roles in the JKD protein.

JKD^{H133D} and JKD^{sub30} have different effects on *SCR* and *CYCD6;1* expression

The divergent phenotypes of JKD^{H133D} and JKD^{sub30} indicate that the two JKD motifs may differentially affect SHR downstream targets to control SHR action range and ACD. JKD is known to differentially regulate at least two SHR targets, namely repressing *CYCD6;1* while activating *SCR* expression (Long et al., 2015a).

We then monitored *CYCD6;1* and *SCR* expression in the roots expressing JKD^{H133D}. *CYCD6;1* expression marks ACDs at the CEI position, and is activated by SHR-SCR protein complex (Figure 6a; Long et al., 2015; Chapter 4; Cruz-Ramírez et al., 2012; Sozzani et al., 2010). In *jkd* roots, *pCYCD6;1::GFP* expression is expanded in association with extra ACDs in GT (Figure 6b; Long et al., 2015). When *pJKD::JKD^{H133D}:CFP* was introduced into *jkd*, *pCYCD6;1::GFP* signal was lost at the corresponding positions of CEI in the root, normal ACDs were not observed, only to reappear at positions where patchy GT separation took place and JKD^{H133D}:CFP expression is low (Figure 6c). This negative effect on transcriptional regulation is supported by transient dual-luciferase promoter assay, where JKD^{H133D} can repress SHR-SCR–mediated *pCYCD6;1* activity slightly further than JKD (Figure 6d).

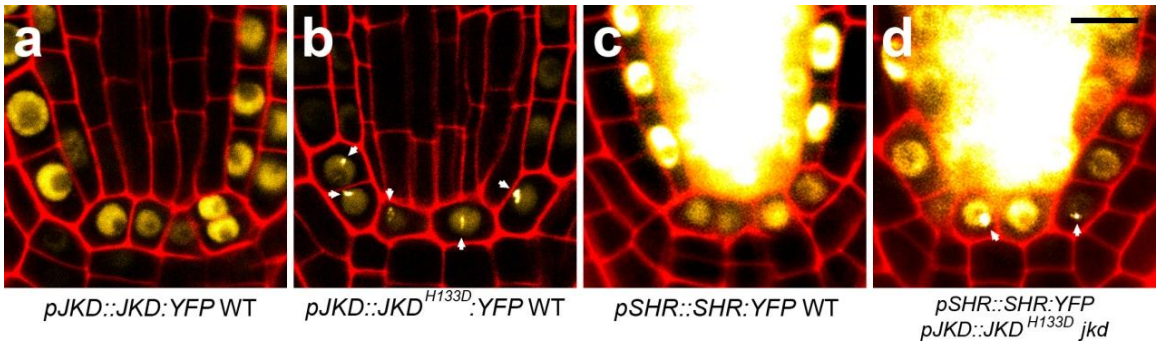

Figure 5. JKD^{H133D} subnuclear bodies in roots.

Roots expressing YFP fusions of JKD (**a**), JKD^{H133D} (**b**) and SHR in wild-type (**c**) or coexpressed with JKD^{H133D} (**d**). White arrows point to JKD^{H133D} subnuclear compartments. Scale bar indicates 10μm.

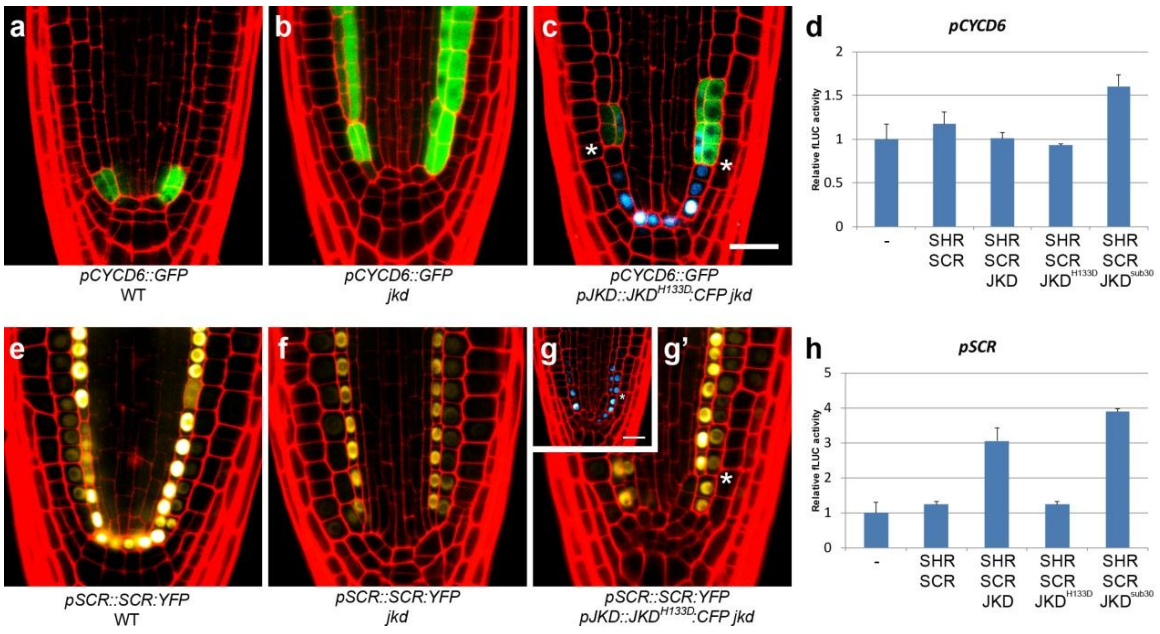

Figure 6. JKD^{H133D} and JKD^{sub30} oppositely regulate root radial pattern.

(**a-c**) *pCYCD6;1*:GFP marker expression in wild-type (**a**), *jkd* (**b**) and *JKD^{H133D}:CFP jkd* roots (**c**). (**d**) Promoter luciferase assay of *pCYCD6;1*. (**e-g'**) SCR:YFP expression in wild-type (**e**), *jkd* (**f**) and *jkd* roots expressing *pJKD::JKD^{H133D}:CFP jkd* (**g'**). The insert shows JKD^{H133D}:CFP expression in the same root (**g'**). (**h**) Promoter luciferase assay of *pSCR*. Error bars indicate standard errors. Scale bars indicate 20μm.

JKD is required for sufficient *SCR* expression, another SHR target, in the GT (Long et al., 2015a; Welch et al., 2007a). In the WT root, *pSCR::SCR:YFP* signal was detected highest in the "U-shaped" domain of QC, CEI and endodermis, and at lower levels in the cortex (Figure 6e; Long et al., 2015; Di Laurenzio et al., 1996). In the *jkd* mutant, *SCR:YFP* expression was reduced in the endodermis and lost in the QC, while weak

signal was detectable in the cortex and epidermis (Figure 6f). In *jkd* plants containing *pJKD::JKD^{H133D}:CFP*, low *SCR:YFP* signal was detected in the unseparated GT, where JKD^{H133D} level is high (Figure 1g, g'). Dual-luciferase promoter assay confirmed JKD^{H133D}'s action on *pSCR*, where addition of JKD^{H133D} to SHR-SCR complex did not induce *pSCR* expression whereas JKD did (Figure 6h).

In planta protein localization and transient expression analyses suggested that JKD^{H133D} exhibit a general repression role on SHR target transcription. On the contrary, JKD^{sub30} enhanced both *pCYCD6;1* and *pSCR* activities when added to cells co-transfected with SHR and SCR in the transient dual-luciferase promoter assay (Figure 6d, h). This data indicates that JKD^{sub30} and JKD^{H133D} mutations have opposite effects on the tested SHR targets. However, further analyses are required to confirm if these two mutants generally represses or activate other *JKD* and/or *SHR* targets.

Interestingly, JKD^{H133D} was found largely excluded from DAPI-stained nuclear DNA (Figure 7a-a''), suggesting that JKD^{H133D} might function as subnuclear localizer to isolate SHR complexes from their target DNA loci to exert its repressive function. Also, JKD^{H133D} subnuclear localization could exhibit sophisticated 3D arrangement (Figure 7b). More analysis is needed to identify the subnuclear bodies where JKD^{H133D} resides and their dynamics in transcriptional regulations.

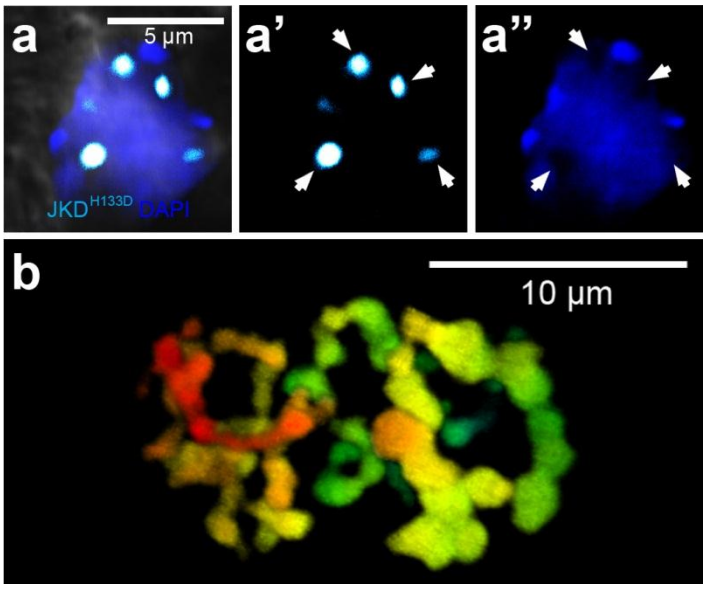

Figure 7. JKD^{H133D} does not colocalize with DAPI.

(**a-a”**) JKD^{H133D}:CFP seems to locate away from DAPI-stained nuclear DNA in protoplast. (**a’**) CFP channel, (**a”**) DAPI chanel. White arrows point to the positions of JKD^{H133D} subnuclear bodies. (**b**) Pseudocolored 3D distribution of the JKD^{H133D}:CFP bodies in the protoplast nucleus. The pseudocolor gradient indicates depth, with red in the front and cyan in the back.

HHD/HHH motifs in BIRD proteins determine subnuclear localization of MGP and NUC but not BIB

The amino acid substitution of JKD^{H133D} locates in the HHD stretch, which is conserved for BIB. MGP and NUC, however, possess a tri-hisitidine stretch (HHH) at this position (Figure 8a). To examine the consequence of this partial conservation in subnuclear localization, we created “JKD-mimics” of MGP (MGP^{HHD}), “MGP-mimics” of JKD (JKD^{HHH}) and “JKD^{H133D} mimics” of BIB (BIB^{DHD}), MGP (MGP^{DHD}) and NUC (NUC^{DHD}) via site-directed mutagenesis, and infiltrated their YFP-fusions into Tobacco leaves.

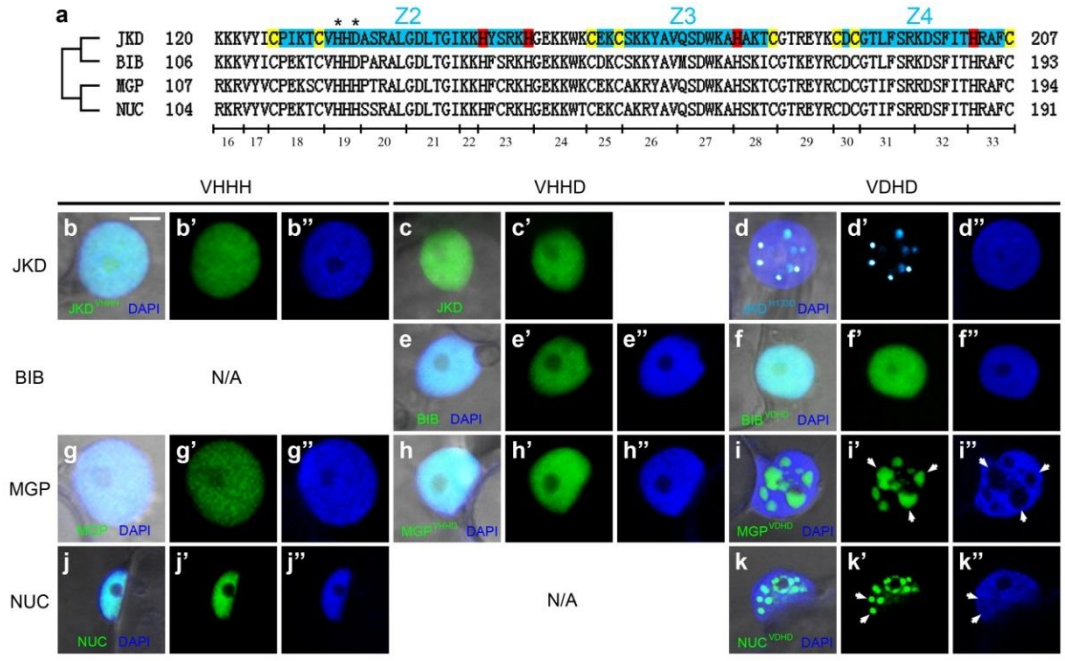

Figure 8. MGP and NUC mutant variants but not BIB mutant can locate into JKD^{H133D}-like subnuclear bodies.

(**a**) Alignment of JKD, BIB, MGP and NUC fragments where the JKD^{H133D} mutation is located. Asterisks indicate the substituted amino acid residues in the semi-conserved motif. (**b-k”**) Fluorescent fusions of MGP- (VHHH), JKD- (VHHD) and JKD^{H133D}-mimics (VDHD) of JKD, BIB, MGP and NUC in transfected tobacco leaf nuclei. Panels marked with ’ are fluorescent protein channels, panels marked by ” are DAPI channels. White arrows point to subnuclear bodies. Scale bar represents 5µm. N/A, image not available.

As shown in Figure 8, JKD showed a slightly punctuated nucleoplasmic localization. With "MGP-mimic", JKD^{HHH} exhibited enhanced signal in the nucleolus, to similar level as cytoplasmic JKD^{HHH} (Figure 8b-c'). Similarly, MGP displayed a slightly stronger nucleolar signal than the "JKD-mimic" MGP^{HHD} (Figure 8g-g''). Despite the nucleolar signal, the "JKD-mimic" and "MGP-mimic" did not drastically alter the subnuclear compartmentalization of tested BIRD proteins.

Like JKD^{H133D} (Figure 8d-d''), the "JKD^{H133D}-mimics" MGP^{DHD} and NUC^{DHD} also located to specific nuclear bodies (Figure 8i-i'', k-k''). MGP^{DHD} also displayed strong exclusion from DAPI-stained nuclear DNA (Figure 8 i-i''), while such effect was less prominent for NUC^{DHD} (Figure 8k-k''). Interestingly, BIB^{DHD} failed to induce punctuated nuclear localization (Figure 8f-f''), indicating that there might be other motifs besides the HHD stretch regulating BIRD protein subnuclear localization.

DISCUSSION

In the present study, we have attempted to identify JKD motifs important for SHR nuclear retention and transcriptional target regulation, and isolated two specific mutants JKD^{H133D} and JKD^{sub30} with disrupted second and fourth zinc finger. JKD^{H133D} confers general transcriptional repression, shows predominant localization to specific nuclear bodies, and we postulated that it exerts its repressive actions by recruiting other transcriptional activators, such as SHR, away from nuclear DNA. In contrast, JKD^{sub30} seems nonfunctional as it cannot restrict extra SHR movement, thus failing to rescue the root patterning defect in *jkd*. Further marker and transcriptional analyses will be required to fully understand its action. Several other JKD mutants (such as JKD^{del1}, JKD^{sub16} and JKD^{L99M} with the conserved leucine substituted) were able to rescue *jkd* phenotype (data not shown), confirming the specific effects of JKD^{H133D} and JKD^{sub30}.

During the interaction study between JKD mutants and SHR, we noticed opposite outcomes from *in vitro* and *in vivo* experiments. Such inconsistency might be caused by

the intrinsic variation between the yeast system and plant cells, or the difference between the nature of deployed techniques. The latter possibility is highly likely, as SplitLUC and FRET-FLIM assays report direct association of tested proteins (Figure 2c, d), while Y2H requires an additional transcriptional activation of the interaction-dependent downstream reporter genes such as *lacZ* (Figure 2a). Being a positive and negative transcriptional regulator (Long et al., 2015a), JKD mutants might have augmented JKD's transcriptional activities while maintaining its binding to SHR, thereby resulting in the different readouts of *in vitro* and *in vivo* analyses. This scenario is supported by the notion that JKD^{H133D} might bestow its repressive function by preventing its interacting transcription factors, from binding DNA, further implying that JKD^{H133D} physically interacts with SHR to translocate it. Alternatively, the interaction between SHR and JKD^{H133D} mutants might require other plant-specific factors which are absent in yeast cells.

Another interesting observation is that, upon overexpression, JKD nuclear distribution is not homogenous, but slightly punctuated. This localization was never observed in Arabidopsis roots, possibly because *JKD* expression level is much lower than that in transfected protoplasts for observation. It is plausible that endogenous JKD protein is distributed in a punctuate manner under physiological conditions but these structures cannot be detected with our confocal imaging system. Implementing super-resolution microscopy for protein localization in the roots will give more insights on the endogenous JKD localization (Schermelleh et al., 2010). Alternatively, the punctuate JKD localization might be an artifact of overexpression. However it is less likely, as JKD overexpression in protoplasts conserved its transcriptional regulations on *CYCD6;1* and *SCR* as in roots. The non-punctuate JKD^{sub30} failed to rescue *jkd* phenotype, suggesting that subnuclear punctuation is correlated with JKD function.

Additionally, JKD can also superimpose its punctuated distribution to SHR, which is otherwise more homogenous when expressed alone or coexpressed with JKD^{sub30}. JKD^{H133D} also forms bigger subnuclear punctuation together with bound SHR. However given the fact that JKD^{H133D} has different transcriptional activity comparing to wild-type JKD, it is likely that JKD^{H133D} compartments are not mere aggregates of JKD punctuate,

but different “nuclear bodies” altogether. Mutation in JKD^{H133D} possibly bestowed its ability to shuttle SHR away from DNA without altering its capacity to spatially guide SHR and other interactors.

Being transcription factors, it is reasonable to envision that JKD-SHR complex should be concentrated to their specific target DNA loci. The more homogenized SHR distribution without JKD indicates that JKD and other BIRD proteins could be the guide for SHR to its targets. Such scenario has been verified for DELLA and SCARECROW-LIKE 3 (SCL3) downstream regulations, where BIRD proteins act as intermediates between these proteins and their target DNA loci (Yoshida et al., 2014a). Additionally, effect of JKD^{sub30} indicates that the last zinc finger of JKD might be crucial for its localizing function on SHR.

Punctuated subnuclear localization has been observed for other plant transcription factors, such as several FLORAL BINDING PROTEINS (FBP) (Immink et al., 2002), circadian regulator GIGANTEA (GI) (Kim et al., 2013) and TCP8 (Valsecchi et al., 2013). It is tempting to speculate that many plant transcription factors are unevenly distributed across the nucleus, and that their localization and dynamics are linked to their transcriptional activity. Links between transcription factor subnuclear compartmentalization and transcriptional regulation have been realized in the animal field (Stein et al., 2000; Corry and Underhill, 2005), and it will be exciting to explore such links in the plant kingdom.

Taken together, our site-directed mutagenesis screen has provided new insight in relation to BIRD proteins function in regulating transcription. However, our analyses did not isolate a JKD variant that loses SHR binding capacity. It is possible that the domains required for SHR binding were not in analyzed region, or multiple motifs within the zinc finger domains are required for such function. Isolating such a mutant would be necessary to fully correlate SHR binding, nuclear retention, transcriptional activity and the regulation of intercellular mobility.

MATERIAL AND METHODS

JKD protein analysis and structure prediction

Homology model of JKD was predicted by the YASARA software package using a Critical Assessment of Structural Prediction (CASP) approved protocol as described in Krieger et al. (2009). Briefly, 155 structural templates were primarily extracted from Uniprot based on a position specific scoring matrix (PSSM) and ranked based on structural quality. 4 templates were kept as templates based on the total score of BLAST alignment score, the WHAT_CHECK quality score in the PDBFinder2 database and the target coverage. The predicted structural models were ranked by their overall quality Z-scores, and the one with highest Z-score (-2.965, model quality commented as “poor”) was selected as the most likely model. Detailed description for YASARA homology modeling can be found at http://www.yasara.org/homologymodeling.htm.

Site-directed mutagenesis

Entry clone of pDONR221 containing *JKD* coding sequence (CDS) was used as a template to create *JKD* zinc finger mutants using the QuikChange II kit (Agilent Technologies). Mutagenic mismatch primers were designed using the QuikChange Primer Design tool (http://www.genomics.agilent.com/primerDesignProgram.jsp) and are listed in Supplementary Table 1. BIB, MGP and NUC mutant variants were created as described above. Resulting clones were confirmed by sequencing.

Yeast two-hybrid assay

Y2H analysis was performed as described in Long et al. (2015). Briefly, *JKD* mutants in pDONR221 were introduced into yeast expression vectors pDest32 (GAL4 BD) and pDest22 (GAL4 AD) by Gateway LR reaction (Invitrogen). Autoactivations were determined by growth on dropout medium supplemented by 3-amino-1,2,4-triazole (3-AT).

A nonautoactivating form of SHR was generated by deleting acidic amino acids 58 to 64 as described by Koizumi et al. (2011). SHR and the JKD mutants were used as baits and interactions were determined by growth on dropout medium supplemented with 5mM 3-AT (SHR) or designated concentration determined in Table 1. Quantification of Y2H was performed with CPRG assay as described in Welch et al. (2007).

Transient luciferase assay in protoplast

Coding sequence (CDS) of *JKD* mutants were introduced into plant expression vector pDuEx-Dc6 by Gateway cloning (Invitrogen). SHR vector for split-LUC assay is as described in Chapter 4. *A. thaliana* Col-0 mesophyll protoplasts were prepared according to Long et al. (2015). Recombined pDuEx-An6 and pDuEx-Dc6 constructs of 2µg each were cotransfected with 1µg of the constitutive *pUBQ::Firefly-LUC* vector. Luciferase activities were measured by using the Dual-Luciferase® Reporter Assay System in a GloMax® 96 Microplate Luminometer (Promega). The obtained LUC levels were normalized using Firefly luciferase, and the relative ratio was determined by comparing this to the obtained with the single transfected pDuEx-An6 fusion samples as described in Cruz-Ramírez et al. (2012).

Promoter assays were performed as described in Long et al. (2015). Protoplasts were transformed with either *pCYCD6::LUC* or *pSCR::LUC* and the effector plasmids. 1µg of *35S::Renilla-LUC* was used as internal control for transfection efficiency. LUC activity was normalized using Renilla luciferase and the relative ratio was determined by comparing this to the obtained with the promoter activity without effectors.

Transient transfection assays in *Nicotiana benthamiana* leaves.

Wild-type *Nicotiana benthamiana* plants were grown under standard greenhouse conditions. For all assays 5 week-old *N. benthamiana* were used. Young leaves were

infiltrated by *Agrobacterium tumefaciens* harboring binary vectors as described in Liu et al. (2010). The infiltrated region was then mounted in water and checked for expression.

Fluorescence lifetime measurements

Coding sequence (CDS) of *JKD* mutants were recombined with cauliflower mosaic virus *35S* promoter and mRFP by Gateway cloning (Invitrogen). SHR and positive control vectors for FRET-FLIM assay is as described in Chapter 3. FRET-FLIM measurements and analysis in mesophyll protoplasts roots are as described in Chapter 3. Frequency-domain FRET-FLIM was performed for protoplast measurements.

Plant DNA constructs and transformation

CDS of wild-type and mutant *JKD, BIB, MGP and NUC* in pDONR221 entry clones were recombined downstream of *35S promoter* with SYFP2 or mRFP by Multisite Gateway cloning (Invitrogen) (Long et al., 2015; Chapter 3). JKD^{H133D} and JKD^{sub30} were fused behind *JKD* promoter to create expression clones containing either SYFP2 or SCFP3A reporters and JKD mutants variants were introduced into wild-type and *jkd* mutant *Arabidopsis thaliana* ecotype Colombia-0 (Col-0) by floral dipping (Clough and Bent, 1998). Fluorescent fusion constructs of *SHR* and *SCR* were described in Long et al. (2015). *pCYCD6:GFP* was as reported in Sozzani et al. (2010).

Plant growth conditions

Growth conditions of *Arabidopsis thaliana* are as described by Sabatini et al. (1999). *jkd-4* is described in Welch et al. (2007). Plants coexpressing fluorescent fusions of JKD mutants and fluorescent markers were generated by crossing.

Confocal microscopy

Roots were mounted in 10µM Propidium iodide for cell wall visualization. After transfection with either WT or mutant protein variants, protein colocalization with DNA was performed in protoplast cells stained with 1.25µg/mL DAPI. Confocal microscopy was performed using a Zeiss LSM710 confocal as described in Long et al. (2015). A C-Apochromat 40x/1.20 W Korr water-immersion objective was used. DAPI fluorescence was detected at 415 – 440 nm with 405 nm excitation and -405 beam splitter; cyan fluorescence was detected at 470 – 485 nm with 458 nm excitation and 458 beam splitter; green fluorescence was detected at 510 – 550 nm with 488nm excitation and 488 beam splitter; yellow detected at 525 – 550 nm with 514 nm excitation and 458/514 beam splitter; and red detected at 600 – 660 nm with 543 nm excitation and 488/543/633 beam splitter, respectively. Protoplasts and roots with single fluorescence were simultaneously observed with the aforementioned setting to confirm limited to no signal bleed through occurred.

SUPPLEMENTARY DATA

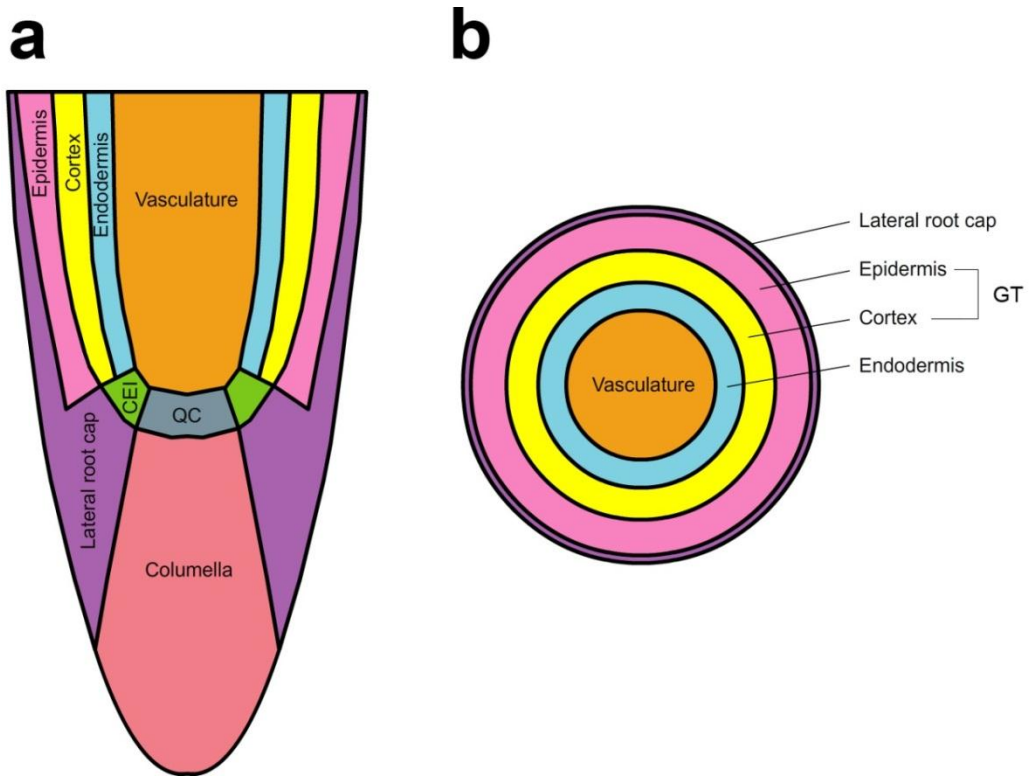

Figure S1. Illustration of Arabidopsis root meristem.

Illustrations of the longitudinal (**a**) and circumferential (**b**) cross sections of Arabidopsis root meristem. Tissue boundaries are drawn without separating individual cells. Different tissues are indicated by different colors. QC, quiescent center; CEI, cortex/endodermis initial; GT, ground tissue.

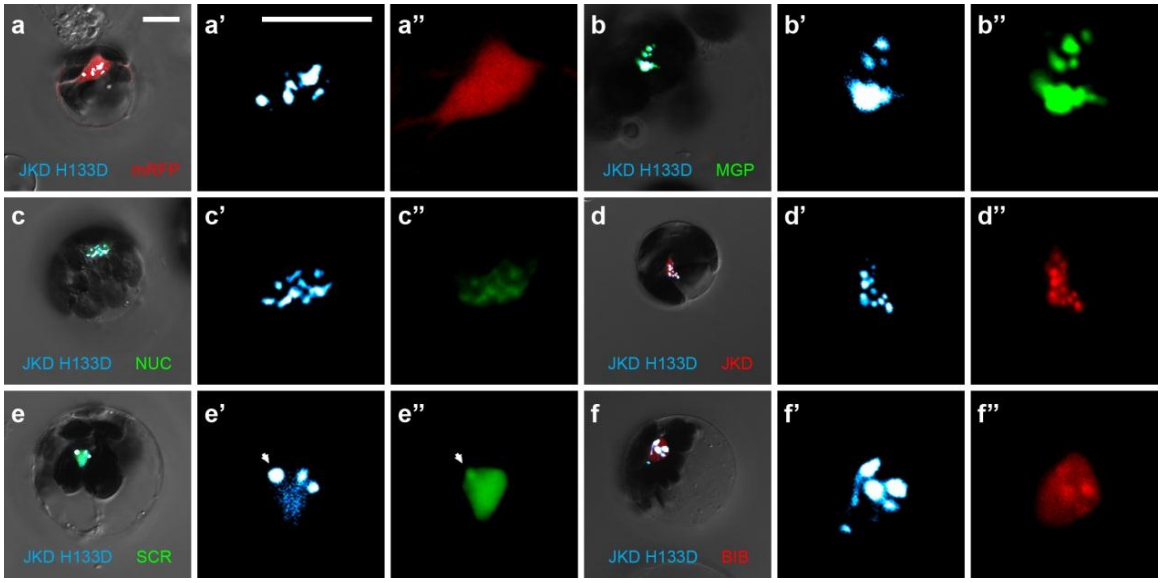

Figure S2. JKD^{H133D} brings SCR, MGP, NUC and BIB into subnuclear bodies.

Coexpression of JKD^{H133D}:CFP with free mRFP (**a-a''**), MGP:YFP (**b-b''**), NUC:YFP (**c-c''**), JKD:mRFP (**d-d''**), SCR:YFP (**e-e''**) and BIB:mRFP (**f-f''**) with zoom-in images of nuclei in separate channels. Scale bars indicates 10µm. White arrow points to mild SCR accumulation in JKD^{H133D} body.

Primer name	SEQUENCE (5'-3')
JKDΔ1F	CAAACTCTTCATCAGCCAATCAACCTGGCACTCC
JKDΔ1R	GGAGTGCCAGGTTGATTGGCTGATGAAGAGTTTG
JKDΔ2F	CTCTTCATCAGCCAAGAAGAAGAGACCAGATCCAGATG
JKDΔ2R	CATCTGGATCTGGTCTCTTCTTCTTGGCTGATGAAGAG
JKDΔ3F	GAAATCAACCTGGCACTGTCATCGCTCTATCGCC
JKDΔ3R	GGCGATAGAGCGATGACAGTGCCAGGTTGATTTC
JKDΔ4F	CTCCAGATCCAGATGCTGATTCGCCAACAACAC
JKDΔ4R	GTGTTGTTGGCGAATCAGCATCTGGATCTGGAG
JKDΔ5F	TGCTGATGTCATCGCTCTAACAACACTCATGGCAA
JKDΔ5R	TTGCCATGAGTGTTGTTAGAGCGATGACATCAGCA
JKDΔ7F	TCGCCAACAACACTCATGGCATGCGAGATCTGC
JKDΔ7R	GCAGATCTCGCATGCCATGAGTGTTGTTGGCGA
JKDΔ8F	GGCAACAAACAGATTCGTGAACAAAGGGTTTCAAAGGG
JKDΔ8R	CCCTTTGAAACCCTTTGTTCACGAATCTGTTTGTTGCC
JKDΔ9F	CGTGTGCGAGATCTGCCAAAGGGACCAGAATT
JKDΔ9R	AATTCTGGTCCCTTTGGCAGATCTCGCACACG
JKDΔ10F	GAGATCTGCAACAAAGGGTTTAATTTACAACTACATCGCCGT
JKDΔ10R	ACGGCGATGTAGTTGTAAATTAAACCCTTTGTTGCAGATCTC
JKDΔ12F	GTTTCAAAGGGACCAGAATTTACAACTAAACCTTCCATGGAAG
JKDΔ12R	CTTCCATGGAAGGTTTAGTTGTAAATTCTGGTCCCTTTGAAAC
JKDΔ13F	CATCGCCGTGGCCACAAGCTAAAGCAACGG
JKDΔ13R	CCGTTGCTTTAGCTTGTGGCCACGGCGATG
JKDΔ14F	GTGGCCACAACCTTCCATGGAAACAAGAAGTGATAAAGAA
JKDΔ14R	TTCTTTATCACTTCTTGTTTCCATGGAAGGTTGTGGCCAC
JKDΔ16F	AACGGTCCAAACAAGAAGTGATAGTATACATATGTCCTATCAAGAC
JKDΔ16R	GTCTTGATAGGACATATGTATACTATCACTTCTTGTTTGGACCGTT
JKDΔ18F	ACAAGAAGTGATAAAGAAGAAAGTATACATAGTACACCATGATGCCTC
JKDΔ18R	GAGGCATCATGGTGTACTATGTATACTTTCTTCTTTATCACTTCTTGT
JKDΔ19F	ACATATGTCCTATCAAGACTTGTGCCTCCAGGGCC
JKDΔ19R	GGCCCTGGAGGCACAAGTCTTGATAGGACATATGT
JKDΔ23F	GGAGACCTCACTGGGATCAAGAAAGGTGAAAAGAAGTG
JKDΔ23R	CACTTCTTTTCACCTTTCTTGATCCCAGTGAGGTCTCC
JKDΔ24F	GAAACACTACAGCCGCAAACACTGTGAAAAGTGTTCTAAGAAAT
JKDΔ24R	ATTTCTTAGAACACTTTTCACAGTGTTTGCGGCTGTAGTGTTTC
JKDΔ25F	CACGGTGAAAAGAAGTGGAAGTCTAAGAAATACGCTGTTCAG

JKDΔ25R	CTGAACAGCGTATTTCTTAGACTTCCACTTCTTTTCACCGTG
JKDΔ26F	GTGGAAGTGTGAAAAGTGTCAGTCTGATTGGAAGGCAC
JKDΔ26R	GTGCCTTCCAATCAGACTGACACTTTTCACACTTCCAC
JKDsub12 AAAAA F	GGTTTCAAAGGGACCAGAATTTACAACTAGCTGCCGCTGCCGCCAACCTTC CATGGAAGCTAAAGCAACGG
JKDsub12 AAAAA R	CCGTTGCTTTAGCTTCCATGGAAGGTTGGCGGCAGCGGCAGCTAGTTGTAA ATTCTGGTCCCTTTGAAACC
JKDsub12 ARRGA F	GACCAGAATTTACAACTAGCTCGCCGTGGCGCCAACCTTCCATGGAAGC
JKDsub12 ARRGA R	GCTTCCATGGAAGGTTGGCGCCACGGCGAGCTAGTTGTAAATTCTGGTC
JKDsub16 AAA F	CATGGAAGCTAAAGCAACGGTCCAAACAAGAAGTGATAGCGGCGGCAGTAT ACATATGTCCTATCAAGACTTGT
JKDsub16 AAA R	ACAAGTCTTGATAGGACATATGTATACTGCCGCCGCTATCACTTCTTGTTTGG ACCGTTGCTTTAGCTTCCATG
JKDsub18 AAAAA F	TAAAGCAACGGTCCAAACAAGAAGTGATAAAGAAGAAAGTATACATAGCTGC TGCCGCGGCTGCTGTACACCATGATGCCTCCAGGGC
JKDsub18 AAAAA R	GCCCTGGAGGCATCATGGTGTACAGCAGCCGCGGCAGCAGCTATGTATACT TTCTTCTTTATCACTTCTTGTTTGGACCGTTGCTTTA
JKDsub18 APIKTA F1	CCAAACAAGAAGTGATAAAGAAGAAAGTATACATAGCTCCTATCAAGACTTGT GT
JKDsub18 APIKTA R1	ACACAAGTCTTGATAGGAGCTATGTATACTTTCTTCTTTATCACTTCTTGTTTG G
JKDsub18 APIKTA F2	GAAGAAAGTATACATATGTCCTATCAAGACTGCTGTACACCATGATGCC
JKDsub18 APIKTA R2	GGCATCATGGTGTACAGCAGTCTTGATAGGACATATGTATACTTTCTTC
JKDsub19 AAAA F	CATATGTCCTATCAAGACTTGTGCAGCCGCTGCTGCCTCCAGGGCCCTTGG AGAC
JKDsub19 AAAA R	GTCTCCAAGGGCCCTGGAGGCAGCAGCGGCTGCACAAGTCTTGATAGGAC ATATG
JKDsub23 AYSRKA F1	GAGACCTCACTGGGATCAAGAAAGCCTACAGCCGCAAA
JKDsub23 AYSRKA R1	TTTGCGGCTGTAGGCTTTCTTGATCCCAGTGAGGTCTC
JKDsub23 AYSRKA F2	TCAAGAAACACTACAGCCGCAAAGCCGGTGAAAAGAAGTG
JKDsub23 AYSRKA R2	CACTTCTTTTCACCGGCTTTGCGGCTGTAGTGTTTCTTGA
JKDsub25 AAAA F	AGCCGCAAACACGGTGAAAAGAAGTGGAAGGCTGCAGCGGCTTCTAAGAA ATACGCTGTTCAGTCTGATTG
JKDsub25 AAAA R	CAATCAGACTGAACAGCGTATTTCTTAGAAGCCGCTGCAGCCTTCCACTTCT TTTCACCGTGTTTGCGGCT
JKDsub26 AAAAAA F	AACACGGTGAAAAGAAGTGGAAGTGTGAAAAGTGTGCTGCGGCAGCCGCT GCTCAGTCTGATTGGAAGGCACATGC
JKDsub26 AAAAAA R	GCATGTGCCTTCCAATCAGACTGAGCAGCGGCTGCCGCAGCACACTTTTCA CACTTCCACTTCTTTTCACCGTGTT
JKDsub28 AAKTA F	CGCTGTTCAGTCTGATTGGAAGGCAGCTGCGAAAACTGCTGGTACTCGTGA G
JKDsub28 AAKTA R	CTCACGAGTACCAGCAGTTTTCGCAGCTGCCTTCCAATCAGACTGAACAGC G

JKDsub30 ADA F	TGCGAAAACTTGTGGTACTCGTGAGTATAAAGCTGACGCTGGCACGTTGTTCTCC
JKDsub30 ADA R	GGAGAACAACGTGCCAGCGTCAGCTTTATACTCACGAGTACCACAAGTTTTCGCA
JKDsub33 ARAFA F	TCTCCAGGAAAGATAGTTTCATCACAGCTAGAGCGTTCGCCGACGCATTAACTG
JKDsub33 ARAFA R	CAGTTAATGCGTCGGCGAACGCTCTAGCTGTGATGAAACTATCTTTCCTGGAGA
JKDsub33 ARAFC F	TCTCCAGGAAAGATAGTTTCATCACAGCTAGAGCGTTCTGCGACG
JKDsub33 ARAFC R	CGTCGCAGAACGCTCTAGCTGTGATGAAACTATCTTTCCTGGAGA
JKD VHHH F	ATCAAGACTTGTGTACACCATCATGCCTCCAGGG
JKD VHHH R	CCCTGGAGGCATGATGGTGTACACAAGTCTTGAT
BIB VDHD F	CGGGTCATGGTCTACGCAAGTCTTCTCTGG
BIB VDHD R	CCAGAGAAGACTTGCGTAGACCATGACCCG
MGP VHHD F	TGCGTCCACCACGATCCGACGAGGG
MGP VHHD R	CCCTCGTCGGATCGTGGTGGACGCA
MGP VDHD F	AAGAGTTGCGTCGACCACGATCCGACGAGGG
MGP VDHD R	CCCTCGTCGGATCGTGGTCGACGCAACTCTT
NUC VDHD F	GAGAAGACATGTGTCGACCATGACTCCTCTAGAGCTC
NUC VDHD R	GAGCTCTAGAGGAGTCATGGTCGACACATGTCTTCTC

Supplementary Table 1. Primers for site-directed mutagenesis.

Underlined residues were substituted.

Chapter 6

SCARECROW-LIKE23 and SCARECROW jointly specify endodermal cell fate but distinctly control SHORT-ROOT movement

Yuchen Long[1,2,5], Joachim Goedhart[3], Martinus Schneijderberg[2], Inez Tepstra[2], Akie Shimotohno[2], Benjamin P. Bouchet[4], Anna Akhmanova[4], Theodorus W.J. Gadella[3], Jr, Renze Heidstra[1,2], Ben Scheres[1,2], Ikram Blilou[1,2#]

[1]Plant Developmental Biology, Plant Sciences, Wageningen University and Research Centre, Droevendaalsesteeg 1, Wageningen, 6708PB, The Netherlands

[2]Molecular Genetics, Department Biology, Padualaan 8, Utrecht, 3581CH, The Netherlands

[3]Swammerdam Institute for Life Sciences, Section of Molecular Cytology, van Leeuwenhoek Centre for Advanced Microscopy, University of Amsterdam, Science Park 904, Amsterdam, 1098 XH, The Netherlands

[4]Cell Biology, Department Biology, Utrecht University, Padualaan 8, Utrecht, 3581CH, The Netherlands

[5]Current address: my current address: Laboratoire de Reproduction et Développement des Plantes, INRA, CNRS, ENS, UCB Lyon 1, 46 Allée d'Italie, 69364 Lyon Cedex 07, France.

[#] For correspondence (email Ikram.blilou@wur.nl)

SUMMARY

Intercellular signaling through trafficking of regulatory proteins is a widespread phenomenon in plants and can deliver positional information for cell fate determination. In the Arabidopsis root meristem, the cell fate determinant SHORT-ROOT (SHR), a GRAS domain transcription factor, acts as a signaling molecule from the stele to the adjacent

layer to specify endodermal cell fate. Upon exiting the stele, SHR activates another GRAS domain transcription factor SCARCROW (SCR) which, together with several BIRD/INDETERMINATE DOMAIN proteins, restricts SHR movement to define a single cell layer of endodermis. Here we report that endodermal cell fate also requires the joint activity of both SCR and its closest homologue SCARECROW-LIKE23 (SCL23). We show that SCL23 protein moves with zonation-dependent directionality. Within the meristem, SCL23 exhibits short-ranged ground-tissue-to-vasculature movement. Away from the meristem, SCL23 displays long-range rootward movement into meristemic vasculature and a bidirectional radio spread, respectively. As a known SHR and SCR target, SCL23 also interacts with SCR and SHR and can restrict SHR intercellular outspread without relying on nuclear retention as SCR does. Collectively, our data show that SCL23 is a mobile protein that regulates SHR movement and acts redundantly with SCR to specify endodermal fate in the root meristem.

Key words: endodermal fate, mobile protein, SCL23, intercellular movement, protein interaction, SCR-SHR complex

INTRODUCTION

In plants, cell-cell trafficking of regulatory proteins is widely used for intercellular communication during cell fate specification (Sparks et al., 2013). In this context, mobile transcription factors can convey positional information in a non-cell-autonomous manner (Scheres, 2001; Dolan, 2006; Han *et al.*, 2014; Gallagher *et al.*, 2014; Long *et al.*, 2015 a).

The maize homeodomain protein KNOTTED1 (KN1) was the first mobile transcription factor described in plants. Loss-of-function *knotted* mutants failed to form shoot meristem, while gain-of-function produced ectopic knots (Schneeberger et al., 1995; Kerstetter et al., 1997). Both KN1 protein and mRNA can traffic within the shoot meristem and across

tissue layers in the leaf (Lucas et al., 1995a; Kim et al., 2002). In addition, KN1 was shown to potentiate its own transport between cells by interacting with plasmodesmata (PD) intercellular membrane-bound channels, and increase its size-exclusion limit (Lucas et al., 1995a; Kragler et al., 2000). KN1 mobility, which requires its homeodomain region, was shown to be necessary to rescue mutant phenotypes (Kim et al., 2002, 2005). In Arabidopsis, SHOOTMERISTEMLESS (STM) and KNAT1 are KN1 orthologs (Reiser et al., 2000; Long et al., 1996; Vollbrecht et al., 2000) which contain the conserved homeodomain to confer their intercellular mobility within the shoot apical meristem, leaves, and stem (Kim et al., 2003b). KNAT1 movement was shown to be required for epidermal cell differentiation, indicating the significance of it mobility during development (Rim et al., 2009).

LEAFY (LFY) was also shown to move between cells in the Arabidopsis flower meristem (Sessions et al., 2000), where it is required for triggering expression of floral identity genes (Weigel et al., 1992; Lohmann et al., 2001). Different from KN1, LFY exhibits a movement pattern resembling diffusion (Wu et al., 2003).

Since the discovery of KN1 and LFY, many mobile transcription factors have been described (Rim et al., 2011; Han et al., 2014; Mähönen et al., 2014). However among all the characterized mobile transcription factors, the GRAS domain protein SHORT-ROOT (SHR) remains the best studied example in which its movement is related to cell fate specification in the root meristem (Nakajima *et al.*, 2001; Sena *et al.*, 2004; Cui *et al.*, 2007; Cruz-Ramírez *et al.*, 2012; Long *et al.*, 2015 b). SHR traffics from the stele to the surrounding cell layer where it binds to its target SCARECROW (SCR), another GRAS domain transcription factor, and acts as a SHR-SCR complex to specify the quiescent center (QC) and promote asymmetric cell division of the cortex/endodermis initial (CEI) (Nakajima et al., 2001a; Sabatini et al., 2003; Heidstra et al., 2004a; Cruz-Ramírez et al., 2012a, 2013). In addition, regulation of radial SHR distribution is essential for specifying endodermal cell fate and stabilizing tissue boundaries in the root meristem; SHR movement is restricted through a nuclear retention mechanism by binding to SCR and several BIRD/INDETERMINATE DOMAIN proteins such as JACKDAW (JKD) and

BALDIBIS (BIB) (Long *et al.*, 2015 b). Together with JKD and BIB, SHR activates SCR to trigger its own nuclear confinement in the endodermis, forming a positive feedback loop which fortifies SHR nuclear accumulation to prevent its outward spread (Long *et al.*, 2015 b).

Here we present an analysis of SCARECROW-LIKE23 (SCL23), another GRAS domain protein closely related to SCR and recently identified as a common SCR and SHR target (Cui et al., 2014). We show that SCL23 is a mobile protein that acts redundantly with SCR to regulate endodermal fate in the root meristem. We show that in the meristem SCL23 exhibits short-range mobility from the ground tissue to the stele while in the transition and elongation zone, SCL23 displays long-range rootward movement into the meristem with the capacity of bidirectional radial spreading. We also show that SCL23 restricts SHR outward movement through a mechanism that does not involve nuclear retention. Furthermore, we demonstrate that SCL23 and SCR antagonistically regulate each other's expression, while their collective activity is required to specify endodermal cell fate

RESULTS

SCL23 interacts with SHR and SCR *in vivo*.

SCR and SHR form protein complex required for controlling asymmetric cell division in the cortex-endodermis initial and its daughter (CEI/D) within the Arabidopsis root (Cruz-Ramírez et al., 2012a). A genetic screen for factors controlling this division identified JKD, member of the BIRD family, as a factor involved in this process. JKD was shown to form protein complexes with both SCR and SHR (Welch *et al.*, 2007; Long *et al.*, 2015 b). SHR is required for endodermal fate specification (Helariutta et al., 2000a) through the collective activities of subsets of BIRD proteins and SCR (Long *et al.*, 2015 b). As BIRD proteins on their own were not competent to confer endodermal fate (Long *et al.*, 2015 b), we hypothesized that a complex involving SHR and SCR may be decisive in instructing endodermal fate.

To identify a potential partner with a redundant role in this process we performed a yeast two-hybrid screen with SCR as bait and selected for candidates with enriched expression in the ground tissue (Birnbaum et al., 2005; Brady et al., 2007) and isolated SCL23, the closest homolog to SCR in Arabidopsis (Lee et al., 2008).

We verified *in vivo* interaction of SCR and SCL23 by performing bimolecular fluorescence complementation (BiFC) assay in Arabidopsis mesophyll protoplasts (Figure 1B, C; (Lee et al., 2008). Interestingly, SCL23 could also bind SHR, and the resulting complex was observed both in the nuclei and cytoplasm of the protoplasts (Figure 1C), while SCL23 interacted with SCR predominantly in the nuclei (Figure 1A, B). We further confirmed the interaction between SCL23 and SHR by Förster resonance energy transfer measurement using fluorescence-lifetime imaging microscopy (FRET-FLIM) approach in protoplasts and HeLa cells (Figure 1E; Figure S1). FRET measurements indicated that SCL23 had comparable binding capacity to SHR as to SCR (Figure 1E), and the SCL23-SHR complex had the same interaction level in the nuclei and cytoplasm in HeLa cells, signified by the homogenous lifetime heat map and the single peak in the lifetime histogram (Figure S1C). Thus, different approaches reveal that SCL23 binds to SCR and SHR, and SHR-SCL23 interaction is observed both in the nuclei and cytoplasm.

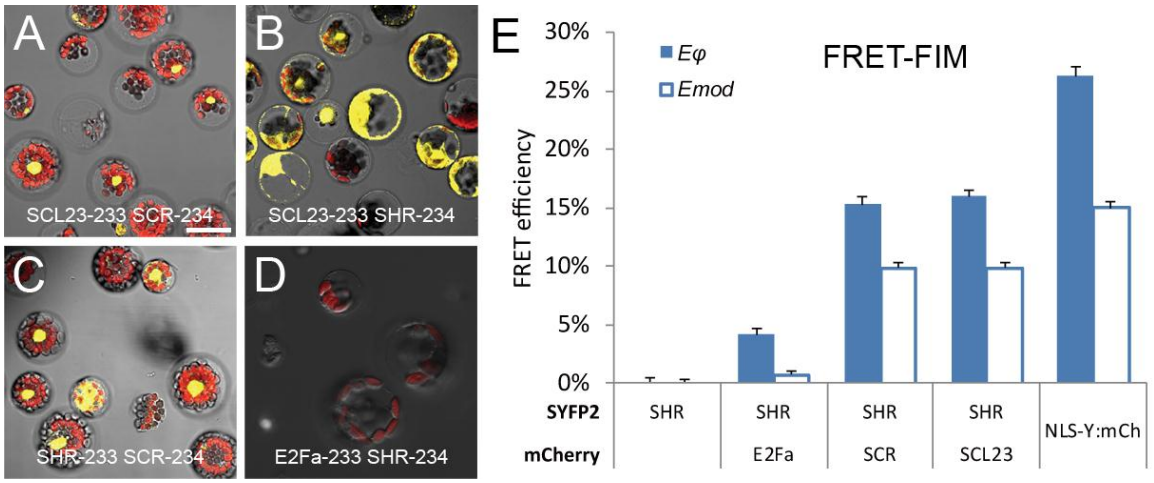

Figure 1. SCL23 binds to SCR and SHR.

A-D BiFC assay in Arabidopsis mesophyll protoplasts showing interactions between SCL23 and SCR or SHR. E2Fa-SHR was used as negative control, while SHR-SCR was used as positive control (Cruz Ramirez et al. 2012). Note the nucleocytoplasmic interaction signal between SCL23 and SHR. Scale bar represents 20 µm. **E** Frequency-domain FRET-FLIM analysis in Arabidopsis mesophyll protoplasts showing interactions between SCR, SCL23 and SHR. Error bars indicate standard errors of means. E2Fa-SHR was used a negative control, while a nuclear-localizing YFP:mCherry tandem was used as positive control (Long et al, 2015). E_{φ}, FRET efficiency derived from fluorescence phase-shift information; E_{mod}, FRET efficiency derived from fluorescence demodulation.

SCR and SCL23 act redundantly to specify endodermal fate

Mutations in *SCR* result in roots with a single ground tissue layer exhibiting mixed cortex and endodermis characteristics (Benfey et al., 1993; Di Laurenzio et al., 1996a). SCL23 displayed close homology to SCR; in addition, SCL23 interacted physically with both SCR and SHR. To assess functional redundancy between these two close homologs, we generated a *scr scl23* double mutant. Single mutants of *scl23* have been reported to have no obvious developmental phenotypes (Lee et al., 2008; Cui et al., 2014). However, root growth and meristem size of *scr scl23* seedlings resembled the *shr* phenotype (Figure 2A-C, D-H). We analyzed the *scr scl23* ground tissue monolayer for endodermal features using the autofluorescence of Casparian strips as a key morphological mark for endodermis. The *scl23* single mutant, similar to WT, displayed Casparian strip marks in its designated endodermal layer (Figure 2E'). In *scr* mutant roots, as previously shown, the ground tissue monolayer retained Casparian strips (Figure 2F'; (Di Laurenzio et al., 1996a). However, in *scr scl23* roots, the mutant monolayer did not show any Casparian strips, similar to *shr* (Figure 2G', H'; (Helariutta et al., 2000a). These data indicate that the *scr scl23* double mutant contains no endodermis tissue and superficially mimics *shr* in root development.

We next examined the *scl23 shr* phenotype and found that it is similar to *shr* (Figure 2 I,I').

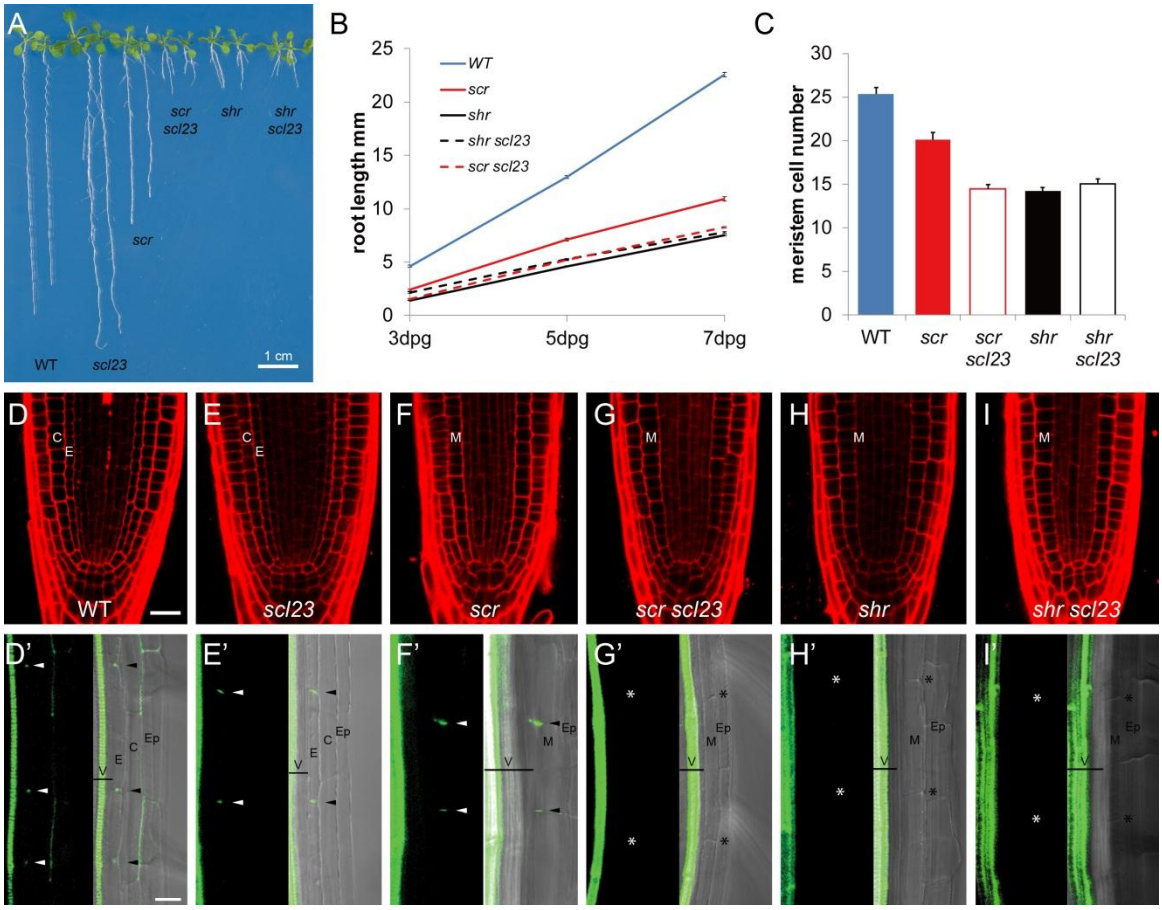

Figure 2. SCL23 and SCR are required for endodermal fate specification.

A Root length of 14 days post-germinations (dpg) seedings of WT, *scl23*, *scr*, *scr scl23*, *shr* and *shr scl23*. **B** Root length quantifications of the genotypes in **A** at 3, 5 and 7 dpg. Error bars represent standard errors of means. WT n=73, *scr* n=48, *scr scl23* n=43, *shr* n=53, *shr scl23* n=52. **C** Meristem cell number determined by cortex cells of the genotypes in **A** at 4 dpg. Error bars represent standard errors of means. WT n=19, *scr* n=20, *scr scl23* n=13, *shr* n=19, *shr scl23* n=15. **D-I** Root meristems of 3 dpg WT (**D**), *scl23* (**E**), *scr* (**F**), *scr scl23* (**G**), *shr* (**H**) and *shr scl23* (**I**). **D'-I'** Casparian strip staining in the genotypes in **D**. Left panel shows the fluorescent signal of Casparian strips and xylems, while right panel shows such signals overlaid with light transmission image. Arrowheads point to Casparian strips. Asterisks marks ground tissue cell wall positions without Casparian strip staining. V, vasculature; E, endodermis; C, cortex; Ep, epidermis; M, ground tissue monolayer. Scale bars represent 20 µm if not specifically indicated in the figure.

SCL23 protein shows stele enrichment in the root meristem

To determine the expression domain of *SCL23*, we generated *pSCL23::NLS-3YFP* and *pSCL23::SCL23:YFP* reporter constructs, and transformed them into wild-type (WT) Arabidopsis. Analysis of promoter activity indicated that the *SCL23* transcription domain

resides predominantly in the mature endodermis and cortex of Arabidopsis roots, starting from the transition zone shootwards, which largely represented the published microarray data (Figure 3A; Birnbaum *et al.*, 2005; Brady *et al.*, 2007). In the meristem, *pSCL23::NLS-3YFP* signal could be detected occasionally in the ground tissue cells adjacent to the stem cell niche (Figure 3A). The SCL23:YFP protein fluorescent signal, however, was observed not only in the ground tissue but also in the stele where no *SCL23* promoter activity was detected (Figure 3B). We found SCL23:YFP localized to both the nuclei and cytoplasm of root cells similar to SHR (Figure 3B). Such a subcellular localization of SCL23, together with its presence in the stele, is consistent with the observed nucleocytoplasmic SCL23-SHR interaction in protoplast cells (Figure 1B).

Figure 3. Root expression pattern of SCL23.

A, B Expression pattern of SCL23 depicted by *pSCL23::NLS-3YFP* (**A**) and *pSCL23::SCL23:YFP* (**B**). Scale bar represents 20 µm.

SCL23 restricts SHR stele exit.

Given the interaction between SCL23 and SHR, the close homology between SCL23 and SCR and the role of SCR to restrict SHR movement, we hypothesized that SCL23 might

also constrain SHR movement. As ectopic SCR expression in the stele abolished SHR outward movement through promoting its nuclear retention (Figure 4C; Koizumi *et al.*, 2012; Long *et al.*, 2015 b), we assessed the significance of the vascular meristematic accumulation of SCL23 protein by increasing its levels in vasculature using *WOODENLEG* promoter (*pWOL*; Bonke *et al.*, 2003). We noticed that in roots expressing *pWOL::SCL23,* the endodermis and cortex failed to completely separate, resulting in patches of ground tissue monolayer in the root meristem (Figure 4B). This phenotype was reminiscent to ectopic SCR expression in the stele. We next monitored SHR movement by introducing *pWOL::SCL23* into *pSHR::SHR:YFP* plants, and found that SHR:YFP could not be detected in the monolayer (Figure 4B). This data indicates that SCL23 is able to constrain intercellular SHR movement.

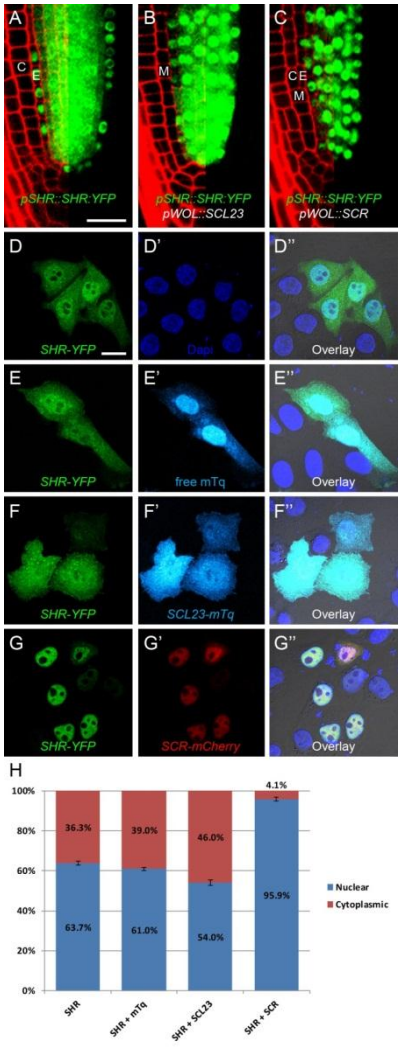

Figure 4. SCL23 restricts SHR outspread without nuclear retention.

A-C SHR:YFP exhibits nucleocytoplasmic localization in the stele while nuclear localization in the endodermis (**A**). *pWOL::SCL23* retards SHR:YFP stele exit, while retaining its nucleocytoplasmic distribution (**B**). *pWOL::SCR* retards SHR:YFP stele exit by nuclear retention (**C**). Both ectopic SCR and SCL23 expressions resulted in a ground tissue monolayer. Left panel shows SHR:YFP signal overlaid with cell walls stained with PI, while right panel shows the SHR:YFP signal only. C, cortex; E, endodermis; M, ground tissue monolayer. **D-G"** HeLa cell analysis of SHR-YFP nuclear retention. SHR-YFP exhibits nucleocytoplasmic localization, similar to that in the stele (**D-D"**). Free mTurquoise (mTq) was used as negative control (**E-E"**). SCL23-mTq fails to enrich SHR-YFP into nuclei (**F-F"**), while SCR-mCherry promotes near-complete SHR-YFP nuclear accumulation (**G-G"**). **H** Quantification of HeLa cell analysis in **D-G"**. Error bars represent standard errors of means. Scale bars represent 20 µm.

SCR was previously described to restrict SHR movement by a mechanism that involves nuclear retention through protein complex formation (Figure 4C; Long *et al.*, 2015 b). We asked whether SCL23 acts similarly to SCR by retaining SHR into the nucleus. Analysis of *pSHR::SHR:YFP* roots with ectopic *pWOL::SCL23* expression revealed that SHR:YFP maintained its nucleocytoplasmic dual localization (Figure 4B). We also introduced SHR, SCR and SCL23 into a heterologous system of HeLa cells to prevent crosstalk from plant-specific factors, and verified that SCL23 did not confer SHR nuclear enrichment as SCR did (Figure 4D-H).

SCL23 and SCR control formative divisions in the ground tissue through mutual repression.

Endodermal SHR activates *SCR* to promote the formative divisions which separates cortex and endodermis (Nakajima et al., 2001a; Cruz-Ramírez et al., 2012a). Since *pWOL::SCL23* blocked SHR stele exit, we asked whether SHR retention resulted in reduced SCR levels which prevented formative divisions. We monitored *pSCR::SCR:CFP* expression in *pWOL::SCL23* lines, and found that, consistent with retarded SHR movement, SCR:CFP accumulation was undetectable in the meristem (Figure 5A-B'). In the transition zone where *pWOL::SCL23:YFP* level was reduced, SCR:CFP reappeared and both ground tissue layers could be detected (Figure 5B, B'). These data suggest that high levels of SCL23 can control formative divisions in the ground tissue through regulating SHR action range.

SHR and SCR are described to share a common set of transcriptional targets including *SCR* itself and *SCL23* (Levesque et al., 2006a; Cui et al., 2007a, 2014). We determined whether *SCL23* is transcriptionally dependent on SCR and/or SHR by qRT-PCR and found a reduced expression in *shr* mutant roots (Fig 4G). This observation was confirmed by a largely reduced SCL23:YFP accumulation in *shr* mutant roots (Figure 5D, D'), and in agreement with a previous study showing *SCL23* regulation by SHR in the shoot (Cui et al., 2014). However, in *scr*, both *SCL23* transcript and SCL23 protein levels were

increased (Figure 5E, E', G) suggesting SCR negatively regulates *SCL23* transcription. We then assessed SCL23 protein level in roots ectopically expressing SCR in the stele under the *pWOL* promoter and found reduced SCL23 expression in the meristem correlating with high *pWOL:SCR:mRFP* expression (Figure 5F, F'). These results indicate that *SCR* represses *SCL23* transcription in the root meristem. Nevertheless, SCL23 is expressed in the endodermis shootward from the meristem where SCR is also present, indicating additional factors are involved in its regulation.

Taken together, these data suggest a mutual repression between SCL23 and SCR, whereby SCL23 can influence SCR levels through its control over SHR accumulation while SCR negatively regulates *SCL23* transcription.

SCL23 protein moves inward from the ground tissue to the stele and rootward from elongation zone to meristem.

The bias in *SCL23* transcript and SCL23 protein localization suggests that SCL23 protein can move from the ground tissue into the central stele and from the elongation zone rootwards to the meristem. Radial movement of SCL23 has also been suggested previously (Rim et al., 2011). To determine SCL23 movement directionality, we ectopically expressed SCL23:YFP under promoters marking different cell types and tracked its mobility between cell layers. We first monitored SCL23 expression under *pCO2* promoter which is expressed predominantly in the cortex (Figure 6A, A'; Heidstra *et al.*, 2004), and found SCL23:YFP signal not only in the cortex but also in the endodermis and pericycle (Figure 6B, B'). Similarly, when SCL23:YFP was driven by the *pEN7* promoter, predominantly expressed in the endodermis (Figure 6C, C'; Heidstra *et al.*, 2004), signal could also be detected spreading into the pericycle from endodermis (Figure 6D, D'). When expressed in the epidermal lineage under the *WEREWOLF* promoter (*pWER*; Figure 6E, E'; Lee and Schiefelbein, 1999), SCL23:YFP kept its nucleocytoplasmic localization but failed to move inwards (Figure 6F, F'). When expressed in the stele under *pWOL* (Figure 6G, G'), SCL23:YFP was restricted to the stele (Figure 6H, H').

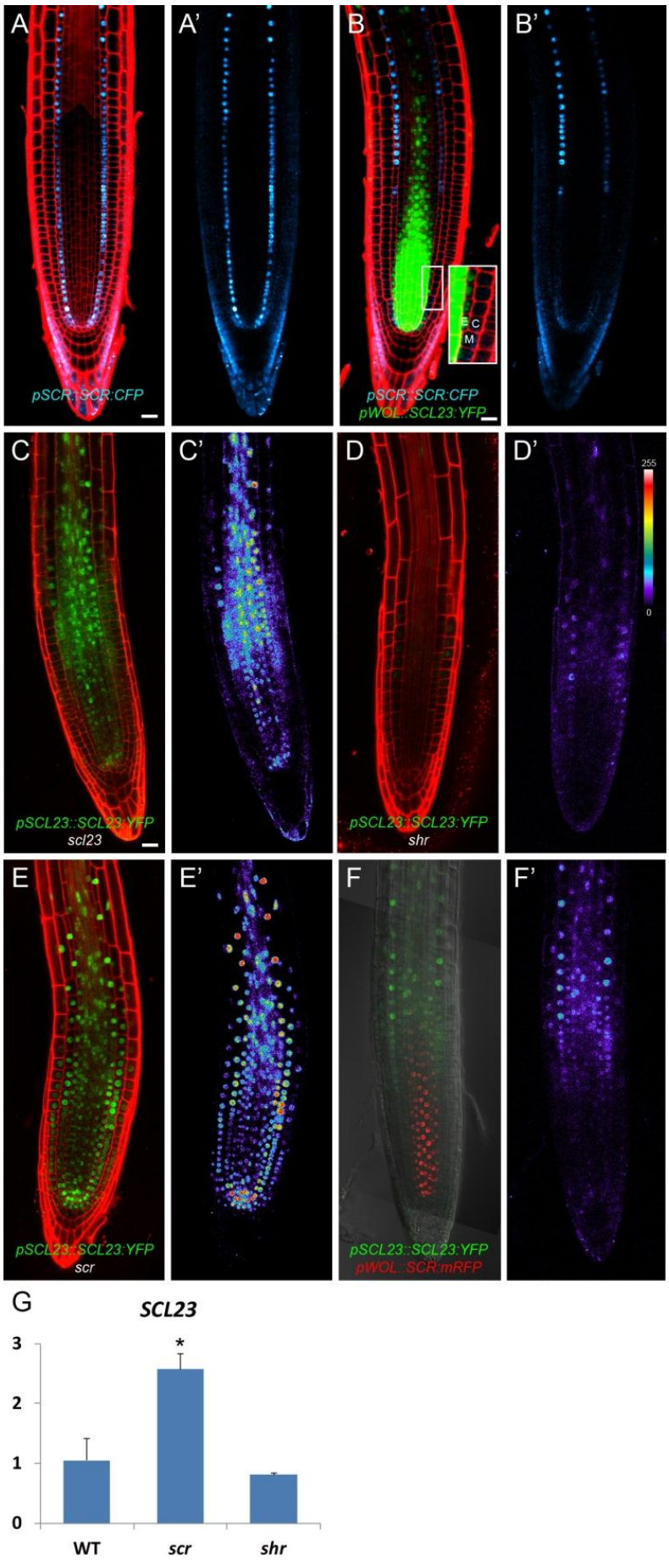

Figure 5. SCL23 and SCR form mutual repression.

A-B' pSCR::SCR:CFP expression in WT root (**A, A'**). Ectopic *pWOL::SCL23:YFP* abolished *pSCR::SCR:CFP* expression in the root meristem, while SCR expression is resumed in the transition zone (**B, B'**). **A'** and **B'** are signals of CFP channel from **A** and **B**. Note that the cyan signal near the stem cell niche in **B'** is excluded from nuclei, and represents auto-fluorescence which is also present in **A'**. **C-F'** *pSCL23::SCL23:YFP* level in *scl23* (**C, C'**), *shr* (**D, D'**), *scr* (**E, E'**) and *pWOL::SCR:RFP* line (**F, F'**). SCL23:YFP signal level is depicted in the intensity heatmap in **C'-F'**. Heatmap pseudo-color scale is as presented. **G** *SCL23* mRNA levels in WT, *scr* ($p = 0.03 < 0.05$, asterisk) and *shr* ($p = 0.18 > 0.05$) determined by qRT-PCR. Error bars represent standard deviations.Scale bars represent 20 μm.

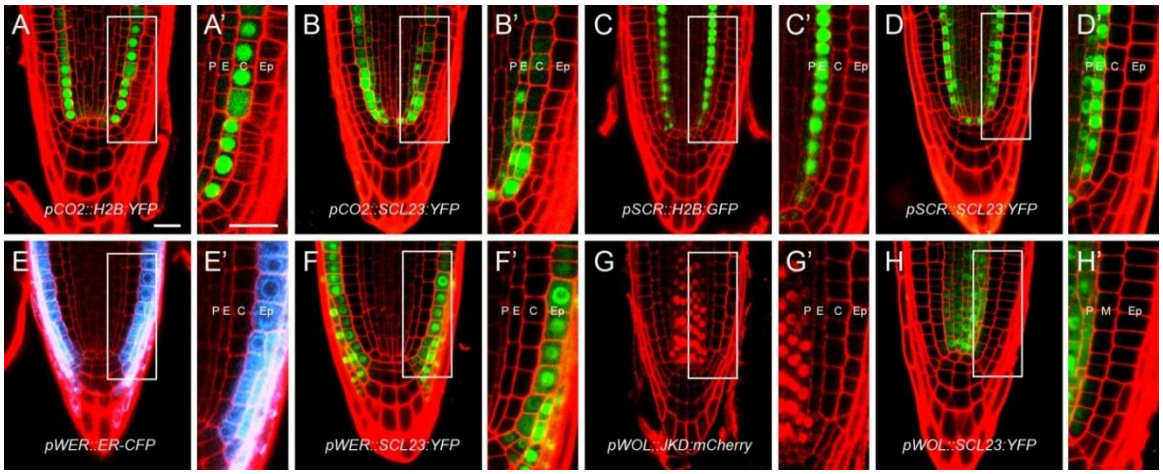

Figure 6. SCL23 protein moves inward from the ground tissue to the stele.

A-H' SCL23 moves from the ground tissue to the stele. *pCO2::H2B:YFP* (**A, A'**), *pCO2::SCL23:YFP* (**B, B'**), *pSCR::H2B:GFP* (**C, C'**), *pSCR::SCL23:YFP* (**D, D'**), *pWER::ER-CFP* (**E, E'**), *pWER::SCL23:YFP* (**F, F'**), *pWOL::JKD:mCherry* (**G, G'**), *pWOL::SCL23:YFP* (**H, H'**). **A'-H'** are enlarged images of the boxed regions in **A-H**. P, pericycle; E, endodermis; C, cortex; Ep, epidermis; M, ground tissue monolayer. Scale bars represent 20 µm.

To test it rootward movement, we constructed SCL23:YFP protein fusion under the promoter of *SODIUM POTASSIUM ROOT DEFECTIVE1* (*pNaKR1*) reported to be active only in the phloem companion cells shootward from the root meristem (Tian et al., 2010). Indeed when *pNaKR1::H2B:YFP* and *pNaKR1::JKD:YFP* were introduced in WT roots, signals were only detected in a subset of vascular cell files in the elongation zone (Figure 7A, B). However, *pNaKR1::SCL23:YFP* signal was detectable not only in the *pNaKR1* domain but also in the meristemic stele, indicating that SCL23:YFP has moved rootwards (Figure 7C). Additionally, weak signal was also visible in the endodermis, cortex and epidermis of *pNaKR1::SCL23:YFP* roots, predominantly in the transition zone (Figure 7C'). This suggests that SCL23 can also move out of the stele. Interestingly, no longitudinal or radial SHR:YFP spread was detected from the *pNaKR1* domain (Figure 7D; Sena *et al.*, 2004). Together with its aforementioned expression pattern, these data confirm that SCL23 protein moves rootward and preferentially inwards, i.e. from the ground tissue into the stele.

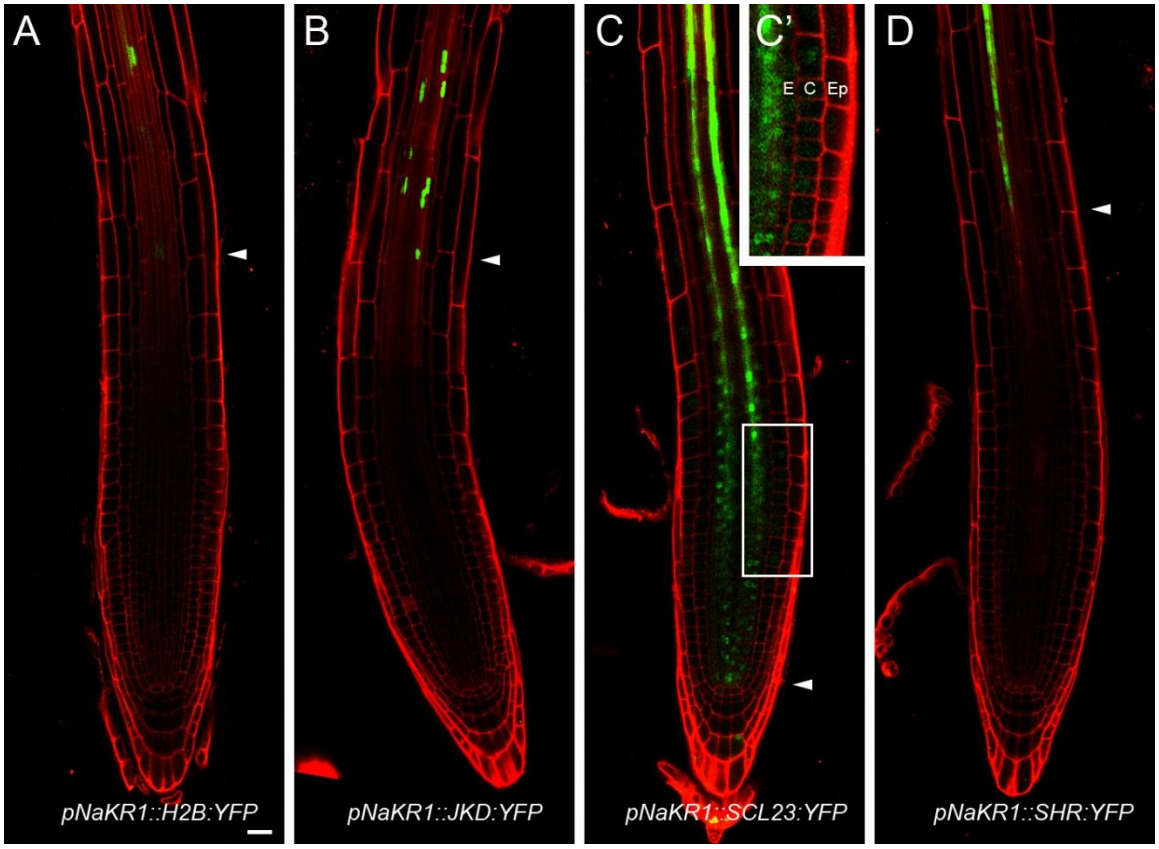

Figure 7. SCL23 protein moves rootward from elongation zone to meristem

A-D SCL23:YFP moves from the *pNaKR1* domain of mature phloem companion cells (**C, C'**), while H2B:YFP (**A**), JKD:YFP (**B**) or SHR:YFP (**D**) does not move from this domain. Arrowheads point to the most rootward signal. Brightness and contrast are increased in **C'** to enhance SCL23:YFP visualization outside the stele.

DISCUSSION

In this report, we identified SCL23 as a mobile protein controlling endodermal specification jointly with its binding partner SCR. SCL23 belongs to the GRAS domain protein family, and is the closest homolog to SCR in monocot and dicot plants (Lee et al., 2008). Interestingly, despite high homologous to SCR, SCL23 lacks the N-terminal region upstream the GRAS domain. It has been shown that SCR lacking this N-terminal region fails to be restricted to nucleus and acquired ability to move outwards when expressed in the stele. In addition, when the N-terminal region of SCR was artificially attached to SHR, it promoted SHR nuclear localization and limited its movement (Gallagher and Benfey, 2009a). These data suggest that the difference in localization and mobility between SCR and SCL23 might be conferred by this region. However, SCR lacking the N-terminal

domain did not mimic SCL23 localization nor acquired ability for inward movement (Cui and Benfey, 2009), indicating that SCL23 might contain specific motifs attributing to its directional intercellular trafficking.

SCL23 is mainly transcribed in the ground tissue starting shootwards from the transition zone, while the protein moves inward to the vasculature and rootwards into the meristem. Despite showing a general inward movement from meristemic ground tissue (Figure 6, Rim *et al.*, 2011), SCL23 protein can spread outward to epidermis as well (Figure 3). This is especially notorious in the transition zone where SCL23 level is high, and indicates that SCL23 movement has zone-specific directional preference, with the meristem favoring ground-tissue-to-stele movement while the transition zone exhibiting a bidirectional radial movement. Such a directional pattern also suggests that SCL23 movement is differentially regulated across the root. Dissecting these root zones and identifying regulators of SCL23 movement will advance our understanding in the control mechanisms of intercellular protein trafficking.

SCL23 contributes to endodermis specification redundantly with SCR and downstream of SHR. Predominantly localized to the stele in meristem, SCL23 might non-cell-autonomously contribute to endodermal fate specification by promoting the stele-originated signal. Alternatively, SCL23 might function cell-autonomously in the transition zone and rootwards, where endodermal SCL23 is more abundant, to mediate endodermis maturation. Additionally, the double mutant *scr scl23* also mimics the *shr* phenotypes in reducing root length and overall plant size. This suggests that SHR action in controlling root and shoot development is mediated by joined action of both SCR and SCL23. Isolating SCL23 targets and domain-specific rescue in the roots will provide more insights on the exact function of SCL23. Interestingly, SCL23 is also involved in the establishment of the bundle sheath, a specialized cell layer outside the leaf vasculature or vein, in the leaf together with SCR and SHR (Cui et al., 2014). The similar molecular determinants for endodermis and bundle sheath confirm that they are analogous cell types (Cui et al., 2014). SHR protein was also found one cell layer outside the leaf vein where it is transcribed, indicating that the SHR movement pattern is also conserved in

roots and leaves (Gardiner et al., 2011). However it remains to be tested whether SHR movement is required for bundle sheath formation. In addition, SCL23 movement has not been documented yet in the aboveground tissues, and it will be interesting to examine whether SCL23 is mobile in leaves.

While we have identified SCL23 as a mobile molecule with distinct trafficking directionality compared to SHR, it is unclear to what extent this movement is relevant for its function. It remains to be established whether SCL23 trafficking is required for SHR movement regulation, endodermis specification, or both. One possibility is that SCL23 might counter SHR outspread by binding and back fluxing SHR. As SHR is equally distributed after the CEI division into the first endodermis and cortex cells (Nakajima et al., 2001a), the early ground tissue expression of *SCL23* might function to reduce SHR activity to prevent additional divisions or maintain a delayed division status in the CEI.

In plants, many transcription factors have been found to translocate between cells and exert functions outside their transcriptional domains (Reviewed by Han *et al.*, 2014). Many of these transcription factors such as LFY and WUSCHEL (WUS) seem to diffuse between cells (Sessions et al., 2000; Yadav et al., 2011), while others such as TARGET OF MONOPTEROS 7 (TMO7) move in a specific direction and/or with a specific range (Schlereth et al., 2010a; Rim et al., 2011). We show that both SHR and SCL23 movements are directional and partially opposite. SHR and SCL23 can form protein complexes with each other and with the immobile SCR to regulate SHR movement range and to specify endodermis. Similarly, the floral homeotic MADS-box proteins DEFICIENS (DEF) and GLOBOSA (GLO) in *Antirrhinum majus* were shown to move within the floral meristem and form protein complexes to specify petal and stamen identities (Schwarz-Sommer et al., 1992; Perbal et al., 1996). It is likely that many more plant developmental processes require the combined activities of mobile transcription factors, and a thorough characterization of these factors is required to understand plant development as a whole.

EXPERIMENTAL PROCEDURES

Y2H screen

A yeast two hybrid library was constructed from Arabidopsis 5 day old roots derived cDNA according to the CloneMiner cDNA Library Construction Kit (Invitrogen) and transferred into pDEST22 using Gateway technology. This library was amplified once and subsequently plasmid DNA was isolated using the Qiagen HiSpeed Plasmid Midi Kit.

Screening was performed with 5mM 3AT (3-Amino-1,2,4-Triazole) to prevent false positive detection due to low autoactivation by the DBD:SCR fusion protein.

Growth condition and plant lines

Growth conditions of *Arabidopsis thaliana* ecotype Columbia-0 (Col-0) are as described by (Sabatini et al., 1999b). Mutant and transgenic lines used are as follows: *scr-3* (Fukaki et al., 1996b); *shr-2* (Nakajima et al., 2001a); *scl23-2* (Lee et al., 2008); *pCO2::H2B:YFP* and *pSCR::H2B:YFP* (Heidstra et al., 2004a); *pWER::ER-CFP* (Willemsen et al., 2008); *pWOL::JKD:mCherry* (Long *et al.*, 2015 b). SHR and SCR fluorescent fusion lines are as described in (Long et al., 2015a). Double mutants were generated by crossing.

Constructs for plants and cells

Coding sequence (CDS) of *SCL23* was amplified using primers in Supplementary Table 1 and subcloned into pDONR221 by Gateway BP reaction (Invitrogen). Approximately 1.7kb upstream of *SCL23* start codon was selected for *SCL23* promoter (*pSCL23*) and introduced into pGEMteasy1R4. Promoters such as *pNaKR1* (Tian et al., 2010), *pCO2* and *pEN7* were also subcloned into pGEMteasy1R4 vectors. *pWER* and *pWOL* are as described in (Hassan et al., 2010). Plant expression vectors were created by Multisite Gateway LR reactions (Invitrogen).

CDS of *SCL23* was also subcloned into HeLa expression vector mTurquoise-N1 (Goedhart et al., 2010b). Other HeLa expression vectors are as described in (Long *et al.*, 2015 b).

Bimolecular fluorescence complementation assay

SCL23 CDS in pDONR221 was recombined into pACR233 vector for BiFC analysis. Other BiFC vectors are as described in (Welch et al., 2007a) and (Cruz-Ramírez et al., 2012a).

A. thaliana Col-0 mesophyll protoplasts were prepared and transfected according to Yoo *et al.* (2007) with following adaptations: 4^{th} and 5^{th} leaves from young seedings were incised on the abaxial side and laid on the surface of enzyme solution for overnight digestion. During transfection, 40% PEG-calcium transfection solution was used. 2×10^5 protoplast cells were used for each transfection. 5µg of each BiFC vectors were transfected. After transfection, W5 solution was used instead of WI, and transfected protoplasts were cultivated overnight under constant light before observation.

FRET-FLIM

SCL23 *CDS* in pDONR221 was introduced between Cauliflower mosaic virus *35S* promoter and *SYFP2* by Multisite Gateway LR reaction (Invitrogen). Constructs used for FRET-FLIM in plants and Hela Cells are described in (Long *et al.*, 2015 b).

Living transfected protoplasts were collected in LabTek chambered coverglass (Nunc) for FLIM measurement according to Goedhart *et al.* (2007). HeLa cells were transfected according to Long, *al.* (2015 b) and FLIM was measured as described in Goedhart *et al.* (2010). CFP-variants and SYFP2-fused samples were exited with a 440 nm modulated diode laser (LDH-M-C-440; PicoQuant) or a 514 nm Argon laser (Melles-Griot) intensity-modulated at a frequency of 75.1 MHz. The light was reflected by a 455DCLP or

a 525DCXR dichroic mirror and emission was passed through a D480/40 or a HQ545/30 band-pass emission filter (Chroma Technology). Emissions were detected using a radio frequency (RF)-modulated image intensifier (Lambert Instruments II18MD) coupled to a charge-coupled device (CCD) camera (Photometrics HQ) as detector. FLIM stacks of 18 phase images were acquired in permutated recording order with an exposure time of 50-1000 ms per image depending on sample brightness. FRET efficiency was calculated as described in Goedhart *et al.* (2007). More than 60 cells were analyzed for each sample.

Confocal microscopy

Roots were mounted in 10µM propidium iodide for cell wall visualization. HeLa cells were transfected and fixed as in Long et al (2015 b). Confocal microscopy was performed using a Leica SP2 and Zeiss LSM710 confocal as described in Wachsman *et al.* (2011) and Long,. (2015 b). Nuclear and cytoplasmic ratio of SHR-YFP was determined by plotting the mean intensities of three regions of intrests in the nucleus and cytoplasm of each HeLa cell with background extraction measured by using ImageJ according to Long et *al.* (2015 b).

Quantitative RT-PCR

Total RNA was extracted from 7-day old seedings (Spectrum Plant Total RNA Kit; Sigma-Aldrich). DNase treatment and cDNA synthesis were performed according to the manufacturer's description (Fermentas). Quantitative RT-PCR was performed using SYBR Green Mastermix (Applied Biosystems). Results were normalized against ACTIN expression.

Casparian strip visualization

6 day-old roots were cleared according to (Alassimone et al., 2010). Cleared roots were mounted in 50% glycerol and Casparian strip autofluorescence was visualized at 520 – 580 nm by 514 nm laser excitation.

Image processing

For images showing long root regions, overlapping confocal images were stitched together with Adobe Photoshop (Figure 3, 5A-F', 7). All root images were rotated to vertical orientation in Adobe Photoshop, and the resulting empty area was filled with black pixels to generate rectangular panels (Figure 2D-I', 3, 4A-C, 5A-F', 6, 7).

SUPPLEMENTARY DATA

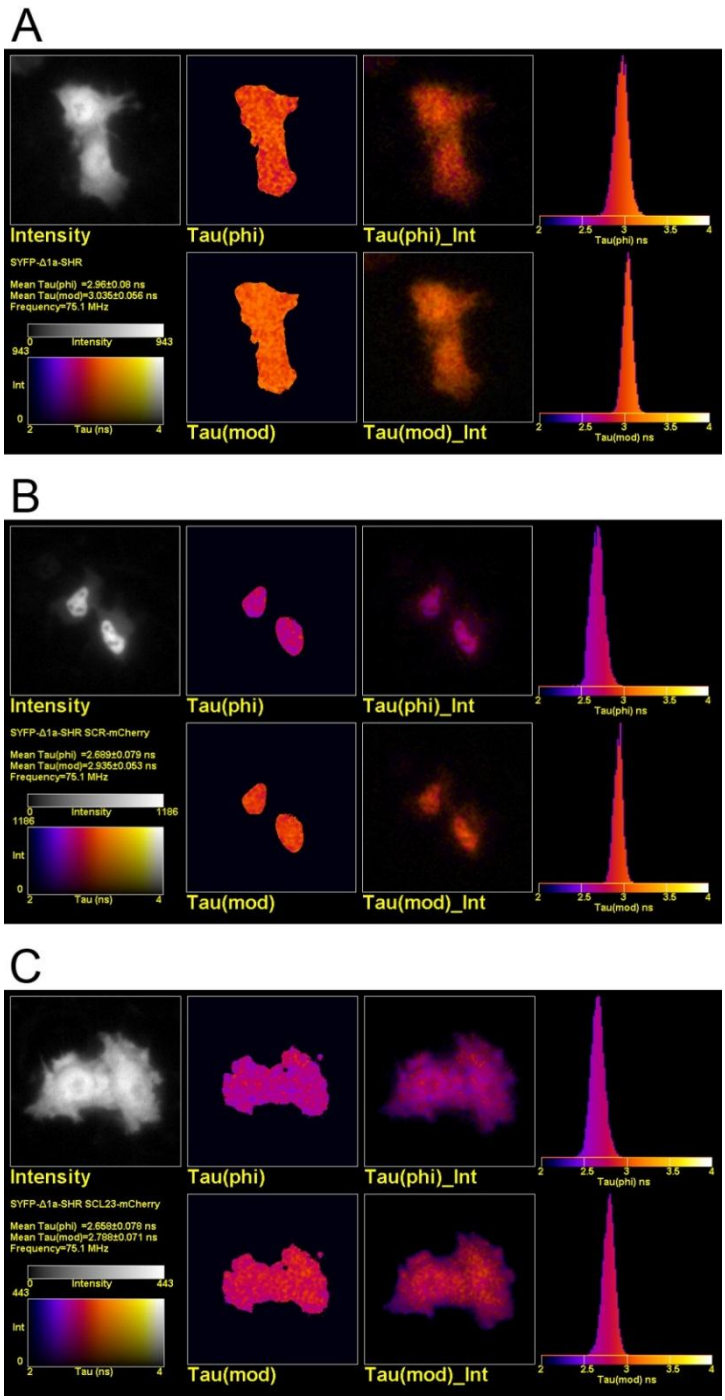

Supplementary Figure 1. FRET-FIM analysis between SHR, SCR and SCL23 in HeLa cells.

A-C Intensity images, fluorescence lifetime heatmaps, fluorescence lifetime heatmaps superposed on intensity images and fluorescence lifetime histograms of SYFP-Δ1a-SHR when expressed alone (**A**), with SCR-mCherry (**B**) or SCL23-mCherry (**C**) in HeLa cells. Intensity and fluorescence lifetime scales are as indicated. Average fluorescence lifetimes based on phase-shift, Tau(phi), and based on demodulation, Tau(mod), are as depicted.

Primer name	Sequnce (5'-3')
pSCL23-R4R1 F	GGGGACAACTTTGTATAGAAAAGTTGCGGCATCCCCATTTGGTAACACAC
pSCL23-R4R1 R	GGGGACTGCTTTTTTGTACAAACTTGCTCGAAAAGAGAAAGGGTTCGAGAG
pCO2-R4R1 F	GGGGACAACTTTGTATAGAAAAGTTGTATCGAGTAACTCCATTATTTACGACTGTGCC
pCO2-R4R1 R	GGGGACTGCTTTTTTGTACAAACTTGTCAAACTCTTGTTGCATTATTGTCAAATCCT
pEN7-R4R1 F	GGGGACAACTTTGTATAGAAAAGTTGTATCGAGCTGCTCCATTAGTCCATATACACAGTT
pEN7-R4R1 R	GGGGACTGCTTTTTTGTACAAACTTGTCTTTTCTTCGTGAATCTCAGAATCTTAAAG
pNaKR1-R4R1 F	GGGGACAACTTTGTATAGAAAAGTTGGCCTTTGTGAAATCGATTTGAGTTAGAAAACCCTC
pNaKR1-R4R1 R	GGGGACTGCTTTTTTGTACAAACTTGGTTTTGTATGGTTTACAAGAAATTTAAGAAAAAGTC
SCL23-221 F	GGGGACAAGTTTGTACAAAAAAGCAGGCTTCATGACTACAAAACGCATAGAC
SCL23-221 R	GGGGACCACTTTGTACAAGAAAGCTGGGTCATCGAACGGCTGAGATTTCC
SCL23-PstI F	AACTGCAGAAATGACTACAAAACGCATAG
SCL23-BamHI R	CGGGATCCCGATCGAACGGCTGAGATTTC
SCL23-qRT-PCR F	ATGACTACAAAACGCATAGACAG
SCL23-qRT-PCR R	GCTTCACGGAGATGATCAG
ACTIN-qRT-PCR F	GGCGAAGATGTGGCAGAGCA
ACTIN-qRT-PCR R	ACGAGGATTCGGTGCAGGACCT

Supplementary Table 1. Primers used in this study.

Chapter 7
General discussion

This thesis describes studies on radial patterning of Arabidopsis roots with an emphasis on the multi-leveled regulation and feedback on the action of the cell fate determinant SHORT-ROOT (SHR). Genetics, bioactivity assays and microscopy techniques were applied to map SHR interactions to SCARECROW (SCR) and BIRD proteins at cellular resolution. The results indicate that these proteins form cell type-specific protein complexes to influence SHR action. These complexes form a network that is responsible for the dynamic process of tissue boundary specification, allowing developmental plasticity of Arabidopsis roots upon network perturbations.

Endodermis, the "frontline" of vasculature

In this thesis we have demonstrated, among other points, how the endodermis is spatially stabilized in the root. Endodermis is an ancient tissue conserved in the roots of ferns and angiosperms, and it functions as a barrier between the outer tissue and the inner vasculature to establish selectivity for compounds taken up from the soil to enter the "vasculature highway". To do this, endodermis locally deposit a hydrophobic cell wall band called Casparian strip, sealing the apoplastic connectivity (transport between cells) and forcing the compounds through the selective endodermal cell layer (Geldner, 2013).

Many plant species has only one single "barrier layer", yet, in *Arabidopsis thaliana* multiple tissues are capable of acquiring endodermal features (Helariutta et al., 2000a; Sena et al., 2004a). To keep this layer adjacent to the vasculature, plants deploy a short-ranged signal from the vasculature to determine endodermal cell fate. SHR serves as such signal, while SCR and the BIRD proteins "wait" outside the vasculature to halt SHR movement, and ensure that endodermal specification occurs only in one layer. SHR movement is conserved among species, orthologs from *Brachypodium distachyon* and

Oryza sativa were shown to move further than AtSHR in Arabidopsis roots, and are able to ectopically induce extra divisions in the outer tissues (Wu et al., 2014). Indeed, both *B. distachyon* and *O. sativa* have many GT layers, however only the innermost layer becomes endodermis, and endogenous OsSHR was shown to only move one layer beyond vasculature in *O. sativa* root (Cui et al., 2007a). It is likely that, despite requiring extra factors, plants use similar regulatory networks to establish a single endodermal layer.

SHR signaling range is unrestricted in the *jkd bib-i* mutant, creating additional layers where outer cells progressively acquire endodermal features (Chapter 2). However, rather than creating multiple endodermis layers, the inner layers are reprogrammed into tissues with vascular properties (Chapter 2). Conversely, when JKD or BIB is ectopically introduced into vasculature, the endodermis-specific *CASPARIAN STRIP DOMAIN PROTEINS 1* (*CASP1*) expression is also induced in the vasculature (data not shown). These data indicate that there are two groups of inputs: SHR originating from inside out and the BIRD proteins expressed on the outside, and the two inputs are converging on the “frontline” to create the boundary layer of endodermis. From this “frontline”, other tissues might also be patterned accordingly, and one example is the endodermis-dependent vasculature patterning with the signal *microRNA165/166* moving from endodermis inward (Carlsbecker et al., 2010; Miyashima et al., 2011). There are likely more vascular patterning signals regulated by the SHR-SCR-BIRD network in the endodermis. In the outer tissues, the SHR-SCR-BIRD pathway may also play significant roles, as during embryogenesis JKD and SCR first express in the outermost cell layer (epidermis), and are progressively shifted inward along with embryonic divisions and SHR movement restriction into endodermal position (data not shown). Among the studied BIRD proteins, only *JKD* expression is prior to *SHR*. Given the fact that early *SCR* expression maintains high in *jkd* embryo, there might be other BIRD proteins required for early embryo patterning and GT formation.

Taken together, we propose that endodermis is a dynamic “frontline” separating the internal and external tissues. Continuous signal exchanges ensure that this “frontline” is

dynamically maintained. With different parameters, this dynamics may also contribute to the generation of multiple GT layers in many plant species and tissue reorganization during regeneration events.

SHR, a "master regulator" under stringent control

SHR is both necessary and sufficient to induce endodermal fate (Benfey et al., 1993; Scheres et al., 1995a; Helariutta et al., 2000a; Sena et al., 2004a). This has led to a description of the SHR protein as the "master regulator" of endodermis in Arabidopsis roots (Chan and Kyba, 2013). What are the mechanisms that dictate SHR action range? Below I will discuss evidence in this thesis that SHR action is controlled at different regulatory levels.

SHR movement is controlled

SHR is a mobile signal of vascular origin that induces endodermal fate in GT cells. To maintain the position of this single tissue layer, intercellular SHR movement is tightly regulated. In this thesis, we demonstrated that JKD and BIB are essential to restrict SHR outspread by retraining SHR into endodermal nuclei (Chapter 2). This is achieved by the combined effect of JKD and BIB forming nuclear complexes with SHR and transcriptionally activating SCR, which also forms nuclear complex with SHR and reinforces SHR nuclear retention. Thus, SHR is halted immediately after exit from the vasculature, and can only induce endodermal fate at such location. When this regulation mechanism is lifted in the *jkd bib-i* background, SHR distribution becomes much wider, forming an outward gradient (Chapter 2, Figure 2L2). This finding indicates that SHR movement might intrinsically have a diffusive property, similar to other mobile transcription factors such as LEAFY (FLY; Wu et al., 2003), and regulation is established by building a nuclear retention-induced "diffusion barrier" to restrict cytoplasmic SHR availability outside the stele. Since SHR moves between cells through plasmodesmata

(Vatén et al., 2011a), intercellular connections of neighboring cytoplasm (Lucas and Lee, 2004), a certain level of cytoplasmic SHR is required for its movement. Yet a cytoplasmic-exclusive SHR mutant failed to move between cells (Gallagher and Benfey, 2009a), indicating that nuclear localization might be important for both restricting and promoting intercellular SHR mobility.

On the other hand, as SHR movement has been suggested to rely on active transport (Koizumi et al., 2011a; Wu and Gallagher, 2013a, 2014), it will be interesting to see how the “transport” and “retention” mechanisms converge to contribute to the final movement pattern of SHR.

In Chapter 6, we described another mobile protein SCL23, whose localization is cytoplasmic and nuclear and coincides with SHR in both subcellular compartments to restrict its outspread without significantly altering its subcellular localization. This further indicates that nuclear retention is not the only mechanism to control SHR distribution. As SCL23 protein is most abundant in the vasculature, it is likely to determine the size of SHR immobile fraction at its source. Additionally, with its preferred outside-in movement direction, it is conceivable that SCL23 may confer SHR back flux into the vasculature, which would add a new mechanism for SHR movement control.

SHR localization is controlled

In a heterologous cell system, SHR exhibits a nucleocytoplasmic dual localization similar to that in the vasculature (Chapter 2), suggesting this is its native subcellular distribution. Addition of JKD, BIB and/or SCR can retain SHR into cell nuclei with various efficiencies (Chapter 2). However, despite the clear effect, it remains unclear how SHR nuclear retention is achieved. It is well established that nucleocytoplasmic trafficking of nuclear proteins relies on the recognition of nuclear localization signal (NLS) and/or nuclear export signal (NES) by the IMPORTIN/EXPORTIN proteins, which mediate transport through the nuclear pore complex. Usually, proteins carrying a NLS are recognized by the

IMPORTIN protein complex, whereas proteins containing a NES rely on EXPORTIN complex for nuclear export (Henderson and Percipalle, 1997; Hübner et al., 1997; Forwood and Jans, 2002). We found multiple putative NLS in JKD, BIB (Chapter 5) and SCR (data not shown), leading the proposition that they bind to the nuclear transport machinery to promote SHR nuclear localization. While imported, nuclear exit might be blocked by a lack of functional NES, by the SHR complex adhering to unknown anchoring factors, or by the sheer size of the SHR complex exceeding the size exclusion limit of the nuclear pores.

SHR transcriptional activity is controlled

SHR can be shuttled in and out of nuclei. This behavior is similar to the STAT proteins which partially rely on its nucleocytoplasmic translocation to regulate its transcriptional activity (Reviewed in Chapter 1). Even when nuclear localized, SHR transcriptional activity can be further regulated in gene-specific and cell-specific manners. JKD, for example, can differentially alter the expression level of at least two SHR targets, namely enhancing *SCR* transcription while repressing *CYCD6;1* transcription. The exact mechanism of this differential regulation is not yet clarified, but might involve different transcription factor assembly at target promoters. A similar scenario has been identified for JKD and other BIRD proteins during gibberellin signaling, where BIRD proteins bind the *SCARECROW-LIKE3* promoter (*pSCL3*) and recruit either DELLA or SCL3 to activate or repress *SCL3* expression (Yoshida et al., 2014a). In this respect, it will be interesting to identify the precise binding motifs for SHR, SCR, JKD and other BIRD proteins in *pSCR*, *pCYCD6;1* and other SHR-SCR targets, and dissect their local protein complex compositions.

SHR is present in the nuclei of quiescent center (QC), CEI/D and endodermis, but specifies endodermal fate only in the endodermis, and activates asymmetric cell divisions (ACD) only in the CEI/D and less frequently in the QC. To explain this differential behavior, Cruz-Ramírez and colleagues (2012) have identified a bistable regulatory circuit with the

active state only in the CEI/D and QC. Interestingly, this indicates that QC is also subjected to ACD, and indeed a similar regulatory circuit is responsible for its regulation (Cruz-Ramírez et al., 2013). However, the QC is mitotically less active comparing to CEI/D (Cruz-Ramírez et al., 2013), indicating that extra factors might repress its division. In Chapter 4, we show that this repression might be sustained by high level of JKD-SHR and BIB-SHR protein complexes, as genetic evidence indicates that JKD and BIB are responsible to repress ectopic ACD in the root (Chapter 2). In the CEI/D where ACD should take place, SHR-SCR complex is enriched, in accordance with its function in inducing divisions (Chapter 3). This SHR-SCR enrichment might be due to reduced JKD- and BIB binding to SHR and/or SCR, and fits with the prediction of the bistable circuit where SHR-SCR activity is enhanced in the CEI/D (Cruz-Ramírez et al., 2012a). Interestingly, in the first endodermal cell adjacent to the CEI/D, both JKD and BIB bind considerably more to SHR comparing to the following endodermal cells (Chapter 4, Figure 3D, L). This is possibly an extra mechanism to prevent subsequent ACD occurring immediately after the CEI/D division, and can work in conjunction with the “flop off” mechanism of the bistable circuit which relies on cell cycle-dependent degradation key regulators, including SHR and SCR (Cruz-Ramírez et al., 2012a). It remains to be established whether the BIRD proteins influence the role of RBR in the “flip-flop” circuit or whether they exert independent control that could enhance the robustness of the position of ACDs.

JKD “buffers” the SHR-SCR-BIRD network

JKD is a component of the SHR-SCR-BIRD regulatory network that regulates the network and root patterning with its homologs BIB, MGP and NUC (Long et al., 2015a), however multiple lines of evidence point to the hypothesis that JKD has additional functions that remain to be deciphered.

The *jkd* root phenotype includes SHR outspread into the cortex and a subsequent extra SHR-driven division, and also a disrupted and dysfunctional QC ((Welch et al., 2007a).

Although it is difficult to assess if there is extra QC divisions in *jkd*, the phenotype favors the conclusion that JKD 1) restricts SHR movement, 2) represses formative divisions and 3) specifies the QC.

In Chapter 2, we have shown that JKD and BIB redundantly restrict SHR movement by trapping it into the nuclei and by transcriptionally activating SCR as another SHR nuclear retainer. In addition, MGP and NUC also contribute to restricting SHR outspread, as in the quadruple mutant *jkd mgi-i nuc-i scr* SHR movement is also unhindered similar to *jkd bib-i* (Chapter 2, Figure 6T). These observations indicate that JKD is redundant to BIB, MGP and NUC to regulate SHR mobility.

JKD has dual functions

Our *in planta* FRET-FLIM results indicate that JKD complex might dominate the Arabidopsis QC and endodermis and is also present in the CEI, while other BIRD complexes such as BIB-SHR and NUC-SCR are either highly cell restricted or overall absent in WT roots (Chapter 4). JKD forms ternary complexes with SHR and SCR, and it is plausible that other regulators are also part of these multimer complexes. When *JKD* is mutated, BIB-SHR and NUC-SCR become more abundant (Chapter 4) in association with their functions identified by genetic analysis (Chapter 2). Taken together, it is likely that BIB and MGP/NUC form two subgroups of the studied BIRD proteins wit opposite regulatory effects, while JKD can and indeed takes over their functions in different cell contexts. The mechanism regulating this dual behavior remains to be elucidated. One possibility is that the presence of BIB or MGP/NUC can alter JKD's activity, and since BIB interaction seems to be QC exclusive while *MGP* and *NUC* are expressed away from QC, they could be the spatial cues for JKD functions. However to answer this, one needs to first complete the FRET-FLIM map with interactions such as MGP-SHR, MGP-SCR, BIB-SCR and NUC-SHR to assess if more BIRD proteins are associated with the SHR-SCR-JKD ternary complex or can form other complexes. Additionally, it will also be interesting to monitor JKD interactions in mutant backgrounds such as *bib-i* single and

mgp-i nuc-i double mutants where mild or no phenotype is observable. This might help to explain how JKD functions redundantly to both the ACD-repressing and ACD-activating BIRD proteins.

JKD may be a molecular guide

In Chapter 5, we found that JKD protein is not uniformly distributed in the nuclei, and it can superimpose its punctuate localization to SHR. We also isolated two JKD mutants that both bind strongly to SHR but give opposite developmental effects and different subnuclear localization of themselves and bound SHR. One mutant is condensed into specific subnuclear foci while the other seemingly fully dispersed in the nucleoplasm (Chapter 5). In combination with phenotypic analysis, we propose that the level of JKD-SHR subnuclear condensation anti-correlates with the occurrence of ACD. It is plausible that JKD is a molecular guide of its interactors and their associated network activity, where native JKD protein can guide SHR and other interactors to their target loci, while the condensing JKD mutant misguide them away. Determining the exact location, identity and dynamics of the JKD subnuclear compartments will help to elucidate how JKD may precisely regulate the output of the network.

Why so complex?

In this thesis, we have introduced and analyzed the SHR-SCR-BIRD regulatory network during root radial patterning. We have shown that Arabidopsis uses this integrated regulatory network to specify QC, CEI/D and endodermis in the root, and this network is likely dynamically regulated by many intertwined feedbacks. In addition, many other factors with relations to differentiation and cell cycle control are also likely to conjointly regulate this network (Cruz-Ramírez et al., 2012a, 2013). This complexity raises many questions that remain to be answered. For example, what is the exact protein complex composition in different cell types? We have shown that different levels of protein

associations are present in cells, which can lead to cell-specific multimers with different conformations. Indeed it is the case for SHR-SCR-JKD complex (Chapter 4), and higher order of protein complexes might also exist for SHR, SCR and other BIRD proteins. Given the fact that many transcription factor complexes contain many subunits (Spitz and Furlong, 2012), it is plausible that these transcriptional regulators form bigger complexes on target promoters that can give rise to different activities. Additionally, RBR is also known to form complexes with SCR and SHR (Cruz-Ramírez et al., 2012a). Although different interactions represent the functions of distinct protein complexes, it is important to determine the exact composition and stoichiometry of each regulatory complex to understand how they perform unique functions. It is a considerable technical challenge to obtain this information given our information that complexes change even in closely related cells.

Quantitative regulation between each factor is another open question. To induce different developmental outcomes, level dependency has been observed at least in SHR (Koizumi et al., 2012a) and SCR (Cui et al., 2007a). 10%~40% reduction of *SCR* by RNAi results in decreased SHR nuclear retention and outward spread (Cui et al., 2007a). The SHR level in *SCRi* GT decreases by ~40%, but is still sufficient to trigger formative divisions together with SCR (Koizumi et al., 2012b). On the other hand, SHR/shr heterozygosity also reduces SHR level in GT by ~40%, inducing extra ACD in the GT too but without enhancing SHR outspread (Koizumi et al., 2012a). As SCR is required to both activate ACD and restrict SHR mobility, these observations indicate that a lower SCR level is sufficient to trigger SHR-dependent divisions, while a higher SCR concentration is required to halt SHR movement. As *SCR* transcription is regulated by SHR, BIRD proteins and itself (Chapter 2), it is very likely that the abundance of SHR and SCR are not linearly related. Small changes in SHR level might significantly alter SCR level, which will in turn affect the amount of SHR retained in the nuclei and availability for downstream regulations. Coupling these with the dynamics of different protein complexes and their transcriptional regulations, interpretation of the network outcome will be challenging and will require the aid of minimalistic theoretical modeling to indicate key parameters that can

subsequently be quantitatively assessed by experiments.

But does this regulatory network need to be so complex? Why do plants not use simple single factors each for QC, CEI and endodermis? The answer might lie in evolution, as the root-like structure is a relatively late invention, and the endodermis arose even later (Raven and Edwards, 2001). For example, the land moss *Physcomitrella patens* does not have root nor endodermis, yet orthologs of *SHR*, *SCR* and *BIRD* genes are found in its genome (data not shown). Obviously these ancient orthologs are not involved in endodermis development, but have other original functions. Plausibly, as the primitive regulatory network evolved, complicated new functions were acquired later, such as regulating GT and specifying endodermis in root plants. As evolution is believed to lack general designs (Zuckerkandl, 2006), the high level of complexity might be the consequence rather than the driving force of new biological structures and functions. Alternatively, the resultant complexity has roles in development that we cannot yet appreciate due to the fact that we have mostly studied development in laboratory conditions rather than in the real world with a vast array of environmental challenges. Whatever its cause, to understand this complexity will be the next challenge.

REFERENCES

Abley, K., De Reuille, P.B., Strutt, D., Bangham, A., Prusinkiewicz, P., Marée, A.F.M., Grieneisen, V.A., and Coen, E. (2013). An intracellular partitioning-based framework for tissue cell polarity in plants and animals. Dev. Camb. Engl. *140*, 2061–2074.

Adjobo-Hermans, M.J.W., Goedhart, J., van Weeren, L., Nijmeijer, S., Manders, E.M.M., Offermanns, S., and Gadella, T.W.J., Jr (2011). Real-time visualization of heterotrimeric G protein Gq activation in living cells. BMC Biol. *9*, 32.

Alassimone, J., Naseer, S., and Geldner, N. (2010). A developmental framework for endodermal differentiation and polarity. Proc. Natl. Acad. Sci. *107*, 5214–5219.

Angel, A., Song, J., Dean, C., and Howard, M. (2011). A Polycomb-based switch underlying quantitative epigenetic memory. Nature *476*, 105–108.

Aouadi, M., Binetruy, B., Caron, L., Le Marchand-Brustel, Y., and Bost, F. (2006). Role of MAPKs in development and differentiation: lessons from knockout mice. Biochimie *88*, 1091–1098.

Axelos, M., Curie, C., Mazzolini, L., Bardet, C., and Lescure, B. (1992). A protocol for transient gene expression in Arabidopsis thaliana protoplasts isolated from cell suspension cultures. Plant Physiol. Biochem. *30*, 123–128.

Band, L.R., Wells, D.M., Fozard, J.A., Ghetiu, T., French, A.P., Pound, M.P., Wilson, M.H., Yu, L., Li, W., Hijazi, H.I., et al. (2014). Systems analysis of auxin transport in the Arabidopsis root apex. Plant Cell *26*, 862–875.

Baum, S.F., Dubrovsky, J.G., and Rost, T.L. (2002). Apical organization and maturation of the cortex and vascular cylinder inArabidopsis thaliana (Brassicaceae) roots. Am. J. Bot. *89*, 908–920.

Bäurle, I., and Laux, T. (2005). Regulation of WUSCHEL Transcription in the Stem Cell Niche of the Arabidopsis Shoot Meristem. Plant Cell *17*, 2271–2280.

Begitt, A., Droescher, M., Knobeloch, K.-P., and Vinkemeier, U. (2011). SUMO conjugation of STAT1 protects cells from hyperresponsiveness to IFNγ. Blood *118*, 1002–1007.

Benfey, P.N., Linstead, P.J., Roberts, K., Schiefelbein, J.W., Hauser, M.T., and Aeschbacher, R.A. (1993). Root development in Arabidopsis: four mutants with dramatically altered root morphogenesis. Dev. Camb. Engl. *119*, 57–70.

Bensimon, A., Heck, A.J.R., and Aebersold, R. (2012). Mass spectrometry-based proteomics and network biology. Annu. Rev. Biochem. *81*, 379–405.

Van den Berg, C., Willemsen, V., Hage, W., Weisbeek, P., and Scheres, B. (1995). Cell

fate in the Arabidopsis root meristem determined by directional signalling. Nature *378*, 62–65.

Birnbaum, K., Jung, J.W., Wang, J.Y., Lambert, G.M., Hirst, J.A., Galbraith, D.W., and Benfey, P.N. (2005). Cell type-specific expression profiling in plants via cell sorting of protoplasts from fluorescent reporter lines. Nat. Methods *2*, 615–619.

Bonke, M., Thitamadee, S., Mähönen, A.P., Hauser, M.-T., and Helariutta, Y. (2003a). APL regulates vascular tissue identity in Arabidopsis. Nature *426*, 181–186.

Bonke, M., Thitamadee, S., Mähönen, A.P., Hauser, M.-T., and Helariutta, Y. (2003b). APL regulates vascular tissue identity in Arabidopsis. Nature *426*, 181–186.

Bonner, J.T. (1998). The origins of multicellularity. Integr. Biol. Issues News Rev. *1*, 27–36.

Brady, S.M., Orlando, D.A., Lee, J.-Y., Wang, J.Y., Koch, J., Dinneny, J.R., Mace, D., Ohler, U., and Benfey, P.N. (2007). A high-resolution root spatiotemporal map reveals dominant expression patterns. Science *318*, 801–806.

Brayer, K.J., and Segal, D.J. (2008). Keep your fingers off my DNA: protein-protein interactions mediated by C2H2 zinc finger domains. Cell Biochem. Biophys. *50*, 111–131.

Bridgeman, J.S., Blaylock, M., Hawkins, R.E., and Gilham, D.E. (2010). Development of a flow cytometric co-immunoprecipitation technique for the study of multiple protein-protein interactions and its application to T-cell receptor analysis. Cytom. Part J. Int. Soc. Anal. Cytol. *77*, 338–346.

Brown, R.S. (2005). Zinc finger proteins: getting a grip on RNA. Curr. Opin. Struct. Biol. *15*, 94–98.

Bücherl, C.A., Esse, G.W. van, Kruis, A., Luchtenberg, J., Westphal, A.H., Aker, J., Hoek, A. van, Albrecht, C., Borst, J.W., and Vries, S.C. de (2013). Visualization of BRI1 and BAK1(SERK3) Membrane Receptor Heterooligomers during Brassinosteroid Signaling. Plant Physiol. *162*, 1911–1925.

Carlsbecker, A., Lee, J.-Y., Roberts, C.J., Dettmer, J., Lehesranta, S., Zhou, J., Lindgren, O., Moreno-Risueno, M.A., Vatén, A., Thitamadee, S., et al. (2010). Cell signalling by microRNA165/6 directs gene dose-dependent root cell fate. Nature *465*, 316–321.

Chan, S.S.-K., and Kyba, M. (2013). What is a Master Regulator? J. Stem Cell Res. Ther. *3*.

Clegg, R.M. (2009). Chapter 1 Förster resonance energy transfer—FRET what is it, why do it, and how it's done. In Laboratory Techniques in Biochemistry and Molecular Biology, T.W.J. Gadella, ed. (Elsevier), pp. 1–57.

Clough, S.J., and Bent, A.F. (1998). Floral dip: a simplified method for Agrobacterium-mediated transformation of Arabidopsis thaliana. Plant J. Cell Mol. Biol. *16*, 735–743.

Colasanti, J., Yuan, Z., and Sundaresan, V. (1998a). The indeterminate gene encodes a zinc finger protein and regulates a leaf-generated signal required for the transition to flowering in maize. Cell *93*, 593–603.

Colasanti, J., Yuan, Z., and Sundaresan, V. (1998b). The indeterminate gene encodes a zinc finger protein and regulates a leaf-generated signal required for the transition to flowering in maize. Cell *93*, 593–603.

Colasanti, J., Tremblay, R., Wong, A.Y.M., Coneva, V., Kozaki, A., and Mable, B.K. (2006a). The maize INDETERMINATE1 flowering time regulator defines a highly conserved zinc finger protein family in higher plants. BMC Genomics *7*, 158.

Colasanti, J., Tremblay, R., Wong, A.Y.M., Coneva, V., Kozaki, A., and Mable, B.K. (2006b). The maize INDETERMINATE1 flowering time regulator defines a highly conserved zinc finger protein family in higher plants. BMC Genomics *7*, 158.

Corbesier, L., Vincent, C., Jang, S., Fornara, F., Fan, Q., Searle, I., Giakountis, A., Farrona, S., Gissot, L., Turnbull, C., et al. (2007). FT protein movement contributes to long-distance signaling in floral induction of Arabidopsis. Science *316*, 1030–1033.

Corry, G.N., and Underhill, D.A. (2005). Subnuclear compartmentalization of sequence-specific transcription factors and regulation of eukaryotic gene expression. Biochem. Cell Biol. Biochim. Biol. Cell. *83*, 535–547.

Crawford, E.W., Jr, and Shimkets, L.J. (2000). The Myxococcus xanthus socE and csgA genes are regulated by the stringent response. Mol. Microbiol. *37*, 788–799.

Crosby, K.C., Pietraszewska-Bogiel, A., Gadella, T.W.J., Jr, and Winkel, B.S.J. (2011). Förster resonance energy transfer demonstrates a flavonoid metabolon in living plant cells that displays competitive interactions between enzymes. FEBS Lett. *585*, 2193–2198.

Cruz-Ramírez, A., Díaz-Triviño, S., Blilou, I., Grieneisen, V.A., Sozzani, R., Zamioudis, C., Miskolczi, P., Nieuwland, J., Benjamins, R., Dhonukshe, P., et al. (2012a). A bistable circuit involving SCARECROW-RETINOBLASTOMA integrates cues to inform asymmetric stem cell division. Cell *150*, 1002–1015.

Cruz-Ramírez, A., Díaz-Triviño, S., Blilou, I., Grieneisen, V.A., Sozzani, R., Zamioudis, C., Miskolczi, P., Nieuwland, J., Benjamins, R., Dhonukshe, P., et al. (2012b). A bistable circuit involving SCARECROW-RETINOBLASTOMA integrates cues to inform asymmetric stem cell division. Cell *150*, 1002–1015.

Cruz-Ramírez, A., Díaz-Triviño, S., Wachsman, G., Du, Y., Arteága-Vázquez, M., Zhang,

H., Benjamins, R., Blilou, I., Neef, A.B., Chandler, V., et al. (2013). A SCARECROW-RETINOBLASTOMA protein network controls protective quiescence in the Arabidopsis root stem cell organizer. PLoS Biol. *11*, e1001724.

Cui, H., and Benfey, P.N. (2009). Interplay between SCARECROW, GA and LIKE HETEROCHROMATIN PROTEIN 1 in ground tissue patterning in the Arabidopsis root. Plant J. Cell Mol. Biol. *58*, 1016–1027.

Cui, H., Levesque, M.P., Vernoux, T., Jung, J.W., Paquette, A.J., Gallagher, K.L., Wang, J.Y., Blilou, I., Scheres, B., and Benfey, P.N. (2007a). An evolutionarily conserved mechanism delimiting SHR movement defines a single layer of endodermis in plants. Science *316*, 421–425.

Cui, H., Levesque, M.P., Vernoux, T., Jung, J.W., Paquette, A.J., Gallagher, K.L., Wang, J.Y., Blilou, I., Scheres, B., and Benfey, P.N. (2007b). An evolutionarily conserved mechanism delimiting SHR movement defines a single layer of endodermis in plants. Science *316*, 421–425.

Cui, H., Hao, Y., and Kong, D. (2012). SCARECROW has a SHORT-ROOT-independent role in modulating the sugar response. Plant Physiol. *158*, 1769–1778.

Cui, H., Kong, D., Liu, X., and Hao, Y. (2014). SCARECROW, SCR-LIKE 23 and SHORT-ROOT control bundle sheath cell fate and function in Arabidopsis thaliana. Plant J. Cell Mol. Biol. *78*, 319–327.

Davies, D.G., Parsek, M.R., Pearson, J.P., Iglewski, B.H., Costerton, J.W., and Greenberg, E.P. (1998). The involvement of cell-to-cell signals in the development of a bacterial biofilm. Science *280*, 295–298.

Dhanasekaran, D.N., Kashef, K., Lee, C.M., Xu, H., and Reddy, E.P. (2007). Scaffold proteins of MAP-kinase modules. Oncogene *26*, 3185–3202.

Dolan, L. (2006). Positional information and mobile transcriptional regulators determine cell pattern in the Arabidopsis root epidermis. J. Exp. Bot. *57*, 51–54.

Dolan, L., Janmaat, K., Willemsen, V., Linstead, P., Poethig, S., Roberts, K., and Scheres, B. (1993a). Cellular organisation of the Arabidopsis thaliana root. Dev. Camb. Engl. *119*, 71–84.

Dolan, L., Janmaat, K., Willemsen, V., Linstead, P., Poethig, S., Roberts, K., and Scheres, B. (1993b). Cellular organisation of the Arabidopsis thaliana root. Dev. Camb. Engl. *119*, 71–84.

Du, T.-G., Schmid, M., and Jansen, R.-P. (2007). Why cells move messages: the biological functions of mRNA localization. Semin. Cell Dev. Biol. *18*, 171–177.

Eggeling, C., Berger, S., Brand, L., Fries, J.R., Schaffer, J., Volkmer, A., and Seidel, C.A.

(2001). Data registration and selective single-molecule analysis using multi-parameter fluorescence detection. J. Biotechnol. *86*, 163–180.

Englbrecht, C.C., Schoof, H., and Böhm, S. (2004). Conservation, diversification and expansion of C2H2 zinc finger proteins in the Arabidopsis thaliana genome. BMC Genomics *5*, 39.

Engstrom, E.M. (2011). Phylogenetic analysis of GRAS proteins from moss, lycophyte and vascular plant lineages reveals that GRAS genes arose and underwent substantial diversification in the ancestral lineage common to bryophytes and vascular plants. Plant Signal. Behav. *6*, 850–854.

Förster, T. (1948). Intermolecular energy migration and fluorescence. Ann. Phys. *437*, 55–75.

Forwood, J.K., and Jans, D.A. (2002). Nuclear import pathway of the telomere elongation suppressor TRF1: inhibition by importin alpha. Biochemistry (Mosc.) *41*, 9333–9340.

Freeman, M. (2000). Feedback control of intercellular signalling in development. Nature *408*, 313–319.

Fujikawa, Y., and Kato, N. (2007). Split luciferase complementation assay to study protein-protein interactions in Arabidopsis protoplasts. Plant J. Cell Mol. Biol. *52*, 185–195.

Fukaki, H., Fujisawa, H., and Tasaka, M. (1996a). SGR1, SGR2, SGR3: novel genetic loci involved in shoot gravitropism in Arabidopsis thaliana. Plant Physiol. *110*, 945–955.

Fukaki, H., Fujisawa, H., and Tasaka, M. (1996b). SGR1, SGR2, SGR3: novel genetic loci involved in shoot gravitropism in Arabidopsis thaliana. Plant Physiol. *110*, 945–955.

Fukaki, H., Wysocka-Diller, J., Kato, T., Fujisawa, H., Benfey, P.N., and Tasaka, M. (1998). Genetic evidence that the endodermis is essential for shoot gravitropism in Arabidopsis thaliana. Plant J. Cell Mol. Biol. *14*, 425–430.

Gadella Jr., T.W.J., Jovin, T.M., and Clegg, R.M. (1993). Fluorescence lifetime imaging microscopy (FLIM): Spatial resolution of microstructures on the nanosecond time scale. Biophys. Chem. *48*, 221–239.

Gallagher, K.L., and Benfey, P.N. (2009a). Both the conserved GRAS domain and nuclear localization are required for SHORT-ROOT movement. Plant J. Cell Mol. Biol. *57*, 785–797.

Gallagher, K.L., and Benfey, P.N. (2009b). Both the conserved GRAS domain and nuclear localization are required for SHORT-ROOT movement. Plant J. Cell Mol. Biol. *57*, 785–797.

Gallagher, K.L., Paquette, A.J., Nakajima, K., and Benfey, P.N. (2004a). Mechanisms regulating SHORT-ROOT intercellular movement. Curr. Biol. CB *14*, 1847–1851.

Gallagher, K.L., Paquette, A.J., Nakajima, K., and Benfey, P.N. (2004b). Mechanisms regulating SHORT-ROOT intercellular movement. Curr. Biol. CB *14*, 1847–1851.

Gallagher, K.L., Sozzani, R., and Lee, C.-M. (2014). Intercellular protein movement: deciphering the language of development. Annu. Rev. Cell Dev. Biol. *30*, 207–233.

Gardiner, J., Donner, T.J., and Scarpella, E. (2011). Simultaneous activation of SHR and ATHB8 expression defines switch to preprocambial cell state in Arabidopsis leaf development. Dev. Dyn. Off. Publ. Am. Assoc. Anat. *240*, 261–270.

Geldner, N. (2013). The endodermis. Annu. Rev. Plant Biol. *64*, 531–558.

Gerritsen, H.C., Agronskaia, A.V., Bader, A.N., and Esposito, A. (2009). Chapter 3 Time domain FLIM: Theory, instrumentation, and data analysis. In Laboratory Techniques in Biochemistry and Molecular Biology, T.W.J. Gadella, ed. (Elsevier), pp. 95–132.

Goedhart, J., Vermeer, J.E.M., Adjobo-Hermans, M.J.W., van Weeren, L., and Gadella, T.W.J., Jr (2007a). Sensitive detection of p65 homodimers using red-shifted and fluorescent protein-based FRET couples. PloS One *2*, e1011.

Goedhart, J., Vermeer, J.E.M., Adjobo-Hermans, M.J.W., van Weeren, L., and Gadella, T.W.J., Jr. (2007b). Sensitive Detection of p65 Homodimers Using Red-Shifted and Fluorescent Protein-Based FRET Couples. PLoS ONE *2*, e1011.

Goedhart, J., van Weeren, L., Hink, M.A., Vischer, N.O.E., Jalink, K., and Gadella, T.W.J., Jr (2010a). Bright cyan fluorescent protein variants identified by fluorescence lifetime screening. Nat. Methods *7*, 137–139.

Goedhart, J., van Weeren, L., Hink, M.A., Vischer, N.O.E., Jalink, K., and Gadella, T.W.J. (2010b). Bright cyan fluorescent protein variants identified by fluorescence lifetime screening. Nat. Methods *7*, 137–139.

Goedhart, J., von Stetten, D., Noirclerc-Savoye, M., Lelimousin, M., Joosen, L., Hink, M.A., van Weeren, L., Gadella, T.W.J., and Royant, A. (2012). Structure-guided evolution of cyan fluorescent proteins towards a quantum yield of 93%. Nat. Commun. *3*, 751.

Gohl, C., Banovic, D., Grevelhörster, A., and Bogdan, S. (2010). WAVE forms hetero- and homo-oligomeric complexes at integrin junctions in Drosophila visualized by bimolecular fluorescence complementation. J. Biol. Chem. *285*, 40171–40179.

Greenhalgh, C.J., and Hilton, D.J. (2001). Negative regulation of cytokine signaling. J. Leukoc. Biol. *70*, 348–356.

Grieneisen, V.A., Xu, J., Marée, A.F.M., Hogeweg, P., and Scheres, B. (2007). Auxin

transport is sufficient to generate a maximum and gradient guiding root growth. Nature *449*, 1008–1013.

Gu, Y., Di, W.L., Kelsell, D.P., and Zicha, D. (2004). Quantitative fluorescence resonance energy transfer (FRET) measurement with acceptor photobleaching and spectral unmixing. J. Microsc. *215*, 162–173.

Hake, S., and Freeling, M. (1986). Analysis of genetic mosaics shows that the extra epidermal cell divisions in Knotted mutant maize plants are induced by adjacent mesophyll cells. Nature *320*, 621–623.

Hall, T.M.T. (2005). Multiple modes of RNA recognition by zinc finger proteins. Curr. Opin. Struct. Biol. *15*, 367–373.

Hall-Stoodley, L., Costerton, J.W., and Stoodley, P. (2004). Bacterial biofilms: from the Natural environment to infectious diseases. Nat. Rev. Microbiol. *2*, 95–108.

Hamers, D., van Voorst Vader, L., Borst, J.W., and Goedhart, J. (2014). Development of FRET biosensors for mammalian and plant systems. Protoplasma *251*, 333–347.

Han, X., Kumar, D., Chen, H., Wu, S., and Kim, J.-Y. (2014). Transcription factor-mediated cell-to-cell signalling in plants. J. Exp. Bot. *65*, 1737–1749.

Hassan, H., Scheres, B., and Blilou, I. (2010). JACKDAW controls epidermal patterning in the Arabidopsis root meristem through a non-cell-autonomous mechanism. Dev. Camb. Engl. *137*, 1523–1529.

Heidstra, R., Welch, D., and Scheres, B. (2004a). Mosaic analyses using marked activation and deletion clones dissect Arabidopsis SCARECROW action in asymmetric cell division. Genes Dev. *18*, 1964–1969.

Heidstra, R., Welch, D., and Scheres, B. (2004b). Mosaic analyses using marked activation and deletion clones dissect Arabidopsis SCARECROW action in asymmetric cell division. Genes Dev. *18*, 1964–1969.

Hejátko, J., Blilou, I., Brewer, P.B., Friml, J., Scheres, B., and Benková, E. (2006). In situ hybridization technique for mRNA detection in whole mount Arabidopsis samples. Nat. Protoc. *1*, 1939–1946.

Helariutta, Y., Fukaki, H., Wysocka-Diller, J., Nakajima, K., Jung, J., Sena, G., Hauser, M.T., and Benfey, P.N. (2000a). The SHORT-ROOT gene controls radial patterning of the Arabidopsis root through radial signaling. Cell *101*, 555–567.

Helariutta, Y., Fukaki, H., Wysocka-Diller, J., Nakajima, K., Jung, J., Sena, G., Hauser, M.T., and Benfey, P.N. (2000b). The SHORT-ROOT gene controls radial patterning of the Arabidopsis root through radial signaling. Cell *101*, 555–567.

Henderson, B.R., and Percipalle, P. (1997). Interactions between HIV Rev and nuclear import and export factors: the Rev nuclear localisation signal mediates specific binding to human importin-beta. J. Mol. Biol. *274*, 693–707.

Heo, J.-O., Chang, K.S., Kim, I.A., Lee, M.-H., Lee, S.A., Song, S.-K., Lee, M.M., and Lim, J. (2011). Funneling of gibberellin signaling by the GRAS transcription regulator scarecrow-like 3 in the Arabidopsis root. Proc. Natl. Acad. Sci. U. S. A. *108*, 2166–2171.

Herbst, R.S. (2004). Review of epidermal growth factor receptor biology. Int. J. Radiat. Oncol. Biol. Phys. *59*, 21–26.

Ten Hove, C.A., Willemsen, V., de Vries, W.J., van Dijken, A., Scheres, B., and Heidstra, R. (2010). SCHIZORIZA encodes a nuclear factor regulating asymmetry of stem cell divisions in the Arabidopsis root. Curr. Biol. CB *20*, 452–457.

Hu, C.-D., Chinenov, Y., and Kerppola, T.K. (2002). Visualization of interactions among bZIP and Rel family proteins in living cells using bimolecular fluorescence complementation. Mol. Cell *9*, 789–798.

Hu, X., Dutta, P., Tsurumi, A., Li, J., Wang, J., Land, H., and Li, W.X. (2013). Unphosphorylated STAT5A stabilizes heterochromatin and suppresses tumor growth. Proc. Natl. Acad. Sci. U. S. A. *110*, 10213–10218.

Huang, C.Y., and Ferrell, J.E. (1996). Ultrasensitivity in the mitogen-activated protein kinase cascade. Proc. Natl. Acad. Sci. *93*, 10078–10083.

Hübner, S., Xiao, C.Y., and Jans, D.A. (1997). The protein kinase CK2 site (Ser111/112) enhances recognition of the simian virus 40 large T-antigen nuclear localization sequence by importin. J. Biol. Chem. *272*, 17191–17195.

Hudry, B., Viala, S., Graba, Y., and Merabet, S. (2011). Visualization of protein interactions in living Drosophila embryos by the bimolecular fluorescence complementation assay. BMC Biol. *9*, 5.

Immink, R.G.H., Gadella, T.W.J., Ferrario, S., Busscher, M., and Angenent, G.C. (2002). Analysis of MADS box protein-protein interactions in living plant cells. Proc. Natl. Acad. Sci. U. S. A. *99*, 2416–2421.

Irie, Y., Borlee, B.R., O'Connor, J.R., Hill, P.J., Harwood, C.S., Wozniak, D.J., and Parsek, M.R. (2012). Self-produced exopolysaccharide is a signal that stimulates biofilm formation in Pseudomonas aeruginosa. Proc. Natl. Acad. Sci. U. S. A. *109*, 20632–20636.

Irie-Sasaki, J., Sasaki, T., Matsumoto, W., Opavsky, A., Cheng, M., Welstead, G., Griffiths, E., Krawczyk, C., Richardson, C.D., Aitken, K., et al. (2001). CD45 is a JAK phosphatase and negatively regulates cytokine receptor signalling. Nature *409*, 349–354.

Iuchi, S. (2001). Three classes of C2H2 zinc finger proteins. Cell. Mol. Life Sci. CMLS *58*,

625–635.

Jiang, H., Patel, P.H., Kohlmaier, A., Grenley, M.O., McEwen, D.G., and Edgar, B.A. (2009). Cytokine/Jak/Stat signaling mediates regeneration and homeostasis in the Drosophila midgut. Cell *137*, 1343–1355.

Jiang, K., Hua, S., Mohan, R., Grigoriev, I., Yau, K.W., Liu, Q., Katrukha, E.A., Altelaar, A.F.M., Heck, A.J.R., Hoogenraad, C.C., et al. (2014a). Microtubule minus-end stabilization by polymerization-driven CAMSAP deposition. Dev. Cell *28*, 295–309.

Jiang, K., Hua, S., Mohan, R., Grigoriev, I., Yau, K.W., Liu, Q., Katrukha, E.A., Altelaar, A.F.M., Heck, A.J.R., Hoogenraad, C.C., et al. (2014b). Microtubule minus-end stabilization by polymerization-driven CAMSAP deposition. Dev. Cell *28*, 295–309.

Jimenez, P.N., Koch, G., Thompson, J.A., Xavier, K.B., Cool, R.H., and Quax, W.J. (2012). The Multiple Signaling Systems Regulating Virulence in Pseudomonas aeruginosa. Microbiol. Mol. Biol. Rev. *76*, 46–65.

Johnson, G.L., and Lapadat, R. (2002). Mitogen-Activated Protein Kinase Pathways Mediated by ERK, JNK, and p38 Protein Kinases. Science *298*, 1911–1912.

Kaiser, D. (2004). Signaling in myxobacteria. Annu. Rev. Microbiol. *58*, 75–98.

Kardash, E., Bandemer, J., and Raz, E. (2011). Imaging protein activity in live embryos using fluorescence resonance energy transfer biosensors. Nat. Protoc. *6*, 1835–1846.

Karimi, M., Bleys, A., Vanderhaeghen, R., and Hilson, P. (2007). Building blocks for plant gene assembly. Plant Physiol. *145*, 1183–1191.

Kelleher, M.T., Fruhwirth, G., Patel, G., Ofo, E., Festy, F., Barber, P.R., Ameer-Beg, S.M., Vojnovic, B., Gillett, C., Coolen, A., et al. (2009). The potential of optical proteomic technologies to individualize prognosis and guide rational treatment for cancer patients. Target. Oncol. *4*, 235–252.

Kerstetter, R.A., Laudencia-Chingcuanco, D., Smith, L.G., and Hake, S. (1997). Loss-of-function mutations in the maize homeobox gene, knotted1, are defective in shoot meristem maintenance. Dev. Camb. Engl. *124*, 3045–3054.

Kholodenko, B.N. (2000). Negative feedback and ultrasensitivity can bring about oscillations in the mitogen-activated protein kinase cascades. Eur. J. Biochem. FEBS *267*, 1583–1588.

Kim, J.Y., Yuan, Z., Cilia, M., Khalfan-Jagani, Z., and Jackson, D. (2002). Intercellular trafficking of a KNOTTED1 green fluorescent protein fusion in the leaf and shoot meristem of Arabidopsis. Proc. Natl. Acad. Sci. U. S. A. *99*, 4103–4108.

Kim, J.-Y., Yuan, Z., and Jackson, D. (2003a). Developmental regulation and significance

of KNOX protein trafficking in Arabidopsis. Dev. Camb. Engl. *130*, 4351–4362.

Kim, J.-Y., Yuan, Z., and Jackson, D. (2003b). Developmental regulation and significance of KNOX protein trafficking in Arabidopsis. Dev. Camb. Engl. *130*, 4351–4362.

Kim, J.-Y., Rim, Y., Wang, J., and Jackson, D. (2005). A novel cell-to-cell trafficking assay indicates that the KNOX homeodomain is necessary and sufficient for intercellular protein and mRNA trafficking. Genes Dev. *19*, 788–793.

Kim, Y., Lim, J., Yeom, M., Kim, H., Kim, J., Wang, L., Kim, W.Y., Somers, D.E., and Nam, H.G. (2013). ELF4 Regulates GIGANTEA Chromatin Access through Subnuclear Sequestration. Cell Rep. *3*, 671–677.

Klug, A. (1999). Zinc finger peptides for the regulation of gene expression. J. Mol. Biol. *293*, 215–218.

Klug, A., and Schwabe, J.W. (1995). Protein motifs 5. Zinc fingers. FASEB J. *9*, 597–604.

Kodama, Y., and Hu, C.-D. (2012). Bimolecular fluorescence complementation (BiFC): a 5-year update and future perspectives. BioTechniques *53*, 285–298.

Koizumi, K., and Gallagher, K.L. (2013). Identification of SHRUBBY, a SHORT-ROOT and SCARECROW interacting protein that controls root growth and radial patterning. Development *140*, 1292–1300.

Koizumi, K., Wu, S., MacRae-Crerar, A., and Gallagher, K.L. (2011a). An essential protein that interacts with endosomes and promotes movement of the SHORT-ROOT transcription factor. Curr. Biol. CB *21*, 1559–1564.

Koizumi, K., Wu, S., MacRae-Crerar, A., and Gallagher, K.L. (2011b). An essential protein that interacts with endosomes and promotes movement of the SHORT-ROOT transcription factor. Curr. Biol. CB *21*, 1559–1564.

Koizumi, K., Hayashi, T., Wu, S., and Gallagher, K.L. (2012a). The SHORT-ROOT protein acts as a mobile, dose-dependent signal in patterning the ground tissue. Proc. Natl. Acad. Sci. U. S. A. *109*, 13010–13015.

Koizumi, K., Hayashi, T., and Gallagher, K.L. (2012b). SCARECROW reinforces SHORT-ROOT signaling and inhibits periclinal cell divisions in the ground tissue by maintaining SHR at high levels in the endodermis. Plant Signal. Behav. *7*, 1573–1577.

Koizumi, K., Hayashi, T., and Gallagher, K.L. (2012c). SCARECROW reinforces SHORT-ROOT signaling and inhibits periclinal cell divisions in the ground tissue by maintaining SHR at high levels in the endodermis. Plant Signal. Behav. *7*, 1573–1577.

Konovalova, A., Wegener-Feldbrügge, S., and Søgaard-Andersen, L. (2012). Two intercellular signals required for fruiting body formation in Myxococcus xanthus act

sequentially but non-hierarchically. Mol. Microbiol. *86*, 65–81.

Kozaki, A., Hake, S., and Colasanti, J. (2004a). The maize ID1 flowering time regulator is a zinc finger protein with novel DNA binding properties. Nucleic Acids Res. *32*, 1710–1720.

Kozaki, A., Hake, S., and Colasanti, J. (2004b). The maize ID1 flowering time regulator is a zinc finger protein with novel DNA binding properties. Nucleic Acids Res. *32*, 1710–1720.

Kragler, F., Monzer, J., Xoconostle-Cázares, B., and Lucas, W.J. (2000). Peptide antagonists of the plasmodesmal macromolecular trafficking pathway. EMBO J. *19*, 2856–2868.

Kremers, G., and Goedhart, J. (2009). Chapter 5 Visible fluorescent proteins for FRET. In Laboratory Techniques in Biochemistry and Molecular Biology, T.W.J. Gadella, ed. (Elsevier), pp. 171–223.

Kremers, G.-J., Goedhart, J., van Munster, E.B., and Gadella, T.W.J., Jr (2006a). Cyan and yellow super fluorescent proteins with improved brightness, protein folding, and FRET Förster radius. Biochemistry (Mosc.) *45*, 6570–6580.

Kremers, G.-J., Goedhart, J., van Munster, E.B., and Gadella, T.W.J. (2006b). Cyan and Yellow Super Fluorescent Proteins with Improved Brightness, Protein Folding, and FRET Förster Radius†,‡. Biochemistry (Mosc.) *45*, 6570–6580.

Krieger, E., Joo, K., Lee, J., Lee, J., Raman, S., Thompson, J., Tyka, M., Baker, D., and Karplus, K. (2009). Improving physical realism, stereochemistry, and side-chain accuracy in homology modeling: Four approaches that performed well in CASP8. Proteins *77 Suppl 9*, 114–122.

Kudryavtsev, V., Felekyan, S., Woźniak, A.K., König, M., Sandhagen, C., Kühnemuth, R., Seidel, C.A.M., and Oesterhelt, F. (2007). Monitoring dynamic systems with multiparameter fluorescence imaging. Anal. Bioanal. Chem. *387*, 71–82.

Kurata, T., Ishida, T., Kawabata-Awai, C., Noguchi, M., Hattori, S., Sano, R., Nagasaka, R., Tominaga, R., Koshino-Kimura, Y., Kato, T., et al. (2005a). Cell-to-cell movement of the CAPRICE protein in Arabidopsis root epidermal cell differentiation. Development *132*, 5387–5398.

Kurata, T., Ishida, T., Kawabata-Awai, C., Noguchi, M., Hattori, S., Sano, R., Nagasaka, R., Tominaga, R., Koshino-Kimura, Y., Kato, T., et al. (2005b). Cell-to-cell movement of the CAPRICE protein in Arabidopsis root epidermal cell differentiation. Dev. Camb. Engl. *132*, 5387–5398.

Kuspa, A., Plamann, L., and Kaiser, D. (1992). A-signalling and the cell density requirement for Myxococcus xanthus development. J. Bacteriol. *174*, 7360–7369.

Ladam, F., and Sagerström, C.G. (2014). Hox regulation of transcription: more complex(es). Dev. Dyn. Off. Publ. Am. Assoc. Anat. *243*, 4–15.

Lassner, M.W., Jones, A., Daubert, S., and Comai, L. (1991). Targeting of T7 RNA polymerase to tobacco nuclei mediated by an SV40 nuclear location signal. Plant Mol. Biol. *17*, 229–234.

Di Laurenzio, L., Wysocka-Diller, J., Malamy, J.E., Pysh, L., Helariutta, Y., Freshour, G., Hahn, M.G., Feldmann, K.A., and Benfey, P.N. (1996a). The SCARECROW gene regulates an asymmetric cell division that is essential for generating the radial organization of the Arabidopsis root. Cell *86*, 423–433.

Di Laurenzio, L., Wysocka-Diller, J., Malamy, J.E., Pysh, L., Helariutta, Y., Freshour, G., Hahn, M.G., Feldmann, K.A., and Benfey, P.N. (1996b). The SCARECROW gene regulates an asymmetric cell division that is essential for generating the radial organization of the Arabidopsis root. Cell *86*, 423–433.

Lawrence, J.R., Korber, D.R., Hoyle, B.D., Costerton, J.W., and Caldwell, D.E. (1991). Optical sectioning of microbial biofilms. J. Bacteriol. *173*, 6558–6567.

Lee, M.M., and Schiefelbein, J. (1999). WEREWOLF, a MYB-related protein in Arabidopsis, is a position-dependent regulator of epidermal cell patterning. Cell *99*, 473–483.

Lee, M.-H., Kim, B., Song, S.-K., Heo, J.-O., Yu, N.-I., Lee, S.A., Kim, M., Kim, D.G., Sohn, S.O., Lim, C.E., et al. (2008). Large-scale analysis of the GRAS gene family in Arabidopsis thaliana. Plant Mol. Biol. *67*, 659–670.

Lemon, B., and Tjian, R. (2000). Orchestrated response: a symphony of transcription factors for gene control. Genes Dev. *14*, 2551–2569.

Levesque, M.P., Vernoux, T., Busch, W., Cui, H., Wang, J.Y., Blilou, I., Hassan, H., Nakajima, K., Matsumoto, N., Lohmann, J.U., et al. (2006a). Whole-genome analysis of the SHORT-ROOT developmental pathway in Arabidopsis. PLoS Biol. *4*, e143.

Levesque, M.P., Vernoux, T., Busch, W., Cui, H., Wang, J.Y., Blilou, I., Hassan, H., Nakajima, K., Matsumoto, N., Lohmann, J.U., et al. (2006b). Whole-genome analysis of the SHORT-ROOT developmental pathway in Arabidopsis. PLoS Biol. *4*, e143.

Levy, D.E., and Darnell, J.E., Jr (2002). Stats: transcriptional control and biological impact. Nat. Rev. Mol. Cell Biol. *3*, 651–662.

Lin, H.W., Thompson, J.W., Morris, K.C., and Perez-Pinzon, M.A. (2011). Signal Transducers and Activators of Transcription: STATs-Mediated Mitochondrial Neuroprotection. Antioxid. Redox Signal. *14*, 1853–1861.

Liongue, C., O'Sullivan, L.A., Trengove, M.C., and Ward, A.C. (2012). Evolution of

JAK-STAT Pathway Components: Mechanisms and Role in Immune System Development. PLoS ONE *7*, e32777.

Liu, L., Zhang, Y., Tang, S., Zhao, Q., Zhang, Z., Zhang, H., Dong, L., Guo, H., and Xie, Q. (2010). An efficient system to detect protein ubiquitination by agroinfiltration in Nicotiana benthamiana. Plant J. Cell Mol. Biol. *61*, 893–903.

Lohmann, J.U., Hong, R.L., Hobe, M., Busch, M.A., Parcy, F., Simon, R., and Weigel, D. (2001). A molecular link between stem cell regulation and floral patterning in Arabidopsis. Cell *105*, 793–803.

Long, J.A., Moan, E.I., Medford, J.I., and Barton, M.K. (1996). A member of the KNOTTED class of homeodomain proteins encoded by the STM gene of Arabidopsis. Nature *379*, 66–69.

Long, Y., Smet, W., Cruz-Ramírez, A., Castelijns, B., de Jonge, W., Mähönen, A.P., Bouchet, B.P., Perez, G.S., Akhmanova, A., Scheres, B., et al. (2015a). Arabidopsis BIRD Zinc Finger Proteins Jointly Stabilize Tissue Boundaries by Confining the Cell Fate Regulator SHORT-ROOT and Contributing to Fate Specification. Plant Cell.

Long, Y., Scheres, B., and Blilou, I. (2015b). The logic of communication: roles for mobile transcription factors in plants. J. Exp. Bot. *66*, 1133–1144.

Lucas, W.J., and Lee, J.-Y. (2004). Plasmodesmata as a supracellular control network in plants. Nat. Rev. Mol. Cell Biol. *5*, 712–726.

Lucas, W.J., Bouché-Pillon, S., Jackson, D.P., Nguyen, L., Baker, L., Ding, B., and Hake, S. (1995a). Selective trafficking of KNOTTED1 homeodomain protein and its mRNA through plasmodesmata. Science *270*, 1980–1983.

Lucas, W.J., Bouché-Pillon, S., Jackson, D.P., Nguyen, L., Baker, L., Ding, B., and Hake, S. (1995b). Selective trafficking of KNOTTED1 homeodomain protein and its mRNA through plasmodesmata. Science *270*, 1980–1983.

Lucas, W.J., Ham, B.-K., and Kim, J.-Y. (2009). Plasmodesmata - bridging the gap between neighboring plant cells. Trends Cell Biol. *19*, 495–503.

Luo, H., and Dearolf, C.R. (2001). The JAK/STAT pathway and Drosophila development. BioEssays *23*, 1138–1147.

Macias, E., Rao, D., Carbajal, S., Kiguchi, K., and DiGiovanni, J. (2014). Stat3 Binds to mtDNA and Regulates Mitochondrial Gene Expression in Keratinocytes. J. Invest. Dermatol. *134*, 1971–1980.

Mähönen, A.P., Bonke, M., Kauppinen, L., Riikonen, M., Benfey, P.N., and Helariutta, Y. (2000). A novel two-component hybrid molecule regulates vascular morphogenesis of the Arabidopsis root. Genes Dev. *14*, 2938–2943.

Mähönen, A.P., Tusscher, K. ten, Siligato, R., Smetana, O., Díaz-Triviño, S., Salojärvi, J., Wachsman, G., Prasad, K., Heidstra, R., and Scheres, B. (2014). PLETHORA gradient formation mechanism separates auxin responses. Nature *advance online publication*.

Malamy, J.E., and Benfey, P.N. (1997). Organization and cell differentiation in lateral roots of Arabidopsis thaliana. Dev. Camb. Engl. *124*, 33–44.

Margolis, B., and Skolnik, E.Y. (1994). Activation of Ras by receptor tyrosine kinases. J. Am. Soc. Nephrol. JASN *5*, 1288–1299.

Markevich, N.I., Hoek, J.B., and Kholodenko, B.N. (2004). Signaling switches and bistability arising from multisite phosphorylation in protein kinase cascades. J. Cell Biol. *164*, 353–359.

Matsuzaki, Y., Ogawa-Ohnishi, M., Mori, A., and Matsubayashi, Y. (2010). Secreted peptide signals required for maintenance of root stem cell niche in Arabidopsis. Science *329*, 1065–1067.

Miyashima, S., Koi, S., Hashimoto, T., and Nakajima, K. (2011). Non-cell-autonomous microRNA165 acts in a dose-dependent manner to regulate multiple differentiation status in the Arabidopsis root. Dev. Camb. Engl. *138*, 2303–2313.

Moreno-Risueno, M.A., Norman, J.M.V., Moreno, A., Zhang, J., Ahnert, S.E., and Benfey, P.N. (2010). Oscillating Gene Expression Determines Competence for Periodic Arabidopsis Root Branching. Science *329*, 1306–1311.

Morrison, D.K., and Davis, R.J. (2003). Regulation of MAP kinase signaling modules by scaffold proteins in mammals. Annu. Rev. Cell Dev. Biol. *19*, 91–118.

Murray, P.J. (2007). The JAK-STAT signaling pathway: input and output integration. J. Immunol. Baltim. Md 1950 *178*, 2623–2629.

Nakagawa, T., Kurose, T., Hino, T., Tanaka, K., Kawamukai, M., Niwa, Y., Toyooka, K., Matsuoka, K., Jinbo, T., and Kimura, T. (2007). Development of series of gateway binary vectors, pGWBs, for realizing efficient construction of fusion genes for plant transformation. J. Biosci. Bioeng. *104*, 34–41.

Nakajima, K., Sena, G., Nawy, T., and Benfey, P.N. (2001a). Intercellular movement of the putative transcription factor SHR in root patterning. Nature *413*, 307–311.

Nakajima, K., Sena, G., Nawy, T., and Benfey, P.N. (2001b). Intercellular movement of the putative transcription factor SHR in root patterning. Nature *413*, 307–311.

Ng, D.C.H., Lin, B.H., Lim, C.P., Huang, G., Zhang, T., Poli, V., and Cao, X. (2006). Stat3 regulates microtubules by antagonizing the depolymerization activity of stathmin. J. Cell Biol. *172*, 245–257.

Nobis, M., McGhee, E.J., Morton, J.P., Schwarz, J.P., Karim, S.A., Quinn, J., Edward, M., Campbell, A.D., McGarry, L.C., Evans, T.R.J., et al. (2013). Intravital FLIM-FRET imaging reveals dasatinib-induced spatial control of src in pancreatic cancer. Cancer Res. *73*, 4674–4686.

Obradovic, Z., Peng, K., Vucetic, S., Radivojac, P., Brown, C.J., and Dunker, A.K. (2003). Predicting intrinsic disorder from amino acid sequence. Proteins *53 Suppl 6*, 566–572.

Obradovic, Z., Peng, K., Vucetic, S., Radivojac, P., and Dunker, A.K. (2005). Exploiting heterogeneous sequence properties improves prediction of protein disorder. Proteins *61 Suppl 7*, 176–182.

O'Connor, K.A., and Zusman, D.R. (1991). Development in Myxococcus xanthus involves differentiation into two cell types, peripheral rods and spores. J. Bacteriol. *173*, 3318–3333.

O'Donnell, A., Odrowaz, Z., and Sharrocks, A.D. (2012). Immediate-early gene activation by the MAPK pathways: what do and don't we know? Biochem. Soc. Trans. *40*, 58–66.

Oeztuerk-Winder, F., and Ventura, J. (2012). The many faces of p38 mitogen-activated protein kinase in progenitor/stem cell differentiation. Biochem. J. *445*, 1–10.

Ogasawara, H., Kaimi, R., Colasanti, J., and Kozaki, A. (2011a). Activity of transcription factor JACKDAW is essential for SHR/SCR-dependent activation of SCARECROW and MAGPIE and is modulated by reciprocal interactions with MAGPIE, SCARECROW and SHORT ROOT. Plant Mol. Biol. *77*, 489–499.

Ogasawara, H., Kaimi, R., Colasanti, J., and Kozaki, A. (2011b). Activity of transcription factor JACKDAW is essential for SHR/SCR-dependent activation of SCARECROW and MAGPIE and is modulated by reciprocal interactions with MAGPIE, SCARECROW and SHORT ROOT. Plant Mol. Biol. *77*, 489–499.

Oldfield, C.J., and Dunker, A.K. (2014). Intrinsically Disordered Proteins and Intrinsically Disordered Protein Regions. Annu. Rev. Biochem. *83*, 553–584.

Owens, D.M., and Keyse, S.M. (2007). Differential regulation of MAP kinase signalling by dual-specificity protein phosphatases. Oncogene *26*, 3203–3213.

Paquette, A.J., and Benfey, P.N. (2005). Maturation of the Ground Tissue of the Root Is Regulated by Gibberellin and SCARECROW and Requires SHORT-ROOT. Plant Physiol. *138*, 636–640.

Pardo, M., and Choudhary, J.S. (2012). Assignment of protein interactions from affinity purification/mass spectrometry data. J. Proteome Res. *11*, 1462–1474.

Perbal, M.C., Haughn, G., Saedler, H., and Schwarz-Sommer, Z. (1996). Non-cell-autonomous function of the Antirrhinum floral homeotic proteins DEFICIENS and

GLOBOSA is exerted by their polar cell-to-cell trafficking. Dev. Camb. Engl. *122*, 3433–3441.

Peremyslov, V.V., Klocko, A.L., Fowler, J.E., and Dolja, V.V. (2012). Arabidopsis myosin XI-K localizes to the motile endomembrane vesicles associated with F-actin. Plant Cell Biol. *3*, 184.

Petricka, J.J., Schauer, M.A., Megraw, M., Breakfield, N.W., Thompson, J.W., Georgiev, S., Soderblom, E.J., Ohler, U., Moseley, M.A., Grossniklaus, U., et al. (2012). The protein expression landscape of the Arabidopsis root. Proc. Natl. Acad. Sci. U. S. A. *109*, 6811–6818.

Petrova, O.E., and Sauer, K. (2009). A Novel Signaling Network Essential for Regulating Pseudomonas aeruginosa Biofilm Development. PLoS Pathog *5*, e1000668.

Planque, N. (2006). Nuclear trafficking of secreted factors and cell-surface receptors: new pathways to regulate cell proliferation and differentiation, and involvement in cancers. Cell Commun. Signal. CCS *4*, 7.

Potenza, E., Domenico, T.D., Walsh, I., and Tosatto, S.C.E. (2014). MobiDB 2.0: an improved database of intrinsically disordered and mobile proteins. Nucleic Acids Res. gku982.

Pysh, L.D., Wysocka-Diller, J.W., Camilleri, C., Bouchez, D., and Benfey, P.N. (1999). The GRAS gene family in Arabidopsis: sequence characterization and basic expression analysis of the SCARECROW-LIKE genes. Plant J. Cell Mol. Biol. *18*, 111–119.

Raven, J.A., and Edwards, D. (2001). Roots: evolutionary origins and biogeochemical significance. J. Exp. Bot. *52*, 381–401.

Reich, N.C., and Liu, L. (2006). Tracking STAT nuclear traffic. Nat. Rev. Immunol. *6*, 602–612.

Reiser, L., Sánchez-Baracaldo, P., and Hake, S. (2000). Knots in the family tree: evolutionary relationships and functions of knox homeobox genes. Plant Mol. Biol. *42*, 151–166.

Richards, D.E., Peng, J., and Harberd, N.P. (2000). Plant GRAS and metazoan STATs: one family? BioEssays News Rev. Mol. Cell. Dev. Biol. *22*, 573–577.

Rim, Y., Jung, J., Chu, H., Cho, W.K., Kim, S., Hong, J.C., Jackson, D., Datla, R., and Kim, J. (2009). A non-cell-autonomous mechanism for the control of plant architecture and epidermal differentiation involves intercellular trafficking of BREVIPEDICELLUS protein. Funct. Plant Biol. *36*, 280–289.

Rim, Y., Huang, L., Chu, H., Han, X., Cho, W.K., Jeon, C.O., Kim, H.J., Hong, J.-C., Lucas, W.J., and Kim, J.-Y. (2011). Analysis of Arabidopsis transcription factor families revealed

extensive capacity for cell-to-cell movement as well as discrete trafficking patterns. Mol. Cells *32*, 519–526.

Roberts, P.J., and Der, C.J. (2007). Targeting the Raf-MEK-ERK mitogen-activated protein kinase cascade for the treatment of cancer. Oncogene *26*, 3291–3310.

Rogers, R.S., Horvath, C.M., and Matunis, M.J. (2003). SUMO Modification of STAT1 and Its Role in PIAS-mediated Inhibition of Gene Activation. J. Biol. Chem. *278*, 30091–30097.

Roppolo, D., De Rybel, B., Tendon, V.D., Pfister, A., Alassimone, J., Vermeer, J.E.M., Yamazaki, M., Stierhof, Y.-D., Beeckman, T., and Geldner, N. (2011). A novel protein family mediates Casparian strip formation in the endodermis. Nature *473*, 380–383.

Sabatini, S., Beis, D., Wolkenfelt, H., Murfett, J., Guilfoyle, T., Malamy, J., Benfey, P., Leyser, O., Bechtold, N., Weisbeek, P., et al. (1999a). An auxin-dependent distal organizer of pattern and polarity in the Arabidopsis root. Cell *99*, 463–472.

Sabatini, S., Beis, D., Wolkenfelt, H., Murfett, J., Guilfoyle, T., Malamy, J., Benfey, P., Leyser, O., Bechtold, N., Weisbeek, P., et al. (1999b). An auxin-dependent distal organizer of pattern and polarity in the Arabidopsis root. Cell *99*, 463–472.

Sabatini, S., Heidstra, R., Wildwater, M., and Scheres, B. (2003). SCARECROW is involved in positioning the stem cell niche in the Arabidopsis root meristem. Genes Dev. *17*, 354–358.

Santuari, L., Scacchi, E., Rodriguez-Villalon, A., Salinas, P., Dohmann, E.M.N., Brunoud, G., Vernoux, T., Smith, R.S., and Hardtke, C.S. (2011). Positional information by differential endocytosis splits auxin response to drive Arabidopsis root meristem growth. Curr. Biol. CB *21*, 1918–1923.

Sarkar, A.K., Luijten, M., Miyashima, S., Lenhard, M., Hashimoto, T., Nakajima, K., Scheres, B., Heidstra, R., and Laux, T. (2007). Conserved factors regulate signalling in Arabidopsis thaliana shoot and root stem cell organizers. Nature *446*, 811–814.

Schaffer, J., Volkmer, A., Eggeling, C., Subramaniam, V., Striker, G., and Seidel, C.A.M. (1999). Identification of Single Molecules in Aqueous Solution by Time-Resolved Fluorescence Anisotropy. J. Phys. Chem. A *103*, 331–336.

Scheres, B. (2001). Plant cell identity. The role of position and lineage. Plant Physiol. *125*, 112–114.

Scheres, B., and Benfey, P.N. (1999). ASYMMETRIC CELL DIVISION IN PLANTS. Annu. Rev. Plant Physiol. Plant Mol. Biol. *50*, 505–537.

Scheres, B., Laurenzio, L.D., Willemsen, V., Hauser, M.T., Janmaat, K., Weisbeek, P., and Benfey, P.N. (1995a). Mutations affecting the radial organisation of the Arabidopsis root

display specific defects throughout the embryonic axis. Development *121*, 53–62.

Scheres, B., Laurenzio, L.D., Willemsen, V., Hauser, M.T., Janmaat, K., Weisbeek, P., and Benfey, P.N. (1995b). Mutations affecting the radial organisation of the Arabidopsis root display specific defects throughout the embryonic axis. Development *121*, 53–62.

Schermelleh, L., Heintzmann, R., and Leonhardt, H. (2010). A guide to super-resolution fluorescence microscopy. J. Cell Biol. *190*, 165–175.

Schlereth, A., Möller, B., Liu, W., Kientz, M., Flipse, J., Rademacher, E.H., Schmid, M., Jürgens, G., and Weijers, D. (2010a). MONOPTEROS controls embryonic root initiation by regulating a mobile transcription factor. Nature *464*, 913–916.

Schlereth, A., Möller, B., Liu, W., Kientz, M., Flipse, J., Rademacher, E.H., Schmid, M., Jürgens, G., and Weijers, D. (2010b). MONOPTEROS controls embryonic root initiation by regulating a mobile transcription factor. Nature *464*, 913–916.

Schneeberger, R.G., Becraft, P.W., Hake, S., and Freeling, M. (1995). Ectopic expression of the knox homeo box gene rough sheath1 alters cell fate in the maize leaf. Genes Dev. *9*, 2292–2304.

Schwarz-Sommer, Z., Hue, I., Huijser, P., Flor, P.J., Hansen, R., Tetens, F., Lönnig, W.E., Saedler, H., and Sommer, H. (1992). Characterization of the Antirrhinum floral homeotic MADS-box gene deficiens: evidence for DNA binding and autoregulation of its persistent expression throughout flower development. EMBO J. *11*, 251–263.

Sena, G., Jung, J.W., and Benfey, P.N. (2004a). A broad competence to respond to SHORT ROOT revealed by tissue-specific ectopic expression. Dev. Camb. Engl. *131*, 2817–2826.

Sena, G., Jung, J.W., and Benfey, P.N. (2004b). A broad competence to respond to SHORT ROOT revealed by tissue-specific ectopic expression. Dev. Camb. Engl. *131*, 2817–2826.

Sessions, A., Yanofsky, M.F., and Weigel, D. (2000). Cell-cell signaling and movement by the floral transcription factors LEAFY and APETALA1. Science *289*, 779–782.

Shin, S.-Y., Rath, O., Choo, S.-M., Fee, F., McFerran, B., Kolch, W., and Cho, K.-H. (2009). Positive- and negative-feedback regulations coordinate the dynamic behavior of the Ras-Raf-MEK-ERK signal transduction pathway. J. Cell Sci. *122*, 425–435.

Sisamakis, E., Valeri, A., Kalinin, S., Rothwell, P.J., and Seidel, C.A.M. (2010). Accurate single-molecule FRET studies using multiparameter fluorescence detection. Methods Enzymol. *475*, 455–514.

Smaczniak, C., Immink, R.G.H., Muiño, J.M., Blanvillain, R., Busscher, M., Busscher-Lange, J., Dinh, Q.D. (Peter), Liu, S., Westphal, A.H., Boeren, S., et al. (2012).

Characterization of MADS-domain transcription factor complexes in Arabidopsis flower development. Proc. Natl. Acad. Sci. *109*, 1560–1565.

Sozzani, R., Cui, H., Moreno-Risueno, M.A., Busch, W., Van Norman, J.M., Vernoux, T., Brady, S.M., Dewitte, W., Murray, J.A.H., and Benfey, P.N. (2010a). Spatiotemporal regulation of cell-cycle genes by SHORTROOT links patterning and growth. Nature *466*, 128–132.

Sozzani, R., Cui, H., Moreno-Risueno, M.A., Busch, W., Van Norman, J.M., Vernoux, T., Brady, S.M., Dewitte, W., Murray, J.A.H., and Benfey, P.N. (2010b). Spatiotemporal regulation of cell-cycle genes by SHORTROOT links patterning and growth. Nature *466*, 128–132.

Sparks, E., Wachsman, G., and Benfey, P.N. (2013). Spatiotemporal signalling in plant development. Nat. Rev. Genet. *14*, 631–644.

Spitz, F., and Furlong, E.E.M. (2012). Transcription factors: from enhancer binding to developmental control. Nat. Rev. Genet. *13*, 613–626.

Stahl, Y., Grabowski, S., Bleckmann, A., Kühnemuth, R., Weidtkamp-Peters, S., Pinto, K.G., Kirschner, G.K., Schmid, J.B., Wink, R.H., Hülsewede, A., et al. (2013). Moderation of Arabidopsis root stemness by CLAVATA1 and ARABIDOPSIS CRINKLY4 receptor kinase complexes. Curr. Biol. CB *23*, 362–371.

Stein, G.S., van Wijnen, A.J., Stein, J.L., Lian, J.B., Montecino, M., Choi, J., Zaidi, K., and Javed, A. (2000). Intranuclear trafficking of transcription factors: implications for biological control. J. Cell Sci. *113 (Pt 14)*, 2527–2533.

Tata, J.R. (2002). Signalling through nuclear receptors. Nat. Rev. Mol. Cell Biol. *3*, 702–710.

Tian, H., Baxter, I.R., Lahner, B., Reinders, A., Salt, D.E., and Ward, J.M. (2010). Arabidopsis NPCC6/NaKR1 is a phloem mobile metal binding protein necessary for phloem function and root meristem maintenance. Plant Cell *22*, 3963–3979.

Tonaco, I.A.N., Borst, J.W., de Vries, S.C., Angenent, G.C., and Immink, R.G.H. (2006). In vivo imaging of MADS-box transcription factor interactions. J. Exp. Bot. *57*, 33–42.

Traas, J., and Vernoux, T. (2010). Oscillating Roots. Science *329*, 1290–1291.

Truernit, E., Bauby, H., Dubreucq, B., Grandjean, O., Runions, J., Barthélémy, J., and Palauqui, J.-C. (2008). High-resolution whole-mount imaging of three-dimensional tissue organization and gene expression enables the study of Phloem development and structure in Arabidopsis. Plant Cell *20*, 1494–1503.

Valsecchi, I., Guittard-Crilat, E., Maldiney, R., Habricot, Y., Lignon, S., Lebrun, R., Miginiac, E., Ruelland, E., Jeannette, E., and Lebreton, S. (2013). The intrinsically

disordered C-terminal region of Arabidopsis thaliana TCP8 transcription factor acts both as a transactivation and self-assembly domain. Mol. Biosyst. *9*, 2282–2295.

Vatén, A., Dettmer, J., Wu, S., Stierhof, Y.-D., Miyashima, S., Yadav, S.R., Roberts, C.J., Campilho, A., Bulone, V., Lichtenberger, R., et al. (2011a). Callose biosynthesis regulates symplastic trafficking during root development. Dev. Cell *21*, 1144–1155.

Vatén, A., Dettmer, J., Wu, S., Stierhof, Y.-D., Miyashima, S., Yadav, S.R., Roberts, C.J., Campilho, A., Bulone, V., Lichtenberger, R., et al. (2011b). Callose biosynthesis regulates symplastic trafficking during root development. Dev. Cell *21*, 1144–1155.

Venugopal, V., Chen, J., Barroso, M., and Intes, X. (2012). Quantitative tomographic imaging of intermolecular FRET in small animals. Biomed. Opt. Express *3*, 3161–3175.

Verveer, P.J., and Hanley, Q.S. (2009). Chapter 2 Frequency domain FLIM theory, instrumentation, and data analysis. In Laboratory Techniques in Biochemistry and Molecular Biology, T.W.J. Gadella, ed. (Elsevier), pp. 59–94.

Vollbrecht, E., Reiser, L., and Hake, S. (2000). Shoot meristem size is dependent on inbred background and presence of the maize homeobox gene, knotted1. Dev. Camb. Engl. *127*, 3161–3172.

Waadt, R., Hitomi, K., Nishimura, N., Hitomi, C., Adams, S.R., Getzoff, E.D., and Schroeder, J.I. (2014). FRET-based reporters for the direct visualization of abscisic acid concentration changes and distribution in Arabidopsis. eLife *3*, e01739.

Wachsman, G., Heidstra, R., and Scheres, B. (2011). Distinct Cell-Autonomous Functions of RETINOBLASTOMA-RELATED in Arabidopsis Stem Cells Revealed by the Brother of Brainbow Clonal Analysis System[W]. Plant Cell *23*, 2581–2591.

Weidtkamp-Peters, S., Felekyan, S., Bleckmann, A., Simon, R., Becker, W., Kühnemuth, R., and Seidel, C.A.M. (2009). Multiparameter fluorescence image spectroscopy to study molecular interactions. Photochem. Photobiol. Sci. Off. J. Eur. Photochem. Assoc. Eur. Soc. Photobiol. *8*, 470–480.

Weigel, D., Alvarez, J., Smyth, D.R., Yanofsky, M.F., and Meyerowitz, E.M. (1992). LEAFY controls floral meristem identity in Arabidopsis. Cell *69*, 843–859.

Welch, D., Hassan, H., Blilou, I., Immink, R., Heidstra, R., and Scheres, B. (2007a). Arabidopsis JACKDAW and MAGPIE zinc finger proteins delimit asymmetric cell division and stabilize tissue boundaries by restricting SHORT-ROOT action. Genes Dev. *21*, 2196–2204.

Welch, D., Hassan, H., Blilou, I., Immink, R., Heidstra, R., and Scheres, B. (2007b). Arabidopsis JACKDAW and MAGPIE zinc finger proteins delimit asymmetric cell division and stabilize tissue boundaries by restricting SHORT-ROOT action. Genes Dev. *21*, 2196–2204.

Widengren, J., Kudryavtsev, V., Antonik, M., Berger, S., Gerken, M., and Seidel, C.A.M. (2006). Single-molecule detection and identification of multiple species by multiparameter fluorescence detection. Anal. Chem. *78*, 2039–2050.

Wildwater, M., Campilho, A., Perez-Perez, J.M., Heidstra, R., Blilou, I., Korthout, H., Chatterjee, J., Mariconti, L., Gruissem, W., and Scheres, B. (2005a). The RETINOBLASTOMA-RELATED gene regulates stem cell maintenance in Arabidopsis roots. Cell *123*, 1337–1349.

Wildwater, M., Campilho, A., Perez-Perez, J.M., Heidstra, R., Blilou, I., Korthout, H., Chatterjee, J., Mariconti, L., Gruissem, W., and Scheres, B. (2005b). The RETINOBLASTOMA-RELATED gene regulates stem cell maintenance in Arabidopsis roots. Cell *123*, 1337–1349.

Willemsen, V., Bauch, M., Bennett, T., Campilho, A., Wolkenfelt, H., Xu, J., Haseloff, J., and Scheres, B. (2008). The NAC domain transcription factors FEZ and SOMBRERO control the orientation of cell division plane in Arabidopsis root stem cells. Dev. Cell *15*, 913–922.

Wright, P.E., and Dyson, H.J. (2015). Intrinsically disordered proteins in cellular signalling and regulation. Nat. Rev. Mol. Cell Biol. *16*, 18–29.

Wu, S., and Gallagher, K.L. (2013a). Intact microtubules are required for the intercellular movement of the SHORT-ROOT transcription factor. Plant J. Cell Mol. Biol. *74*, 148–159.

Wu, S., and Gallagher, K.L. (2013b). Intact microtubules are required for the intercellular movement of the SHORT-ROOT transcription factor. Plant J. Cell Mol. Biol. *74*, 148–159.

Wu, S., and Gallagher, K.L. (2014). The movement of the non-cell-autonomous transcription factor, SHORT-ROOT relies on the endomembrane system. Plant J. Cell Mol. Biol. *80*, 396–409.

Wu, L., Bijian, K., and Shen, S.-S. (2009). CD45 recruits adapter protein DOK-1 and negatively regulates JAK–STAT signaling in hematopoietic cells. Mol. Immunol. *46*, 2167–2177.

Wu, S., Lee, C.-M., Hayashi, T., Price, S., Divol, F., Henry, S., Pauluzzi, G., Perin, C., and Gallagher, K.L. (2014). A plausible mechanism, based upon SHORT-ROOT movement, for regulating the number of cortex cell layers in roots. Proc. Natl. Acad. Sci. *111*, 16184–16189.

Wu, X., Dinneny, J.R., Crawford, K.M., Rhee, Y., Citovsky, V., Zambryski, P.C., and Weigel, D. (2003). Modes of intercellular transcription factor movement in the Arabidopsis apex. Dev. Camb. Engl. *130*, 3735–3745.

Xavier, J.B. (2011). Social interaction in synthetic and natural microbial communities. Mol. Syst. Biol. *7*, 483.

Xu, T., Wen, M., Nagawa, S., Fu, Y., Chen, J.-G., Wu, M.-J., Perrot-Rechenmann, C., Friml, J., Jones, A.M., and Yang, Z. (2010). Cell Surface- and Rho GTPase-Based Auxin Signaling Controls Cellular Interdigitation in Arabidopsis. Cell *143*, 99–110.

Xue, B., Dunbrack, R.L., Williams, R.W., Dunker, A.K., and Uversky, V.N. (2010). PONDR-FIT: a meta-predictor of intrinsically disordered amino acids. Biochim. Biophys. Acta *1804*, 996–1010.

Yadav, R.K., Perales, M., Gruel, J., Girke, T., Jönsson, H., and Reddy, G.V. (2011). WUSCHEL protein movement mediates stem cell homeostasis in the Arabidopsis shoot apex. Genes Dev. *25*, 2025–2030.

Yang, J., Chatterjee-Kishore, M., Staugaitis, S.M., Nguyen, H., Schlessinger, K., Levy, D.E., and Stark, G.R. (2005). Novel roles of unphosphorylated STAT3 in oncogenesis and transcriptional regulation. Cancer Res. *65*, 939–947.

Yoo, S.-D., Cho, Y.-H., and Sheen, J. (2007a). Arabidopsis mesophyll protoplasts: a versatile cell system for transient gene expression analysis. Nat. Protoc. *2*, 1565–1572.

Yoo, S.-D., Cho, Y.-H., and Sheen, J. (2007b). Arabidopsis mesophyll protoplasts: a versatile cell system for transient gene expression analysis. Nat. Protoc. *2*, 1565–1572.

Yoshida, H., Hirano, K., Sato, T., Mitsuda, N., Nomoto, M., Maeo, K., Koketsu, E., Mitani, R., Kawamura, M., Ishiguro, S., et al. (2014a). DELLA protein functions as a transcriptional activator through the DNA binding of the INDETERMINATE DOMAIN family proteins. Proc. Natl. Acad. Sci. 201321669.

Yoshida, H., Hirano, K., Sato, T., Mitsuda, N., Nomoto, M., Maeo, K., Koketsu, E., Mitani, R., Kawamura, M., Ishiguro, S., et al. (2014b). DELLA protein functions as a transcriptional activator through the DNA binding of the INDETERMINATE DOMAIN family proteins. Proc. Natl. Acad. Sci. 201321669.

Young, C.L., Britton, Z.T., and Robinson, A.S. (2012). Recombinant protein expression and purification: a comprehensive review of affinity tags and microbial applications. Biotechnol. J. *7*, 620–634.

Zhang, D., Iyer, L.M., and Aravind, L. (2012). Bacterial GRAS domain proteins throw new light on gibberellic acid response mechanisms. Bioinforma. Oxf. Engl. *28*, 2407–2411.

Zhang, S., Ma, C., and Chalfie, M. (2004). Combinatorial marking of cells and organelles with reconstituted fluorescent proteins. Cell *119*, 137–144.

Zhang, Z.-L., Ogawa, M., Fleet, C.M., Zentella, R., Hu, J., Heo, J.-O., Lim, J., Kamiya, Y., Yamaguchi, S., and Sun, T. (2011). Scarecrow-like 3 promotes gibberellin signaling by antagonizing master growth repressor DELLA in Arabidopsis. Proc. Natl. Acad. Sci. U. S. A. *108*, 2160–2165.

Zuckerkandl, E. (2006). Intelligent design and biological complexity. Gene *385*, 2–18.

Zusman, D.R., Scott, A.E., Yang, Z., and Kirby, J.R. (2007). Chemosensory pathways, motility and development in Myxococcus xanthus. Nat. Rev. Microbiol. *5*, 862–872.

(2000). Jak-Stat signal transduction pathway through the eyes of cytokine class II receptor complexes. Publ. Online 22 May 2000 Doi101038sjonc1203524 *19*.

English Summary

Cell-cell communication is key to coordinated cellular functions in multicellular organisms. In addition to the signaling molecules found in animals, plants also frequently recruit mobile transcription factors, to deliver positional information. The best studied example is SHORT-ROOT (SHR), a transcription factor which moves from the central vasculature outward to specify the cell fates of quiescent center (QC), the stem cell cortex/endodermis initial and its daughter (CEI/D) and endodermis in the adjacent cell layer in the root of the model organism *Arabidopsis thaliana*. SHR is also required together with its downstream target SCARECROW (SCR) for the formative divisions of CEI/D and the separation of endodermis and cortex. Intensive studies have revealed that SHR intercellular mobility is linked to its subcellular localization, while formative divisions at the CEI/D position is determined by a nested regulatory network involving SHR and SCR. Despite these advances, additional regulatory mechanisms are needed to fully explain the regulation of SHR movement and action range, as summarized in Chapter 1 of this Thesis.

SHR movement was shown to be regulated by a zinc finger protein JACKDAW (JKD). Chapter 2 describes the function of three JKD homologs – BALDIBIS (BIB), MAGPIE (MGP) and NUTCRACKER (NUC) – and members of the “BIRD protein family”, and observed that they constrain SHR movement through nuclear retention and that they can fine-tune transcription of key SHR targets including *SCR* and *CYCLIN D6* (*CYCD6*). JKD and the studied BIRD proteins promote tissue specifications to continuously stabilize tissue boundaries in the root meristem, highlighting the developmental plasticity in plants.

SHR, SCR and the BIRD proteins are largely present in the QC, CEI/D and endodermis, yet different cell types are specified by their interplay. Being able to physically bind each other, it is also likely that they form protein complexes in these cells. We hypothesized that SHR, SCR and JKD might form distinct protein complexes in QC, CEI/D and endodermis to precisely regulate their behaviors, and set off to develop methods to analyze this dynamic complex formation in living roots. In Chapter 3, we optimized the

imaging technique Förster resonance energy transfer (FRET) measured by fluorescence lifetime imaging microscopy (FLIM) for Arabidopsis roots, and observed that SHR-SCR interaction is enriched in the CEI/D.

In Chapter 4, we confirmed that enhanced SHR-SCR interaction correlates with formative divisions, while JKD binds SHR and SCR in spatially complementary manners to repress undesired formative divisions away from CEI/D. Binding competition assays also suggest that higher order protein complexes are present for SHR, SCR and BIRD proteins. Together, these data indicate that differential protein interactions are associated with different cell fate specifications, and suggest how multicellular organisms might employ a limited set of regulatory factors to trigger various developmental processes.

JKD fine-tunes SHR's transcriptional activity on different targets. In Chapter 5, we show that JKD can act as a guiding molecule for SHR into specific subnuclear bodies. We generated two JKD mutant variants with opposite effect on SHR regulation: one enhances SHR subnuclear body localization while repressing *SCR* and *CYCD6* expression, the other fails to enrich SHR into subnuclear structures but enhances *SCR* and *CYCD6* transcription. Our data provide evidence for a role of JKD subnuclear compartmentalization as a means to regulate target gene expression.

In Chapter 6, we analyzed the function of SCARECROW-LIKE23 (SCL23), the closest homolog of SCR in Arabidopsis. We show that SCL23 is also a mobile protein with opposite directionality to SHR in the root meristem and that it restricts SHR movement without relying on nuclear retention as SCR does, adding more complexity towards SHR regulation during root development.

In Chapter 7, an overview is given to the new data generated in this thesis.

Samenvatting in het Nederlands

Cel - cel communicatie is de sleutel tot gecoördineerde cellulaire functies in meercellige organismen. Naast een belangrijke functie van klein moleculaire signaalstoffen vergelijkbaar met die in dierlijke systemen (maar anders wat betreft identiteit), maken planten ook vaak gebruik van mobiele transcriptiefactoren voor het geven van positionele informatie.

Het best bestudeerde voorbeeld omvat de transcriptie factor SHORT-ROOT (SHR), in het model organisme Arabidopsis thaliana, welk eiwit van het centrale vaatstelsel naar buiten beweegt om de celtypes specificeren in de aangrenzende cellaag, zijnde het quiescent center (QC), de cortex/endodermis initiaal en haar dochter (CEI/D) en de endodermis. SHR is ook vereist samen met zijn "target" SCARECROW (SCR) voor formatieve celdeling van de CEI/D en het scheiden van endodermis and cortex identiteit. Onderzoek heeft aangetoond dat intercellulaire SHR mobiliteit is verbonden met zijn subcellulaire localisatie terwijl formatieve celdeling op de CEI/D positie wordt bepaald door een regulatoir netwerk waarbij SHR en SCR een essentiele rol spelen. Ondanks deze inzichten, zijn additionele regulatoire mechanismen nodig om transport en de actieradius van SHR volledig te verklaren, zoals samengevat in Hoofdstuk 1 van dit proefschrift.

SHR mobiliteit wordt gereguleerd door een zinkvinger-eiwit JACKDAW (JKD). In Hoofdstuk 2 is de functie geanalyseerd van drie JKD homologen – BALDIBIS (BIB), MAGPIE (MGP) en NUTCRACKER (NUC) – ook behorend tot de zogenoemde BIRD familie, en laten zien dat ze transport van SHR beperken door nucleaire retentie en bovendien transcriptie kan "fine-tunen" van belangrijke SHR gereguleerde genen met inbegrip van *SCR* en *CYCLIN D6* (*CYCD6*). JKD en de bestudeerde BIRD eiwitten bevorderen weefsel specificatie door het continu te stabiliseren van identiteitsgrenzen in het wortelmeristeem en daarmee de ontwikkeling plasticiteit van planten accentueert.

SHR, SCR en de BIRD eiwitten zijn aanwezig in de QC, CEI/D en endodermis. Desalnietemin worden door hun samenspel verschillende celtypen gevormd. Onze hypothese was dat SHR, SCR en JKD verschillende eiwitcomplexen in QC, CEI/D en

endodermis kunnen vormen om hun gedrag nauwkeurig te reguleren. Wij hebben methoden ontwikkeld en geoptimaliseerd om deze dynamische complexvorming te analyseren in levende wortels. Hoofdstuk 3 beschrijft de optimalisatie van de Förster resonance energy transfer (FRET) techniek, gemeten met behulp van fluorescentie levensduur imaging microscopie (FLIM), voor Arabidopsis wortels en laat zien dat SHR - SCR interactie is verhoogd in de CEI/D.

In Hoofdstuk 4 wordt bevestigd dat SHR - SCR interactie correleert met formatieve celdeling, waarbij JKD bind aan SHR en SCR om ongewenste formatieve celdeling buiten de CEI/D te onderdrukken. Bindingstudies suggereren ook dat hogere orde eiwitcomplexen voor SHR, SCR en BIRD eiwitten aanwezig zijn. Samen duiden deze gegevens op een mechanisme waarbij differentiële eiwit interacties zijn geassocieerd met specificatie van verschillende celtypen. Deze resultaten suggereren dat meercellige organismen een beperkte set van regulatoire factoren kunnen gebruiken voor het activeren verschillende ontwikkelingsprocessen.

JKD beinvloed de transcriptie-activiteit van SHR. Hoofdstuk 5 laat het effect zien van twee JKD mutant varianten met een tegengesteld effect op SHR accumulatie en functie. Eén vartiant verhoogd subnucleaire SHR lokalisatie terwijl tegelijktijd *SCR* en *CYCD6* expressie wordt onderdrukt, terwijl een andere JKD variant *SCR* en *CYCD6* transcriptie bevordert maar geen effect heeft op subnucleaire SHR verrijking. Deze resultaten leveren bewijs voor een functie van JKD subnucleaire accumulatie voor het reguleren van genexpressie.

Hoofdstuk 6 beschrijft de functie van SCARECROW - LIKE23 (SCL23), het meest homologe familielid van SCR in Arabidopsis. De resultaten laaten zien dat SCL23 ook een mobiel eiwit is en op zijn beurt de mobiliteit van SHR beperkt maar niet via nucleaire retentie zoals SCR doet. Deze gegevens voegen meer complexiteit toe aan regulatie SHR activiteit tijdens wortelontwikkeling.

In hoofdstuk 7 wordt een overzicht gegeven van de nieuwe gegevens gegenereerd in dit proefschrift.

Acknowledgements

It has been a great challenge to complete this PhD, and I would have not been able to do this without the help of many people.

First and foremost, I would like to thank Ben and Ikram for encouraging, permitting, making the effort to initiate, financing and extending the finance of my PhD. Without you, I would have prematurely ended my track of higher education long ago.

I would like to thank Ikram and Ben for the intensive discussion, guidance and supervision during my PhD. I have learned a lot from you, both in sciences and ethics.

I would like to thank Ikram for the tremendous help and support in the laboratory. Working with you has been a great experience.

I would like to thank the collaborators in Amsterdam, specifically Joachim, Mark, Marten and Dorus. Your education and help on initializing the FRET-FLIM analysis and your critical opinions were invaluable for the progress.

I would like to thank the collaborators in Düsseldorf, specifically Yvonne, Steffi and Rüdiger. Thank you for all the help with the FRET-FLIM set-up, data processing and discussion, without which I would not accomplish a big part of this thesis. Thank Yvonne and Barbara for frequently sparing their confocal appointments for my measurements. Also, thank you all for preventing my starvation, dehydration, hypothermia and possible eventual death in the dark, cold confocal room.

I would like to thank the collaborators in Utrecht, specifically Ben, Kai and Anna. Thank you for sharing your HeLa cell facility and opening up new doorways for the project.

I would like to thank the nightshift companions: Dudu, Akie and Ikram. Thank you for the great company, the in-depths discussions, the cola-and-snack time, the share-of-feelings, the hearty encouragements and the wonderful dinners we had in the dark corridors.

I would like to thank the gentlemen of the office: Alfredo, Kalika, Guy and Hongtao. Thank you for setting examples on the qualities of endurance and faithfulness.

I would like to thank Sara for the insightful and mind-opening discussions.

I would like to thank the BIRD crew: Nicola, Roeska, Wouter, Martinus, Wim, João and Sunny. Thank you for your great help. You are the proud of the BIRD team.

I would like to thank the Dutch colleagues: Ben, Renze, Viola, René, Inez, Anja, Colette, Albert, Hugo, Vera, Maartje, Maaike, Klaartje, Sabine, Bas and everyone I might have missed. Thank you for helping me to integrate into the Dutch society.

I would like to thank the international colleagues: Ikram, Akie, Alfredo, Kalika, Sara, Gabino, AP, Tom, Violaine, Bea, Guy, Stephen, Klementina, Babu, Luca, Serena, Bandan and everyone I might have mised. Thank you for making integration unnecessary in this foreign land.

I would like to thank the Chinese colleagues and friends: Dudu, Ming, Hongtao, Zhong, Dongping, Wenkun, Fengfeng and Jingkun. Thank you for making this place feeling more like home.

I would like to thank the ex-students of the group: Nicola, Angie, Jelmer, Jos, Roeska, Richard, Evert, Wouter, Martinus, Mara, Daan, Christophe, Alberto, Tiemen, Sabrina, Pascal, Leny, Jurgen, Fons, Martijs, Gert-jan and everyone else I might have missed. Thank you for keeping me young.

I would like to thank my Taichi fellows, especially Mara, Daan, Frits, Uroš, Jie and Lan. Thank you for keeping me health, both physically and mentally.

I would like to thank my Parkour fellows. Thank you for showing me that I can “go over” the obstacles.

I would like to thank my family, especially my mother, my father, my grandfather and Ikram my mother No. 2. Thank you for your unconditional support and encouragement throughout all this time. 感谢我的母亲，父亲，祖父和家人这些年对我无保留的支持与鼓励。

Last but not least, I would like thank my wife Mengying. Thank you for all your care, your tolerance, your sacrifices and your love. Thank you for giving me a home.

Curriculum vitae

Yuchen Long (龙宇尘) was born on 28 April 1987 in the crowded city of Beijing, China. In this city he received exceptional education at home, kindergarten, elementary school, middle school and high school. At the age of eighteen, he ventured to the Netherlands for higher education at the Hogeschool van Arnhem en Nijmegen (HAN University of Applied Sciences). He majored in Plant Biotechnology and undertook two internships, the first in Prof. Gerco Angenent's laboratory in Wageningen, the Netherlands under the supervision of Mr. Guodong Wang and the second in Prof. Ben Scheres's laboratory in Utrecht, the Netherlands under the supervision of Dr. Ikram Blilou. In year 2009, he obtained his Bachelor of Applied Science degree with full marks in the graduation thesis. In the same year, he was lucky enough to join Prof. Ben Schere's laboratory as a PhD candidate to study Arabidopsis root development under the supervision of Prof. Ben Scheres and Dr. Ikram Blilou. In year 2012 he moved with Prof. Ben Schere's laboratory to Wageningen, the Netherlands and continued his PhD training. In year 2014, he joined Prof. Arezki Boudaoud's laboratory in Lyon, France to study biomechanics and Arabidopsis shoot development.

Cover designed by Yuchen Long

Printed by CPI-Wöhrmann Print Service – Zutphen

ISBN: 978-94-6203-875-2